THE
LONDON, EDINBURGH, AND DUBLIN
PHILOSOPHICAL MAGAZINE
AND
JOURNAL OF SCIENCE.

[SEVENTH SERIES.]

JULY 1931.

I. *The Viscous Layer associated with a Circular Cylinder.* *By* J. J. GREEN, *B.Sc., A.R.C.Sc., D.I.C., Ph.D. Busk Student, Beit Scientific Research Fellow* *.

[Plates I.–III.]

Summary.

THIS research was pursued with the intention of testing the truth of the Prandtl Boundary Layer Theory, when applied to a circular cylinder. Assuming that the circumferential velocity of the fluid close to the cylinder is expressible as a power series, in distance from the surface, whose coefficients are functions of the distance along the surface, a theoretical-step-by-step solution of the Prandtl Boundary Layer Equations is developed and compared with observations of the actual air-flow in the layer.

It is found that the solution agrees with observation as far round the cylinder as 67°, within the limits of experimental error, and that by employing a modified method of solution the range of agreement is extended up to the point of break-away of the boundary layer (75°). Further light is thrown on the conditions existing at this point, and the reasons for the break-away occurring there.

Further Advance.—It is found that all the Prandtl approximations are not valid at the point of break-away, and further advance can only be made by incorporating

* Communicated by Prof. L. Bairstow, F.R.S.

other assumptions when attempting to simplify the viscous fluid equations for solution.

Experimental Observations of the Air-flow in the Boundary Layer.

THE cylinder used in these experiments was hollow and of aluminium—6 in. external diameter; the surface at the mid-section, where the measurements were made, was polished so as to preclude any possibility of accidental disturbance in the flow. The cylinder was mounted symmetrically in the 4-ft. wind tunnel at the Royal College of Science where the experimental work was done. By employing the balance spindle as mounting, the cylinder could be freely rotated and clamped in any position. A wind speed of 30 ft./sec. was employed throughout the work.

The circumferential velocities were measured by means of a pitot tube of the normal type. This consisted of a short length ($\frac{1}{2}$ in.) of hypodermic syringe needle let into a 1-in. length of larger bore tube. The finer tube was flattened at the end to yield a slot of an approximate width of 1/50 in., the tube itself being of the order of 1 mm. external diameter. Connexion to the Chattock tilting gauge was effected by the use of small bore rubber tubing. The liquid reservoir of the gauge, to which the pitot was connected, was filled up, as far as possible, with water, and the gauge was employed in a position just outside the tunnel to minimize the length of connecting tubing. By reducing the volume of air on the pitot side of the gauge in this manner rapidity of use was secured.

The pitot tube was adjusted to be tangential to the surface at the mid-section of the cylinder and perpendicular to its axis; its distance from the surface was variable by means of a micrometer screw, operating an arm and bent shaft passing through a small slot in the cylinder wall, the micrometer being fixed to the inside surface of the cylinder. Adjustment was made from the tunnel roof by incorporating a bevel gear and shaft, all enclosed within the cylinder, and by the provision of a second circular dial and pointer (see Plates I. and II.).

The tangential velocity distribution along cylinder normals was explored from as near the cylinder as possible, and moving in steps of 0·005 in. Starting from the 0·0°, or nose position, the normals were chosen at 5° intervals (by rotating the cylinder) until the point was reached where

TAB

Velocity Measurements near the Sur

V = Channel speed = 30 ft./sec.

s_0 = distance round cylinder in deg

n = distance of centre of pitot tube

R_1 = gauge reading corrected to sta

R = original gauge reading.

q_1 = deduced velocity in ft./sec.

$s°$.	5°.			10°.			15°.			
n.	R.	R_1.	q_1.	R.	R_1.	q_1.	R.	R_1.	q_1.	R.
0·00166	3·12	0·05	3·76	3·01	0·14	6·31	2·83	0·41	10·80	2·60
0·0025	3·16	0·09	5·06	3·09	0·22	7·90	3·02	0·60	13·05	2·88
0·00333	,,	,,	,,	3·12	0·29	9·10	3·10	0·68	13·90	3·07
0·004166	—	—	—	3·18	0·33	9·70	3·16	0·74	14·50	3·19
0·005	—	—	—	,,	,,	,,	3·20	0·78	14·90	3·22

$s°$.	30°.			35°.			40°.			
n.	R.	R_1.	q_1.	R.	R_1.	q_1.	R.	R_1.	q_1.	R.
0·00166	1·94	1·49	20·6	1·79	2·19	25·00	0·69	1·99	23·8	0·21
0·0025	2·48	2·03	24·0	2·13	2·53	26·83	1·62	2·92	28·8	1·39
0·00333	2·93	2·48	26·6	2·71	3·11	29·80	2·50	3·80	32·9	2·36
0·004166	3·09	2·64	27·4	2·99	3·39	31·10	2·88	4·18	34·5	2·78
0·005	3·15	2·70	27·7	3·0	3·4	31·10	3·05	4·35	35·2	3·00
0·00583	,,	,,	,,	3·03	3·43	31·20	3·12	4·42	35·4	3·06
0·0066	—	—	—	3·05	3·45	31·30	3·14	4·44	35·6	3·15

$s°$.	55°.			60°.			65°.			
n.	R.	R_1.	q_1.	R.	R_1.	q_1.	R.	R_1.	q_1.	R.
0·0016̇	−0·82	2·83	28·40	−1·61	2·60	27·20	−1·95	2·52	26·8	−2·15
0·0025	0·52	4·17	34·50	−0·16	4·05	33·95	−0·63	3·84	33·1	−0·78
0·003̇	1·87	5·52	39·60	1·52	5·73	40·40	0·91	5·38	39·2	0·89
0·00416̇	2·55	6·20	42·00	2·34	6·55	43·25	2·11	6·58	43·3	1·98
0·005	2·90	6·55	43·25	2·78	6·99	44·60	2·62	7·09	45·0	2·43
0·00583̇	3·03	6·68	43·65	3·03	7·24	45·40	2·91	7·38	45·8	2·84
0·0066	3·10	6·75	43·80	3·09	7·30	45·60	3·06	7·53	46·2	2·98
0·0075	,,	,,	,,	,,	,,	,,	,,	,,	,,	,,
0·0083̇	—	—	—	—	—	—	—	—	—	—

[*To face page 3.*

LE I.

face of a Cylinder in an Air-stream.

d = diameter of cylinder = 6 in.

rees.

from surface (as fractions of diam. d).

tic pressure conditions.

20°.		25°.		
R_1.	q_1.	R.	R_1.	q_1.
0·72	14·3	2·45	1·25	18·9
1·00	16·9	2·75	1·55	21·0
1·19	18·4	2·93	1·73	22·2
1·31	19·3	3·06	1·86	23·0
1·34	19·5	3·12	1·92	23·4

45°.		50°.		
R_1.	q_1.	R.	R_1.	q_1.
2·36	25·93	−0·47	2·48	26·60
3·54	31·75	1·00	3·95	33·55
4·51	35·80	2·23	5·18	38·40
4·93	37·50	2·80	5·75	40·45
5·15	38·30	3·03	5·98	41·20
5·21	38·50	3·10	6·05	41·50
5·30	38·80	3·12	6·07	41·60

67°.		69°.			71°.			72°.		
R_1.	q_1.	R.	R_1.	q_1.	R.	R_1.	q_1.	R.	R_1.	q_1.
2·35	25·85	−2·47	2·03	24·0	−2·52	1·95	23·6	−2·45	1·95	23·6
3·72	32·60	−1·08	3·42	31.2	−1·21	3·26	30·5	−1·43	2·97	29·1
5·39	39·20	0·50	5·00	37·7	0·10	4·57	36·1	−0·07	4·33	35·1
6·48	43·00	1·76	6·26	42·2	1·52	5·99	41·3	1·15	5·55	39·7
6·93	44·40	2·38	6·88	44·2	2·11	6·58	43·2	2·03	6·43	42·7
7·34	45·70	2·82	7·32	45·6	2·71	7·18	45·2	2·60	7·00	44·6
7·48	46·10	2·92	7·42	46·0	2·82	7·29	45·5	2·70	7·10	45·0
,,	,,	3·03	7·52	46·4	3·00	7·47	46·1	3·02	7·42	46·0
—	—	,,	,,	,,	,,	,,	,,	3·13	7·53	46·3

the flow tended to change from laminar to turbulent motion; over this region of transition the readings were taken at 2° and 1° intervals. The velocity distribution at positions behind the point of break-away was also observed.

By measurement with a cathetometer microscope at its nearest point to the surface, the centroid of the pitot slit was found to be 0·01 in from the cylinder.

(*Note.* When a pitot is placed in a field where the velocity gradient is large, there is some doubt in assuming that the recorded pressure is that at the centroid of the pitot aperture. In conjunction with this there is the problem of interference when the pitot is very close to the surface. These points have been investigated fairly exhaustively by other observers (Stanton, Thom, etc.) and with tubes of various sizes. It is shown that errors, if any, due to the first assumption are smaller than the experimental errors, except when the pitot is just touching the surface, in which case its reading is slightly too large.)

The experimental results are given in Table I.

Column (1) gives n, the actual distance, in terms of d, of the centre of the pitot slit from the surface of the cylinder, after correction of the micrometer settings for the 0·01 in. mentioned above. d = diameter of cylinder.

Column (2) gives the gauge reading R, one side of the gauge being connected to the pitot, the other side to the static hole in the tunnel wall.

Column (3) gives R_1, the gauge readings corrected to the conditions of static pressure at the various points considered by employing the curve of pressure distribution round the cylinder, as obtained experimentally for use in the theoretical treatment of the Prandtl equations.

Column (4) gives the deduced velocities q_1 corresponding to gauge readings R_1,

$R_1 = K.\frac{1}{2}\rho q_1^2$, where K is a constant for the gauge.

Actually

$q_1^2 = 284{\cdot}4\ R_1$ for the gauge used, where q_1 is in ft./sec.

The observed velocity distributions are plotted in figs. 9, 9*a*, 9*b*, etc. The rise of velocity through the boundary layer, as the distance from the surface increases, to very clearly defined limiting values, is exhibited quite plainly.

The observations suggest a thickness of nearly 0·03 in. for the boundary layer from 0° to 45° round the cylinder. After this point the layer begins to slowly thicken, and at 67° is 0·04 in. The thickening, or rather opening, out now

rapidly increases, and at 72° the layer thickness is 0·05 in. and 0·07 in. at 73°. The point of break-away is considered to be in this region.

A curve showing the value of $\bar{q}$R against $s°$ is given in fig. 5. $\bar{q}=\bar{q}_1/V$, where $\bar{q}_1$ is the limiting velocity at any particular section, V is the channel speed of 30 ft./sec., R is Reynolds's number for the experiment ($0{\cdot}943 \times 10^5$), and $s°$ is the distance round the cylinder in degrees.

The Theoretical Velocity Distribution in the Boundary Layer.

It will be shown that the second of the Prandtl Boundary Layer equations indicates that the pressure in the layer is independent of r (or n), and hence the value of the pressure at any particular point is the same as that at the corresponding point just outside the layer, and we can assume that this distribution of pressure outside is independent of the conditions inside the layer.

For the development of the theoretical flow and the evaluation of the skin friction, it was necessary to measure the pressure distribution round the cylinder experimentally. The theoretical determination of the pressure distribution would be too difficult owing to turbulence outside the boundary layer, both in the initial stream and after the break-away.

A short tube was let into the cylinder wall from the inside near the mid-section, and the external surface was smoothed off to remove all roughness from the edges of the pressure hole which was formed by the end of the tube set flush with the surface. A rubber tube was connected to the short metal tube and led away through the interior of the cylinder to the Chattock gauge. The other side of the gauge was connected to the static pressure hole in the tunnel wall.

In all the experimental work great care was taken to guard against leakage, and prior to use the apparatus was tested by the U-tube method usually employed for that purpose.

By rotating the cylinder, readings for the pressure distribution were made at the various positions required. By continuing the range covered by the readings well round the nose or 0° position, the point of maximum pressure ($\frac{1}{2}\rho V^2$) accurately determined the location of the nose, and errors in the positioning of the pressure hole relative to the angle scale of the balance were thus eliminated.

At the value of $s = 68{\cdot}5^{\circ}$ from the nose the pressure is a minimum, and the transition from laminar to turbulent flow occurs soon after this. In the first set of readings, the pressure oscillations were too large for extreme accuracy to be attained, and so two further sets of readings were taken, with capillary tubes introduced into the rubber lead connecting to the gauge, to damp out oscillations. Allowance

TABLE II

Pressure Distribution round Cylinder.
$Vd/\nu = 0{\cdot}943 \times 10^5$.

s°.	R.	s°.	R.
−45	−1·99	70	−4·47
−40	−1·10	75	−4·15
−35	−0·25	80	−3·95
−30	+0·56	85	−3·84
−25	1·30	90	−3·80
−20	1·98	95	−3·83
−15	2·49	100	−3·83
−10	2·90	105	−3·73
− 5	3·09	110	−3·65
+ 0	3·16	115	−3·61
5	3·09	120	−3·60
10	2·85	125	−3·61
15	2·40	130	−3·63
20	1·87	135	−3·68
25	1·19	140	−3·69
30	0·41	145	−3·64
35	−0·40	150	−3·62
40	−1·30	155	−3·64
45	−2·15	160	−3·70
50	−2·95	165	−3·75
55	−3·65	170	−3·82
60	−4·21	175	−3·83
65	−4·47	180	−3·80

s° = distance round cylinder, in degrees.
R = gauge reading (mean of three sets of values).

was made in these cases for the time-lag during which readings became steady.

The agreement between the three sets of readings was very good, even in the turbulent region. The mean of the three sets of readings is given in Table II., and fig. 1 shows the curve of pressure distribution ($P/\rho V^2$ plotted against s°).

Experiments performed to test the constancy of static

pressure through the boundary layer indicate that over distances of 2 mm. or thereabouts the pressure is constant and equal to that on the surface of the cylinder at the position considered.

(*Note.* Since the static hole in the tunnel wall is not opposite the position occupied by the cylinder in the tunnel,

Fig. 1.

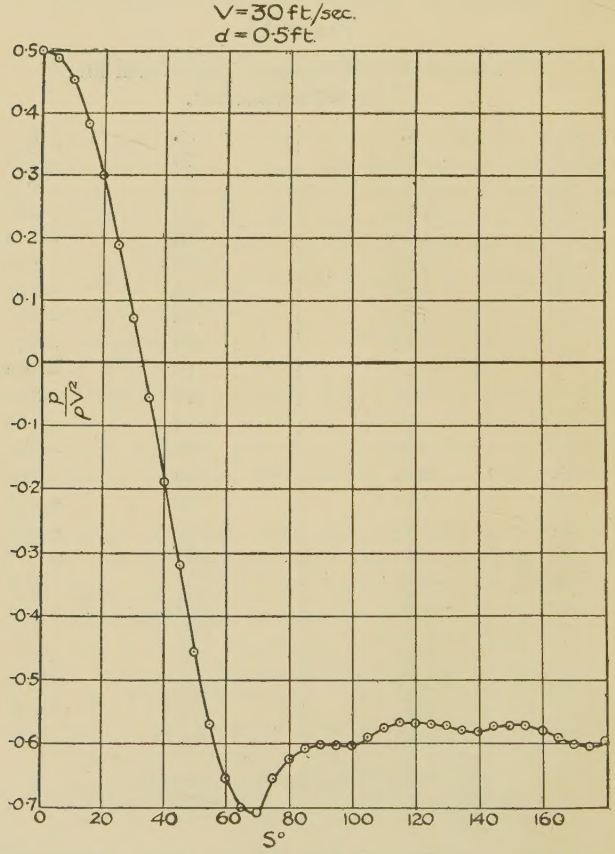

Wind speed, V, = 30 ft./sec.; diameter of cylinder, d, = 0·5 ft.; and ν, the kinematic viscosity coefficient for air, = 0·000159 ft.²/sec. Hence Reynolds's number, R, = $Vd/\nu = 0{\cdot}943 \times 10^5$ for the experiments described.

an investigation was made as to the difference in static pressure between the two points. This was undertaken in two ways, the results from both indicating that there was

no difference in static pressure between the two positions, and hence no correction was applied to the pressure readings for the fact that the cylinder and static hole were not at the same position on the tunnel centre-line.)

Mathematical Theory. Derivation of Prandtl's Boundary Layer Equations.

The general equations of steady motion in two dimensions, as given by Lamb, are

$$u\frac{\partial u}{\partial x}+v\frac{\partial u}{\partial y}=\nu\nabla^2 u-\frac{1}{\rho}\frac{\partial p}{\partial x}, \quad \ldots \quad (1)$$

$$u\frac{\partial v}{\partial x}+v\frac{\partial v}{\partial y}=\nu\nabla^2 v-\frac{1}{\rho}\frac{\partial p}{\partial y}, \quad \ldots \quad (2)$$

and the equation of continuity

$$\frac{\partial u}{\partial x}+\frac{\partial v}{\partial y}=0. \quad \ldots \quad (3)$$

Non-dimensional Form of (1), (2), *and* (3) *as Applied to a Cylinder.*

This form is deduced by dividing lengths and velocities by representative lengths and velocities respectively.

Let V, the relative velocity of the cylinder and fluid far from it, be the representative velocity, and let d, the diameter of the cylinder, be the representative length. Then we can re-write equation (1) as

$$\left\{\frac{u}{\mathrm{V}}\cdot\frac{\partial\frac{u}{\mathrm{V}}}{\partial\frac{x}{d}}+\frac{v}{\mathrm{V}}\cdot\frac{\partial\frac{u}{\mathrm{V}}}{\partial\frac{y}{d}}\right\}\frac{\mathrm{V}^2}{d}$$

$$=\nu\left\{\frac{\partial^2\frac{u}{\mathrm{V}}}{\left(\partial\frac{x}{d}\right)^2}+\frac{\partial^2\frac{u}{\mathrm{V}}}{\left(\partial\frac{y}{d}\right)^2}\right\}\frac{\mathrm{V}}{d^2}-\frac{1}{\rho}\cdot\frac{\partial p}{\partial\frac{x}{d}}\cdot\frac{1}{d};$$

i.e.,

$$\frac{u}{\mathrm{V}}\cdot\frac{\partial\frac{u}{\mathrm{V}}}{\partial\frac{x}{d}}+\frac{v}{\mathrm{V}}\cdot\frac{\partial\frac{u}{\mathrm{V}}}{\partial\frac{y}{d}}$$

$$=\frac{\nu}{\mathrm{V}d}\left\{\frac{\partial^2}{\left(\partial\frac{x}{d}\right)^2}+\frac{\partial^2}{\left(\partial\frac{y}{d}\right)^2}\right\}\cdot\frac{u}{\mathrm{V}}-\frac{\partial\frac{p}{\rho\mathrm{V}^2}}{\rho\frac{x}{d}}. \quad (4)$$

If, then,

(*a*) lengths are measured with the diameter of the cylinder as unity,

(*b*) velocities are measured as fractions of V, the channel speed,

(*c*) pressures are measured as fractions of ρV^2,

the equations of motion become

$$u\frac{\partial u}{\partial x}+v\frac{\partial u}{\partial y}=\frac{1}{R}\nabla^2 u-\frac{\partial p}{\partial x}, \quad . \quad . \quad . \quad . \quad (5)$$

$$u\frac{\partial v}{\partial x}+v\frac{\partial v}{\partial y}=\frac{1}{R}\nabla^2 v-\frac{\partial p}{\partial y}, \quad . \quad . \quad . \quad . \quad (6)$$

$$\frac{\partial u}{\partial x}+\frac{\partial v}{\partial y}=0, \quad . \quad . \quad . \quad . \quad . \quad . \quad . \quad (7)$$

where R is Reynolds's number.

To express in Curvilinear Coordinates.

With the coordinate axes as shown, s denoting dis-

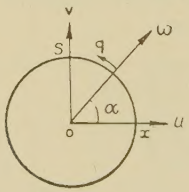

tances round the cylinder, r distances normal from the surface, and the velocities w and q as shown,

$$u=-q\sin\alpha+w\cos\alpha, \qquad v=q\cos\alpha+w\sin\alpha,$$

$$\frac{\partial}{\partial x}=\left(\frac{\partial s}{\partial x}\right)_y\frac{\partial}{\partial s}+\left(\frac{\partial r}{\partial x}\right)_y\frac{\partial}{\partial r}=-\sin\alpha.\frac{\partial}{\partial s}+\cos\alpha.\frac{\partial}{\partial r},$$

$$\frac{\partial}{\partial y}=\left(\frac{\partial s}{\partial y}\right)_x\frac{\partial}{\partial s}+\left(\frac{\partial r}{\partial y}\right)_x\frac{\partial}{\partial r}=\cos\alpha.\frac{\partial}{\partial s}+\sin\alpha.\frac{\partial}{\partial r},$$

$$\nabla^2=\left(\frac{\partial^2}{\partial x^2}+\frac{\partial^2}{\partial y^2}\right)=\frac{\partial^2}{\partial s^2}+\frac{\partial\alpha}{\partial s}\cdot\frac{\partial}{\partial r}+\frac{\partial^2}{\partial r^2};$$

and with $\alpha = \pi/2$ the three equations of motion become

$$\left.\begin{aligned} -q\frac{\partial q}{\partial s} - w\frac{\partial q}{\partial r} - wq\cdot\frac{\partial \alpha}{\partial s} &= \frac{1}{\mathrm{R}}\left\{-\frac{\partial^2 q}{\partial s^2} + q\left(\frac{\partial \alpha}{\partial s}\right)^2 \right. \\ &\quad \left. - 2\frac{\partial w}{\partial s}\cdot\frac{\partial \alpha}{\partial s} - \frac{\partial q}{\partial r}\cdot\frac{\partial \alpha}{\partial s} - w\frac{\partial^2 \alpha}{\partial s^2} - \frac{\partial^2 q}{\partial r^2}\right\} + \frac{\partial p}{\partial s}, \\ q\frac{\partial w}{\partial s} + w\frac{\partial w}{\partial r} - q^2\frac{\partial \alpha}{\partial s} &= \frac{1}{\mathrm{R}}\left\{\frac{\partial^2 w}{\partial s^2} - w\left(\frac{\partial \alpha}{\partial s}\right)^2 \right. \\ &\quad \left. - 2\frac{\partial q}{\partial s}\cdot\frac{\partial \alpha}{\partial s} + \frac{\partial w}{\partial r}\cdot\frac{\partial \alpha}{\partial s} - q\frac{\partial^2 \alpha}{\partial s^2} + \frac{\partial^2 w}{\partial r^2}\right\} - \frac{\partial p}{\partial r}, \\ \frac{\partial q}{\partial s} + \frac{\partial w}{\partial r} + w\cdot\frac{\partial \alpha}{\partial s} &= 0. \end{aligned}\right\} \quad . \quad . \quad . \quad . \quad (8)$$

Prandtl's Approximate Equations for a Boundary Layer.

(*a*) R is supposed large compared with unity.

(*b*) q is supposed large compared with w (no turbulence).

(*c*) Derivatives with respect to r are supposed large compared with those with respect to s.

The first is an arbitrary condition, and satisfied in the experiments where $\mathrm{R} = 0{\cdot}94 \times 10^5$.

The second condition will hold if the motion is laminar.

The third condition is less clear, but on examination is found to be a remarkably good assumption up to the point of break-away, but not beyond.

The equations then deduced * are

$$\left.\begin{aligned} -q\frac{\partial q}{\partial s} - w\frac{\partial q}{\partial r} &= -\frac{1}{\mathrm{R}}\frac{\partial^2 q}{\partial r^2} + \frac{\partial p}{\partial s}, \\ 0 &= \frac{\partial p}{\partial r}, \\ \frac{\partial q}{\partial s} + \frac{\partial w}{\partial r} &= 0. \end{aligned}\right\} \quad . \quad . \quad . \quad (9)$$

The second equation should really be interpreted as meaning

$$\frac{\partial p}{\partial r} \text{ is small compared with } \frac{\partial p}{\partial s} \quad . \quad . \quad . \quad (10)$$

* Bairstow, Journ. Roy. Aero. Soc. xxix. (1925).

For the middle equation (8) yields the result

$$\left\{\frac{\partial p}{\partial r}\right\}_{\text{boundary}} = \frac{1}{\mathrm{R}}\left\{\frac{\partial^2 w}{\partial r^2} + \frac{1}{r}\frac{\partial w}{\partial r}\right\}_{\text{boundary}}, q = w = 0, \quad (11)$$

and from first equation (8)

$$\left\{\frac{\partial p}{\partial s}\right\}_{\text{boundary}} = \frac{1}{\mathrm{R}}\left\{\frac{\partial^2 q}{\partial r^2} + \frac{1}{r}\frac{\partial q}{\partial r}\right\}_{\text{boundary}},$$

and by assumption (*b*) this must be greater than

$$\left\{\frac{\partial p}{\partial r}\right\}_{\text{boundary}}.$$

The importance of this equation lies in the simplification introduced by considering $\frac{\partial p}{\partial s}$ to be sensibly independent of r, a limitation which rests on the solid basis of empirical argument.

The solution suggested by Professor Bairstow commences with the assumption that

$$q\mathrm{R} = \frac{n}{\lfloor 1}f_0 + \frac{n^2}{\lfloor 2}f_1 + \frac{n^3}{\lfloor 3}f_2 + \ldots = \sum_{\alpha=1}\frac{n^\alpha}{\lfloor \alpha}f_{\alpha-1}, \quad . \quad (12)$$

where f_0, f_1, etc., are functions of s only, and n is that part of r which lies beyond the boundary, so that

$$\frac{\partial}{\partial n} = \frac{\partial}{\partial r}.$$

From the third equation (9),

$$\frac{\partial}{\partial r}w = -\frac{\partial}{\partial s}q.$$

$$\therefore \quad \frac{\partial}{\partial n}\mathrm{R}w = -\frac{\partial}{\partial s}\mathrm{R}q = -\sum_{\alpha=1}\frac{n^\alpha}{\lfloor \alpha}\frac{\partial}{\partial s}f_{\alpha-1}$$

and

$$\mathrm{R}w = -\sum_{\alpha=1}\frac{n^{\alpha+1}}{\lfloor \alpha+1}\frac{\partial}{\partial s}f_{\alpha-1}. \quad . \quad . \quad . \quad . \quad (13)$$

From first equation (9), multiplying throughout by R^2,

$$-q\mathrm{R}.\frac{\partial q\mathrm{R}}{\partial s} - w\mathrm{R}.\frac{\partial q\mathrm{R}}{\partial n} = -\frac{\partial^2}{\partial n^2}q\mathrm{R} + \mathrm{R}^2\frac{\partial p}{\partial s}, \quad . \quad (14)$$

and using (12) and (13) this becomes

$$-\sum_{\beta=1}\frac{n^{\beta}}{\lfloor\beta}f_{\beta-1}\sum_{\gamma=1}\frac{n^{\gamma}}{\lfloor\gamma}\frac{\partial}{\partial s}f_{\gamma-}$$

$$+\sum_{\beta=1}\frac{n^{\beta+1}}{\lfloor\beta+1}\frac{\partial}{\partial s}f_{\beta-1}\sum_{\gamma=1}\frac{n^{\gamma-1}}{\lfloor\gamma-1}f_{\gamma-1}$$

$$=-\sum_{\alpha=2}\frac{n_{\alpha-2}}{\lfloor\alpha-2}f_{\alpha-1}+\mathrm{R}^2\frac{\partial p}{\partial s},\quad\ldots\quad(15)$$

i. e.,

$$-\sum_{\alpha=2}n^{\alpha}\sum_{\beta=1}\frac{f_{\beta-1}}{\lfloor\beta}\cdot\frac{f'_{\alpha-\beta-1}}{\lfloor\alpha-\beta}$$

$$+\sum_{\alpha=2}n^{\alpha}\sum_{\beta=1}\frac{f_{\beta-1}}{\lfloor\beta-1}\cdot\frac{f'_{\alpha-\beta-1}}{\lfloor\alpha-\beta+1}$$

$$=-\sum_{\alpha=0}\frac{n^{\alpha}}{\lfloor\alpha}f_{\alpha-1}+\mathrm{R}^2\frac{\partial p}{\partial s},\quad\ldots\quad(16)$$

where $\alpha=\beta+\gamma$ or $\gamma=\alpha-\beta$,

i. e.,

$$-\sum_{\alpha=2}n^{\alpha}\sum_{\beta=1}f_{\beta-1}\cdot f'_{\alpha-\beta-1}\cdot\frac{\alpha-2\beta+1}{\lfloor\beta\cdot\lfloor\alpha-\beta+1}$$

$$=-\sum_{\alpha=0}n^{\alpha}\frac{f_{\alpha+1}}{\lfloor\alpha}+\mathrm{R}^2\frac{\partial p}{\partial s}.$$

By differentiation of (12) with $n\to 0$,

$$f_0=\mathrm{R}\left(\frac{\partial q}{\partial n}\right)_{\text{boundary}}.$$

Hence $f_0=$skin friction,

when $\alpha=0$, $f_1=\mathrm{R}^2\frac{\partial p}{\partial s}$,

$\alpha=1$, $f_2=0$;

$$\alpha>1\quad\sum_{\beta=1}f_{\beta-1}f'_{\alpha-\beta-1}\cdot\frac{\alpha-2\beta+1}{\lfloor\beta\cdot\lfloor\alpha-\beta+1}=\sum_{\alpha=2}\frac{1}{\lfloor\alpha}f_{\alpha+1}.\qquad(17)$$

Hence

$$\frac{1}{\lfloor 2}f_3=\frac{1}{\lfloor 1\lfloor 2}f_0f_0',$$

$$\frac{1}{\lfloor 3}f_4=\frac{2}{\lfloor 1\lfloor 3}f_0f_1'+0.$$

$$\frac{1}{\lfloor 4}f_5 = 0 + \frac{1}{\lfloor 2\ \lfloor 3}f_1 f_1' - 0,$$

$$\frac{1}{\lfloor 5}f_6 = \frac{4}{\lfloor 1\ \lfloor 5}f_0 f_3' + 0 + 0 - \frac{2}{\lfloor 4\ \lfloor 2}f_3 f_0'$$

$$= \frac{4}{\lfloor 5}(f_0 f_0'' + (f_0')^2) - \frac{1}{\lfloor 4}f_0 (f_0')^2$$

$$= \frac{1}{\lfloor 5}\{4 f_0^2 f_0'' - f_0 (f_0')^2\},$$

$$\frac{1}{\lfloor 6}f_7 = \frac{5}{\lfloor 1\ \lfloor 6}f_0 f_4' + \frac{3}{\lfloor 2\ \lfloor 5}f_1 f_3' + 0 - \frac{1}{\lfloor 4\ \lfloor 3}f_3 f_1' - \frac{3}{\lfloor 5\ \lfloor 2}f_4 f_0'$$

$$= \frac{5}{\lfloor 6}f_0\{2 f_0 f_1'' + 2 f_0' f_1'\} + \frac{3}{\lfloor 2\ \lfloor 5}f_1\{f_0 f_0'' + (f_0')^2\}$$

$$- \frac{1}{\lfloor 4\ \lfloor 3}f_1' f_0 f_0' - \frac{3}{\lfloor 5}f_0' f_0 f_1'$$

$$= \frac{10}{\lfloor 6}f_0^2 f_1'' - \frac{13}{\lfloor 6}f_6 f_0' f_1' + \frac{9}{\lfloor 6}(f_0 f_0'' f_1 + (f_0')^2 f_1),$$

$$\frac{1}{\lfloor 7}f_8 = \frac{6}{\lfloor 1\ \lfloor 7}f_0 f_5' + \frac{4}{\lfloor 2\ \lfloor 6}f_1 f_4' + 0 + 0$$

$$- \frac{2}{\lfloor 5\ \lfloor 3}f_4 f_1' - \frac{4}{\lfloor 6\ \lfloor 2}f_5 f_0'$$

$$= \frac{6}{\lfloor 7}f_0\{2 f_1 f_1'' + 2(f_1')^2\} + \frac{2}{\lfloor 6}f_1\{2 f_0 f_1'' + 2 f_0' f_1'\}$$

$$- \frac{2}{\lfloor 5\ \lfloor 3}f_1'\{2 f_0 f_1'\} - \frac{2}{\lfloor 6}f_0'\{2 f_1 f_1'\}$$

$$= \frac{40}{\lfloor 7}f_0 f_1 f_1'' - \frac{16}{\lfloor 7}f_0 (f_1')^2,$$

$$\frac{1}{\lfloor 8}f_9 = \frac{7}{\lfloor 1\ \lfloor 8}f_0 f_6' + \frac{5}{\lfloor 2\ \lfloor 7}f_1 f_5' + 0 + \frac{1}{\lfloor 4\ \lfloor 5}f_3 f_3' - 0$$

$$- \frac{3}{\lfloor 6\ \lfloor 3}f_5 f_1' - \frac{5}{\lfloor 7\ \lfloor 2}f_6 f_0'$$

$$= \frac{7}{\underline{8}} f_0\{4(2f_0 f_0' f_0'' + f_0^2 f_0''') - (2 f_0' f_0'' f_0 + (f_0')^3)\}$$

$$+ \frac{5}{\underline{2}\,\underline{7}} 2f_1\{f_1 f_1'' + (f_1')^2\}$$

$$+ \frac{1}{\underline{4}\,\underline{5}} f_0 f_0'\{f_0 f_0'' + (f_0')^2\} - \frac{1}{\underline{6}} f_1'\{f_1 f_1'\}$$

$$- \frac{5}{\underline{7}\,\underline{2}} f_0'\{4 f_0^2 f_0'' - f_0 (f_0')^2\},$$

$$= \frac{7}{\underline{8}} f_0^3 f_0''' - \frac{24}{\underline{8}} f_0^2 f_0' f_0'' + \frac{27}{\underline{8}} f_0 (f_0')^3$$

$$+ \frac{40}{\underline{8}} f_1^2 f_1'' - \frac{16}{\underline{8}} f_1 (f_1')^2.$$

Hence

$$qR = \frac{n}{\underline{1}} f_0 + \frac{n^2}{\underline{2}} f_1 + 0 + \frac{n^4}{\underline{4}} f_0 f_0' + \frac{n^5}{\underline{5}} 2 f_0 f_1' + \frac{n^6}{\underline{6}} 2 f_1 f_1'$$

$$+ \frac{n^7}{\underline{7}} \{4 f_0^2 f_0'' - f_0 (f_0')^2\} + \frac{n^8}{\underline{8}} f_7 + \frac{n^9}{\underline{9}} f_8 + \frac{n^{10}}{\underline{10}} f_9, \text{ etc.}$$

. . . (18)

This series was not convenient for the evaluation of qR and the determination of f_0 (skin friction), since a large number of terms were required before qR reached its limiting value. A form which agrees with (18) when n is small, and which reaches a limit readily found by successive approximation, is developed below.

From (18) we have

$$\frac{1}{f_0} \cdot \frac{\partial}{\partial n} qR = 1 + n \frac{f_1}{f_0} + \frac{n^3}{\underline{3}} \cdot f_0' + \frac{5n^4}{5\,\underline{4}} \cdot 2 f_1' + \frac{n^5}{\underline{5}} 2 f_1' \cdot \frac{f_1}{f_0}$$

$$+ \frac{n^6}{\underline{6}} \cdot \frac{f_6}{f_0} + \frac{n^7}{\underline{7}} \cdot \frac{f_7}{f_0} + \frac{n^8}{\underline{8}} \cdot \frac{f_8}{f_0} + \frac{n^9}{\underline{9}} \cdot \frac{f_9}{f_0} \ldots \text{etc.}$$

$$= 1 + n \frac{f_1}{f_0} + \frac{n^3}{3} f_0' + \frac{4n^4}{5} \cdot 2 f_1' + \frac{n^4}{5} \cdot 2 f_1' \left(1 + n \frac{f_1}{f_0}\right)$$

$$+ \frac{n^6}{\underline{6}} \cdot \frac{f_6}{f_0} + \frac{n^7}{\underline{7}} \cdot \frac{f_7}{f_0} + \frac{n^8}{\underline{8}} \cdot \frac{f_8}{f_0} + \ldots \text{etc.}$$

$$\therefore \quad \frac{1}{f_0}\cdot\frac{\partial}{\partial n}qR=\left(1+n\frac{f_1}{f_0}\right)\left(1+\frac{n^4}{\lfloor 5}2f_1'\right)+\frac{n^3}{\lfloor 3}f_0'+\frac{8n^4}{\lfloor 5}f_1'$$
$$+\frac{n^6}{\lfloor 6}\cdot\frac{f_6}{f_0}+\frac{n^7}{\lfloor 7}\frac{f_7}{f_0}+\frac{n^8}{\lfloor 8}\frac{f_8}{f_0}+\ldots \text{ etc.} \quad . \quad (19)$$

In the final method of solution employed, the above expression for $\frac{1}{f_0}\frac{\partial}{\partial n}qR$ was used, but an initial device consisted in expression (19) exponentially, thus:

$$\frac{1}{f_0}\cdot\frac{\partial}{\partial n}qR=\left(1+n\cdot\frac{f_1}{f_0}\right)\left(1+\frac{n^4}{\lfloor 5}2f_1'\right)$$
$$\times\left\{1+\frac{\frac{n^3}{\lfloor 3}f_0'+\frac{8}{\lfloor 5}n^4f_1'+\frac{n^6}{\lfloor 6}\frac{f_6}{f_0}+\frac{n^7}{\lfloor 7}\frac{f_7}{f_0}+\ldots}{\left(1+n\frac{f_1}{f_0}\right)\left(1+\frac{n^4}{\lfloor 5}2f_1'\right)}\right\}$$
$$=\left(1+n\frac{f_1}{f_0}\right)\left(1+\frac{n^4}{\lfloor 5}2f_1'\right)e^{\overset{\mathrm{F}(n)}{\left(1+n\frac{f_1}{f_0}\right)\left(1+\left(\frac{n^4}{\lfloor 5}\right)\cdot 2f_1'\right)}}$$
$$\ldots \quad (21)$$

with $\mathrm{F}(n)$ as yet undetermined.

To determine $\mathrm{F}(n)$: if we write

$$1+\frac{\frac{n}{\lfloor 3}f_0'+\frac{8n^4}{\lfloor 5}f_1'+\frac{n^6}{\lfloor 6}\frac{f_6}{f_0}\ldots}{\left(1+n\frac{f_1}{f_0}\right)\left(1+\frac{n^4}{\lfloor 5}\cdot 2f_1'\right)}\equiv e^{\log\left(1+\frac{\frac{n^3}{\lfloor 3}f_0'+\frac{8n^4}{\lfloor 5}f_1'+\frac{n^6}{\lfloor 6}\frac{f_6}{f_0}\ldots}{\left(1+n\frac{f_1}{f_0}\right)\left(1+\frac{n^4}{\lfloor 5}\cdot 2f_1'\right)}\right)}$$

and then expand the logarithm

$$\left|\ \log(1+x)=x-\frac{x^2}{2}+\frac{x^3}{3}-\frac{x^4}{4}\ldots \text{ when } x<1\ \right|,$$

we have

$$\left\{\frac{\frac{n^3}{\lfloor 3}f_0'+\frac{8n^4}{\lfloor 5}f_1'+\frac{n^6}{\lfloor 6}\frac{f_6}{f_0}\ldots}{\left(1+n\frac{f_1}{f_0}\right)\left(1+\frac{n^4}{\lfloor 5}2f_1'\right)}\right\}-\frac{1}{2}\left\{\frac{\frac{n^3}{\lfloor 3}f_0'+\frac{8n^4}{\lfloor 5}f_1'+\frac{n^6}{\lfloor 6}\frac{f_6}{f_0}+\ldots}{\left(1+n\frac{f_1}{f_0}\right)\left(1+\frac{n^4}{\lfloor 5}2f_1'\right)}\right\}^2$$
$$+\frac{1}{3}\{\text{do.}\}^3\ldots \text{ etc.}=\frac{\mathrm{F}(n)}{\left(1+n\frac{f_1}{f_0}\right)\left(1+\frac{n^4}{\lfloor 5}2f_1'\right)}.$$

$$\therefore \quad F(n)=\frac{n^3}{\lfloor 3}f_0'+\frac{8n^4}{\lfloor 5}f_1'+\frac{n^6}{\lfloor 6}\frac{f_6}{f_0}$$
$$-\frac{1}{2}\frac{\left(\frac{n^3}{\lfloor 3}f_0'+\frac{8n^4}{\lfloor 5}f_1'+\frac{n^6}{\lfloor 6}\frac{f_6}{f_0}\right)^2}{\left(1+n\frac{f_1}{f_0}\right)\left(1+\frac{n^4}{\lfloor 5}2f_1'\right)}+\frac{1}{3}. \quad . \quad . \quad (22)$$

Now assume that terms involving powers of n greater than the sixth may be ignored in a first approximation. Then

$$F(n)=\frac{n^3}{\lfloor 3}f_0'+\frac{8n^4}{\lfloor 5}f_1'+\frac{n^6}{\lfloor 6}\frac{f_6}{f_0}-\frac{1}{2}\frac{\left(\frac{n^3}{\lfloor 3}f_0'\right)^2}{\left(1+n\frac{f_1}{f_0}\right)\left(1+\frac{n^4}{\lfloor 5}2f_1'\right)},$$

$$. \quad . \quad . \quad (23)$$

and hence (21) is completely known in terms of the f functions.

The method of solution briefly, then, was to evaluate the f functions at various positions round the cylinder, and insert in eqnation (21) plotting $\frac{1}{f_0}\frac{\partial}{\partial n}.qR$ for various values of n. Integration would then yield $\frac{1}{f_0}qR$, giving the theoretical velocity distribution through the boundary layer.

There were two drawbacks to this method of analysis :—

(1) The logarithmic expansion $\{\log(1+x)\}$ was not always valid, since when n was large, x sometimes ceased to be fractional.

(2) The curves for $\frac{1}{f_0}\frac{\partial}{\partial n}qR$ when plotted exhibited sudden drops to zero at large n values, and this was deemed not to be in accordance with the truth ; the belief that the velocity gradient falls steadily and smoothly to zero at the outside edge of the boundary layer seemed more logical.

In face of these limitations equation (21) was no longer employed to deduce a solution ; but, instead, the full expression for $\frac{1}{f_0}\frac{\partial}{\partial n}qR$ contained in (19) was employed (up to and including the term $\frac{n^8}{8}\frac{f_8}{f_0}$), in conjunction with the boundary conditions, viz., $q=0$ and $w=0$ when $n=0$ (on the surface);

Table III.

Summary of Data for use in the Theoretical Work.

$$R = V d/\nu = 0{\cdot}943 \times 10^5.$$
$$R^2 = 0{\cdot}89 \times 10^{10}.$$

$s°$.	$\frac{s}{\text{diams.}}$	$\frac{p}{\rho V^2}$.	$\frac{f_1}{10^6} \equiv \frac{R^2}{10^6}\frac{\partial}{\partial s}\frac{p}{\rho V^2}$.	$\frac{f_1'}{10^8} \equiv \frac{\partial}{\partial s}\frac{f_1}{10^8}$.	$\frac{f_1''}{10^{10}} \equiv \frac{\partial}{\partial s}\frac{f_1'}{10^{10}}$.	$\frac{1}{10^3}\bar{q}R$, expt.	$\frac{1}{10^3}\bar{q}R$, Bernoulli.
0	0	0·500	0	− 992	− 80·0	0	0
5	0·0436	0·489	− 4800	−1228	− 31·1	15·7	14·0
10	0·0872	0·453	−10400	−1260	+ 15·1	30·8	28·9
15	0·1308	0·383	−15700	−1100	+ 55·6	45·8	45·7
20	0·1744	0·300	−19900	− 806	67·0	61·0	59·7
25	0·2180	0·189	−22750	− 539	45·4	73·8	74·4
30	0·2616	0·071	−24900	− 420	13·4	85·5	87·5
35	0·3052	−0·055	−26700	− 397	8·5	97·4	99·5
40	0·3488	−0·189	−28200	− 234	66·7	109·0	110·8
45	0·3924	−0·319	−28550	+ 234	174·0	119·3	121·0
50	0·4360	−0·457	−26000	1170	158·0	129·0	130·5
55	0·4796	−0·570	−20080	1517	31·1	137·0	138·0
60	0·5232	−0·655	−12950	1505	− 10·7	142·3	143·5
65	0·5668	−0·70	− 6230	1637	+169·0	146·0	146·1
67	0·5838	−0·707	− 2230	+2150	+445·0	146·4	146·5
69	0·6015	−0·710	+ 1330	3110	800·0	146·0	146·5
71	0·6185	−0·704	8450	—	—	145·0	145·5
72	0·6270	−0·695	+12230	—	—	145·0	145·0
73	0·6355	−0·680	12000	—	—	144·0	144·5

$$\frac{1}{10^3}\bar{q}R \text{ (Bernoulli)} = \frac{\sqrt{2}}{10^3} R \sqrt{\left(0{\cdot}5 - \frac{p}{\rho V^2}\right)}.$$

and further, that the tangential velocity must be asymptotically equal to the velocity $\bar{q}$ just outside the boundary layer*. Hence, as we pass into the main stream, $\frac{\partial q}{\partial n}$ must vanish, and also $\frac{\partial^2 q}{\partial n^2}$ must be zero, and $\bar{q}$ is given (from a knowledge of the pressure) by Bernoulli's equation. In the theoretical treatment the value of q employed was that actually measured, a value not anywhere sensibly departing from the Bernoulli value, even at points beyond the region of break-away.

Fig. 2.

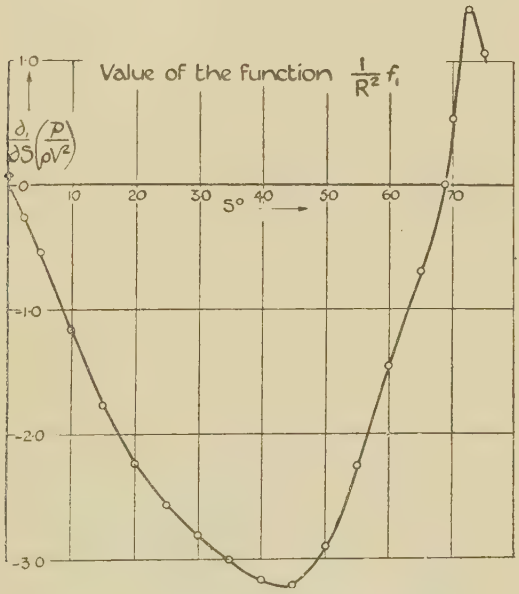

Evaluation of the f Coefficients.

In Table III. the pressure-readings are given, reduced to fractions of ρV^2, and the corresponding curve is shown in fig. 1. This curve was then graphically differentiated, a process corrected to very great accuracy by integration of the curve obtained and comparison with the original pressure-distribution curve. After a little practice it was possible to obtain exact curves of the differential without finding the process too laborious. Fig. 2 shows the differentiated curve

* See p. 27.

giving values of $\frac{\partial}{\partial s}\left(\frac{p}{\rho V^2}\right)$, and column 4 of Table III. then indicates the value of f_1 derived from equation (17). By

Fig. 3.

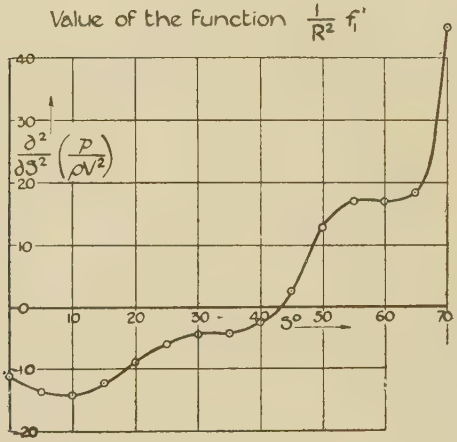

Fig. 4.

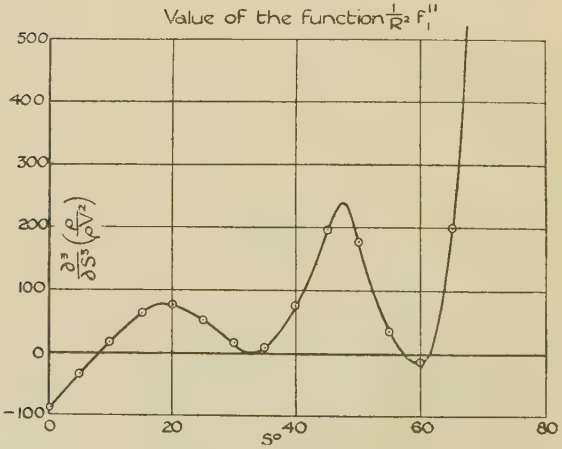

further graphical differentiation the values of f_1' and f_1'' were deduced. Figs. 3 and 4 contain the curves of

$$\frac{\partial^2}{\partial s^2}\left(\frac{p}{\rho V^2}\right) \quad \text{and} \quad \frac{\partial^3}{\partial s^3}\left(\frac{p}{\rho V^2}\right),$$

and columns 5 and 6 of Table III. give the tabulated values of f_1' and f_1'' for the various positions round the cylinder. Generally it was found advisable to divide by powers of ten to get convenient numbers. Columns 7 and 8 of Table III. contain the experimental and the Bernoulli values for the limiting velocity $\bar{q}$ (multiplied by Reynolds's number) respectively.

The two sets of values are plotted in fig. 5; the agreement is almost exact for at least 90° round the cylinder.

Knowing the values of f_1 and its derivatives at all positions round the cylinder, it only remains to evaluate f_0 and its derivatives before $\frac{1}{f_0}\frac{\partial}{\partial n}qR$ can be determined and the

Fig. 5.

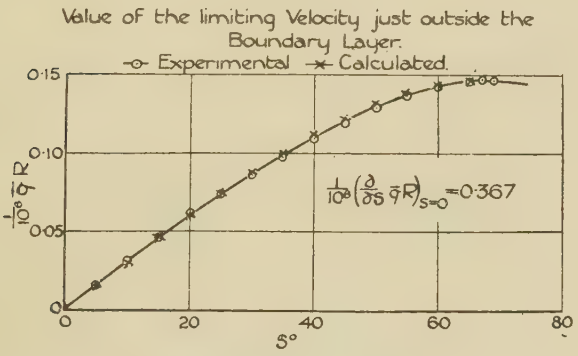

theoretical velocity distribution plotted for comparison with experimental measurement.

Near the 0° position, where $\frac{f_1}{f_0}$ is large and negative, it appears, from trial calculations, that

$$\frac{1}{f_0}\frac{\partial}{\partial n}qR \doteqdot 1+n\frac{f_1}{f_0},$$

and by integration,

$$\frac{1}{f_0}\bar{q}R \doteqdot \bar{n}+\frac{\bar{n}^2}{\underline{2}}\frac{f_1}{f_0}, \quad \text{where } \bar{n} \text{ is the value of } n,$$

which makes

$$\frac{\partial}{\partial n}qR=0 \quad (\text{at } n=0, \frac{1}{f_0}\bar{q}R=0).$$

TABLE IV.

Calculated Values of Skin Friction and its Derivatives.

$V = 30$ ft./sec.
$d = 0{\cdot}5$ ft.

$s°$.	s diams.	$\frac{f_0}{10^6}$, 1st approx.	$\frac{f_0}{10^6}$.	$\frac{f_0'}{10^6}$.	$\frac{f_0''}{10^6}$.	$\frac{f_0'''}{10^6}$.
0	0	0·00	0·00	281·00	−1380	
						13000
5	0·0436	12·25	11·10	233·15	− 813	
						74000
10	0·0872	25·30	21·50	268·00	+2415	
						−123800
15	0·1308	37·90	33·80	255·80	−2985	
						+ 95000
20	0·1744	49·25	43·40	215·50	+1155	
						− 84000
25	0·2180	58·00	52·70	186·10	−2505	
						+ 68000
30	0·2616	65·10	59·40	141·40	+ 463	
						− 23000
35	0·3052	72·10	65·70	139·70	− 540	
						500
40	0·3488	78·40	71·31	117·60	− 518	
						− 33000
45	0·3924	82·40	75·40	63·65	−1957	
						− 10000
50	0·4360	81·90	76·18	− 31·25	−2393	
						+ 17000
55	0·4796	74·18	72·75	−119·35	−1652	
						− 5000
60	0·5232	60·70	65·93	−196·10	−1870	
						+ 9400
65	0·5668	41·00	55·75	−268·70	−1461	
						− 14813
67	0·5838	26·00	50·72	−316·70	−4044	
69	0·6012	0·00	45·50			
71	0·6186	imaginary	38·00			
72	0·6274	⋮	27·00			
73	0·6361	⋮	5·00			

Hence, when $\frac{\partial}{\partial n} qR$ is zero,

$$1 + \bar{n}\frac{f_1}{f_0} \doteqdot 0.$$

$$\therefore \quad \bar{n} \doteqdot -\frac{f_0}{f_1},$$

and, substituting this value of $\bar{n}$,

$$\frac{1}{f_0}\bar{q}\mathrm{R} \doteqdot -\frac{f_0}{f_1}+\frac{1}{2}\left(\frac{f_0}{f_1}\right)^2 \cdot \frac{f_1}{f_0}.$$

Fig. 6.

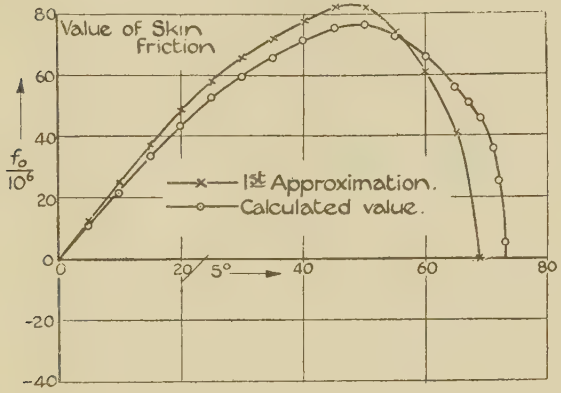

Fig. 7.

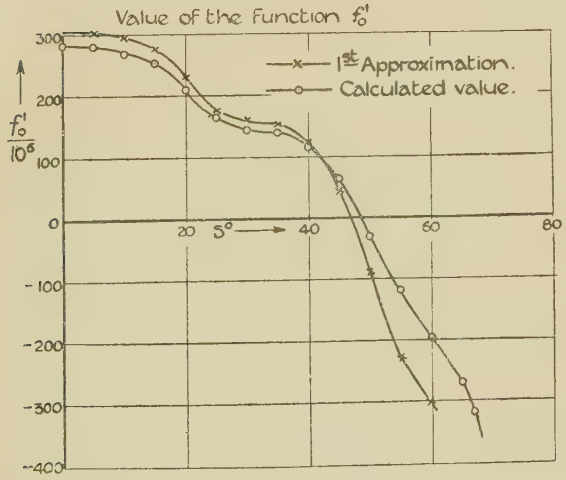

This yields

$$f_0^2 \doteqdot -2f_1 . q\mathrm{R}. \quad . \quad . \quad . \quad . \quad . \quad (24)$$

Knowing f_1 and $\bar{q}\mathrm{R}$, we have a first approximation for f_0.

Values thus calculated are given in Column 3, Table IV., and plotted in fig. 6, and first approximate values of f_0' found by graphical differentiation are plotted in fig. 7.

A second approximate value for f_0' at the 0° position is obtained from equation (24).

We have

$$f_0^2 \doteqdot -2f_1 . \bar{q}\mathrm{R},$$

but at S°=0°,

$$f_0=0 \quad \text{and} \quad \bar{q}\mathrm{R}=0.$$

But by Taylor's theorem

$$f_0 = sf_0' + \frac{s^2}{\lfloor 2} f_0'' \ldots \doteqdot sf_0'.$$

Similarly expanding

$$f_1 \doteqdot sf_1' \quad \text{and} \quad \bar{q}\mathrm{R} \doteqdot s . \frac{\partial}{\partial s}\bar{q}\mathrm{R},$$

we have

$$s^2(f_0')^2 \doteqdot -2s . \overline{f_1' \Big|}_{s=0} . s . \frac{\partial}{\partial \mathrm{S}}\bar{q}\mathrm{R}.$$

$$\therefore \quad (f_0')^2 \doteqdot \left(-2f_1' . \frac{\partial}{\partial s}\bar{q}\mathrm{R}\right)_{s=0} .$$

$(f_1')_{s=0}$ is known, and $\left(\frac{\partial}{\partial s} q\mathrm{R}\right)_{s=0}$ is the slope at $s=0$ of the curve given in fig. 5. It was found that the two approximate values for f_0' agreed fairly closely.

An approximate value for f_0'' at 0° could be found by taking the slope of the f_0' curve at that point, but actually in the work described f_0'' at 0° was found by solving equation (19) for the 5° position, omitting the terms involving f_7 and f_8, and using a method similar to that described below. By this means f_0'' between 0° and 5° was evaluated, and the result was taken as a close approximation to the value of f_0'' at the 0° position.

Method of Procedure.

Having obtained values for the f_0 coefficients at 0°, their values at 5° are deduced by employing Taylor's expansion. Thus

$$(f_0)_{s+ds} = (f_0)_s + ds(f_0')_s + \frac{ds^2}{\lfloor 2}(f_0'')_s + \frac{ds^3}{\lfloor 3}(f_0''')_s, \quad (25)$$

and values of (f_0''') are assumed for the evaluation of f_0, f_0', and f_0'' at the position $s+ds$. These values are then employed as initial values and the process repeated for the

next step round the cylinder. In this manner the f_0 coefficients were determined, and appear tabulated in Table IV. (p. 20), divided by powers of ten for convenience.

Having determined all the f functions, the solution of equation (19) can be effected.

The complete procedure for the 45° position—chosen at random—is included in the paper to indicate the method, and the final results only are given for the other positions.

At 45° the f_1 functions are as indicated in Table V. (p. 24). At 40°, the preceding position, f_0, f_0', and f_0'' are known, and a value for f_0''' between 40° and 45° is guessed. The guess can be arrived at by inspection of the f_0 and f_0' curves, which have been calculated (second approximation) up to this point.

Three different values for f_0''' are taken, covering a range which, it is hoped, will enclose the correct value, and the three corresponding values of f_0, f_0', and of f_0'' are computed for the 45° position. This enables the evaluation of the coefficients $f_0, f_1, f_3, f_4, \ldots f_8$ and their insertion in equation (19), the process being shown in Table V. for the three distinct values of f_0'''. The last line of the table designated (sum + AB) gives the values of $\frac{1}{f_0}\frac{\partial}{\partial n}qR$. This is plotted, as in fig. 8, and the areas of the three curves found by integration. This yields three values for $\frac{1}{f_0}\bar{q}R$ corresponding to the three different values of f_0'''. Table III. (p. 16) gives the value of $\bar{q}R$ at 45°, and hence three values for f_0 can be found by division. The correct value of f_0''' is that one which makes the initial assumed value of f_0 equal to the final value obtained. The usual method adopted was to plot the two values of f_0 against the corresponding value of f_0''', and to find the point of intersection of the two curves (marked "assumed" and "calculated") shown in fig. 8. This gives f_0''' with considerable accuracy.

When plotting the values of $\frac{1}{f_0}\frac{\partial}{\partial n}qR$ for large n values, it was found that the series contained insufficient terms to make the value $\frac{1}{f_0}\frac{\partial}{\partial n}qR$ fall to zero. In view of this fact, large values of n were excluded and the curve was smoothed off to zero by eye in such a manner that when $\frac{\partial}{\partial n}qR$ is zero, $\frac{\partial^2}{\partial n^2}qR$ is also zero.

Table V.

Complete Calculations for the 45° Position.

At $s=40°$ $\frac{f_0}{10^6}=71{\cdot}31$, $\frac{f_0'}{10^6}=117{\cdot}6$, $\frac{f_0''}{10^6}=-518$.

$s=45°$ $\frac{f_1}{10^6}=-28550$, $\frac{f_1'}{10^8}=234$, $\frac{f_1''}{10^{10}}=174$, and $\frac{1}{10^6}qR=0{\cdot}1193$.

$ds=5°=0{\cdot}0436$ diameters.

$$\left(\frac{f_0}{10^6}\right)_{45°}=71{\cdot}31+(0{\cdot}0436)117{\cdot}6+(0{\cdot}0436)^2(-259)+(0{\cdot}0436)^3\frac{k_3}{6}=75{\cdot}95+0{\cdot}0000138\,k_3,$$

$$\left(\frac{f_0'}{10^6}\right)_{45°}=117{\cdot}6-(0{\cdot}0436)518+(0{\cdot}0436)^2\frac{k_3}{2}=95+0{\cdot}00095\,k_3,$$

$$\left(\frac{f_0''}{10^6}\right)_{45°}=-518+0{\cdot}0436\,k_3=-518+0{\cdot}0436\,k_3,$$

where $k_3\equiv{}_{40}\left(\frac{f_0'''}{10^6}\right)_{45}$.

k_3.	$\frac{f_0}{10^6}$.	$\frac{f_0'}{10^6}$.	$\frac{f_0''}{10^8}$	$\frac{f_0'''}{10^6}$.	$\frac{1}{\lfloor 6}\frac{1}{10^{12}}\frac{f_6}{f_0}$.	$\frac{1}{10^2}\frac{f_1}{f_0}$.	$\frac{1}{\lfloor 7}\frac{1}{10^{14}}\frac{f_7}{f_0}$.	$\frac{1}{\lfloor 8}\frac{1}{10^{16}}\frac{f_8}{f_0}$.
0	75·95	95·0	− 518	0	− 231	−3·76	2770	−4960
−30000	75·54	66·5	−1826	−30000	− 773	−3·78	3470	−4960
−60000	75·12	38·0	−3134	−60000	−1307	−3·80	4170	−4960

TABLE V. (*cont.*).

$k_2 \longrightarrow$	0				−30000				−60000			
$a = 100\,n \longrightarrow$	0·1.	0·2.	0·25.	0·3.	0·1.	0·2.	0·25.	0·3.	0·1.	0·2.	0·25.	0·3.
$\frac{a^3}{3}\frac{f_0'}{10^6}$	+0·0158	+0·1263	+0·2470	+0·4275	+0·0110	+0·0985	+0·1730	+0·2990	+0·0063	+0·0505	+0·0988	+0·1710
$\frac{8}{\lfloor 5}\,a^4\frac{f_1'}{10^8}$	+0·00156	+0·0249	+0·0610	+0·1263	+0·00156	+0·0249	+0·0610	+0·1263	+0·00156	+0·0249	+0·0610	+0·1263
$\frac{1}{\lfloor 6}\,\frac{a^6}{10^{12}}\frac{f_6}{f_0}$	−0·0002	−0·0148	−0·0564	−0·1685	−0·0008	−0·0495	−0·1890	−0·5640	−0·0013	−0·0836	−0·3190	−0·9530
$\frac{1}{\lfloor 7}\,\frac{a^7}{10^{14}}\frac{f_7}{f_0}$	+0·0003	+0·0354	+0·1690	+0·6050	+0·0003	+0·0444	+0·2120	+0·7590	+0·0004	+0·0534	+0·2540	+0·9130
$\frac{1}{\lfloor 8}\,\frac{a^8}{10^{16}}\frac{f_8}{f_0}$	0	−0·0127	−0·0755	−0·326	0	−0·0127	−0·0755	−0·326	0	−0·0127	−0·0755	−0·326
Sum	0·0175	0·1590	0·345	——	0·0121	0·1055	0·1815	0·2940	0·0069	0·0325	0·0193	——
$A = \left(1 + \frac{a}{10^2}\frac{f_1}{f_0}\right)$.	0·624	0·248	0·060	−0·128	0·622	0 244	0·055	−0·134	0·620	0·240	0·050	−0·140
$B = \left(1 + \frac{a^4}{\lfloor 5}\,2\,\frac{f_1'}{10^8}\right)$.	1·0004	1·0062	1·0153	1·0316	1·0004	1·0062	1·0153	1·0316	1·0004	1·0062	1·0153	1·0316
(A) (B)	0·6242	0·2493	0·0610	−0·1320	0·6222	0·2453	0·0559	−0·138	0·6202	0·2413	0·0508	−0·144
Sum+(A)(B) ...	0 642	0·408	0·406	——	0·634	0·351	0·237	0·156	0·627	0·274	0·070	——

TABLE V. (*cont.*).

k_3.	0.	-30000.	-60000.
Areas.	0·00191.	0·001605.	0·00138.
$\frac{f_0}{10^6}$	$\frac{0\cdot1193}{0\cdot00191}=62\cdot5$	$\frac{0\cdot1193}{0\cdot001605}=74\cdot35$	$\frac{0\cdot1193}{0\cdot00138}=86\cdot5$

By cross-plotting (fig. 8), the balance-value of $k_3 = {}_{40}\left(\frac{f_0'''}{10^6}\right)_{45} = -33000$.

Hence $\left(\frac{f_0}{10^6}\right)_{45} = 75\cdot4$, $\left(\frac{f_0'}{10^6}\right)_{45} = 63\cdot65$, $\left(\frac{f_0''}{10^6}\right)_{45} = -1957$, ${}_{40}\left(\frac{f_0'''}{10^6}\right)_{45} = -33000$.

Slight variations in the shapes of the curves when near to zero can hardly affect appreciably the areas of the curves. The effect of large variations in the method of smoothing off to zero was examined for the 5° position (see fig. 8 *a*) and

Fig. 8.

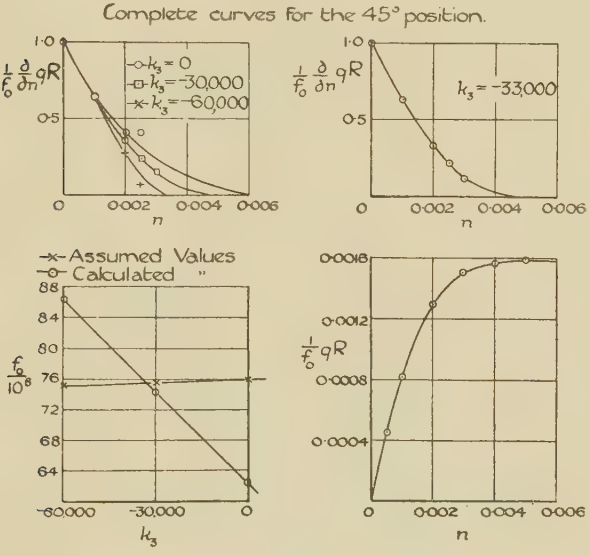

Fig. 8 *a*.

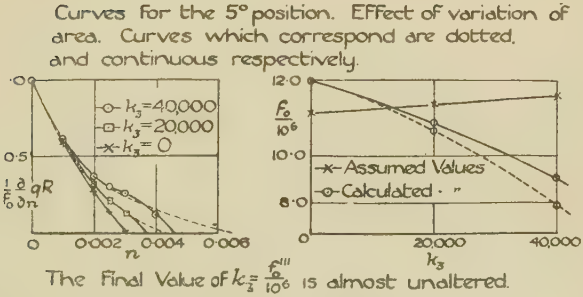

was found to have a very slight influence on the final result for f_0'''.

An inspection of the relative magnitude of the calculated terms in equation (19) will readily reveal the truth as to the sufficiency of terms. Should the value of the term involving f_8 be of the same magnitude as the calculated

value of $\frac{1}{f_0}\frac{\partial}{\partial n}qR$ for that particular value of n, the number of terms is insufficient, and the calculation for this value of n is ignored when smoothing off the curve, and only the calculations for smaller values of n are taken into account.

Having determined the correct value of f_0''', the computation is repeated in each case, the values of $\frac{1}{f_0}\frac{\partial}{\partial n}qR$ plotted, and the integration performed for the production of the velocity distribution curves $\left(\frac{1}{f_0}qR \text{ plotted against } n\right)$, which represent the complete solution of the boundary-layer equations.

The solution presented no difficulty up to the point 67° round the cylinder; at this point the terms involving f_7 and f_8 were large, and approaching in magnitude to the value of $\frac{1}{f_0}\frac{\partial}{\partial n}qR$, and it was obvious that there were insufficient terms in the series to allow the solution to be continued. An extension of the number of terms included would have involved further graphical differentiations, and it is quite likely that the accuracy would be reduced accordingly, it being suggested that the third graphical differentiation was a safe limit to this process.

In fig. 10 the values of qR for various distances from the surface are plotted against distance round the cylinder in degrees.

In order to investigate the position and nature of the break-away, it was desirable to extend the solution for another 5° or 6°.

Before doing this, the solution at 67° was checked. Taking the values of qR at various distances from the surface as given by the solution, and multiplying by $\frac{\partial}{\partial s}qR$ at the corresponding positions (found by graphical differentiation of the curves in fig. 10), the product $qR\frac{\partial}{\partial s}qR$ is obtained.

Re-write equation (14) as

$$\frac{\partial^2}{\partial n^2}qR - wR\frac{\partial}{\partial n}qR = qR\frac{\partial}{\partial s}qR + R^2\frac{\partial p}{\partial s},$$

and then the right-hand side is known, since $R^2\frac{\partial p}{\partial s}$ is known,

for various values of n. Calling this $\mathrm{F}(n)$, we have

$$\frac{\partial}{\partial n}\left(\frac{\partial}{\partial n}q\mathrm{R}\right)-w\mathrm{R}\left(\frac{\partial}{\partial n}q\mathrm{R}\right)=\mathrm{F}(n),$$

and by the equation of continuity

$$-w\mathrm{R}=\int\frac{\partial}{\partial s}q\mathrm{R}\,.\,dn,$$

and is determined by integration.

Hence the equation is reduced to a first-order linear differential equation and the solution is given by

$$\frac{\partial}{\partial n}q\mathrm{R}=\frac{1}{e^{\int -w\mathrm{R}\,dn}}\left\{\int e^{\int -w\mathrm{R}\,dn}\mathrm{F}(n)\,dn+\text{const.}\right\},$$

and the constant is found to be f_0.

The value of $\frac{\partial}{\partial n}q\mathrm{R}$ for various values of n agreed exactly with the initial solution at 67° given in the form $\frac{1}{f_0}\frac{\partial}{\partial n}q\mathrm{R}$ plotted against n, which verified the solution at that point.

Method of Solution after 67°.

Since both $q\mathrm{R}$ and $\frac{\partial}{\partial s}q\mathrm{R}$ are changing rapidly in this neighbourhood, very small steps were taken, two of 2° each, followed by two of 1° each.

The curves for velocity, given in fig. 10, were carefully continued by eye, employing the values of $\frac{\partial}{\partial s}q\mathrm{R}$ to give the correct slope. The extrapolated values of the velocity at the end of the next step, thus obtained, were assumed to give the correct solution of the equations, and by employing them to give the values of $\frac{\partial}{\partial n}q\mathrm{R}$ and $\frac{\partial^2}{\partial n^2}q\mathrm{R}$ the viscous equation (14) could again be reduced to a first-order linear equation which, on solution, gave the values of $\frac{\partial}{\partial s}q\mathrm{R}$ at the point considered. This value was then utilized to extrapolate the velocity curves to the next point, where the process was repeated. In this manner the theoretical solution was examined at 69°, 71°, 72°, and 73° round the cylinder. In

Table VI. the details in full for the 69° position are given, and the final results only for the other positions are added.

Equation (14) can be written

$$qR\frac{\partial}{\partial s}qR-\frac{\partial}{\partial n}qR\int\frac{\partial}{\partial s}qR\,.\,dn=\left(\frac{\partial^2}{\partial n^2}qR-R^2\frac{\partial p}{\partial s}\right).$$

$$\therefore\quad \frac{\partial}{\partial s}qR-\frac{1}{qR}\cdot\frac{\partial}{\partial n}qR\int\frac{\partial}{\partial s}qR\,.\,dn=\frac{1}{qR}\left(\frac{\partial^2}{\partial n^2}qR-R^2\frac{\partial p}{\partial s}\right),$$

TABLE VI.

Details of the Method Employed from 69° to 73°.

$$s=69°,\quad \frac{f_0}{10^6}=45{\cdot}5,\quad \frac{1}{10^6}R^2\frac{\partial p}{\partial s}=1330.$$

n.	0·0.	0·0005.	0·001.	0·002.	0·003.	0·004.
$\frac{1}{10^6}qR$	0	0·0221	0·045	0·0863	0·1155	0·1323
$\frac{1}{10^6}\frac{\partial}{\partial n}qR$	45·5	45·0	43·7	36·0	22·3	10·9
$\frac{1}{10^6}\frac{\partial^2}{\partial n^2}qR$	1330	−1820	−4550	−11130	−13950	−8650
$\frac{1}{10^6}\left(\frac{\partial^2}{\partial n^2}qR-R^2\frac{\partial p}{\partial s}\right)$.	0	−3150	−5880	−12460	−15280	−9980
$f(n)$	0/0	−142500	−130500	−144000	−132300	−75500
$f(n)=\frac{1}{qR}\frac{\partial}{\partial n}qR$	∞	2035	970	417	193	82·5
$\int -f(n)\,dn$	0	−1·385	−2·035	−2·675	−2·960	− 3·080
$e\int -f(n)\,dn$	1	0·250	0·131	0·069	0·052	0·046
$\phi(n)e\int -f(n)\,dn$	0/0	−35625	−17100	−9940	−6870	−3470
$\int\phi(n)e\int -f(n)\,dn\,dn$ ...	0	−24·375	−35·625	−48·125	−56·375	−61·375
$\int\frac{\partial}{\partial s}qR\,dn$	0	−97·5	−272·0	−698·0	−1084·0	−1335·0 → $-wR$
$\frac{1}{10^6}\frac{\partial}{\partial s}qR$	0	——	−0·39	−0·40	−0·312	−0·20

TABLE VI. (*cont.*).

$s = 71°$, $\frac{f_0}{10^6} = 38{\cdot}0$, $\frac{1}{10^6} R^2 \frac{\partial p}{\partial s} = 8450.$

n.	0·0.	0·0005.	0·001.	0·002.	0·003.	0·004.
$\frac{1}{10^6} qR$	0	0·0171	0·036	0·076	0·106	0·125
$\frac{1}{10^6} \frac{\partial}{\partial n} qR$	38·0	39·2	39·9	35·7	23·6	14·4
$\int \frac{\partial}{\partial s} qR\, dn$	0	−306·0	−822·5	−1926	−2910	$-3570 \rightarrow -wR$
$\frac{1}{10^6} \frac{\partial}{\partial s} qR$	0	——	−1·08	−1·07	−0·85	− 0·375

$s = 72°$, $\frac{f_0}{10^6} = 27{\cdot}0$, $\frac{1}{10^6} R^2 \frac{\partial p}{\partial s} = 12230.$

n.	0·0.	0·0005.	0·001.	0·002.	0·003.	0·004.
$\frac{1}{10^6} qR$	0	0·0141	0·029	0·069	0·099	0·121
$\frac{1}{10^6} \frac{\partial}{\partial n} qR$	27·0	28·1	34·6	35·1	25·4	16·75
$\int \frac{\partial}{\partial s} qR\, .\, dn$	0	−279	−728	−1860	−2920	$-3740 \rightarrow -wR$
$\frac{1}{10^6} \frac{\partial}{\partial s} qR$	0	——	−1·00	−1·155	−0·93	− 0·725

$s = 73°$, $\frac{f_0}{10^6} = 5{\cdot}0$, $\frac{1}{10^6} R^2 \frac{\partial p}{\partial s} = 12000.$

n.	0·0.	0·0005.	0·001.	0·0015 0·002.	0·003.	0·004.
$\frac{1}{10^6} qR$	0	0·004	0·015	0·0385 0·0575	0·083	0·103
$\frac{1}{10^6} \frac{\partial}{\partial n} qR$	5·0	15·0	37·0	42·0 31·5	22·5	16·5
$\int \frac{\partial}{\partial s} qR\, .\, dn$	0	2125	23600	68800	100300	$122000 \rightarrow -wR$
$\frac{1}{10^6} \frac{\partial}{\partial s} qR$	0	——	46·4	39·2	27·0	19·8

which can be written as

$$\frac{\partial}{\partial n}\chi_n - f(n)\chi_n = \phi(n),$$

where

$$\chi_n = \int \frac{\partial}{\partial s} q\mathrm{R} \,.\, dn,$$

and $f(n)$ and $\phi(n)$ are known.

The solution of this first-order linear equation is, then,

$$\chi_n = \int \frac{\partial}{\partial s} q\mathrm{R} \,.\, dn = \frac{1}{e^{\int -f(n)\,dn}} \left[\int e^{\int -f(n)\,dn} \phi(n)\, dn + \text{const.} \right],$$

when

$$n = 0, \quad (\chi_n)_{n=0} = 0 = \text{const.}$$

Hence the solution yields the value of

$$-w\mathrm{R} = \int \frac{\partial}{\partial s} q\mathrm{R}\, dn,$$

and by graphical differentiation the value of $\frac{\partial}{\partial s} q\mathrm{R}$ for any particular value of n is determined.

At 73° the solution falls; from 70° the value of f_0 has been falling rapidly, and is of only a small positive magnitude at 73°. At the same time the velocity has been rapidly falling, as indicated by the steepness of the curves in fig. 10 at this position. The value of $\frac{\partial}{\partial s} q\mathrm{R}$ has rapidly grown to a large negative figure, which means that $w\mathrm{R}$ (the value of $\int -\frac{\partial}{\partial s} q\mathrm{R}\, dn$) has reached a large positive value, and has become comparable with the falling value of $q\mathrm{R}$. This violates Prandtl's original assumption. In addition, the value of $\frac{\partial}{\partial s} q\mathrm{R}$ is of the same magnitude as $\frac{\partial}{\partial n} q\mathrm{R}$, which violates another of the Prandtl assumptions.

The fact that the solution at 73° demands a large positive value for $\frac{\partial}{\partial s} q\mathrm{R}$ indicates the sudden change of conditions here, and a failure of the Prandtl equations to account for the flow at this point. For this reason 73° is assumed to be the position where the break-away commences.

Discussion of Results.

A very marked agreement exists between the solution and the observed flow in the boundary layer, and this is claimed to be within the limits of experimental error.

The solution is free from that limitation of range which has characterized other methods, the agreement with experiment being good up to the point of break-away of the boundary layer.

The solution substantiates the gradual increase in boundary-layer thickness indicated by the observations, together with the very sudden increase over the range 69° to 73°.

The mathematical prediction of the break-away commencing at 73° is in accord with photographic records (see Pls. I.–III.) which will be referred to later, and with present ideas regarding the location and cause of break-away.

The Break-away of the Boundary Layer.

The physical interpretation of the cause of transition from laminar to turbulent flow is derived from an examination of the layer conditions.

Fluid particles near the surface have very small velocities, and hence, whilst the pressure along the surface is falling, these particles will continue in the direction of main-stream flow ; but after the point of minimum pressure (69°) the speed of the particles must decrease owing to the reversal in direction of the pressure gradient, and so the fluid just behind the point of minimum pressure will be at rest, and further round the cylinder the tendency is for a back-flow. The effect of this is that the forward flow in the boundary layer is forced to leave the surface, and a sheet of discontinuity is formed which ultimately breaks up into vortices. This is shown very well in Pls. I.–III.

By reference to the pressure-distribution curve it is found that the point of maximum back-pressure gradient is 73°, a reasonable position to assign for the commencement of break-away, and in agreement with the mathematical arguments.

The position of transition from laminar flow to turbulence is therefore indicated by the change in layer-thickness and the sudden fall in skin-friction.

The Boundary Layer Theory.

The results of this solution seem to accord so well with actual facts that the hypothesis of a boundary layer in

which the viscous terms are of the same order of magnitude as the inertia terms seems a very reasonable assumption for deriving the flow pattern close to a circular cylinder.

A rapid examination of the value of the neglected terms in deriving the Prandtl equations in comparison with those retained was made, and the results shown in Table VII. for the range of the solution. It is shown that the neglected terms are almost insignificantly small, except at the break-away position, a justification for the approximations employed.

TABLE VII.

Examination of the Terms neglected in the Derivation of the Prandtl Equations.

	Order of terms.	Order of neglected terms.			
S°.	Retained.	$\left(\frac{\partial a}{\partial s}\right)\frac{\partial q}{\partial n}$.	$q\left(\frac{\partial a}{\partial s}\right)^2$	$\frac{\partial^2 q}{\partial s^2}$.	$wq\,\frac{\partial a}{\partial s}$.
5°	10^{+3}	10^{1}	10^{-1}	10^{+1}	10^{+1}
35°	10^{+4}	10^{2}	10^{-1}	10^{+1}	10^{+2}
67°	10^{+4}	10^{2}	10^{-1}	10^{+1}	10^{+2}
71°	10^{+4}	10^{2}	10^{-1}	10^{+1}	10^{+2}
72°	10^{+4}	10^{2}	10^{-1}	10^{+1}	10^{+2}
73°	10^{+4}	10^{2}	10^{-1}	10^{+3}	10^{+4}

$\frac{\partial a}{\partial s}$ = curvature of surface $= \frac{1}{r}$, where r = radius of cylinder.

$w = -\int \frac{\partial}{\partial s} q \,.\, dn.$

The neglected terms not included in the above Table were assumed to be of even smaller order than those examined.

The rising importance of some of the neglected terms at 73° is indicated, and justifies the rejection of the Prandtl equations at this point.

Other Solutions of the Equations.

The solution for a flat plate, due to Blasius *, in which

* H. Blasius, Thesis Göttingen, 1907 (*Zs. f. Math. u. Phys.* 1908).

the hypothesis is adopted that $\frac{\partial p}{\partial s}$ is small enough to be negligible, was applied to the case of the circular cylinder, and the velocity distribution plotted in figs. 9, 9 *a*, 9 *b*, etc. (this has only been done approximately). The results are

Figs. 9–9 *h*.

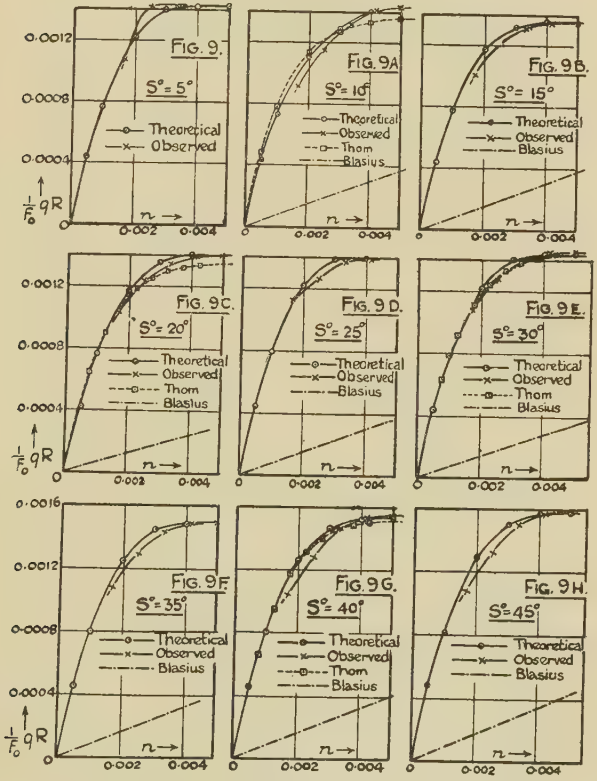

n = Distance from the surface in fractions of 'd' the diameter of the cylinder.

$R = 0{\cdot}943 \times 10^5$ S°= Distance round cylinder in degrees.

sufficient to show that Blasius's solution fails hopelessly when applied to a circular cylinder; this was only to be expected, since the assumption that $\frac{\partial p}{\partial s}$ is negligible is untrue in the case of a circular cylinder where $\frac{\partial p}{\partial s}$ is found to be a large controlling factor.

Dr. Thom * has derived a solution of the boundary-layer equations based on an early assumption that the character of the velocity distribution through the layer is almost independent of the position round the cylinder. His second

Figs. 9 *i*–9 *l*.

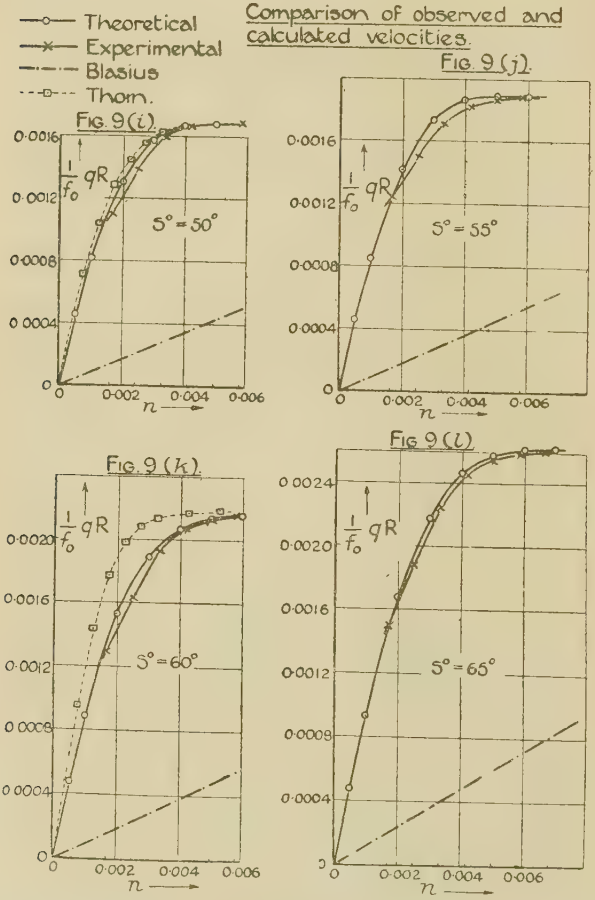

approximation, which makes allowance for errors due to his original assumption, yields velocity curves which are in excellent agreement with observation. These are also shown plotted in figs. 9, 9 *a*, etc.

* R. & M. 1176; also A. Page in R. & M. 1179.

There is a limitation to the range of Thom's solution, which is no longer valid after the velocity gradient $\frac{\partial q}{\partial s}$ has become small or negative; this occurs at about 55° for $R = 0{\cdot}94 \times 10^5$. His solution at 50° is not in as good

Figs. 9 *m*–9 *n*.

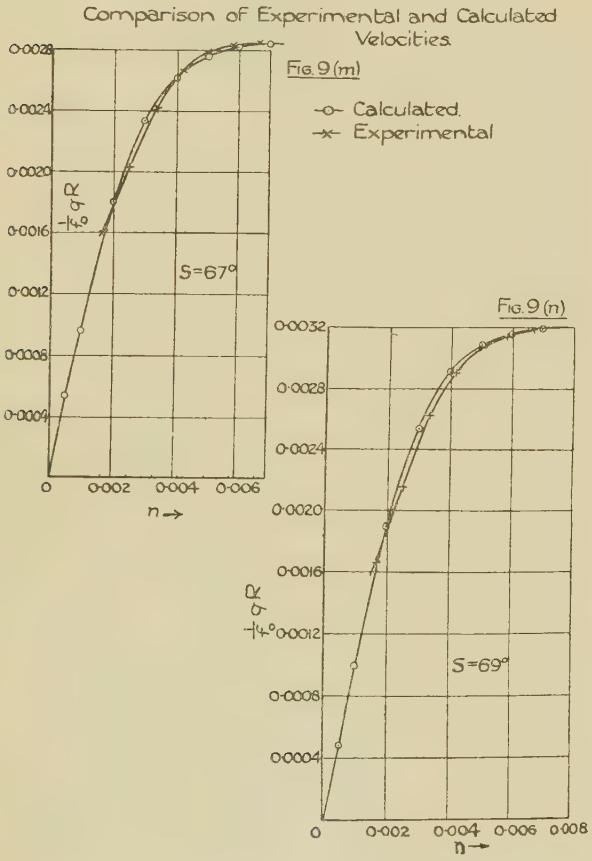

agreement as it was between 0° and 50°, and at 60° the discrepancy is very large.

Conclusion.

A solution of the boundary-layer equations has been developed for the complete range of laminar flow round a

circular cylinder. Considerable success has been achieved with the method, which, it is claimed, is not prohibitively laborious.

It is suggested that in unaltered form it could be profit-

Fig. 9 *o*.

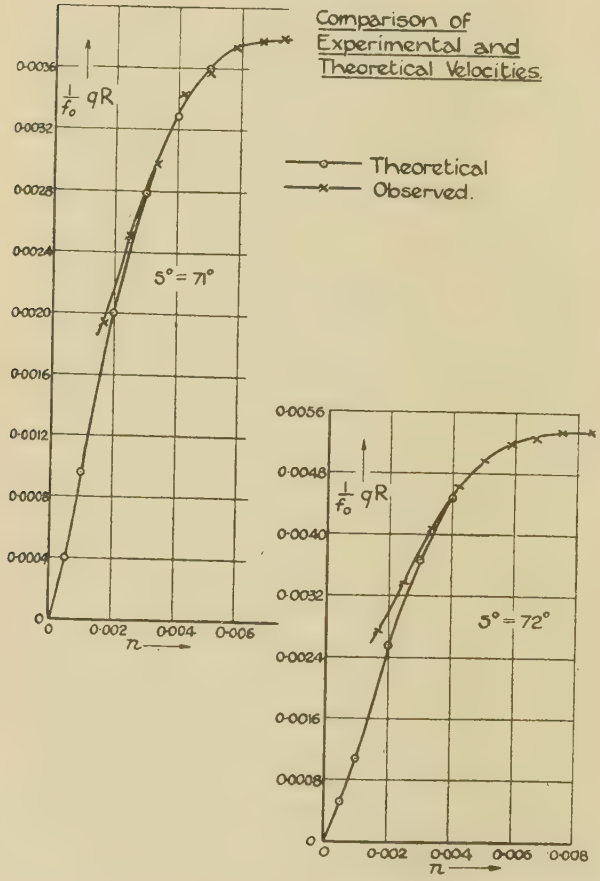

ably applied to the case of an aerofoil, and would probably achieve some fair degree of success.

In some of the readings behind the position of break-away negative values were indicated for the velocity close to the surface, and abrupt discontinuities were discovered in the curves which, it is suggested, might be due to the vortex

sheet which is undoubtedly present in that region (80° to 90°). In view of these possible uncertainties, observations beyond the break-away are not included in the paper. It is suggested that an examination for the existence of back-flow in the range 75° to 90° might be more helpful in indicating the exact conditions behind the transition point, and may

Fig. 10.

Calculated Velocities in the Boundary Layer.

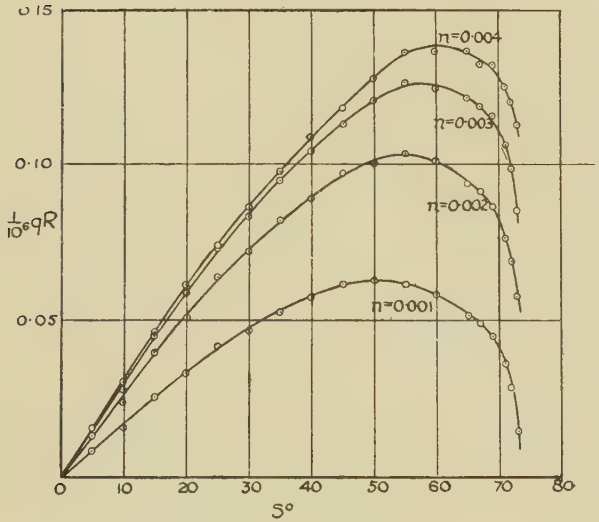

By Graphically Differentiating these curves the value of $\frac{\partial}{\partial s} qR$ was obtained and $w R$ (where w = normal velocity) was evaluated, for each position, by integrating the curve of $-\frac{\partial}{\partial s} qR$ plotted against n for that position under consideration.

It was deemed unnecessary to include these curves in the paper.

suggest other approximations that could be included in the viscous equations to enable further progress to be made.

In conclusion, I wish to acknowledge my indebtedness to Professor Bairstow for his guiding influence throughout the work.

Description of Plates.

PLATE I.

FIG. 1.—This is a photograph of the pitot tube used in the velocity measurements and indicates its attachment to a shaft passing through the surface of the cylinder.

FIG. 2.—In this photograph the pitot tube is shown with the cylinder mounted in position in the wind-tunnel. A sketch is added which indicates the method of measurement.

FIG. 3.—*Investigation of the Break-away.* The object of this photograph was to obtain an initial rough estimate of the location of the break-away. Two pieces of ordinary medical bandage were stuck to the front of the cylinder and their ends allowed to trail out, as shown: one piece was frayed at the ends to obtain a more definite indication of the change in flow. With the wind on, it was found that the bandage violently oscillated in the region of turbulence but was quite still in the laminar region. The photograph indicates the change in flow as taking place between 70° and 80°, agreeing quite well with the mathematical prediction of breakdown in laminar flow: $Vd/\nu = 0{\cdot}943 \times 10^5$.

The remaining photographs were secured with the aid of liquid titanium tetrachloride *. The cylinder was coated with it, and evaporation ensued when the wind was turned on. This yielded dense smoke, which enabled the flow in the neighbourhood of the cylinder to be examined.

Since good definition is only obtained by taking short exposures (1/25 second), the plates suffer somewhat in intensity.

The photographs were taken direct, employing a camera outside the tunnel, and it is suggested that the photographic results might have been better had it been possible to employ the shadow method outlined in the paper by L. F. Simmons and N. S. Dewey (R. & M. 1334).

Sketches are added to indicate the salient features in each plate. Small chalk-marks on the surface of the cylinder were employed to mark the degrees, which are easily elucidated by reference to the sketches.

* R. & M. 1334. Aeronautical Research Committee, L. F. Simmons and N. S. Dewey.

PLATE II.

FIGS. 4 & 5.—These are intended to indicate the laminar flow on the front portion of the cylinder, the formation of a vortex sheet between 70° and 80°, and its final break up into eddies. The wind-speed was of the order of 1 ft./sec., and Reynolds's number then $=3{\cdot}0\times10^3$.

FIG. 6.—Is a closer view of the break-away of the boundary layer and the formation of eddies behind the cylinder: $Vd/\nu=3{\cdot}0\times10^3$.

PLATE III.

FIGS. 7 & 8.—These are close-ups of the break-away, intended to indicate the general nature of the transition. The vortex sheet appears to be tangential to the surface between 70° and 80°; in fact its formation commences here, and for that reason the transition to turbulent flow is taken as originating in this neighbourhood. The suggestion of back-flow near to the final point of break-away is very marked, and the undulating nature of the smoke towards the rear of the cylinder is, perhaps, worthy of notice: $Vd/\nu=3{\cdot}0\times10^3$.

FIG. 9.—This was the result of photographing a cylinder moving in the water-tank at the Royal College of Science. The flow was exhibited by employing suspended milk-particles illuminated by mercury-vapour lamps. The formation of a wide wake after the point where the boundary layer breaks away is evident from this plate: $V\doteqdot1/12$ ft./sec., $d=3$ in., $Vd/\nu\doteqdot1700$.

II. *The Compressibilities of the Permanent Gases.* *By* WILLIAM WILD *.

THE accurate determination of atomic weights by means of the "Limiting Density" method of Berthelot requires accurate knowledge of gaseous compressibilities at pressures below atmospheric. As a measure of the compressibility it is customary to use a coefficient

$$1+\lambda=\frac{p_0v_0}{p_1v_1}$$

* Communicated by Prof. R. Whytlaw-Gray.

at a temperature 0° C., *i. e.*, the ratio of the pressure-volume products of a constant mass of gas pertaining to zero and one atmospheric pressure respectively. It is now possible to determine values of this constant to within 1 part in 10,000, an accuracy that is required to give atomic weights comparable with those obtained by stoichiometric methods.

Moles[1] has examined the existing data for oxygen and nitrogen, and maintains that those determinations alone are of value which have been carried out

(1) At the temperature of melting ice, − 0° C.

(2) Between 0 and 1 atmosphere pressure.

With the first stipulation one cannot disagreee, for there is no satisfactory method of reducing $(1+\lambda)$ values from one temperature to another.

The restriction of the pressure range to beneath one atmosphere is more questionable. Many determinations of the pressure × volume product at 0° C. have been carried out at pressures between 20 and 100 atmospheres. The results are accurately represented by the equation

$$pv = A + B \cdot p + C \cdot p^2,$$

where A, B, and C are constants for a given temperature. From such relations the values of (pv) at 0 and 1 atmosphere and hence that of $(1+\lambda)$ can be found by substitution. Now Moles maintains that the range of extrapolation is too great. In practice the values at high pressures are determined relative to that at one atmosphere, the value of p_1v_1 being taken as unity. In this sense we may regard p_1v_1 as an experimentally determined point on the curve.

A consideration of the existing data for six permanent gases (H_2, N_2, O_2, He, Ne, and A) is illuminating. On the average, the $(B \cdot p)$ term contributes 1 part in 1500 and the $(C \cdot p^2)$ term only 1 part in 500,000 of the total value of (pv) at one atmosphere. To obtain $(1+\lambda)$ values accurate to 1 part in 10,000 we may neglect the $(C \cdot p^2)$ term, and expect to obtain reliable figures if the present values of (B) are correct to within 10 per cent. The values of (B) derived by different observers are in agreement by more than this amount (the same units being used in the comparison). The above statements are in agreement with conclusions, drawn from low pressure measure-

ments, that the isotherms are linear to within 1 part in 20,000.

Since the intermolecular forces operating to cause the observed variations from ideal behaviour are undoubtedly the same in both regions, we might expect the more complicated expressions obtaining in the high pressure region to reproduce the data in the domain of low pressures. The enhanced effect of these forces at high pressures permits more accurate evaluation of the constants of the above equation.

A justification of the arguments advanced has been sought in the existing data. The result of a comparison of $(1+\lambda)$ values derived from high pressure work with those obtained from low pressure experiments is given below for six gases—hyrdogen, nitrogen, oxygen, helium, neon, and argon.

High Pressure Data.

Extensive data have been obtained in this region since 1915, the 0° C. isotherms of the above gases being known with considerable certainty. In all cases the values of (pv) at high pressures have been compared with that at a standard low pressure by direct comparison. The workers at Leiden have expressed their results in an equation,

$$pV = A_v + B_v.\left(\frac{1}{V}\right) + C_v.\left(\frac{1}{V}\right)^2 + D_v.\left(\frac{1}{V}\right)^4, \quad . \quad \text{(Leiden)}$$

where (pV) is taken as unity at atmospheric pressure. The values of the constants A_v, B_v, C_v, etc. were evaluated from the measurements.

Holborn and collaborators [3], of the Reichsanstalt at Berlin, use an expansion in powers of (p),

$$pV = A + B.p + C.p^2 + D.p^4, \quad . \quad \text{(Berlin)}$$

where the pressure unit is the metre of mercury and $(pv)=1$ at this pressure. Verschoyle uses this equation also, but prefers the Leiden units [4].

By using the published constants the present writer has calculated the values of (pv) at zero pressure and at one atmosphere, deducing therefrom the values of $(1+\lambda) = p_0v_0/p_1v_1$ for each of the above gases. When using the Berlin measurements to derive p_1v_1 it is necessary to

substitute $p=0{\cdot}760$ in their equation. The results of the calculation are given below in Table I.

The work of different observers is in excellent agreement, the maximum deviation of the figures for any one gas being less than 1 part in 10,000 in every case.

Table I.

Values of $(1+\lambda)$ at O° C. from high pressure work.

Observer.	H_2.	N_2.	O_2.	He.	Ne.	A.
Onnes [2]	0·99942	1·00041	1·00096	0·99949	0·99959	—*
Holborn & Otto [3]	0·99938	1·00046	1·00098	0·99947	0·99952	1·00098
Verschoyle [4] ..	0·99937	1·00049	—	—	—	—
Mean	0·99939	1·00045	1·00097	0·99948	0·99956	1·00098

* Professor Masson of the University of Durham informs me that Onnes' data on argon are in error, due to "side trapping" of a small amount of gas in one limb of the piezometer, after measurement of its volume at one atmosphere.

Low Pressure Data.

Direct Method.

The accurate determination of the pressure and corresponding volume of a constant mass of gas at a series of pressures between 200 and 800 mm. has long been regarded as the best method of finding $(1+\lambda)$ values. Great care has to be taken to obtain the desired accuracy, since the permanent gases deviate very little from ideal behaviour in this region.

The figures of Leduc and Rayleigh were obtained at room temperatures, and will be discarded for this reason. Those of Jacquerod and Scheuer were obtained with gases of uncertain purity [1]; whilst Burt's data for helium and neon are unsatisfactory, as he only did readings on one filling of gas in each case.

Recent publications from the Geneva Laboratory contain valuable contributions: they relate to a series of measurements on hydrogen [5], two series on oxygen [5, 6], and two series for nitrogen [7, 8]. The method and apparatus employed was unchanged throughout the five series: for this reason, I have combined the two sets

of figures to obtain a final average for both oxygen and nitrogen. The results of these calculations are summarized below :—

Gas.	No. of experiments.	Final average.
H_2	6	0·99935
O_2	12+ 7=19	1·00086
N_2	15+14=29	1·00043

As the gases used were prepared by a variety of methods the results should not contain any constant error due to impurity.

The very beautiful work of Heuse and Otto does not seem to have been considered from this standpoint. They have carried out measurements of the 0° C. isotherms [9, 10] for all the six gases, using the refined technique of Burt and Howarth [11]. Determinations were carried out at certain fixed pressures by the use of a multiple point manometer, the volumes occupied by the gas being found from the weights of mercury withdrawn from the apparatus. Two series of experiments were performed with the whole of the apparatus immersed in melting ice :

(1) A volume of gas was chosen, so that the whole pressure range could be covered (5 or 6 points between 0·3–1·2 metres of mercury).

(2) Larger volumes of gas were used, so that PV values at two adjacent pressures only could be found with any one filling of gas.

It was found for all six gases that PV was a linear function of the pressure. Of 53 points measured in Series I. the greatest deviation from the straight line was 1 in 11,000, and the average deviation between observed and calculated figures only 1 in 30,000. The results were expressed in Berlin units, *i.e.*, $pV=1$ at 0° C. and 1 metre pressure, by the equation

$$pV = A + x_0 \cdot p \qquad (A \text{ and } x_0 \text{ are constants}).$$

Hence $A=(pV)_0/(pV)_{1\text{ metre}}$. Again, at $p=1$ metre $pV=1$, giving $A=1-x_0$. The calculation of $(1+\lambda)$ values from these results does not seem to have been carried out previously. This constant can be derived by use of the equation

$$(1+\lambda) = \frac{(pv)_0}{(pv)_{1\text{ atm.}}} = \frac{A}{A + x_0 \times (0{\cdot}760)} \quad \text{and} \quad A = 1 - x_0.$$

Using this equation, I have carried out the necessary computations. The results are given below, together with Heuse and Otto's values for (x_0):

Gas.	$x_0 . 10^5$.			No. of Expts.	$(1+\lambda)$.
	Series I.	Series II.	Mean.		
He	+ 70	+ 68	+ 69	6	0·99948
H_2.....	+ 74	+ 79	+ 76	7	0·99942
N_2	− 63	− 63	− 63	5	1·00048
O_2	−124	−132	−128	4	1·00097
Ne.....	+ 59	+ 64	+ 62	3	0·99953
A.....	−124	—	−124	1	1·00094

This is probably the finest work done in the field.

Table II. summarizes all the reliable determinations carried out at low pressures.

TABLE II.

$(1+\lambda)$ values at 0° C.; low pressure data.

Observer.	H_2.	N_2.	O_2.	He.	Ne.	A.
Chappuis ..	0·99942	1·00043	—	—	—	—
Gray & Burt.	—	—	1·00097	—	—	—
Geneva	0·99935	1·00043	1·00086	—	—	—
Heuse & Otto	0·99942	1·00048	1·00097	0·99948	0·99953	1·00094
Mean	0·99940	1·00045	1·00093	0·99948	·099953	1·00094

Here again there is close agreement between the work of different observers.

The Indirect Density Method.

There is another method, which can be carried out at low pressures. This is due to Guye [12], and is best suited for gases of high molecular weight. The very refined density determinations of Baxter and Starkweather [13, 14] have rendered possible its extension to some of the permanent gases.

It depends on an accurate knowledge of the densities of a gas at 0° C. and 760 mm. pressure (the normal density)

and at several lower pressures. If, then, the value of PV at 1 atmosphere is put equal to unity, the value of PV at any other pressure (p) is given by

$$(\mathrm{PV}) = \mathrm{P\ (in\ atmos.)} \times \frac{\text{normal density}}{\text{density at ``P'' atmos.}}.$$

Baxter and Starkweather carried out density determinations at several pressures (including 1 atm.), and derived the PV values as above. These were plotted against pressure, an isotherm linear to more than 1 in 10,000 being obtained in each case, the slope of which was evaluated by the "method of least squares." The values of PV at zero and one atmosphere pressure were found, and that of $(1+\lambda)$ computed.

Their experiments on oxygen, nitrogen, neon, and argon gave the values quoted in Table III. Baxter's work is unique. As the density of gas is very sensitive to impurity, the accuracy of this method is perhaps somewhat lower than that of the direct method.

TABLE III.

N_2.	O_2.	Ne.	A.
1·00040	1·000927	0·99941	1·00107

DISCUSSION.

TABLE IV.

Comparison of the mean values of $(1+\lambda)$.

Method.	H_2.	N_2.	O_2.	He.	Ne.	A.
High pressure..	0·99939	1·00045	1·00097	0·99948	0·99956	1·00098
Low pressure ..	0·99940	1·00045	1·00093	0·99948	0·99953	1·00094
Density.....	—	1·00040	1·00093	—	0·99941	1·00107
Final Mean..	0·99939	1·00044	1·00094	0·99948	0·99951	1·00099

The mean values of $(1+\lambda)$ from Tables I., II., and III. are collected together in Table IV. The agreement between the different sets of figures is striking. In particular the values from high pressure work agree in all cases

with those from low pressure measurements to within 1 part in 20,000. Moreover, as reference to Tables I. and II. indicates, the former data are as consistent amongst themselves as are the latter. We may then conclude that it is justifiable to include values of $(1+\lambda)$ deduced from high pressure experiments in any calculation of the most probable values of this coefficient. The values obtained in this way are now so accurate that their exclusion (considered necessary by Guye and Moles) seems unjustified. In this connexion it is interesting to compare the data of the Reichsanstalt, Berlin; for Heuse and Otto state that the gases used for both sets of measurements were prepared by identical methods.

TABLE V.

Data of the Reichsanstalt, Berlin (Holborn, Heuse, & Otto).

Method.	H_2.	N_2.	O_2.	He.	Ne.	A.
Low pressure..	0·99942	1·00048	1·00097	0·99948	0·99953	1·00094
High pressure..	0·99938	1·00046	1·00098	0·99947	0·99952	1·00098
$\Delta \times 10^5$	—4	—2	+1	—1	—1	+4

The correspondence of the two series is satisfying evidence of the reliability of the high pressure method.

The density method gives a value for neon 1 in 10,000 lower and for argon 1 in 10,000 higher than those obtained by other methods. Reference to the original publications shows that the readings from which they were obtained are very consistent. Taking this in conjunction with close agreement found in the cases of oxygen and nitrogen with the results from other sources, it seems reasonable to conclude that the deviations are not due to any inherent defect in the density method.

Accordingly, in deriving the "final means" of Table IV., an average was taken of all the data contained in Tables I., II., and III., giving equal weight to every value quoted irrespective of the method of determination. These mean values of $(1+\lambda)$ may be regarded as the best available at the present time. It is very difficult to arrive at any estimate of the probable errors of a single determination

in the case of high pressure work. The probable errors of the mean values, given below, were obtained by regarding all the individual values as equally reliable, and thus using the familiar formula

$$\text{Probable error} = 0{\cdot}6745 \,.\, \left(\frac{\Sigma\Delta^2}{n(n-1)}\right)^{\frac{1}{2}}.$$

The results of this survey are summarised below.

Gas.	$(1+\lambda)$ from Table IV.
H_2	$0{\cdot}99939 \pm 0{\cdot}00001$
N_2	$1{\cdot}00044 \pm 0{\cdot}00001$
O_2	$1{\cdot}00094 \pm 0{\cdot}000013$
He	$0{\cdot}99948 \pm 0{\cdot}000005$
Ne	$0{\cdot}99951 \pm 0{\cdot}000025$
A	$1{\cdot}00099 \pm 0{\cdot}000026$

I wish to thank Professor Whytlaw-Gray, F.R.S., for suggesting this survey and for his interest in its progress. My thanks are also due to Professor Masson of Durham for helpful suggestions. The work was carried out whilst the author was in receipt of a maintenance grant from the Department of Scientific and Industrial Research, for which aid the writer wishes to express his appreciation.

References.

(1) Moles, *Zeit. für Anorg. Chem.* clxvii. p. 40 (1927).
(2) Onnes and collaborators, many papers in *Comm. Phys. Lab.* at Leiden; see also Landolt-Börnstein Tabellen.
(3) Holborn and Otto, *Zeit. für Physik*, xxxiii. p. 1 (1925).
(4) Verschoyle, Proc. Roy. Soc. A, cxi. p. 552 (1926).
(5) Guye and Batuecas, *J. Chim. Phys.* xx. p. 308 (1923).
(6) Batuecas, Maverick, and Schlatter, *J. Chim. Phys.* xxii. p. 131 (1925).
(7) Batuecas, Maverick, and Schlatter, *J. Chim. Phys.* xxvi. p. 548 (1929).
(8) Maverick, *J. Chim. Phys.* xxvii. p. 36 (1930).
(9) Heuse and Otto, *Ann. der Physik*, Band 2, viii. Heft, p. 1012 (1929).
(10) Heuse and Otto, *Ann. der Physik*, Band 4, vi. Heft, p. 778 (1930).
(11) Burt and Howarth, Trans. Farad. Soc. xx. p. 544 (1924).
(12) Guye, *J. Chim. Phys.* xvii. p. 141 (1919).
(13) Baxter and Starkweather, Proc. Nat. Acad. Sci. xiv. p. 57 (1928).
(14) Baxter and Starkweather, Proc. Nat. Acad. Sci. xv. p. 441 (1929).

Department of Inorganic Chemistry,
University of Leeds.
November 14th, 1930.

III.—*On the Molecular Spectra of Mercury, Zinc, Cadmium, Magnesium, and Thallium.* *By* H. Hamada. (*From the Laboratory of Physics, Sendai, Japan* *.)

[Plates IV. & V.]

Introduction.

A NUMBER of papers have recently appeared on the spectral excitation of diatomic mercury molecules, and the energy states of these molecules, which emit the band and the continuous spectrum, have been brought out fairly clearly. To obtain a more general conception of the energy states of such a loosely bound molecule as mercury it is desirable to extend the investigation to other metallic vapours. In order to investigate the emission spectrum of molecules which have a small amount of dissociation energy it is necessary to devise an apparatus capable of concentrating excited molecules in a suitable quantity. One of the devices adopted for this purpose is the hollow cathode designed by Schüler †. By his special investigation it was found that the atoms at the slit of the cathode are mainly in excited states of the lower energies in large concentration in addition to the normal state. It is to be expected, therefore, that the molecular spectrum will be excited with a sufficient intensity at the slit of the hollow cathode when the density of metallic vapour is suitably high.

The hollow cathode used in this experiment is a closed iron tube 6 cm. in length and 2 cm. in diameter. An iron cover, the thickness of which varied from 5 to 10 mm., and having a small aperture 2 or 3 mm. in diameter in it, is screwed to one end of the tube. For heating purposes a nichrome wire was coiled on a sheet of mica wound closely round the tube. The gas occluded in this cathode system was pumped out during the long duration of heating, first without inserting the metal in the cathode and by keeping it at a temperature of about 1000° C. for ten hours, by which time the mica changes to a white and hard substance. Next, metal is inserted in the hollow space of the cathode, and heated again for a long time at a moderate temperature. The anode is a double-

* Communicated by Prof. J. Okubo.

† H. Schüler, *Zs. f. Phys.* xxxv. p. 323 (1926).

walled cylinder of copper, and is always cooled by circulating water in the intervening space.

The discharging current was supplied from a D.C. generator of 3500 volts. The potential difference between the two electrodes falls below 100 volts as soon as the metallic vapour glows intensely at the small aperture of the cathode, and the current density was varied from 30 to 100 milliamp. The favourable condition for the excitation of the molecular spectrum is that of a comparatively low voltage and weak current, but there are, of course, some limitations to these values, for the less stable the glow

Fig. 1.

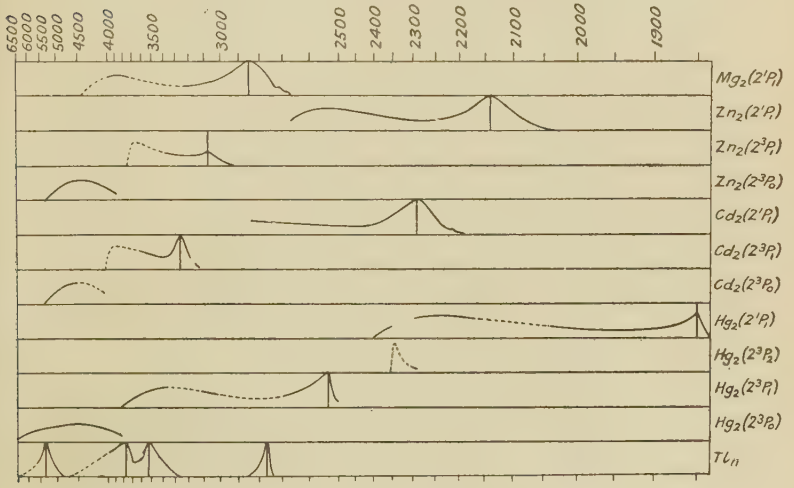

becomes the lower is the voltage and the weaker is the current applied. The spectrograms were taken by using three types of quartz spectrographs, Hilger E 1, E 2, and E 31. The metals studied in this experiment were mercury, cadmium, zinc, calcium, magnesium, and thallium.

Experimental Results.

1. *Mercury.*

(*a*) The continuous spectrum having a maximum intensity at the resonance line λ 1849 Å ($1^1S_0 - 2^1P_1$) seems to extend to a region of shorter wave-length than 1837, where it fades away owing to the strong absorption

(fig. 1). The intensity of this continuous spectrum on the longer wave-length side decreases gradually as the wave-length increases, and reaches a minimum at about 1950. Then, after increasing again to a maximum at about 2260, it decreases gradually to about 2400. Wood's band series at about 2346 is superimposed on this spectrum, and

Table I.

λ.	ν.	Δν.	λ.	ν.	Δν.
2167	46142	227	2094	47733	148
2156	46369	203	2088	47881	154
2147	46572	214	2081	48035	162
2137	46786	213	2074	48197	161
2127	46999	182	2067	48358	146
2119	47181	192	2061	48504	146
2110	47373	183	2055?	48650	138
2102	47556	177	2049	48788	126
			2044	48914	

Fig. 2.

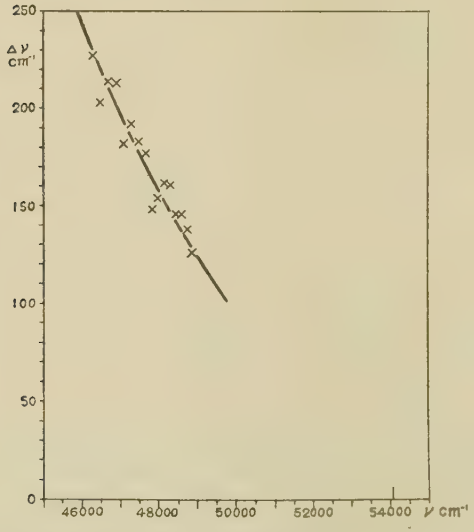

also, as it is masked by well-developed lines of higher terms in the region of a wave-length longer than 2170, the structure of this " band system " can only be observed in the region 2167–2044. The annexed table (Table I.) contains the wave-lengths corresponding to the intensity maxima of these diffused bands, and it is certain that the convergence point of these flutings falls nearly at the resonance line 1849 (fig. 2). For reasons explained later

it will be confirmed that the so-called Steubing's band series to which these bands belong is emitted by Hg_2 molecules in consequences of transitions from the 2^1P_1 level to the normal level, in agreement with the theoretical conclusion of H. Kuhn.

(*b*) The shorter wave-length side of another remarkable continuous spectrum having a maximum intensity at 2537 ($1^1S_0-2^3P_1$) extends to about 2500, but as it was masked by the band system 2513–2450 it was impossible to trace it further. On the longer wave-length side this continuous spectrum has a minimum at about 2770 and a second maximum at 3370, and it was possible to trace it, especially under the circumstance that the continuous band about 4850 appears very faint, up to the region at about 3820 (fig. 1). The wave-lengths corresponding to the maxima of intensity of the coarse structure of this spectrum in the region between 3009 and 2703, coincide quite well with those already found by Lord Rayleigh * in the absorption, but not with those in the emission. The convergence limit of these coarse structure bands falls at a position a little shorter than the resonance line*, and it will be concluded that the band system is emitted as consequences of transitions to the normal state from various vibrational levels of the excited 2^3P_1 state. On observing the spectrum with a spectrograph of greater dispersion a series of narrow bands having nearly equal differences of frequency 49 cm.$^{-1}$ in the region between 3341–3132 in the continuous band about 3300 was found (Table II.), and the intensity of the series varies periodically with each set of five bands (Pl. IV., *c*). This period is very near the value 230 cm.$^{-1}$, which is the extrapolated value of the frequency difference of Lord Rayleigh's bands towards the longer wave-length side, and therefore it may be considered that these bands are longer wave members of Rayleigh's bands in addition to the finer structure due to the vibrations in the normal state.

It may be remarked here that a well-known narrow band 2540 of unknown origin appears also beyond the resonance line.

(*c*) The convergence limit of the fluted bands at 2346 (Table III.) is estimated nearly at the forbidden line 2270.

* Lord Rayleigh, Proc. Roy. Soc. cxvi. p. 702 (1927).

and this band system is closely connected with the 2^3P_2 state of the molecule.

(*d*) The continuous spectrum about 4850 seems to be very intense in the circumstances under which atoms or molecules in the 2^3P_0 state are concentrated, and, for this and other reasons, it is probable that this spectrum is closely connected with the 2^3P_0 molecular state. It is

Table II.

λ.	ν.	Δν.	λ.	ν.	Δν.
3336·7	29961	47	3251·9	30743	49
3331·4	30008	54	3246·7	30792	48
3325·5	30062	49	3241·6	30840	51
3320·0	30111	55	3236·3	30891	46
3314·0	30166	48	3231·5	30937	45
3308·8	30214	51	3226·8	30982	50
3303·2	30265	46	3221·6	31032	48
3298·2	30311	50	3216·6	31080	51
3292·8	30361	52	3211·3	31131	51
3287·2	30413	44	3206·1	31182	
3282·4	30457	50			
3277·0	30507	46			
3272·1	30553	47	3162·4	31613	51
3267·1	30600	49	3157·3	31664	50
3261·8	30649	48	3152·3	31714	46
3256·7	30697	46	3147·7	31760	50
			3142·8	31810	

Table III.

λ.	ν.	Δν.
2345·5	42622	126
2338·6	42748	88
2333·8	42836	88
2329·0	42924	85
2324·4	43009	67
2320·8	43076	52
3218·0	43128	54
2315·1?	43182	54
2312·2	43236	52
2309·4	43288	

to be regretted that the maximum at 2650 was so feeble as to make it impossible to detect it in the conditions of this experiment.

(*e*) Another remarkable band system appears in the region between 2450 and 2513 (Pl. V., *f*). In this system the bands of shorter wave-length than 2496 are shaded towards the longer wave-length side and have their heads at 2450, 2457, 2463 ?, 2470, 2476, 2483 ?, 2489, and 2496, while in a part of the longer wave there are observed only

two maxima of intensity, at 2504 and 2513, without showing any sharp head. This system is considered to be emitted probably from Hg_3 molecules in the 2^3P_1 state.

Beside the continuous and band spectrum described above, another band system was observed in the region between 3948 and 3822 which has already been described by J. Stark. But it was difficult to confirm whether this was due to any kind of mercury molecule or to some impurity.

2. *Cadmium.*

(*a*) The continuous spectrum having the maximum intensity at the resonance line 2289 ($1^1S_0-2^1P_1$) extends to about 2191, passing over and beyond the continuous band at 2214. On the longer wave-length side of this spectrum there is a minimum of intensity at about 2450, and then the intensity increases gradually up to the region at 2850. Beyond that region the intensity was modified by the superimposition of the band system at 3015–2895. Mohler and Moore's absorption flutings "Cd II." which are believed to be either the band system $1^1S_0-2^1P_1$ of Cd_2 or the spectrum of an impurity, could not be observed in this experiment owing to the crowding of many atomic lines.

(*b*) Another continuous spectrum having a maximum intensity at the resonance line 3261 ($1^1S_0-2^3P_1$) seemed to extend beyond the region at 3178, where it was covered by a continuous band (Pl. IV., *b*). The longer wave-length part of this continuous spectrum has a minimum at about 3370 and the second maximum at 3939, and it terminates suddenly at the 4044 band. In the region between 4044 and 3664 was found a system of bands having a coarse structure. The longer three ($n'=0$, 1, 2) of them possess finer structures, while the others show only maxima of intensity in a diffused nature (Table IV.). The convergence limit of these coarser bands falls probably near the resonance line 3261, though the band series does not appear long enough to confirm this. For the reason subsequently mentioned it is considered that this coarser structure belongs to the vibrational states of 2^3P_1, while the finer structure is due to the normal state of the Cd_2 molecules.

A band of a diffused nature appears in the region

3186–3148 (maximum 3178), the origin of which could not be determined.

(*c*) A spectrum corresponding to the green fluorescence radiation of mercury is emitted in the region between 5400 and 4058 (Pl. IV., *b*). By studying the distribution of intensity of this band system it was ascertained that there is a maximum at about 4530 and that the intensity on the longer wave-length side of it decreases rapidly,

Table IV.

λ.	ν.	Δν.	Δν.
4044	24722	92	
4029	24814	105	
4012	24919	100	
3996	25019		(462)
3966	25208	83	
3953	25291	90	
3939	25381	90	
3925	25471	144?	
3903?	25615		(479)
3879	25773	87	
3866	25860	107	
3850	25967	95	
3836	26062		(359)
3813	26219		236
3779	26455		233
3746	26688		230
3714	26918		190
3688	27108		177
3664	27285		

Table V.

λ.	ν.	Δν.	λ.	ν.	Δν.
4463	22401	122	4319	23148	124
4439	22523	117	4296	23272	114
4416 ?	22640	123	4275	23386	121
4392	22763	120	4253	23507	122
4369	22883	137	4231	23629	118
4343	23020	128	4210	23747	

and on the shorter wave side gradually, until it is superimposed on the 2^3P_1 band system with very feeble intensity. Another characteristic of this system is that it possesses a distinct structure consisting of twelve bands in the region between 4463 and 4210 (Table V.). The band system is perhaps emitted from the 2^3P_0 state of the Cd_2 molecules, and the distinct structure is due to various vibrational levels of the normal state.

(*d*) A continuous band, without showing any structure and extending into the region between 2136 and 2112, possesses a maximum at 2124.

Another remarkable band system was observed in the region between 3015 and 2895 on the shorter wave-length side of the resonance line $1^1S_0-2^3P_1$ (Pl. V., *e*). Each of these bands was shaded towards the red and their heads were at 2895, 2903, 2913, 2924, 2934, 2945, 2956, and the remaining ones showed no definite heads but maxima of intensity at 2969, 2981?, 2993, 3004, and 3015. From the analogous band systems in the cases of mercury and zinc it is probably emitted from the Cd_3.

It may here be remarked that a system of narrow bands exist having intensity maxima at 3379, 3362, 3344, 3310, and 3293, but it is not clear whether this system is due to any cadmium molecule or to traces of impurity contained in the metal.

3. *Zinc.*

(*a*) The continuous spectrum having a maximum of intensity at the resonance line 2139 ($1^1S_0-2^1P_1$) is observable up to the region at about 2035. The longer wave-length branch of this spectrum possesses, analogous to the cases of mercury and cadmium, a minimum and the second maximum of intensity at about 2300 and 2550, and it could be traced up to the region of about 2670, where it is masked by the band system 2826–2679. The series of fluted bands * observed by Mohler and Moore ("Zn I") seems to be a part of the 2^1P_1 band system of Zn_2 as conjectured by them, or else it is due to impurity; but to my regret it was impossible to observe any structure of this continuous spectrum, on account of the development of many atomic lines. The band at 2064 was too faint to be observed.

(*b*) The band system possessing a maximum of intensity at resonance line 3076 ($1^1S_0-2^3P_1$) extends up to about 2936 on its shorter wave-length side. On the longer wave-length part of this system the second maximum was found at 3688, and it faded away suddenly at 3763 (fig. 1). The coarse structure of this system was observed in the region between 3575 and 3411 (Table VI.), and its convergence limit falls probably nearly on the

* S. Mrozowski, *Zs. f. Phys.* lxii. p. 314 (1930).

resonance line 3076 ; this system is probably due to the 2^3P_1 state of the Zn_2 molcules. In this system other narrow bands possessing the maximum of intensity at 3749, 3727, 3706, and 3688 are observed, and these may be considered as the finer structure due to vibrational levels of the ground state, but this is not certain.

A diffuse band having a maximum intensity at 3052 is a similar one to the band at 3178 in cadmium. In the region between 3893 and 3776 another continuous band of unknown origin appeared with a maximum of intensity at 3787.

(*c*) A continuous spectrum extends widely in the region between about 5350 and 3890. The maximum of this was measured to be at about 4450, and it was very hard to determine the distribution of intensity on the shorter wave side, as the continuous band at 3787 masked it.

Table VI.

λ.	ν.	Δν.
3575?	27964	421
3522	28385	318
3483	28703	241
3454	28944	194
3431	29138	170
3411	29308	

Though this spectrum does not show any structure, it will be considered, from similar spectra in the cases of mercury and cadmium, that this is perhaps emitted from the 2^3P_0 state of excitation of the Zn_2 molecules.

(*d*) It must be remarked here that another new system of bands was found in this investigation. This is situated on the shorter wave-length side of the resonance line $1^1S_0-2^3P_1$ and covers the region between 2826 and 2679 (Pl. V., *d*). In a part of the shorter wave-length of this system there is a series of bands shaded towards the longer wave-length and having sharp heads at 2679, 2689, 2702, 2714?, 2726, and 2739, while maxima of intensity at 2753?, 2766?, 2781, 2795, 2810, and 2826 are observed without showing sharp heads in the part where the wave-length is longer. The relative intensity of this and the Zn_2 band systems described above varies with conditions of experiment, and it was ascertained that the emission of this band system is intense at conditions of higher density of vapour, as in the cases of the mercury

2513–2450 band system and the cadmium 3015–2895 band system, and the emission centres of this system are probably the Zn_3 molecules.

Three bands, with maxima of intensity at 3134, 3113, and 3097, and shaded towards the red, are probably those corresponding to that in 3379–3293 in the case of cadmium.

4. *Calcium.*

Calcium also emits a continuous spectrum accompanying the resonance line 4227 ($1^1S_0-2^1P_1$). It extends in the region between 5100 and 3980. Owing to the many atomic lines and the bands due to calcium oxide it was impossible to trace it further beyond these positions of wave-lengths, but it is conjectured that the band series due to the 2^1P_1 state may be observable in the red or infra-red regions.

TABLE VII.

λ.	ν.	Δν.	λ.	ν.	Δν.
3681	27159	420	3418	29248	259
3625	27579	370	3388	29507	255
3577	27949	348	3359	29762	(220)
3533	28297	340	3334?	(29982)	(220)
3491	28637	298	3310	30202	212
3455	28935	313	3287	30414	204
			3265	30618	

5. *Magnesium.*

(*a*) The continuous spectrum about the resonance line 2852 ($1^1S_0-2^1P_1$) of this metallic vapour broadens also very widely in the conditions of this experiment. The diminution of intensity on the shorter wave-length side of this spectrum is comparatively slow up to 2669, where it terminates, while on the longer wave-length side there was found a minimum at 3300 and the second maximum at 3880, beyond which point the spectrum gradually decreases in intensity up to the 4412 band, where the band system suddenly breaks off (Pl. IV., *a*). In the region between 3681 and 3265 it shows a coarse structure with maxima of intensity at positions given in the above table (Table VII.), and the convergence limit of these fluted bands falls near the resonance line 2852 (fig. 3); it is certain that this system is emitted from the 2^1P_1 state of the Mg_2 molecules. A finer structure, possessing

the maxima of intensity at 4412, ——, ——, 4251, 4203, 4156, 4112, and 4068 is probably caused by various vibration levels of the normal state. A continuous band with a maximum of intensity at 2681 was recorded in the plate, but it was not possible to say whether this belongs to this system or not.

(*b*) The continuous spectrum about the resonance line $1^1S_0-2^3P_1$ does not appear. Two bands with maxima of intensity at 4662 and 4608 respectively were observed on the longer wave-length side of this resonance line, and

Fig. 3.

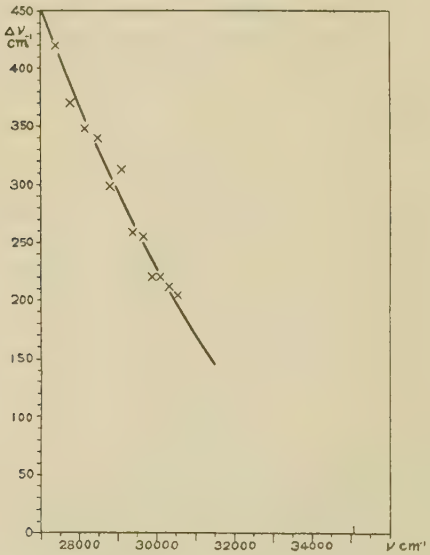

these bands shaded off towards the red. Another narrow band was also recorded at 2713.

6. *Thallium.*

(*a*) Thallium emits a spectrum of quite a different character from those of the five metallic vapours previously described.

An unsymmetrical " band " with a maximum intensity at about 3776 covers the region between 4635 and 3680 (Pl. V., *g*). The interesting characteristic of this band

system is that there was found a sharp edge at 3770·7; beyond there the intensity diminishes very rapidly up to about 3680, while several bands having maximum intensities at positions 4635 (weak), 4405 (medium), 4308 (w.), 4237 (m.), 4187 (strong), 4133 (w.), 4071 (s.), and 4004 (s.) were observed on the continuous background, which is always increasing towards the 3776 line, and on the shorter wave-length side of the 4004 band the structure disappears and only the traces of feeble maxima at 3923, 3857, and 3800 on the continuous spectrum could be observed. Each band is broad and diffuse, but seems to be rather shaded towards the shorter wave-length. It will be conjectured, from the appearances of the band system above mentioned, that the molecules emitting these bands of shorter wave-lengths than 4004 are in an unstable state. Mixing helium (1–2 cm. Hg) with the vapour the edge at 3770·7 together with the band structure as above described does not appear, and there only remains an intense continuous spectrum in the region between 3816 and 3708 (Pl. V., *h*).

(*b*) Another unsymmetrical "band" at the line 2768 was observed. The shorter wave-length end was measured to be at about 2740, while the longer wave-length side seems to extend over the region at about 2850, where it meets with the shorter wave-length branch of the band at 2922–2918. This system has a sharp edge at 2766·3 similar to that of the system at 3776, but no structure was observed.

(*c*) A symmetrical "band" covering the region between about 6500 and 4900 appears in connexion with the line 5350. On the longer wave-length branch there was observed four diffused bands, and the wave-lengths corresponding to maxima of intensity were measured to be at about 6042, 5758, 5621, and 5548. Another symmetrical band about the lines 3529–19 is extended in the region longer than 3260, and the end of the longer wave-length meets the shorter end of the system at 3776. There was found a weak maximum at 3600.

(*d*) Under conditions of higher vapour density the lines 3230, 3092, and 2922–18 are also broadened and the continuous spectrum of molecular origin almost covers the visible and the ultra-violet region up to 2768. Some maxima of intensity at 3446, 3156, and 3050 on the continuous background were found.

Discussion of the Results.

The photometric measurement of the photographic records obtained are summarized in fig. 1, in which the intensity of a continuous spectrum is denoted by a full line, and that of the region with some structure by a dotted line. It was very hard to measure the intensity of the region in which another system of bands is superimposed on it, and it remains blank. From the results obtained in this experiment it may be generally stated that a "band system" emitted from diatomic molecules of mercury, cadmium, zinc, and magnesium vapours has two broad maxima and one flat minimum of intensity. One of these maxima always coincides with the resonance line $1^1S_0-2^1P_1$ or $1^1S_0-2^3P_{0,1,2}$ and the other lies at the region of longer wave-length than this resonance line. In the region about this second maximum there

Fig. 4.

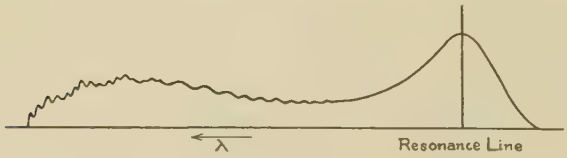

was found a generally coarse structure, each band occasionally accompanying some finer structure, while no bands were observed in the region near the resonance line. The intensity of the shorter wave-length side from the resonance line gradually decreases and terminates rather suddenly at a certain position, and that of the longer wave-length side from the second maximum decreases also gradually to a certain point at where the band system suddenly fades. The distribution of intensity as a whole of this spectrum is to be represented as given in fig. 4. Next will be given here some theoretical interpretation and discussions of the results obtained in the light of recent considerations put forward by M. Born, J. Franck, E. U. Condon, J. G. Winans, and H. Kuhn*.

* M. Born and J. Franck, *Zs. f. Phys.* xxxi. p. 411 (1925); J. Franck, Trans. Faraday Soc. xxi. p. 536 (1925-26); E. U. Condon, Phys. Rev. xxxii. p. 858 (1928); J. G. Winans, Phil. Mag. vii. p. 555 (1929); H. Kuhn, *Naturwiss.* xvi. p. 352 (1928); H. Kuhn, *Zs. f. Phys.* lxiii. p. 458 (1930).

It is generally accepted that the normal molecule in these metallic vapours is a diatomic one loosely combined by the polarization force, while when in an excited state it is a little more firmly combined by the interaction of the normal and the excited atoms. And as the energy of dissociation of the molecule in the normal or excited state is here believed to be much smaller than that of the excitation of the atom, the potential energies of the molecule in these two states may be represented by curves like those as shown in fig. 5. The system of bands therefore will be emitted as consequences of transitions

Fig. 5.

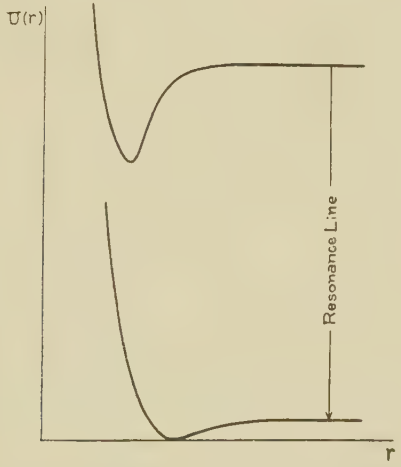

from the molecular state 2^3P_0, 2^3P_1, 2^3P_2, or 2^1P_1 to 1^1S_0. (This notation means that in the molecule one of the atoms is normal and the other is in the state of corresponding atomic level.) The excited states of these molecules will result from the normal state as consequences of absorbing light quanta or the collisions of the first and the second kind. Further, the collisions between the normal and excited atoms play a great rôle in the production of excited molecules.

As was shown by M. Born and J. Franck, a stable excited molecule is formed from a normal atom and an excited one as the result of the triple collisions ; however, even when no such triple collisions occur, the pair of colliding atoms

behaves as a quasi-molecule, and the spectrum due to such quasi-molecules may be expected to be emitted intensely in a highly dissociated vapour, which is usually considered to be a monatomic one. The characteristic of the intensity distribution of the continuous spectrum emitted by quasi-molecules can be deduced from the character of the potential energy curves shown in fig. 5. The probability of electronic transition is greater when colliding atoms are widely separated than when they approach near together, and therefore the intensity of the continuous spectrum due to the quasi-molecules will gradually increase to a maximum at the resonance line from the highest frequency, which corresponds to the transition to the potential minimum of the normal state*, and then decreases as it proceeds to the longer wave-length side. The reason why no structure was found about the maximum at the resonance line may well be understood.

The distribution among the vibrational states of excited stable (quantized) molecules differs with experimental conditions; but in definite circumstances there will be the most predominant vibrational state of a comparatively low quantum number. And a system of bands, consisting of a band having a maximum intensity corresponding to the most predominant vibrational state and many numbers of bands of decreasing intensity on both wave-length sides of it, will be emitted on the red side of the resonance line. On the longer wave-length side the system will suddenly break off or melt into the continuous spectrum of wide or narrow breadth.

For these reasons it is to be expected that in the distribution of intensity of the band system emitted by the excited molecules there will be found two maxima and one minimum between them. One of these maxima corresponds to that emitted by excited quasi-molecules and the other to that emitted by excited stable molecules.

As the vibrational energy levels of molecules in a normal state are very close together while those in an excited state are moderately separated it may be inferred that in the band system due to stable molecules a coarse and sometimes a finer structure corresponding to vibrational levels in an excited and a normal state is emitted. The decreasing rate of the differences of frequencies between

* J. G. Winans, *loc. cit.*

two successive coarser bands is extremely great at a few bands from that with $n'=0$, and then gradually smaller as it proceeds towards the bands with higher quantum numbers of vibration. This interesting fact is very well understood from the consideration which H. Kuhn has well expressed. It is to be expected that the frequency of convergence of the coarser bands will fall somewhere between the frequency of the resonance line and this frequency plus the energy of dissociation in frequency unit, in accordance with the relative position of the two potential curves, as was approximately confirmed by the results of this experiment. The convergence frequency is capable of being extrapolated graphically from the curve representing the variation of the differences of frequencies with the frequency of the maximum of the coarser band. but because the curve is always concave towards the axis of frequency the linearly extrapolated value is smaller than the true convergence, even when there is a sufficient number of bands observed ; moreover, when only a few bands with smaller quantum numbers of vibration are observed, the converging frequency linearly extrapolated will be much too small, as may be expected from Kuhn's opinion.

The energy of dissociation of molecule in the normal or the excited states can be calculated approximately from the difference of energies corresponding to the frequency of the resonance line and that of the shortest or the longest wave-length limit of the band system : but it should be stated here that in the latter case the approximate calculation will be possible only when the finer structure appears in the limiting band with $n'=0$. In both cases of this band $n'=0$ falls in the continuous region of the potential curve in the normal state, and if the longer wave-length region of the band system is really continuous the energy of dissociation of an excited molecule calculated in this manner will certainly be overestimated. Table VIII. (p. 66) gives the values, calculated from the observed values, of the energy of dissociation of the metallic molecules used in this experiment. These energies of dissociation of normal molecules are always a little greater than the values already obtained by other observers. For example, those for molecules Zn_2 ,Cd_2, and Hg_2 are 0·29, 0·24, and $\geq$0·07 volt respectively, while Winans calculated them to be 0·25 and 0·20 volt for Zn_2

and Cd_2 from the limits of the absorption spectra, and Franck and Grotrian obtained 0·04 volt and Koernicke 0·06 volt for Hg_2. These discrepancies can be well explained by taking into account the effect of the kinetic energies of colliding atoms at the temperatures of this experiment, as Oldenberg has discussed in detail.

The intensity of a band depends generally on the concentration of the initial state and the probability of transition between initial and final state. In the case of quasi-molecules the continuous spectrum accompanying forbidden lines $1^1S_0-2^3P_0$ and $1^1S_0-2^3P_2$ is lacking, while that with the line $1^1S_0-2^3P_1$ is excited, and the greater the intensity the greater is the triplet separation in the atomic spectrum. And the continuous band due to the transition $1^1S_0-2^1P_1$ is emitted intensely in the case of all the metals. From these results it seems that the intensity rule for the atomic line holds good very well in

TABLE VIII.

	1^1S_0.	2^3P_0.	2^3P_1.	2^3P_2.	2^1P_1.
Mg_2	0·30	—	—	—	$\fallingdotseq 1·5$
Ca_2	$>0·18$	—	—	—	?
Zn_2	0·29	$<1·7$	$\fallingdotseq 0·7$	—	$<\fallingdotseq 1·2$
Cd_2	0·24	$\begin{cases} <1·4 \\ >0·9 \end{cases}$	$\fallingdotseq 0·7$	—	?
Hg_2	$\fallingdotseq 0·07$	$<2·8$	$\begin{cases} <1·6 \\ >1·1 \end{cases}$	$\fallingdotseq 0·2$	$<1·5$

the case of the continuous spectrum emitted by quasi-molecules, but regarding the stable molecules similar reasoning does not hold good. The distribution of intensity in one and the same band system differs according to the ratio of the concentration of the quasi-molecules and of the stable molecules; therefore the relative intensity of the continuous spectrum near the resonance line and of that in the longer wave-length differs with experimental conditions. The distribution of intensity of the band series emitted by stable molecules depends mainly on the distributions of molecules in the vibrational levels in the initial state.

The symmetrical and asymmetrical bands accompanying the lines in the spectrum of thallium is probably due to thallium molecules, but nothing could be deduced as to

whether the molecule is diatomic or not. At any rate, the structure of the band systems at 3776 and 5350 differs from that of the diatomic one. The continuous branch extending in the shorter wave-length side from edges at 3770·7 or 2766·3 in the 3776 band or 2768 band may be explained as the excess of energy due to the kinetic energies of the colliding atoms.

The author wishes to express his thanks to Professor J. Okubo, who suggested this problem, for his continued help and advice throughout the experiment, and also to the Saito Gratitude Foundation for the cost of apparatus used in this experiment.

Sendai, Japan.
October 1930.

IV. *The Significance of Bode's Law in Relation to Satellite Systems.* *By* V. V. Narliker, *B.A., Isaac Newton Student, Cambridge* *. (*With an Addition by* Sir Joseph Larmor.)

[Note.—By Sir J. Larmor (March 17).—The interest of this paper rests on the fact that the same common ratio is found to arise in the four nearly geometric progressions, which express the sequence of distances of planets from the Sun and of systems of satellites from their central planet. If this numerical ratio is taken as C, equal to $\frac{1}{4}$B in the notation of the paper *infra*, the final expressions for log distances for the systems of Saturn, Uranus, Jupiter, and the solar planetary system are somewhat closely of the forms, for what they may be worth, and to the degree of approximation exhibited in the tables,

$$A+C.4n,\quad A'+C.6n,\quad A''+3.8n, \text{ and } A'''+C.11n \text{ resp.},$$

where n is an integer. In other words, the log distances of positions of planets and satellites are for all the systems of the type const. $+ Cm$, where m is an integer ; but only a few of these possible positions, sets of equidistant ones, are

* Read at the Royal Astronomical Society, March 12, 1931. Communicated by Sir Joseph Larmor.

occupied in each case, the others not having acquired a satellite. The last, rather more remote, expression belongs to the system of planets.

Mr. Narliker advances the consideration that if there is anything real in Bode's empirical law for the planets, the relation might be expected to extend in some cognate form to the satellite systems: for whatsoever may be the course of evolution that produced the solar planetary system, it is reasonable to expect that the same general type of evolution may have been operative for the satellite systems attached to the planets. Perhaps the natural tendency has been to regard Bode's law as an accidental coincidence; but one notes that Sir George Darwin was inclined to regard it as a subject for serious discussion, on the view that deviations from a regular law may conceivably have accumulated from secondary causes such as tidal friction.

Since the paper was written it came under our notice that the same subject had been explored recently by M. Pierucci in *Rend. dei Lincei* (June 15, 1930, p. 1099), referring back to six previous papers in greater detail, published in *Il Nuovo Cimento*. As Mr. Narliker informs me, he gives two geometric progressions, one for Mercury, Venus, Earth, and Mars, and the other for Jupiter, Saturn, Uranus, and Neptune. He tries different geometrical progressions expressing distances in different units, without adjustment, however, by least squares. This procedure is adopted for systems of satellites and some of the periodic comets as well.

But our attention has just now been directed to an earlier discussion by Miss M. A. Blagg with assistance from the late Prof. H. H. Turner, in 'Monthly Notices R. Astronomical Soc.' lxxiii. (April 1913) pp. 414–422. The procedure is difficult to follow, and is avowedly provisional and tentative: it revealed at an early stage the same feature, common to all the satellite systems, that captured our attention, but in our case in the different form *supra* that the common ratio of the successive distances for all the systems is the same B (equal to 4C) or a simple multiple thereof. So far as one remembers, there is no reference to Miss Blagg's striking discovery in the large literature on this subject, of long-standing historical interest ever since the times of Kant and Laplace, and still unsettled, of possible modes of evolution of a planetary system, whether in memoirs published by the Royal Astronomical Society and elsewhere, or, so far as one has found out, in the current handbooks on Astronomy; and it may be held that though

the main idea is so simple, or even because it is so easily grasped, it ought not to remain thus completely buried.

The trend of Miss Blagg's mode of discussion, as far as one has been able to follow it, seems to aim at merging all the satellites into one scheme, notwithstanding that they belong in groups to different systems. The final formula for distances (d) is, after logarithms have been taken,

$$\log(d/\mathrm{A}) = n \log 1{\cdot}7275 + \log\{\mathrm{B} + f(\theta)\}, \qquad \theta = \alpha + \beta n$$

for integral values of n; here the last term is of the nature of a correction to the main term, which itself involves a common ratio for successive distances equal to 1·7275, being, as above, very remarkably the same for all the systems. This mode of correction of the simple law of geometric progression is explored. A graph for $f(\theta)$ plotted against n seems to have been obtained by tabular methods, and is presented on a special plate, with the points belonging to the various satellites and planets marked along the curve, apparently occurring almost in random order. It thus appears to present itself as a unique universal graph (possibly some sort of a mean) common to all the satellite systems, and this notwithstanding that in an accompanying table of values of A, B, α, β, the values given for the constants α and β which occur in θ are very different for the four systems. As it stands, this contradiction seems patent. It is possible that α and β are virtually eliminated by introducing some linear correlation, in such wise that the four constants reduce really to two. That the separate graphs for the four systems may be forced into coincidence by uniform expansions and shrinkages in this way is natural enough, provided they are all nearly straight; but here the complex undulatory form of the final graph is evidence that there may be something real behind it. However this may be, the process of transferring the value of $f(\theta)$ from this one universal graph connecting $f(\theta)$ with n, into the formula, is found apparently (p. 420) to give good results for the four systems, the Sun, Jupiter, Saturn, and Uranus, when appropriate values of the remaining two constants A and B are introduced, peculiar to each system.

In contrast with this, the procedure of the present paper has kept the four systems distinct, avoiding any merging of their constituent members in mixed array along one empirical curve such as that for $f(\theta)$: this course is in keeping with the initial presumption from which it starts, that if the systems have arisen from similar origins, they may be

expected to be more or less like one another, but not so identical as to form a single compound system *.

For this reason, unless Bode's law is to be definitely abandoned, it is considered to be worth while to put on record, for the judgment of students of astronomy, this digest of carefully verified calculations of independent type and aim.—J. L.]

BODE'S law, discovered in 1772, assigns fairly well the distances of the major planets from the Sun. No explanation has yet come of the law, and it is generally considered to be an accident. Some considerations are here presented which may go against that view.

Leaving aside the exceptional case of the Moon, satellites in general may be supposed to have evolved from the respective primaries, presumably by the same kind of process by which the planets may have been born from the Sun. Hence, if Bode's law is not accidental, a trace of it or of an analogue should be found in the satellite systems; and a search is thus worth while. It is easily seen that the satellites of Uranus obey the actual law fairly well; there being, however, no inner satellite corresponding to Mercury, though a blank position hardly forms an objection to the rule. But there is a cognate relation, a modification of Bode's, which holds more widely with about the same approximation as Bode's for most of the satellite systems. The main feature is that, for all the systems, distances increase in geometrical progressions, while simple relations hold for the common ratios in these progressions.

* The universal direction of revolution common to almost all the bodies in all the component systems is already closely tied up with the once famous theories of secular stability, developed by Laplace and Lagrange, and focussed especially in this connexion by the theorems (of rotational momentum) announced by Laplace in 1784 (*cf.* the *Exposition du Système du Monde*). This analysis is surely the original and powerful pioneer for the modern science of evolutional dynamics, which has acquired its main stimulus and most of its progress on the physical side from Lord Kelvin. Though of course mathematically incomplete for very long range, the analysis is ample to show that a newly arrived body revolving the opposite way in the solar system would have very little chance of maintaining regular orbital motion, and that the progress of its elimination from the system would soon become precipitate: much less could such exceptional bodies have any chance of survival in the original settling down of the evolution of the raw material towards an ordered system. Sir John Herschel, as late as 1850, continued to insist on *Design* in this evolution, in the original Newtonian manner.

Let us now tabulate our results for the planets.

TABLE I.

The Bode Relation for the Planetary System.

Planet.	Mean relative dist. from Sun.	Per cent. departure from G. M. of the two adjac. distances *.	Empirical series in G. P.	Distances by Bode's Law.	Per cent. departure from formula †.
Mercury ...	3·87	—	—	4	−3·4
Venus	7·23	14	3	7	3·2
Earth	10·00	−4·9	6	10	—
Mars	15·23	−6	12	16	−5·1
Asteroids...	26	−8	24	28	−7·7
Jupiter ...	52·03	4·3	48	52	·1
Saturn ...	95·38	−4·7	96	100	−4·8
Uranus ...	191·9	11·8	192	196	−2·1
Neptune ...	300·7	7·9	—	—	—
Pluto	400	—	384	388	3

* Thus for Venus, for example, $\frac{7\cdot23-\sqrt{3\cdot87\times10}}{7\cdot23}\times100=14$ approx. etc.

† For Venus $\frac{7\cdot23-7}{7\cdot23}\times100=3\cdot2$ approx. etc.

If the unit of distance is ten times the Earth's distance from the Sun, Bode's law may be stated in the form

$$d=\cdot04+\cdot015\times2^n$$

or $$\log(d-\cdot04)=\log\cdot015+2\cdot72n\log(1\cdot29)_{n=1,2,\ldots8}.$$

In this form the formula does not hold good for Mercury ($n=0$) and for Neptune ($n=8$). But if Neptune is omitted as for some reason outside the series it holds for the new outer planet Pluto with that value ($n=8$).

Lastly, some remarks arise about the satellites not considered here. The distances of the last four satellites of Jupiter are 160·6, 164·6, 330, 338 : it is worth remarking that $\frac{330}{160\cdot6}=\frac{338}{164\cdot6}=2\cdot05$. The distances of the last five satellites of Saturn are 8·84, 20·48, 24·82, 59·68, 216·8. Now 8·79, 25·54, 74·2, 215·6 is a geometrical series, with a common ratio which is very nearly the same as the ratio of the two omitted distances, suggesting that they may be on another series of the same kind.

TABLE II.

(*a*) Saturn (first five satellites).

Mean dist. in equat. radius of planet.	Per cent. departure from G.M. of two adj. dists.	Empirical series in G.P.	Distances by formula.	Per cent. departure from formula.
3·11	—	3·06	3·10	·3
3·99	1·8	3·95	3·99	—
4·94	−1·6	5·09	5·13	−3·8
6·33	−4·3	6·57	6·61	−4·4
8·84	—	8·48	8·52	3·6

Formula: $\log(d-\cdot04)=\log 3\cdot06+n\log(1\cdot29)$, $n=0, 1, 2\ 3, 4$.

(*b*) Uranus.

7·35	—	7·28	7·32	·4
10·20	−9	10·69	10·73	−5·1
16·80	10	15·70	15·74	6·3
22·40	—	23·00	23·04	−2·8

Formula: $\log(d-\cdot04)=\log 7\cdot28+\frac{3n}{2}\log(1\cdot29)$, $n=0, 1, 2, 3$.

(*c*) Jupiter (the four large satellites).

5·90	—	5·74	5·78	2·0
9·40	− ·1	9·53	9·57	−1·8
14·99	−5	15·82	15·86	−5·8
26·38	—	26·27	26·31	·3

Formula: $\log(d-\cdot04)=\log 5\cdot74+2n\log(1\cdot29)$, $n=0, 1, 2, 3$.

Our search thus brings to notice principally the three formulæ:

$$\log(d-\cdot04)=\mathrm{A}+\mathrm{B}n \text{ (Saturn)}$$
$$=\mathrm{A}'+\mathrm{B}\tfrac{3}{2}n \text{ (Uranus)}$$
$$=\mathrm{A}''+\mathrm{B}2n \text{ (Jupiter)},$$

closely related to one another, and also, but not so closely, to Bode's law for the planets when stated in the form

$$\log(d-\cdot04)=\mathrm{A}'''+\mathrm{B}(2\cdot72n).$$

In conclusion, I should like to express my thanks to Prof. Sir J. Larmor for valuable suggestions while this note was being prepared; also to Dr. W. M. Smart for correcting a mistake in one of the formulæ.

V. *The Origin of the Light from the Negative Glow. By* R. H. Sloane, *M.Sc., and* K. G. Emeléus, *M.A., Ph.D., Department of Physics, The Queen's University of Belfast* *.

THE excited systems in the negative glow responsible for the radiation might be produced in two ways; in the first by the absorption of energy by a less excited state ("excitation"), and in the second by neutralization of a positive ion by an electron, without the immediate return of the neutral system to its ground state "(recombination"). There has been much controversy as to which process is effective, and it is only recently that it has been realized that either may preponderate according to the conditions of discharge.

Paschen †, from the presence of continuous spectra near the series limits in helium, has now shown that recombination is important in the negative glow of the hollow cathode discharge-tube developed by him for spectroscopic purposes. Dewey ‡, from the breadth of the lines in the negative glow of an arc from a hot cathode in helium, also concluded that recombination was responsible for the formation of the majority of the excited atoms. In both instances, however, as has been pointed out by Seeliger §, the discharges are much heavier than in the class of "normal" discharges, in which the negative glow is situated in front of a cold plane cathode, with a cathode fall just sufficient or a little more than sufficient to maintain the discharge, so that the origin of the light from the latter remained an open question. It has now been shown by Druyvesteyn ‖ in two investigations that such negative glows in argon and neon give an excitation light. In the first the spectrum of the light was compared with that of the afterglow which persists for a short time after the voltage across the tube has been reduced to too small a value to maintain the discharge. The afterglow was relatively rich in high members of certain series of Ne I and Ar I, and since the afterglow under these

* Communicated by the Authors.
† Paschen, *Berl. Ber.* xvi. p. 135 (1926).
‡ Dewey, Phys. Rev. xxxii. p. 918 (1928).
§ Seeliger, *Phys. Zeit.* xxx. p. 329 (1929).
‖ Druyvesteyn, *Zeit. f. Phys.* lvii. p. 292 (1929); lxii. p. 764 (1930).

circumstances gives a recombination light *, it was concluded that the ordinary light of the negative glow must be due to some other process, presumably excitation. In the second investigation a cold cathode discharge was run at a very low potential (50-65 volts), and it was found that the first appearance of Ne II lines coincided with the cathode fall in potential reaching the value needed for their excitation from the ground state of the neutral atom. It may be remarked in this connexion that the chance of spark spectra being due to recombination must fall off rapidly with increase in the order of the spectrum, from lack of multiply charged ions.

Summarizing these results—with special reference to spectra of neutral atoms, with which alone we are now concerned—it has been shown :

(*a*) that the negative glow of a heavy discharge from a hot cathode gives a recombination spectrum (Dewey) ;

(*b*) the same is true of the negative glow of a cold cathode discharge with special geometry of the electrode system (Paschen) ;

(*c*) The negative glow of the " normal " glow discharge from a cold cathode in argon and neon gives an excitation spectrum (Druyvesteyn).

In this paper we show that Druyvesteyn's conclusions for argon and neon are supported by two other lines of evidence, viz., the general similarity of the intensity distribution in the arc spectrum (Ar I) of the negative glow and of the positive column at the same low current density, and, less definitely, by the magnitude of the electron concentrations and temperatures in the negative glow found by Emeléus and Harris † and Emeléus and Brown ‡. On the one hand the spectrum of the positive column is definitely an excitation spectrum §, and on the other it appears by comparison with similar investigations by Kenty ‖ and by Mohler ¶ that the electron temperatures

* Mohler, ' Physical Review, Supplement,' i. p. 216 (1929).
† Emeléus and Harris, Phil. Mag. iv. p. 49 (1927).
‡ Emeléus and Brown, Phil. Mag. vii. p. 17 (1929).
§ Compton, Turner, and McCurdy, Phys. Rev. xxiv. p. 597 (1924).
‖ Kenty, Phys. Rev. xxxii. p. 624 (1928).
¶ Mohler, *loc. cit.*

are too high, and, to a less extent, their concentrations too small, for recombination usually to be of importance.

To compare the spectra of the negative glow and positive column the tubes shown in the figure were used. Fig. 1 *a* shows the form used for observation of the negative glow ; it consisted of two parallel plates of nickel $2 \times 22{\cdot}5$ cm. mounted in a soda-glass tube of 3 cm. diameter. The negative glow, which occupied the middle of the tube, was viewed through the end (fig. 1 *b*), which was blown to a thin bulb. The positive column tube is shown in fig. 1 *c*. This also was 3 cm. in diameter, and produced in the straight part a feebly striated positive column about 10 cm. long, which was again viewed end-on ; the negative glow remained in the side tube. The apparatus was

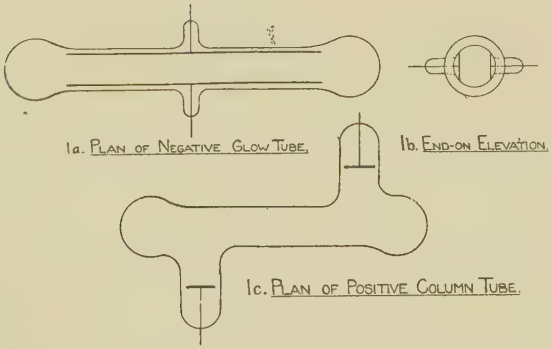

exhausted by a Langmuir diffusion-pump, backed by an oil-pump ; pressures were read on a McLeod gauge. A single large liquid-air trap protected the discharge-tube from condensible vapours. The argon (containing 0·1 per cent. nitrogen initially) was stored at approximately atmospheric pressure in a tube connected with the main apparatus through a misch-metal arc, from which charges were passed into the main apparatus. It was found desirable to have a second purifying arc connected directly with the discharge-tube, and to keep this running whilst making an exposure ; the cathode of this was a tray of small pieces of commercial cerium. The first few plates showed the Balmer lines, although the discharge-tube had been baked out in a furnace, and the purifying arc and connecting tubes heated with a gas-flame ; these disappeared after the purifying arc and the tubing up

to the liquid-air trap had been thoroughly degassed in one large furnace with the discharge-tube.

The discharge-tubes were run off the 440 volt d.c. mains in series with either a wire resistance of approximately 1700 ohms or a saturated diode; the current density was never more than 10^{-4} amp. per cm.^{2} The pressures used were between 0·1 and 0·8 mm. Hg. The spectrum of the discharge was taken with a glass single prism instrument giving the visible spectrum on a quarter plate. A disk cut to the form of a logarithmic spiral was rotated in front of the slit, the wedge-length of the lines being used to check the visual estimates of their intensities. Exposures of up to thirteen hours were made on Agfa Andresa plates, which were developed under standardized conditions. The plates were measured on the laboratory comparator, taking known argon lines as standards, and some 100 Ar I lines between λ 4628 and λ 5928 identified from Meissner's tables *; Rosenthal's table † was used for identification of Ar II. The only foreign lines were those due to nickel from the electrodes ‡. As is well-known, spark-lines are almost absent from the positive column. Tables were drawn up for comparison of the relative intensities of lines in each series of Ar I, for the negative glow, the positive column, and for the conditions employed by Meissner, with visual estimates of intensity on a 10 to 000 scale for our plates, Meissner's scale being 100 to 0. Portions of some forty series, mostly short, were investigated. Results for two of them are shown in Tables I and II.

Fewer lines were recorded for the positive column, the light from which is extremely feeble, but the fall of intensity in a series is much the same as in the negative glow. In no case is there the enhancement of high members in the negative glow which was found by Kenty § and by Druyvesteyn ‖ in the afterglow. Since the positive column gives an excitation spectrum we conclude, in agreement with Druyvesteyn, that the same is true of the negative glow of this discharge. The slow decrease in intensity with increase in m in Meissner's list

* Meissner, *Zeit. f. Phys.* xxxix. p. 172 (1926); xl. p. 839 (1927).

† Rosenthal, *Ann. d. Phys.* iv. p. 49 (1930).

‡ A trace of the 3914 N_2^+ head occasionally appeared, but did not affect the intensities in the Ar I spectrum.

§ Kenty, *loc. cit.*

‖ Druyvesteyn, *loc. cit.*

may indicate that he has recorded, in part at least, a recombination spectrum, as might be expected from the fact that he used an interrupted discharge and a high current density, but it is possible that the electrons in his discharge-tube had higher average energy, which would increase the intensity of high members of series *.

TABLE I.

Comparison of intensities in the series $2p_9$–md_4' of Ar I.

Wave-length.	m.	Intensity.		
		Meissner.	Positive column.	Negative glow.
6032.....	5	30	Outside range of plate.	
5496.....	6	20	8	10
5221.....	7	10	4	5
5060.....	8	10	000	4
4956.....	9	9	—	1
4886.....	10	6	—	000
4835.....	11	6	—	—
4799.....	12	6	—	—
4770.....	13	2	—	—
4748.....	14	3	—	—
4730.....	15	3	—	(Ar II 4731 and 4732.)
4716.....	16	0	—	—

A dash indicates that a line was not found on our plates.

TABLE II.

Comparison of intensities in the series $2p_6$–md_4' of Ar I.

Wave-length.	m.	Intensity.		
		Meissner.	Positive column.	Negative glow.
6213.....	5	10	Outside range of plate.	
5682.....	6	10	1	6
5410.....	7	10	000	3
5246.....	8	5	—	000
5142.....	9	4	—	—
5070.....	10	2	—	—
5017.....	11	2	—	(Ar II 5017 and 5018.)

Turning to the evidence afforded by probe measurements for an excitation spectrum, reference has first to be made to an investigation by Mohler †, in which the effect of current density on the spectrum, other conditions

* Peteri and Elenbaas, *Zeit. f. Phys.* liv. p. 92 (1929).
† Mohler, Phys. Rev. xxxi. p. 187 (1928).

being similar, has been shown. With tubes of special design containing cæsium vapour continuous spectra appeared at the 1 S, 2 P, and 3 D limits when a current of 0·5 amp. was passed, but were absent with a current of 0·015 amp. These continuous spectra furnish a measure of the amount of recombination. By analogy it might be supposed that recombination could not occur with the low current densities in our tubes. It is known, however, from Druyvesteyn's observations on the "aureole" of argon light round the negative glow in a neon-argon mixture that recombination may occur under special circumstances even with low current density, so that it is necessary to consider the conditions of discharge in more detail.

In a region like the negative glow, which is almost field-free*, the factors to be taken into account are :

(1) the nature of the gas,

(2) the temperature of the electrons,

(3) the concentrations of positive ions and electrons, which must be nearly equal to satisfy Poisson's relation.

With regard to (1) and (2) it is, however, probably safe to use for a starting-point the rough criterion † that recombination is not of importance for electron temperatures of more than one volt. Reference to the data given by Emeléus and Harris ‡ and Emeléus and Brown § then shows that in almost all cases studied in argon and neon the electron temperatures were greater than this. The exceptions in Emeléus and Harris's work occur for a discharge in argon at 0·52 mm. pressure (table iii. of their paper), when in a very narrow region in the middle of the negative glow the temperature was 0·7 volt and the electron concentration $7 . 10^8$ per c.c. A similar case is recorded in Table I. of Emeléus and Brown's paper, when an electron temperature of 0·5 volt was found in the middle of the negative glow, the pressure being 1·36 mm., and a few others occur in data summarized in figs. 5 and 6 of the same paper. The trend of these results has been confirmed by other measurements made

* We now believe the large reversed fields found by Emeléus and Harris at the negative glow boundary of the cathode dark space to be spurious.

† *Cf.* Mohler and Bœckner, Bureau of Standards Journal of Research, ii. p. 489 (1929).

‡ Emeléus and Harris, *loc. cit.*

§ Emeléus and Brown, *loc. cit.*

here with these gases. Summarizing them, we may say that with neon and argon under these conditions the temperature of the slowest group of electrons present (faster groups obviously need not be considered) falls below 1 volt only occasionally, in the middle of the negative glow, so that recombination spectra, if occurring at all, would only be expected there. That much recombination does take place is unlikely:

(*a*) from the small electron concentrations, relative to those found by Kenty when recombination was occurring;

(*b*) because the electron temperatures, although less than 1 volt, are rather higher than those for which recombination has been reported;

(*c*) in no instance has the colour of the negative glow (in argon) been noticed to approach the yellow-green of the pure recombination spectrum *. (This would in any event be partially masked by blue Ar II lines.)

Taken together these indicate that recombination, even under these relatively favourable conditions, was at least not the predominant source of the excited neutral atoms.

It would be natural to assume that these results for argon and neon apply generally to all similar low-current glows. To do this would, however, be unjustifiable. For example, in an investigation of helium in progress here it has been found that the spectra (He I) of the negative glow and anode glow, in addition to showing the pronounced differences to be expected from the presence of numerous fast electrons in the negative glow, also have, in some instances at least, a definite difference in the rate of decrease of intensity with increase of m in a series. This occurs both in singlet and triplet series, examples of which are given in Table III. (p. 80).

The intensities are eye estimates for exposures on Agfa rapid panchromatic plates in which the lines 5876 and 4472 were about equally intense. The electron concentrations and temperatures for the negative glow were approximately 9.10^8 at 0·6 volt, 5.10^7 at 7 volts, and 7.10^6 at 39 volts, and for the anode glow $3{\cdot}5.10^6$ at 0·8 volt, 5.10^6 at 3·4 volts, and 4.10^5 at 34 volts. It cannot be decided without further evidence whether the presence of high members in the spectrum of the negative glow is due to excitation by the fastest group of electrons or to recombination of the slowest group, or the extent to which it

* Kenty, *loc. cit.*

is perhaps due to both. This emphasizes that absence of high members shows absence of recombination, but their presence does not necessarily show that it is occurring: each discharge must be considered on its merits, and it seems to us that no general statement can yet be made as to the origin of the light.

Two further points arise from the work described here, viz., the fate of the ions and electrons which escape recombination in the negative glow and the parts played by the various groups of electrons in the excitation process. It is proposed to deal with these later.

In conclusion, it must be pointed out that in any discharge there will certainly be a small amount of recombination

Table III.

Comparison of intensities in the series 2^1P–m^1D (left-hand columns) and 2^3P–n^3D (right-hand columns) of He I.

Wave-length.	m.	Intensity. Anode glow.	Intensity. Negative glow.	Wave-length.	n.	Intensity. Anode glow.	Intensity. Negative glow.
6678....	3	2	2	5876....	3	7	7
4922....	4	1	2	4472....	4	10	10
4388....	5	0	2	4026....	5	3	8
4144....	6	—	1	3819....	6	0	3
				3705....	7	—	2
				3634....	8	—	0

light due to the low-velocity "tail" of the groups of electrons; all that has been shown in the present cases is that the extent to which this occurs is generally negligible.

Summary.

Druyvesteyn's conclusion that the negative glow of the normal glow discharge in neon and argon gives an excitation light has been shown to be in agreement with the similarity of the intensity distribution for Ar I lines in the negative glow and positive column, and also to agree with the electrical analysis of the negative glow. It is pointed out, with special reference to helium, that this conclusion is not necessarily valid for all gases.

We are indebted to Mrs. Emeléus for help with the experiments, and to Mr. Brown and Mr. Cowan for furnishing data for the discharge in helium.

VI. *Some Numerical Calculations of Atomic Scattering Factors.* *By* R. W. James, *Manchester University, and* G. W. Brindley, *Leeds University* *.

Introduction.

IT is our intention in this paper to give a summary of the work which has so far been done on the theoretical determination of the scattering factors of atoms for X-rays, and to base upon it methods of calculating them empirically which shall be sufficiently accurate to use in determining parameters in the analysis of crystal structures. The scattering factors for a number of atoms have already been tabulated by W. L. Bragg and J. West [1] in a paper on the calculation of crystal parameters, but more data are now available, and it seems worth while to collect together such information as may be of use to those engaged in analysing structures.

Part I.—*Theoretical.*

In the direct analysis of a crystal, by the use of Fourier series for example, what is determined is the distribution of scattering matter in the unit cell of the structure, and it is the scattering power of the whole unit which is measured, and which is used in the calculation. In most determinations, however, it is necessary at some stage in the work to make use of our knowledge that the electrons, to which the scattering is due, are collected together in the atoms in clusters having very nearly spherical symmetry. If to each atom a characteristic scattering power is assigned, the scattering power of the whole unit may be calculated in terms of those of the individual atoms, the phase differences introduced by the distribution of the atoms in the unit cell being taken into account. In any real crystal structure, the arrangement of the outer electrons of the atoms must be to some extent distorted from spherical symmetry, and this procedure of assigning a definite scattering power to each atom, and assuming it to remain the same for a given type of atom from crystal to crystal, can only be an approximation. Experience shows, however, that the departure from spherical symmetry is not important. The scattering at any appreciable angle is

* Communicated by Prof. W. L. Bragg, F.R.S.

due mainly to the inner electrons of the atoms, for which the departure from spherical symmetry due to the packing of the atoms in the crystal is small, and the scattering powers of atoms in simple crystals in general depend only on the angle through which the radiation has been scattered, and not on the direction in which it has passed through the crystal. Since nothing definite is known of the distortions introduced into the electron arrangement by packing the atoms into a crystal, any theoretical calculation of the atomic scattering factors must be made for the free atoms or ions, and must therefore be approximate [2]; but since the outer electrons contribute little to the scattered radiation at large angles of scattering, the error introduced by this is not great.

All the earlier calculations of atomic scattering factors [3] [4] [5] [6] were based on the assumption that the atom contained electrons which scattered according to the classical laws of electrodynamics. The further assumption was made that the frequency of the incident radiation was large compared with the absorption frequencies of the electrons in the atoms, so that they could be treated as free electrons, scattering according to the law of J. J. Thomson. According to this law, if plane-polarized radiation of unit amplitude falls on an electron the amplitude of the scattered radiation at unit distance from the electron and at a point in the plane of polarization of the incident radiation is e^2/mc^2. To get the amplitude of the radiation scattered from a cluster of electrons, such as an atom, we must add together their individual contributions, taking into account the phase differences introduced by the fact that they are distributed through a region whose dimensions are comparable with the wavelength of the radiation. The scattered amplitude at unit distance from the atom then becomes $f \cdot e^2/mc^2$, where f is a number which approaches the number of electrons in the atom for very small angles of scattering, but falls away rapidly with increasing angle, owing to the interference between the contributions from the different parts of the atom. It is with this scattering factor f that this paper is concerned.

In any actual measurement of the scattering factor we can only deal with the effect of an enormous number of atoms acting together, so that it is the average distribution of electrons in the atom which must be taken into account

in calculating f. Matters are further complicated by the fact that the atoms in a crystal are subject to thermal oscillations, so that the average distribution of the electrons in the region of any atom is more diffuse than that calculated for the atom at rest. This effect is a property of the crystal in which the atom occurs, and not of the atom itself.

To a first approximation we may consider each atom of the crystal to vibrate as a whole. Then, if f_0 is the scattering factor for the atom at rest, and f that for the same atom in a crystal at temperature T, it was shown by Debye [7] that

$$f = f_0 \cdot e^{-M}, \quad . \quad . \quad . \quad . \quad . \quad . \quad . \quad (1)$$

where

$$M = 8\pi^2 \bar{u}^2 (\sin\theta)^2/\lambda^2, \quad . \quad . \quad . \quad . \quad . \quad (2)$$

$\bar{u}^2$ being the mean square displacement of the atom at temperature T in a direction perpendicular to the atomic planes at which X-ray reflexion is considered as taking place at a glancing angle θ. We can therefore separate the temperature factor e^{-M} from the factor f_0, which depends on the spatial distribution of the electrons in the atom at rest. It is perhaps well to emphasise at this point that the temperature correction is not a small one, and for soft crystals may be very considerable. Actual examples will be given later.

It is easy to show that if $U(r)$ is the radial density of charge in the atom, so that $U(r) \cdot dr$ is the average number of electrons lying within distances r and $r+dr$ from the centre of the atom, then

$$f_0 = \int_0^\infty U(r) \cdot \frac{\sin kr}{kr} \cdot dr, \quad . \quad . \quad . \quad . \quad (3)$$

where $k = 4\pi(\sin\theta)/\lambda$.

f_0 and f are therefore both functions of $(\sin\theta)/\lambda$, and the f-curve of an atom plotted as a function of $(\sin\theta)/\lambda$ should be independent of the wave-length of the radiation.

A theoretical calculation of f_0, the scattering factor for the atom at rest, thus involves the determination of $U(r)$, the average radial charge-density in the atom. Once $U(r)$ is known as a function of r, it is easy to integrate equation (3) numerically, and so to determine f_0 for any value of $(\sin\theta)/\lambda$. In the first theoretical calculation of

f_0, that due to Hartree [8], an orbit model of the atom, based on spectroscopic data, was assumed, and the time average of the electron density was treated as a classical distribution of charge scattering according to Thomson's formula. This made no allowance for the incoherent scattering, which the Compton effect showed must exist, and, moreover, the agreement between the general form of Hartree's f-curves and those observed for certain atoms in crystals was far from satisfactory. Williams [9], and, independently, Jauncey [10], made attempts to correct the theoretical f-curves for the Compton effect, and, with reasonable assumptions, obtained curves of the right general type.

The development of the wave-mechanics theory of scattering by Wentzel [11], Waller [12] [13], and others has, however, made it possible to treat the problem in a more satisfactory way and at the same time to retain the form of equation (3). The matter has been dealt with in detail elsewhere [18], and here it will only be necessary to state the results. Waller, to whom this development of the theory of scattering from bound electrons is mainly due, has shown that if the frequency of the incident radiation is large compared with the absorption frequency of the bound electron, and yet not so large that relativity corrections become appreciable, the *total* scattering from a bound electron is still that given by Thomson's formula. This total scattering is, however, composed of two parts, one consisting of incoherent radiation of changed wave-length, corresponding to the Compton scattering, the other of coherent radiation of the same wave-length as the incident radiation. It is, of course, this latter part with which we are concerned in the calculation of f_0. The importance of Waller's results lies in the fact that they provide a method of calculating $\mathrm{U}(r)$ in terms of the wave-function of the electron. If ψ is the wave function of the electron at any point, $|\psi|^2 dv$ may be interpreted as giving the probability that an electron will be found in the element of volume dv in the neighbourhood of the point considered. $|\psi|^2$, suitably normalized, so that $\int |\psi|^2 dv$ throughout space is equal to the number of electrons in the atom, may therefore in a certain sense be considered as an average electron density. Waller shows that, within the limits of frequency we have considered, the coherent scattering from an atom may be

obtained by treating this "charge-density" as scattering classically, so that $U(r)$ in formula (3) is given by

$$U(r) = 4\pi r^2 |\psi|^2 \quad . \quad . \quad . \quad . \quad . \quad . \quad (4)$$

If, therefore, Schrödinger's equation can be solved for the electrons in the atom, $U(r)$, and hence f_0, can be calculated.

Waller's original treatment was limited to a single electron in an atom. He has, however, shown that it can be extended, at all events as a close approximation, to atoms containing many electrons. The calculation of ψ^2 for an atom containing a single electron can, of course, be made directly from the solution of Schrödinger's equation for the hydrogen atom. The accurate solution for an atom with n electrons would, however, involve an equation with $3n$ variables, and is impracticable, so that some approximate method must be used. Pauling [14] obtained an approximate solution by treating each electron in the atom as hydrogen-like, subject to a Coulomb field due to an effective nuclear charge which was estimated for each group of electrons. The most accurate approximate method is, however, that due to Hartree [15], the so-called method of self-consistent fields, which applies to completed electron groups having spherical symmetry. Scattering factors calculated by Hartree's method for Na^+, Cl^-, K^+, and Al agreed very well with those obtained from experiments on the absolute intensity of reflexion of X-rays from crystals of rock-salt [16] [17] [13], sylvine [19], and metallic aluminium [20], in which the temperature factors were also measured, so that allowance could be made for the heat motions.

The available experimental evidence seems therefore to show that the method of self-consistent fields leads to reliable values of f_0, but the labour of calculating fields by this method is very considerable, especially for the higher atomic numbers, and it is hardly practicable to embark upon it each time a new f-curve is required. In the second part of this paper we shall show how it is possible to use the known f-curves as a basis for the interpolation of others. Self-consistent fields have now been calculated for a number of atoms between hydrogen and calcium, $Z=20$, but for none between calcium and rubidium, $Z=37$, nor for any greater value of Z. Interpolation methods thus become very uncertain for $Z>20$,

and there are no data for calculating f_0 from self-consistent fields for the heavier atoms. Fortunately the method for calculating atomic fields introduced by Thomas [21] and independently by Fermi [22], which treats the atom as a quantized electron gas obeying the exclusion principle, gives a reasonably good approximation for these atoms, whereas it breaks down for the lighter ones. By using the two methods it is therefore possible to cover the range of atomic numbers with a fair degree of approximation.

It is important to realize that the methods of calculating f_0 outlined above all assume that the radiation which is scattered has a frequency considerably greater than the critical absorption frequency of any of the atomic electrons. If molybdenum radiation is used, this is the case for most of the atoms encountered in crystal analysis. If, however, copper or iron radiation is used it may frequently happen that the conditions are not fulfilled. In the analysis of alloys, for example, the absorption frequencies of the electrons in the specimen must often be comparable with the frequency of the incident radiation. When the frequency of the latter approaches that of the K absorption edge of the irradiated atom, the dispersion terms in the scattering formula become important, and the value of f_0 for a given value of $(\sin\theta)/\lambda$ will no longer be independent of the wave-length. As the frequency of the radiation passes from values below to values above that corresponding to the absorption edge, the K electrons no longer scatter in phase with the others, and the value of f may be expected to drop possibly by two or even more units. Since the K electrons, which contribute considerably to the scattering at all angles, are those concerned, the drop in f will affect the whole curve. The existence of an effect of this kind was first shown experimentally by Mark and Szillard [23], and some recent work by Wyckoff [25] and Miss Armstrong [24] on the scattering of different wave-lengths by nickel demonstrates it very clearly. All the data from the second part of this paper must therefore be applied with the possibility of this effect in view. For heavy atoms the L electrons may of course be affected as well.

Before going on to discuss the actual calculation of f_0 it will be well to recall briefly a few important general considerations. Each electron may be considered as replaced for the purpose of calculating f by a more or less

diffuse distribution of charge, having spherical symmetry. For the inner electrons this distribution is compact, and most of the charge lies within a region whose dimensions are small compared with the wave-length of the radiation whose scattering is considered. The f-values for such a group of electrons will decrease very slowly with increasing $(\sin\theta)/\lambda$, and the K electrons of the atom will thus contribute not far short of two units to f_0 at all angles of scattering at which measurements can be made with the wave-lengths generally used. The outermost electrons, on the other hand, correspond to a diffuse distribution of charge, the bulk of which lies at distances from the atomic centre comparable with or greater than the wave-length. The f-curve for such a distribution will fall away very rapidly with increasing $(\sin\theta)/\lambda$, and at large angles of scattering the outer electrons make very small contributions to f, which is due, at all events for the lighter atoms, almost entirely to the K electrons. Thus, although the charge distributions for the outer electrons are known with less certainty than those for the inner ones, the uncertainty matters very little*. If these ideas are kept in mind, the justification of some of the approximations made in the second part of the paper will be apparent. In fig. 1 we show the contribution of a single electron of each of the groups in the potassium ion to f_0.

Part II.—*The Numerical Calculation of* f_0.

In this part of the paper we shall consider some methods by which f_0, the scattering factor for the atom at rest, may be estimated numerically, and shall also discuss the possibility of applying corrections to these calculated values to take account of the thermal vibrations of the atoms in actual substances. We shall deal first with methods of interpolation, based on our knowledge of the electron distributions in those atoms to which the method of self-consistent fields has been applied. There are two possible lines of attack; either we may try to estimate $U(r)$ by interpolation from known distributions, and then calculate f_0, or we may interpolate for f_0 directly.

* Considerations of the same kind show that it is difficult, if not impossible, to distinguish between the different states of ionization of an atom by measuring its f-curve. (See, for example, James, Brindley, and Wood, *loc. cit.* (10).)

As the result of a number of trials a method of the second type was chosen, which we shall proceed to describe in some detail.

The calculations are based on charge distributions obtained by Hartree's method for the following atoms and ions: He, Li, O neutral, F^-. Na, Na^+, Al^+, Al^{++}, Al^{+++}, Si^{+4}, Cl^-, K^+, Ca^{++}, and Rb^+. The scattering factors were first of all calculated for all the separate electron groups in these atoms and ions, and relationships were sought between the f_0-curves for the

Fig. 1.

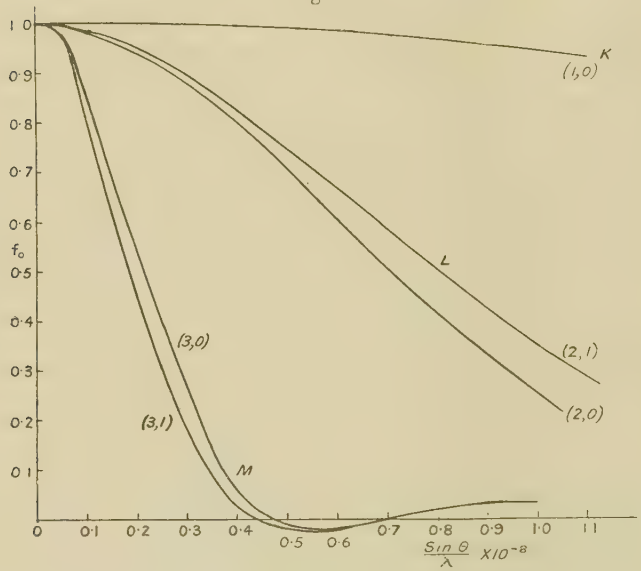

Contributions of one electron to f_0 in each of the electron groups of K^+.

same electron group in atoms with varying atomic number Z. It was found that if f_0 for the K electrons was plotted against $(1/Z) \cdot (\sin\theta)/\lambda$, the curves for all the atoms or ions were practically coincident so that for any K electron the value of f_0 as a function of $(\sin\theta)/\lambda$ could be estimated very quickly for any value of Z. It is easy to see the physical significance of this result. As Z increases the electrons become more tightly bound, and there is a greater charge-density for smaller values of r. Now for the K electrons in a hydrogen-like atom $Z \cdot r_{\max.}$ is constant,

$r_{max.}$ being the value of r for which the radial charge-density is a maximum. The same is approximately true for atoms which are not hydrogen-like, and to the same degree of approximation $r_{max.}$ is proportional to $1/Z$. If all the charge were concentrated at the radius $r_{max.}$, f_0 for the electron would be equal to $\sin\beta/\beta$, where $\beta = 4\pi r_{max.} (\sin\theta)/\lambda$, so that the f-curves would be exactly coincident if plotted against $(1/Z).(\sin\theta)/\lambda$, and although the actual distribution is diffuse, the approximate agreement of the f-curves remains.

Now, owing to the interaction of the electrons in the atoms the product $Z.r_{max.}$ is not constant for a given group of electrons. We might, however, take $(Z-s).r_{max.}$ as constant, and consider this relation as defining a screening parameter s which makes allowance for the interaction. For our purpose it is better to define the screening parameter in a rather different way, which, however, comes to very nearly the same thing. Suppose f_0 for a single electron of a group is plotted against $1/(Z-s).(\sin\theta)/\lambda$ for as many atoms as possible; then s may be defined as having values which make all the curves as nearly coincident as possible. The coincidence of the f_0-curves obtainable in this way is surprisingly close. For a given atomic number, Z, the value of the screening parameter, s, depends on the electron group considered, but the value for a given group will of course also vary with Z. For the idea of a screening parameter to be of use it is essential that it should not vary too rapidly with Z, so that its value for a given atom whose field is not known can be determined by interpolation with some certainty. Ideally then we shall have, characteristic of an electron of a given group, a common f_0-curve, the same for all the atoms containing the group, the abscissæ of which are values of $1/(Z-s).(\sin\theta)/\lambda$. If now s can be determined for any atom of atomic number Z, the f_0 curve for an electron in that atom as a function of $(\sin\theta)/\lambda$ can at once be obtained from the common f_0-curve. If, for example, the common curve has an ordinate f_x at an abscissa x, we shall have $f_0 = f_x$ when $(\sin\theta)/\lambda = x.(Z-s)$ for the atom of atomic number Z. By treating each electron in the same way the f_0-curve for the whole atom can be built up.

Before proceeding further it will be well to indicate the notation to be used in describing the electron groups.

It is only the radial charge distribution which is of importance for our purpose, since we shall in nearly every case

TABLE I.—(1, 0) electrons.

Values of f_0.

$\frac{1}{Z-s}\cdot\frac{\sin\theta}{\lambda}$	H.	He.	Li.	O.	F^-.	Na^+.	Al^{+3}.	Si^{+4}.	Cl^-.	K^+.	Ca^{+2}.	Rb^+.
0	1·00	1·00	1·00	1·00	1·00	1·00	1·00	1·00	1·00	1·00	1·00	1·00
0·005	—	—	—	1·00	1·00	1·00	1·00	1·00	1·00	1·00	1·00	1·00
0·01	1·00	1·00	1·00	1·00	1·00	1·00	1·00	1·00	1·00	1·00	1·00	1·00
0·015	—	- -	—	$\cdot99_5$	·99	$\cdot99_5$	$\cdot99_5$	$\cdot99_5$	1·00	1·00	1·00	1·00
0·02	$\cdot99_5$	$\cdot99_5$	$\cdot99_5$	·99	·99	$\cdot99_5$	$\cdot99_5$	$\cdot99_5$	$\cdot99_5$	$\cdot99_5$	$\cdot99_5$	$\cdot99_5$
0·025	—	—	—	$\cdot98_5$	$\cdot98_5$	·99	·99	·99	$\cdot99_5$	·99	·99	·99
0·03	·99	·99	$\cdot98_5$	·98	$\cdot97_5$	$\cdot98_5$	$\cdot98_5$	$\cdot98_5$	·99	$\cdot98_5$	$\cdot98_5$	$\cdot98_5$
0·035	—	—	—	$\cdot97_5$	·97	·98	$\cdot97_5$	$\cdot97_5$	·98	·98	·98	
0·04	$\cdot97_5$	$\cdot97_5$	·97	$\cdot96_5$	$\cdot96_5$	·97	·97	$\cdot96_5$	$\cdot97_5$	·97	·97	
0·045	—	—	—	$\cdot95_5$	$\cdot95_5$	·96	·96	·96	$\cdot96_5$	·96	·96	
0·05	·96	·96	·95	$\cdot94_5$	·95	·95	·95	·95	$\cdot95_5$	·95	·95	
0·055	—	—	—	$\cdot93_5$	·94	$\cdot93_5$	·94	$\cdot93_5$	$\cdot94_5$	·94	·94	
0·06	·94	$\cdot93_5$	·92	·92	·93	$\cdot92_5$	·93	$\cdot92_5$	·93	$\cdot92_5$		
0·065	—	—	—	·91	·92	·91	$\cdot91_5$	·91	$\cdot91_5$			
0·07	·91	·90	·89	·89	·91	·90	$\cdot90_5$	·90				
0·075	—	—	—	·88	·90	$\cdot88_5$	·89	$\cdot88_5$				
0·08	$\cdot87_5$	$\cdot86_5$	·86	$\cdot86_5$	·88	·87	$\cdot87_5$	·87				
0·085	—	—	—	$\cdot84_5$	·87	$\cdot85_5$	·86					
0·09	$\cdot84_5$	$\cdot83_5$	·83	·83	·85	·84						
0·095	—	—	—	$\cdot81_5$	$\cdot83_5$	$\cdot82_5$						
0·10	·81	·80	·80	$\cdot79_5$	·82	$\cdot80_5$						
0·15	·63	·61	·63	·63								
0·20	·48	·46	$\cdot47_5$									
0·25	·35	·34	·34									
0·30	·25	·25	$\cdot24_5$									
0·35	·18	$\cdot17_5$	$\cdot18_5$									
0·40	·13	·13	$\cdot13_5$									
0·45	·09	·10										
0·50	·07	$\cdot07_5$										
0·55	$\cdot05_5$	$\cdot06_5$										
0·60	·04	·05										
0·65	$\cdot03_5$	$\cdot04_5$										
0·70	·03											

Z	1	2	3	8	9	11	13	14	17	19	20	37
s	0	0·30	0·30	0·40	0·45	0·50	0·50	0·50	0·50	0·50	0·50	0·50

be dealing with completed groups which have spherical symmetry. We shall therefore denote an electron group by the total quantum number, n, and the quantum number l of Schrödinger's theory, each of which is common to all the electrons of a given group. A group will accordingly be denoted by the symbol (n, l). If n_k is the older Bohr notation for the same group, we have the relation $l=k-1$. The number of nodes in the radial wave-function, exclusive

TABLE II.—(2, 0) electrons.

Values of f_0.

$\frac{1}{Z-s}\cdot\frac{\sin\theta}{\lambda}$.	Li.	O.	F^-.	Na^+.	Al^{+3}.	Si^{+4}.	Cl^-.	K^+.	Ca^{+2}.	Rb^+.
0	1·00	1·00	1·00	1·00	1·00	1·00	1·00	1·00	1·00	1·00
0·005	·99	$\cdot99_5$	·99	$\cdot99_5$	·99	·99	$\cdot98_5$	·99	·99	·99
0·01	$\cdot96_5$	$\cdot97_5$	$\cdot96_5$	$\cdot97_5$	$\cdot96_5$	·97	·96	$\cdot96_5$	$\cdot96_5$	·97
0·015	$\cdot92_5$	$\cdot93_5$	$\cdot92_5$	·94	$\cdot92_5$	$\cdot93_5$	·93	·93	·93	·93
0·02	·88	·88	$\cdot87_5$	·89	$\cdot87_5$	$\cdot88_5$	·88	$\cdot88_5$	·88	$\cdot88_5$
0·025	$\cdot82_5$	$\cdot81_5$	$\cdot82_5$	·83	$\cdot81_5$	$\cdot82_5$	·82	$\cdot82_5$	·82	$\cdot82_5$
0·03	·76	·75	·76	$\cdot75_5$	·75	·76	$\cdot75_5$	·76	$\cdot75_5$	·75
0·035	$\cdot68_5$	·68	·68	$\cdot68_5$	$\cdot67_5$	·69	·69	$\cdot68_5$	·68	·68
0·04	$\cdot60_5$	·61	$\cdot60_5$	·61	·60	·62	·62	$\cdot60_5$	·61	
0·045	·53	$\cdot53_5$	·53	·54	·53	·54	·55	·53	$\cdot53_5$	
0·05	·46	·47	$\cdot45_5$	·48	$\cdot46_5$	·47	·48	·46	·46	
0·055	$\cdot39_5$	$\cdot40_5$	$\cdot38_5$	·41	·40	·40	$\cdot40_5$	$\cdot39_5$	$\cdot39_5$	
0·06	$\cdot33_5$	$\cdot34_5$	·33	$\cdot34_5$	·34	$\cdot34_5$	$\cdot33_5$	·33	·33	
0·07	$\cdot24_5$	·24	·24	$\cdot23_5$	$\cdot23_5$	·23	·22	$\cdot21_5$	·22	
0·08	·17	·16	·16	·15	·15	·14	·14			
0·09	·11	·10	·10	$\cdot08_5$	$\cdot07_5$	·08	·08			
0·10	·06	$\cdot05_5$	$\cdot05_5$	$\cdot03_5$	$\cdot02_5$	$\cdot03_5$				
0·11	—	·02	·03	0	0	·01				
0·12	—	·00	·01	−·02	$-\cdot00_5$	$-\cdot00_5$				
Z	3	8	9	11	13	14	17	19	20	37
s	1·62	3·0	3·3	3·6	3·9	4·0	4·0	4·0	4·0	4·0

of those for $r=0$ and $=\infty$, is equal to $n-(l+1)$. Electrons for which $l=0$ have, individually, spherically symmetrical charge distribution; those for which $l\neq0$ cannot be treated as spherically symmetrical unless the completed group is considered. The inclusive terms K, L, M, . . . electrons are applied in the usual way to electrons for which the total quantum number n is 1, 2, 3, ... and so on.

We shall now consider some of the numerical results. In Tables I., II., and III. values of f_0 are given for a series of values of $1/(Z-s) \cdot (\sin\theta)/\lambda$ for one (1, 0), one (2, 0), and one (2, 1) electron for all the atoms and ions for which the charge distributions are known. The values of Z and s

TABLE III.—(2, 1) electrons.

Values of f_0

$\frac{1}{Z-s} \cdot \frac{\sin\theta}{\lambda}$.	O.	F^-.	Na^+.	Al^{+3}.	Si^{+4}.	Cl^-.	K^+.	Ca^{+2}.	Rb^+.
0	1·00	1·00	1·00	1·00	1·00	1·00	1·00	1·00	1·00
0·005	·99$_5$	·98	·99$_5$	·99	·99	·99$_5$	·99	·99	·99$_5$
0·01	·98	·94$_5$	·98	·97$_5$	·97$_5$	·98	·97$_5$	·97$_5$	·97$_5$
0·015	·95	·90	·95	·95	·94$_5$	·95	·94$_5$	·94$_5$	·95
0·02	·90$_5$	·85$_5$	·91	·90$_5$	·91$_5$	·90$_5$	·91	·90$_5$	·91
0·025	·86	·80$_5$	·86	·86	·87	·86	·86$_5$	·86	·86$_5$
0·03	·80	·76	·80	·81	·82	·80$_5$	·81	·81	·81$_5$
0·035	·74	·71$_5$	·74	·75	·76	·75	·75$_5$	·75$_5$	·76
0·04	·68	·66	·68	·69$_5$	·70	·69$_5$	·70	·70	
0·045	·62$_5$	·61	·62$_5$	·64	·64$_5$	·64	·64$_5$	·64	
0·05	·57	·55	·56$_5$	·58	·58	·58	·58$_5$	·58$_5$	
0·055	·52	·50$_5$	·51$_5$	·52	·52$_5$	·52$_5$	·53	·52$_5$	
0·06	·47	·45	·46$_5$	·47	·47	·47	·47	·47	
0·07	·37$_5$	·36	·37	·37	·37$_5$	·37	·36$_5$	·36	
0·08	·30	·28	·29	·28$_5$	·29	·28$_5$	·28		
0·09	·23$_5$	·22$_5$	·22$_5$	·22	·22	·20$_5$			
0·10	·18	·18	·17	·17	·16$_5$				
0·11	·14	·14$_5$	·13	·12$_5$	·12				
0·12	·11	·11$_5$	·10	·08$_5$	·08$_5$				
0·13	·08	·09	·08	·06	·06				
0·14	·06	·06$_5$	·05$_5$		·04				
0·15	·04	·04$_5$	·04						
Z	8	9	11	13	14	17	19	20	37
s	4·1	4·9	4·9	4·9	4·9	5·0	5·0	5·0	5·0

are given at the foot of each table. To enable the results to be visualized more easily, the values of s are plotted against Z in fig. 2. A glance at the numbers given in the table shows that if s is rightly chosen f_0, when expressed as a function of $1/(Z-s) \cdot (\sin\theta)/\lambda$. is almost independent of Z. For the (1, 0) electrons the agreement is particularly good, and may be compared with the wide divergence between the f_0-curves for these electrons for atoms with

large and small Z plotted in the usual way against $(\sin\theta)/\lambda$. For the (2, 0) and (2, 1) electrons the differences between the various curves plotted as functions of $1/(Z-s)$. $(\sin\theta)/\lambda$ are a little larger than for the (1, 0) electrons, but they are still quite small. The curve for the (2, 1) electron of the negative fluorine ion differs slightly from those for the other (2, 1) electrons, but this is not serious, and may

Fig. 2.

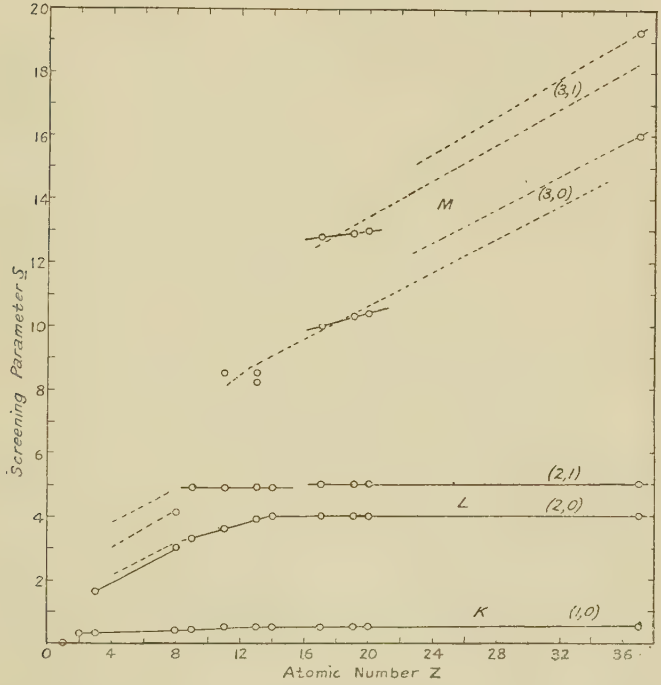

easily be due to the difficulty of calculating the charge distributions for the outer electrons in negative ions.

One point of some interest arose in the calculations. Although the way in which s was determined was somewhat arbitrary—actually a graphical method of successive approximation was used—it was quite clear that s could not in general be regarded as a smooth function of Z. In consequence, the interpolation of s is rendered somewhat uncertain in some regions of Z. For the K electrons the value of s is small everywhere, so that the lack of

smoothness of s as a function of Z is not important. When Z is greater than about 30, the precise value given to s is not important, since it is in any case only a small fraction of Z. We therefore consider that the method will give values of f_0 for the K electrons of any atom with all needful accuracy.

The L *Electrons.*—For the (2, 0) electrons s varies over a larger range than for the (1, 0) electrons, and is not small compared with Z if the latter is less than about 20. In the region between Z=8, O, and Z=20, Ca, enough values of s are known to determine as accurately as is necessary how it varies with Z, and since s for the (2, 0) electrons is the same for rubidium as for calcium, it seems probable that it is constant between Z=20 and Z=37. For Z<8 we have only one value of s, that for Li, Z=3, so that there is some uncertainty for the (2, 0) electrons from Z=4 to Z=7. The effect of possible errors in s on the values of f_0 in this region are considered below.

For the (2, 1) electrons s remains practically constant between Z=9 and Z=37, but we have no information as to how it varies when Z is less than 8. If we accept Stoner's assignment of electrons to the groups, this affects only Z=5, 6, and 7, and since in these atoms there are only a few (2, 1) electrons, the possible error in s will not have a very large effect on f_0. We consider therefore that the method is accurate enough for all K and L electrons for Z<37, but that the error in f_0 for these electrons will be greatest in the region Z=4 to Z=7. Let us then examine the case of carbon, and see how f_0 will vary for likely variations in s. From an inspection of fig. 2 it will be seen that s probably lies between the following extreme values for the different electron groups; for the (1, 0) electrons between 0·3 and 0·4; for the (2, 0) electrons between 2·5 and 2·7; for the (2, 1) electrons between 3·8 and 4·4. Using these values of s, we can calculate by means of Tables I., II., and III., the extreme limits within which the f_0-curve for carbon is likely to lie. These limits are shown in fig. 3 by the dotted lines, and we may perhaps take as the most likely f-curve that which lies halfway between them. It will be seen that it is unlikely that the error in f_0 is greater than 0·2 at any point. For values of $(\sin\theta)/\lambda$ greater than about 0·45 the error is very small, for here only the K electrons contribute appreciably to f_0. The uncertainties in the value of

f_0 for the K and L electrons are not therefore likely to be more than about 0·2 even in this unfavourable region of Z; they are likely to be much smaller for values of Z outside this region.

The M *Electrons.*—With the M electrons we are on much less safe ground. Rubidium is the only atom containing (3, 2) electrons for which the charge distribution has been calculated, and this alone gives no information as to how f_0 will vary for this group of electrons from atom to atom.

Fig. 3.

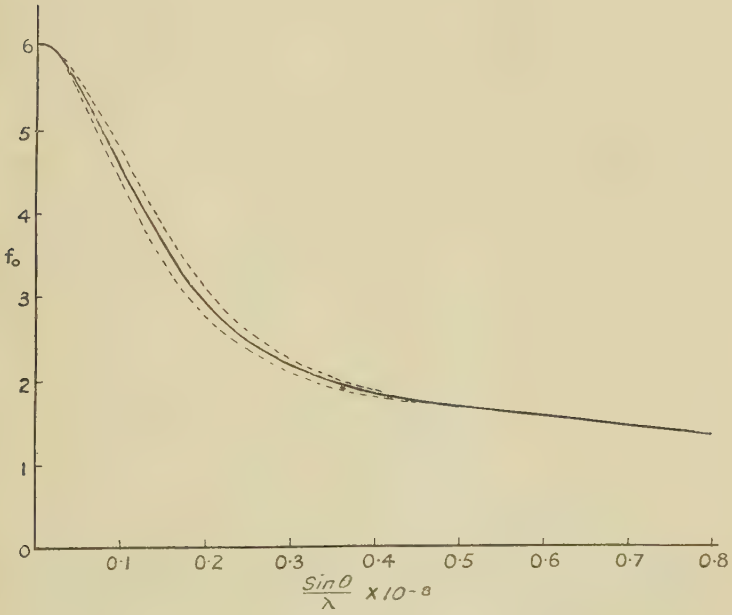

We shall therefore consider for the moment only the (3, 0) and (3, 1) electrons. The results for the (3, 0) electrons are given in Tables IV. and V. In Table IV. values of f_0 are given for different values of $(\sin\theta)/\lambda$, and it will be noticed how rapidly f_0 diminishes with increasing $(\sin\theta)/\lambda$ for the ions with the smaller values of Z, Na, Al^+, and Al^{++}. In Table V. values of $1/(Z-s).(\sin\theta)/\lambda$ are given for a series of definite values of f_0, instead of values of f_0 being given for definite values of $1/(Z-s).(\sin\theta)/\lambda$, as in Tables I., II., and III. This is a

TABLE IV.

Values of f_0 for (3, 0) electrons.

$(\sin\theta)/\lambda \times 10^{-8}$.	Na.	Al+.	Al++.	Cl−.	K+.	Ca++.	Rb+.
0·0	1·00	1·00	1·00	·100	1·00	1·00	1·00
0·025	·93	·97	·98				
0·05	·63	·85	·89	·97	·98	·98	·99
0·075	·35	$\cdot 71_5$	$\cdot 76_5$				
0·10	·15	$\cdot 56_5$	·61	·81	·85	·87	·98
0·125	·04	$\cdot 41_5$	·47				
0·15	$-\cdot 00_5$	·28	·33	·59	·69	$\cdot 73_5$	$\cdot 94_5$
0·175	−·02	$\cdot 15_5$	·20				
0·20	$-\cdot 02_5$	$\cdot 06_5$	·10	·38	$\cdot 54_5$	·61	$\cdot 90_5$
0·25	$-\cdot 01_5$	$-\cdot 01_5$	$-\cdot 01_5$	$\cdot 21_5$	·40	$\cdot 47_5$	$\cdot 85_5$
0·30	$\cdot 00_5$	$-\cdot 04_5$	−·05	$\cdot 09_5$	·27	·34	·80
0·35	·01	$-\cdot 02_5$	$-\cdot 03_5$	$\cdot 02_5$	$\cdot 14_5$	$\cdot 20_5$	·74
0·40	$\cdot 00_5$	$\cdot 00_5$	·00	−·01	$\cdot 05_5$	·10	·67
0·5	—	$\cdot 02_5$	$\cdot 02_5$	−·03	−·01	·01	$\cdot 53_5$
0·6	—	·02	·02	$-\cdot 01_5$	−·02	−·02	·40
0·7	—	—	—	−·01	·00	−·02	·28
0·8	—	—	—	·02	·02	·00	·18
0·9	—	—	—	$\cdot 01_5$	·03	·02	$\cdot 10_5$
1·0	—	—	—	·01	·03	·02	·05
1·1	—	—	—	—	—	—	·01

TABLE V.

(3, 0) electrons.

$$\frac{1}{Z-s}\cdot\frac{\sin\theta}{\lambda}\times 10^{-8}.$$

f_0.	Na.	Al+.	Al++.	Cl−.	K+.	Ca++.	Rb+.
1·00	0	0	0	0	0	0	0
0·9	·0110	·0095	·0101	·0110	·0096	·0090	·0099
0·8	·0145	·0135	·0140	·0148	·0133	·0132	·0144
0·7	·0175	·0177	·0178	·0178	·0168	·0171	·0180
0·6	·0210	·0208	·0213	·0210	·0210	·0212	·0212
0·5	·0245	·0245	·0247	·0242	·0247	·0250	·0249
0·4	·0280	·0282	·0285	·0277	·0288	·0289	·0288
0·3	·0323	·0325	·0326	·0319	·0330	·0327	·0325
0·2	·0370	·0370	·0370	·0364	·0374	·0365	·0370
0·1	·0436	·0425	·0417	·0424	·0427	·0415	·0430
0·0	·0580	·0520	·0501	·0545	·0540	·0540	·0540
s	8·5	8·5	8·2	10·0	10·3	10·4	16·0
Z	11	13	13	17	19	20	37

matter of practical convenience in the actual calculation, owing to the very rapid fall of f_0 with increasing $(\sin\theta)/\lambda$.

There are some points of special interest: first, it will be seen from fig. 2 that for the (3, 0) electrons s is definitely not a smooth function of Z. For argon-like ions s appears to vary in a linear way with Z, but the values of s for Rb^+, for Na, and for Al do not lie on this line. The estimation of s between Z=20 and Z=37 is uncertain, and the most that can be done is to suppose

TABLE VI.

Values of f_0 for (3, 1), (3, 2), (4, 0), and (4, 1) electrons.

	(3, 1).				Rb^+.		
$(\sin\theta)/\lambda\times10^{-8}$.	Cl^-.	K^+.	Ca^{++}.	Rb^+.	(3, 2).	(4, 0).	(4, 1).
0·0	1·00	1·00	1·00	1·00	1·00	1·00	1·00
0·05	·90	·98	·97	·99	·99	$\cdot96_5$	$\cdot95_5$
0·10	·62	$\cdot80_5$	$\cdot84_5$	$\cdot97_5$	·97	·82	$\cdot74_5$
0·15	·37	·62	$\cdot69_5$	·94	·94	$\cdot62_5$	·52
0·20	·21	·45	$\cdot53_5$	·90	$\cdot89_5$	·43	·29
0·25	·12	·31	$\cdot37_5$	·85	$\cdot84_5$	·27	·13
0·30	·05	·18	$\cdot24_5$	$\cdot79_5$	·79	$\cdot12_5$	·04
0·4	$-\cdot01_5$	$\cdot02_5$	·06	·66	·66	−·01	−·03
0·5	$-\cdot01_5$	−·02	−·01	·53	$\cdot53_5$	−·03	−·02
0·6	·00	−·02	−·01	·40	·41	−·01	·01
0·7	·01	$-\cdot00_5$	$-\cdot00_5$	·28	·31	$\cdot01_5$	$\cdot02_5$
0·8	·02	$\cdot01_5$	·00	$\cdot18_5$	$\cdot22_5$	$\cdot02_5$	$\cdot02_5$
0·9	$\cdot01_5$	·03	·02	$\cdot11_5$	·16	$\cdot02_5$	·02
1·0	·01	·03	$\cdot02_5$	·06	$\cdot10_5$	·02	·03

that its values will lie somewhere between the two broken lines in fig. 2. For Z<17 s will probably lie in the region of the lower broken line. From the general point of view this indefiniteness is not at all satisfactory, but for the special purpose of this section, the numerical evaluation of f_0, the results are of some value, as we shall see later. The second point of special interest is that the values of s for Al^+ and Al^{++} are different. So far it has been assumed that in the calculation of the f-curve for an electron the value of s may be supposed to depend only on the (n, l) group in which it occurs and on the value of Z. A little consideration will, however, show that the result of adding a second (3, 0) electron to A^{++} is not

simply to double the charge density of that group. The interaction of these electrons with each other and, to a lesser extent, with those of other groups will cause the charge density of each to become more diffuse, so that the value of s will be slightly increased by the addition of another electron to the same group. This second order effect is not, however, of great importance in the numerical estimation of f_0. Clearly s will vary most with the number of electrons in the group when the group is

TABLE VII.

(3, 1) electrons.

$$\frac{1}{Z-s}\cdot\frac{\sin\theta}{\lambda}\times 10^{-8}.$$

f_0.	Cl^-.	K^+.	Ca^{++}.	Rb^+.
1·00	0	0	0	0
0·9	·0119	·0121	·0113	·0113
0·8	·0160	·0168	·0165	·0168
0·7	·0201	·0210	·0210	·0210
0·6	·0246	·0257	·0255	·0252
0·5	·0288	·0303	·0300	·0295
0·4	·0339	·0356	·0341	·0339
0·3	·0400	·0412	·0392	·0385
0·2	·0489	·0480	·0457	·0443
0·1	·0625	·0570	·0535	·0522
0·0	·0850	·0695	·0640	·0640
Z	17	19	20	37
s	12·8	12·9	13·0	19·3

almost empty, and very little when it is almost full. Now when there are few electrons in an outer group their contributions to f_0 will be small except at very small values of $(\sin\theta)/\lambda$, so that when the second order effect is likely to be appreciable the electrons in any case make only a small contribution to f. When, however, an electron group is nearly full the charge density is relatively compact. The contribution of the group to f_0 is more important, but the uncertainty in s due to the second order effect is less so.

The values of f_0 for a (3, 1) electron are given in Table VI. Their variation with $(\sin\theta)/\lambda$ is similar to that for the (3, 0)

electrons, and once again the values of $1/(Z-s).(\sin\theta)/\lambda$ are tabulated for definite values of f_0. These values, together with the appropriate values of s, are shown in Table VII. Here, again, s is an approximately linear function of Z for the argon-like ions, but the value of s for rubidium is not collinear with the argon-like values. The uncertainty in s for $20>Z>37$ is indicated in fig. 2 by the broken lines.

We shall now examine how far the data contained in Tables I. to VII. and in fig. 2 are likely to be of use in estimating f_0-curves for atoms and ions with $Z<37$. For atoms containing only K and L electrons it has already been shown that the method is fairly satisfactory. M electrons are first found in Na, but for $Z=11$, 12, and 13 their distributions are so diffuse that it is only at very small values of $(\sin\theta)/\lambda$ that they make any appreciable contribution to f_0. Between $Z=13$ and $Z=17$ the uncertainty in s is so small that f_0 can be calculated for atoms and ions with $Z=14$, 15, and 16 accurately enough. The method is thus applicable with fair certainty up to $Z=20$. It remains to investigate its usefulness between $Z=20$ and $Z=37$, and, with this end in view, we shall consider the case of copper ($Z=29$) in detail. From fig. 2 we obtain the following values of s:—

For two (1, 0) electrons	$s=$	0·50	K.
„ two (2, 0) „	$s=$	4·0	L.
„ six (2, 1) „	$s=$	5·0	L.
„ two (3, 0) „	$s=$	13·0–14·0	M.
„ six (3, 1) „	$s=$	16·0–17·0	M.
„ ten (3, 2) „	$s=$	?	M.
„ one (4, 0) „	$s=$	?	N.

For the K and L groups there is little doubt as to the value of s, and the values of f_0 calculated for these electrons with the aid of Tables I., II., and III. should be quite accurate enough. For the (3, 0) and (3, 1) groups s will probably lie within the limits given above, and in Table VIII. we show the variations in the value of f_0 for these groups corresponding to the assumed variations in s. The mean value of f_0 is taken in each case in calculating the values of f_0 for Cu and Cu^+ which are given in Table IX. With the information at our disposal we can obtain no reliable information as to the contribution of the ten (3, 2) electrons. The values of f_0 for the different groups

of Rb show, however, that the contribution of a (3, 2) electron is not unlike that of a (3, 1) electron, and all that can be done for copper is to assume that the ten (3, 2) electrons make a contribution equal to that of ten (3, 1) electrons. This is, of course, not satisfactory. All that can be claimed is that the f-curve should be fairly reliable for values of $(\sin\theta)/\lambda$ greater than about 0·5, since at such values the M electrons make in any case

TABLE VIII.

Contributions of (3, 0) and (3, 1) electrons to f_0 for Cu calculated using two different values of s.

$(\sin\theta/\lambda)$ $\times 10^{-8}$.		0	0·1	0·2	0·3	0·4	0·5	0·6	0·7	0·8	0·9	1·0	1·1
$2\times$ (3, 0)	$s=13$,	2·00	1·91	1·65	1·32	1·00	0·62	0·36	0·14	0·04	−·02	−·04	−·04
	$s=14$,	2·0	1·90	1·62	1·26	0·90	0·56	0·26	0·10	0·01	−·03	−·04	−·01
$6\times$ (3, 1)	$s=16$,	6·00	5·73	4·92	3·93	2·88	1·86	1·08	0·51	0·12	−·09	−·12	−·12
	$s=17$,	6·00	5·67	4·71	3·63	2·55	1·53	0·78	0·27	−·06	−·12	−·09	−·06

only a small contribution to f_0. Even this amount of information may, however, be of value in crystal analysis. We shall return to the case of copper when discussing other methods of obtaining f-curves.

It is now quite evident that our lack of knowledge of the (3, 2) electrons prevents our estimating with any certainty the f_0-curves for atoms which contain many of them. In atoms having only one or two such electrons their contribution to f_0 will be small, and the error will not be important. The following table shows the probable numbers of (3, 2) and (4, 0) electrons in some atoms :—

	Z.	K. (1, 0).	L. (2, 0).	L. (2, 1).	M. (3, 0).	M. (3, 1).	M. (3, 2).	N. (4, 0).
K.....	19	2	2	6	2	6	—	1
Ca.....	20	2	2	6	2	6	—	2
Sc.....	21	2	2	6	2	6	1	2
Ti.....	22	2	2	6	6	6	2	2
V.....	23	2	2	6	2	6	3	2

In all these atoms the (4, 0) electrons have a charge-density so diffuse that their contribution to f_0 will be negligible except for small $(\sin\theta)/\lambda$. In Sc, Ti, and V the (3, 2) electrons are not "outer electrons." Their charge distributions will have approximately the same degree of diffuseness as those of the (3, 0) and (3, 1) electrons. The f_0-curves for the (3, 2) electrons will not fall to zero rapidly like those for the (4, 0) electrons, or like those for (3, 1) electrons in an outer group. A close enough approximation to the contribution of the (3, 2) electrons to f_0 for Z=21, 22, and 23 may be made by taking a mean of the curves for (3, 1) and (3, 0), for an inspection of the data for the different atoms shows that electrons with the same Z and the same total quantum number have very similar f-curves.

It seems therefore fair to say that the method of interpolation based on the Hartree distributions can be used with some degree of confidence up to Z=23 or 24, but that for greater values of Z it must be used with caution except for quite large values of $(\sin\theta)/\lambda$, where the uncertainty in the contributions from the M and N electrons is unimportant.

f_0 Factors from Thomas Fields.

The method of interpolation breaks down, as we have seen, for atomic numbers greater than about 25 owing to absence of numerical data upon which interpolations may be based. For higher atomic numbers, a fair approximation can be obtained by using the Thomas-Fermi method [21] [22] of calculating the atomic fields. This method, as applied to the calculation of f_0, has been described by W. L. Bragg and J. West [1] in the paper already referred to, and we shall not discuss it in detail here. The Thomas f-curves for all the atoms are alike, except for a difference in scale both in the ordinates and the abscissæ. If we have the f-curve for an atom of atomic number Z_0, and wish to obtain that for one of atomic number Z, we proceed as follows:—To obtain the value of f_0 for $\sin\theta/\lambda=x$ for the atom Z we take the value of f_0 from the curve for Z_0 at $(\sin\theta)/\lambda=x(Z_0/Z)^{\frac{1}{3}}$ and multiply the value so obtained by Z/Z_0.

Thomas worked out the charge distribution for cæsium, and the f_0-curve calculated from this by Bragg and

West, which is reproduced in this paper (Table IX.) may be taken as standard. This method treats the atom as an electron gas, and such a procedure is evidently more justifiable for heavy atoms, containing many electrons, in which the peculiarities of the individual electrons will be to some extent averaged out, than for light ones, in which such individual peculiarities are important. It is interesting to compare the f-values for rubidium calculated from the Hartree field and from the Thomas field*. It will be seen that the agreement is very close except for small values of $(\sin\theta)/\lambda$, and that the differences here are largely due to the fact that the

TABLE IX.

Standard f_0-curve for Cs. N=55 Thomas model.

$\frac{\sin\theta}{\lambda}\cdot 10^{-8}$.	f_0.	$\frac{\sin\theta}{\lambda}\cdot 10^{-8}$.	f_0.
0	55	1·0	17·0
0·1	50·7	1·1	15·6
0·2	43·8	1·2	14·5
0·3	37·6	1·3	13·2
0·4	32·4	1·4	12·3
0·5	28·7	1·5	11·3
0·6	25·8	1·6	10·4
0·7	23·2	1·7	9·6
0·8	20·8	1·8	9·2
0·9	18·8	1·9	8·6
		2·0	8·1

Thomas curve applies, as always, to the neutral atom, while the Hartree curve applies to the ion.

The case of copper is also instructive. We give in fig. 4 three curves—one obtained, in the manner described above, by interpolation (which, as we have seen, is not very trustworthy in this region of Z), another for neutral copper obtained by the Thomas method, and a third calculated from an approximation to the self-consistent field for copper for which we are indebted to Prof. Hartree. It will be seen that, while the curves differ in detail, there is a very fair general agreement amongst them, although the case of copper is favourable neither to the method of interpolation nor to the Thomas method. In this atom the group of ten (3, 2) electrons has just been completed,

* See Table X.

and the concentration of charge in the M region will be notably more compact than that predicted by the Thomas method. The Thomas curve therefore falls away more rapidly for small values of $(\sin\theta)/\lambda$ than it should for the true distribution. The agreement between the Hartree

Fig. 4.

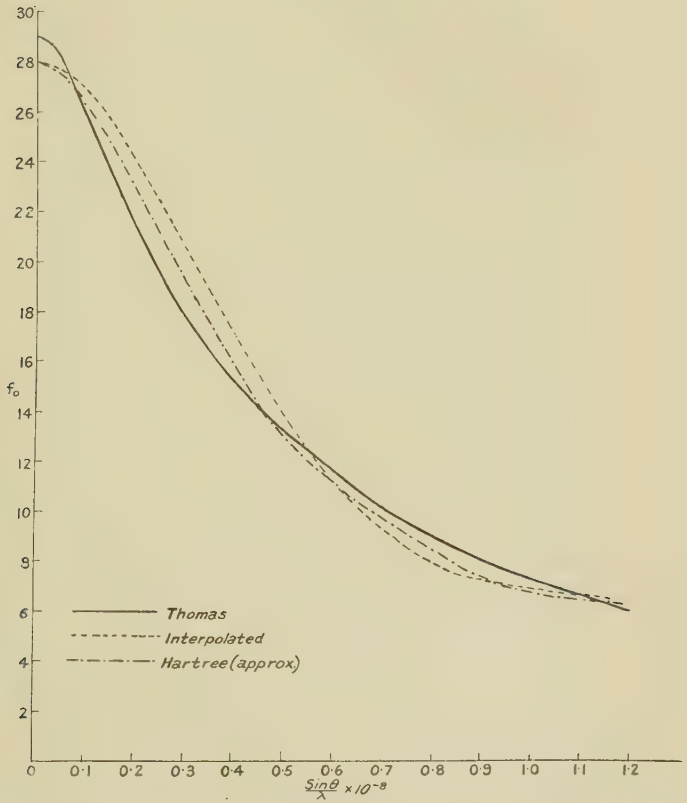

f_0-curves for copper obtained by different methods.

curve and the interpolated curve for large values of $(\sin\theta)/\lambda$ should be noted.

Tables of f_0.

In Table X. we give the values of f_0 for different values of $(\sin\theta)/\lambda$ for a considerable number of atoms and ions.

Table X.

Atomic scattering factors f_0.

$(\sin\theta)/\lambda \times 10^{-8}$.	0	0·1	0·2	0·3	0·4	0·5	0·6	0·7	0·8	0·9	1·0	1·1	Remarks.
H	1·0	0·81	0·48	0·25	0·13	0·07	0·04	0·03	0·02	0·01	0·00	0·00	W
He	2·0	1·88	1·46	1·05	0·75	0·52	0·35	0·24	0·18	0·14	0·11	0·09	H
Li^+	2·0	1·96	1·8	1·5	1·3	1·0	0·8	0·6	0·5	0·4	0·3	0·3	H
Li (neut.)	3·0	2·2	1·8	1·5	1·3	1·0	0·8	0·6	0·5	0·4	0·3	0·3	H
Be^{+2}	2·0	2·0	1·9	1·7	1·6	1·4	1·2	1·0	0·9	0·7	0·6	0·5	I
Be (neut.)	4·0	2·9	1·9	1·7	1·6	1·4	1·2	1·0	0·9	0·7	0·6	0·5	I
B^{+3}	2·0	2·0	1·9	1·8	1·7	1·6	1·4	1·3	1·2	1·0	0·9	0·7	I
B (neut.)	5·0	3·5	2·4	1·9	1·7	1·5	1·4	1·2	1·2	1·0	0·9	0·7	I
C	6·0	4·6	3·0	2·2	1·9	1·7	1·6	1·4	1·3	1·2	1·0	0·9	I
N^{+5}	2·0	2·0	2·0	1·9	1·9	1·8	1·7	1·6	1·5	1·4	1·3	1·16	I
N^{+3}	4·0	3·7	3·0	2·4	2·0	1·8	1·65	1·55	1·5	1·4	1·3	1·15	I
N (neut.)	7·0	5·8	4·2	3·0	2·3	1·9	1·65	1·55	1·5	1·4	1·3	1·15	I
O (neut.)	8·0	7·1	5·3	3·9	2·9	2·2	1·8	1·6	1·5	1·4	1·35	1·25	H
O^{-2}	10·0	8·0	5·5	3·8	2·7	2·1	1·8	1·5	1·5	1·4	1·35	1·25	I+H
F^-	10·0	8·7	6·7	4·8	3·5	2·8	2·2	1·9	1·7	1·55	1·5	1·35	H
F (neut.)	9·0	7·8	6·2	4·45	3·35	2·65	2·15	1·9	1·7	1·6	1·5	1·35	H
Ne	10·0	9·3	7·5	5·8	4·4	3·4	2·65	2·2	1·9	1·65	1·55	1·5	I
Na+	10·0	9·5	8·2	6·7	5·25	4·05	3·2	2·65	2·25	1·95	1·75	1·6	H
Na	11·0	9·65	8·2	6·7	5·25	4·05	3·2	2·65	2·25	1·95	1·75	1·6	H
Mg^{+2}	10·0	9·75	8·6	7·25	5·05	4·8	3·85	3·15	2·55	2·2	2·0	1·8	I
Mg	12·0	10·5	8·6	7·22	5·05	4·8	3·85	3·15	2·55	2·2	2·0	1·8	I
Al^{+3}	10·0	9·7	8·9	7·8	6·65	5·5	4·45	3·65	3·1	2·65	2·3	2·0	H
Al^{+2}	11·0	10·3	9·0	7·75	6·6	5·5	4·5	3·7	3·1	2·65	2·3	2·0	H
Al+	12·0	10·9	9·0	7·75	6·6	5·5	4·5	3·7	3·1	2·65	2·3	2·0	H
Al	13·0	11·0	8·95	7·75	6·6	5·5	4·5	3·7	3·1	2·65	2·3	2·0	H+I
Si^{+4}	10·0	9·75	9·15	8·25	7·15	6·05	5·05	4·2	3·4	2·95	2·6	2·3	H
Si^{+2}	12·0	11·1	9·55	8·2	7·15	6·05	5·05	4·2	3·4	2·95	2·6	2·3	H+I
Si	14·0	11·35	9·4	8·2	7·15	6·1	5·1	4·2	3·4	2·95	2·6	2·3	H+I
P^{+5}	10·0	9·8	9·25	8·45	7·5	6·55	5·65	4·8	4·05	3·4	3·0	2·6	I
P (neut.)	15·0	12·4	10·0	8·45	7·45	6·5	5·65	4·8	4·05	3·4	3·0	2·6	I
P^{-3}	18·0	12·7	9·8	8·4	7·45	6·5	5·65	4·85	4·05	3·4	3·0	2·6	I
S (neut.)	16·0	13·6	10·7	8·95	7·85	6·85	6·0	5·25	4·5	3·9	3·35	2·9	I
S^{+6}	10·0	9·85	9·4	8·7	7·85	6·85	6·05	5·25	4·5	3·9	3·35	2·9	I
S^{-2}	18·0	14·3	10·7	8·9	7·85	6·85	6·0	5·25	4·5	3·9	3·35	2·9	I
Cl	17·0	14·6	11·3	9·25	8·05	7·25	6·5	5·75	5·05	4·4	3·85	3·35	H+I
Cl^-	18·0	15·2	11·5	9·3	8·05	7·25	6·5	5·75	5·05	4·4	3·85	3.35	H
A	18·0	15·9	12·6	10·4	8·7	7·8	7·0	6·2	5·4	4·7	4·1	3·6	I
K+	18·0	16·5	13·3	10·8	8·85	7·75	7·05	6·44	5·9	5·3	4·8	4·2	H
Ca^{+2}	18·0	16·8	14·0	11·5	9·3	8·1	7·35	6·7	6·2	5·7	5·1	4·6	H
Sc^{+3}	18·0	16·7	14·0	11·4	9·4	8·3	7·6	6·9	6·4	5·8	5·35	4·75	I
Ti^{+4}	18·0	17·0	14·4	11·9	9·9	8·5	7·85	7·3	6·7	6·15	5·65	5·05	I
Ti^{+2}	20·0	18·7	15·5	12·5	10·1	8·5	7·8	7·25	6·7	6·15	5·65	5·05	I
Cu+	28·0	27·0	24·0	20·7	17·3	14·0	11·3	9·4	8·0	7·3	7·0	6·7	I
Cu+	28·0	26·3	23·0	19·2	15·8	13·0	11·2	9·7	8·4	7·4	6·7	6·5	H(approx.)
Cu	29·0	25·8	21·4	17·8	15·2	13·3	11·7	10·2	9·1	8·1	7·3	6·7	T
Rb+	36·0	33·6	28·7	24·6	21·4	18·9	16·7	14·6	12·8	11·2	9·9	8·9	H
Rb	37·0	33·4	28·2	23·6	20·4	17·9	15·9	14·0	12·4	11·2	10·2	9·9	T

I=calculated by method of interpolation.
H=calculated from Hartree distribution.
T=calculated from Thomas model.
W=calculated from hydrogen wave-function (ground state).

Up to atomic number 22 the values are calculated from Hartree fields or interpolated from them by the method we have described. For Z greater than 22 values can be obtained from the Thomas field. In the special cases of copper and rubidium values are given obtained from the Hartree fields and also from the Thomas fields. In the last column of the table the sources of the figures are indicated. For a number of atoms f_0 is given for different states of ionization. The method of calculation used is not always strictly justifiable, for it assumes spherical symmetry in the electron group, which is attained only for a completed (n, l) group or for a single electron with $l=0$. In neutral chlorine, for example, the (3, 1) group is incomplete, and to obtain f_0 for it we have simply subtracted the contribution of a single (3, 1) electron, or, more strictly, one-sixth of the contribution of six (3, 1) electrons to f_0 for the negative ion, in which the group is completed. Since the uncertainties introduced in this way affect on the whole only the outer electron groups, the corresponding uncertainties in f_0 will usually be small.

For atoms such as nitrogen, silicon, sulphur, and phosphorus, which often occur as the central member of a complex ion, we have tabulated f_0 for several states of ionization; but it is certain that the picture of such a group as a spherically symmetrical central ion surrounded by spherically symmetrical oxygen ions is far too simple. The whole ion must be a complex group, with the outer electrons of the constituent atoms forming a single system. The use of separate f_0 curves for the individual atoms can only be an approximation, whatever assumption as to the state of ionization is made.

The Temperature Factor.

It was pointed out in the first part of this paper that the values of f_0 calculated from the atomic charge distributions refer to the scattering from an atom supposed at rest, whereas in any actual crystal the atoms are in a state of thermal vibration. This, in effect, increases the volume occupied by the average atom, and so causes the f-curve to fall away with increasing $(\sin\theta)/\lambda$ more rapidly than it would do were the atoms at rest. To allow for the thermal vibrations we must multiply f_0 by a factor e^{-M}, M being proportional to the mean square displacement of the atoms of the type considered. It is evidently

these corrected values of f which are required in crystal analysis, and we must therefore consider the possibility of applying a temperature correction. It may be said at once that no general rules can be given. The temperature factor will differ for the same kind of atom in different crystals, and since atoms of different kinds in a compound crystal will not in general have the same mean amplitude of vibration, it will differ for different kinds of atom in the same crystal. Moreover, unless a crystal is cubic, the amplitude of vibration will depend on the crystallographic direction, and hence the actual f will not in general be spherically symmetrical.

For simple cubic crystals formulæ for the temperature factor were first deduced by Debye [7] and were later modified by Waller [26]. Actual measurements of the factor for simple crystals such as rock-salt [17] [27], sylvine [19], and aluminium [20] have shown it to be well represented by Waller's modification of Debye's formula for temperatures not too near the melting-point of the crystal and we shall therefore use it as a basis for making temperature corrections. The Debye-Waller formula for M is

$$\mathrm{M} = \left\{ \frac{6h^2}{mk\Theta} + \frac{1}{4} \right\} \frac{\phi(x)}{x} \frac{\sin^2\theta}{\lambda^2},$$

h being Planck's constant, m the mass of an atom of the lattice, k Boltzmann's gas constant, Θ the characteristic temperature of the crystal lattice, and $x = \Theta/\mathrm{T}$, T being the absolute temperature. The function $\phi(x)$ is tabulated by Debye [7], and we give the values again in Table XI. for convenience. The term 1/4 in the bracket allows for the zero-point energy of the lattice. The formula applies only to crystals of a simple type containing one kind of atom. For simple binary compounds, in which the forces keeping the two kinds of atom in place are of much the same order, a good approximation to M is obtained by taking m to be the mean mass of the two atoms. If the characteristic temperature is known the temperature factor can be calculated.

The characteristic temperature is obtained from the variation of the specific heat of the crystal with temperature. For all simple crystals of the type we are considering the curves connecting the atomic heat and

the absolute temperature are of the same shape, apart from a difference of scale of the temperature axis, and can be made to coincide if each is plotted with its temperature reckoned as a multiple of a certain value

TABLE XI.

Values of $\frac{\phi(x)}{x}$ after Debye. $\frac{\phi(x)}{x} = \frac{1}{x^2}\int_0^x \frac{\xi d\xi}{e^{\xi}-1}$.

x.		x.		x.		x.	
0	1	1·2	0·740	3	0·483	9	0·183
0·2	0·950	1·4	0·704	4	0·388	10	0·164
0·4	0·904	1·6	0·669	5	0·321	12	0·137
0·6	0·860	1·8	0·637	6	0·271	14	0·114
0·8	0·818	2·0	0·607	7	0·234	16	0·103
1·0	0·778	2·5	0·540	8	0·205	20	0·0822

Θ, characteristic of each crystal. On the Einstein-Debye theory of specific heats we have $\Theta = h\nu/k$, where ν is the limiting frequency of the elastic vibrations of the crystal lattice. Θ^2 is thus a measure of the restoring force on the displaced lattice points, and so is larger the greater this force, or, in other words, the harder the crystal. We give in Table XII. the values of the characteristic temperatures for a number of crystals, compiled from a paper by Schrödinger [28].

TABLE XII.

Values of the characteristic temperature, Θ.

Substance.	Θ.	Substance.	Θ.
Pb	88	KCl	230
Tl	96	Zn	235
Hg	97	NaCl	281
I	106	Cu	315
Cd	168	Al	398
Na	172	Fe	453
KBr	177	CaF_2	474
Ag	215	FeS_2	645
Ca	226	Diamond	1860

As a general rule we can say that the harder the crystal the smaller its temperature factor, because the more work which has to be done to displace the atoms from their mean positions the less will be the mean atomic displacement

at any given temperature. For simple crystals the characteristic temperature is a convenient measure of the hardness in this sense, and for such crystals a very good practical estimate of the temperature factor can be obtained by applying Debye's formula. In general, however, a crystal whose structure is being determined will be of a more complex type, to which the simple formula for M will not apply. Moreover we shall not, as a rule, have the data necessary to estimate an approximate characteristic temperature, for this would involve a knowledge of the variation of the specific heat of the crystal at low temperatures. Neither, in general, shall we know anything of the elastic properties of the crystal, from which an estimate of Θ could also be made. Nevertheless, if we are able by quite simple tests, for example by scratching the crystal, to get some idea of its hardness relative to the substances in Table XII. we can estimate an effective Θ for it, and taking m as the mean atomic weight of the material, can arrive at a value of M which will at least be a rough guide as to the order of the temperature effect. It cannot be claimed that such a procedure will give more than a very rough idea, but even this may be of considerable value. For a crystal such as diamond the temperature factor is nearly negligible at any reasonable temperature, whereas for soft crystals, such as rock-salt for example, it is very considerable. In fig. 5 we give f-curves for the sodium ion at rest (curve A), in a crystal of rock-salt at the absolute zero (curve B), in a crystal of rock-salt at 17° C. (curve D), and in a crystal of sodium fluoride at 17° C. (Curve C). Curve C is compiled from results obtained by Wyckoff and Armstrong [29] and by Havighurst [30]. The difference between A and B is due to the zero-point vibration of the lattice, and that between C and D no doubt mainly, at all events at the larger values of $(\sin\theta)/\lambda$, to the difference in hardness of NaCl and NaF. In the latter crystal the atoms can approach more closely than in the former, so that the attractive forces are stronger and the thermal agitation at a given temperature consequently less [31].

It is important in crystal analysis to know whether to expect a temperature factor of the order of that for diamond or of that for rock-salt, and by estimates of the kind proposed it should be possible to get this amount of information. It must be emphasized once more, however,

that the temperature factor estimated in this way can only be very approximate. For one thing it will be a mean temperature factor, to be applied to all atoms of the crystal, of whatever kind and however situated, whereas, strictly speaking, a separate factor should be applied to each kind of atom, depending on the nature of its binding and on its situation. Where possible it is of course far better to obtain an estimate of the temperature factor by actually measuring the intensity of a high

Fig. 5.

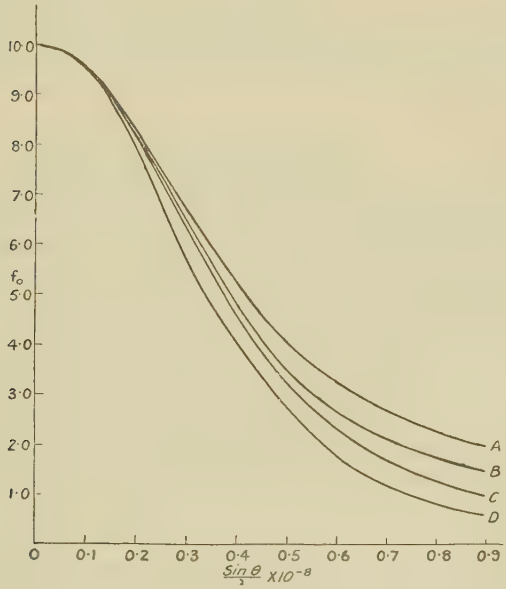

for sodium ion { A, ion at rest. B, at absolute zero. C, in NaF at 17° C. D, in NaCl at 17° C.

order spectrum at two temperatures. Care must, however, be taken in the interpretation of such measurements, since a change of temperature may alter the structure parameters, and so produce a change in the intensity of the spectrum which has nothing to do with atomic vibrations, and which may be larger than the effect due to this cause.

Concluding Remarks.

This paper was undertaken with the idea of making available for general use the data at our disposal concerning the charge distributions for various atoms and ions. We had in view its application to crystal analysis by means of X-rays, and it is therefore the atomic scattering factors for X-rays which have been tabulated. The results may, however, be of interest to those engaged in work on the diffraction of electrons by crystals. In this case also there is an atomic scattering factor which is related in a simple way to the scattering factor for X-rays[32] [33] [34]. For electrons the scattering due to the nucleus must also be taken into account. The atomic scattering factor for electrons which corresponds to f for X-rays is

$$(Z - f) \cdot \operatorname{cosec}^2 \theta,$$

where Z is the nuclear charge of the scattering atom, f the scattering factor applicable to X-ray scattering, and θ half the angle through which the electrons have been scattered. Electron-scattering factors also can therefore be calculated from the figures in the tables.

We have been mainly concerned in this paper with the theoretical calculation of f_0. We give, however, for convenience references in the bibliography to a number of the more important papers on the practical measurement of f which have not been specifically mentioned in the text, but we have made no attempt to make this list exhaustive.

We are indebted for much of the numerical data used in the preparation of the tables in this paper to Prof. D. R. Hartree and his co-workers, and we should like to take this opportunity of thanking him for the interest he has shown and for the help which he has always been ready to give. Our thanks are also due to Prof. W. L. Bragg, F.R.S., for much helpful criticism and advice.

Summary.

(1) A general account is given of the nature of the atomic scattering factor f and of methods of calculating it theoretically.

(2) Two methods of calculating numerically the scattering factor f_0 for the atom at rest, with sufficient

accuracy for use in crystal analysis, are discussed: (*a*) A method of interpolation, based on the values of f_0 calculated for those atoms for which the charge distributions have been determined by Hartree's method of self-consistent fields. This method appears to give reliable values up to atomic number 25. The limitations of the method are discussed. Tables are given for calculating f_0 for the different electron groups. (*b*) The method based on the Thomas-Fermi method of approximating to the atomic charge distributions.

(3) Tables of f_0 for a considerable number of atoms and ions are given.

(4) The possibility of applying a temperature correction to f based on the physical properties of the crystal is considered.

References.

(1) W. L. Bragg and J. West, *Z. f. Krist.* lxix. p. 118 (1928).
(2) G. W. Brindley and R. G. Wood, Phil. Mag. vii. p. 616 (1929).
(3) C. G. Darwin, Phil. Mag. xxvii. pp. 315, 675 (1914).
(4) A. H. Compton, Phys. Rev. ix. p 29 (1917).
(5) P. Debye and P. Scherrer, *Phys. Zeitschr.* xix. p. 474 (1918).
(6) W. L. Bragg, R. W. James, and C. H. Bosanquet, Phil. Mag. xli. p. 309 (1921); xlii. p. 1 (1921); xliv. p. 433 (1922).
(7) P. Debye, (*a*) *Verh. der Deutsch. Phys. Ges.* xv. pp. 678, 738, 867 (1913); (*b*) *Ann. der Phys.* xliii. p. 49 (1914).
(8) D. R. Hartree, Phil. Mag. l. p. 289 (1925).
(9) E. J. Williams, Phil. Mag. ii. p. 657 (1926).
(10) G. E. M. Jauncey, Phys. Rev. xxix. p. 605 (1927).
(11) G. Wentzel, *Z. f. Phys.* xliii. pp. 1, 779 (1927).
(12) I. Waller, Phil. Mag. iv. p. 1228 (1927); 'Nature,' cxx. p. 155 (1927); *Naturwissenschaften*, xv. p. 969 (1927); *Z. Phys.* li. p. 213 (1928).
(13) I. Waller and D. R. Hartree, Proc. Roy. Soc. A, cxxiv. p. 119 (1929).
(14) L. Pauling, Proc. Roy. Soc. A, cxiv. p. 181 (1927).
(15) D. R. Hartree, Camb. Phil. Soc. Proc. xxiv. pp. 89, 111 (1928).
(16) R. W. James and E. M. Firth, Proc. Roy. Soc. A, cxvii. p. 62 (1927).
(17) I. Waller and R. W. James, Proc. Roy. Soc. A. cxvii. p. 214 (1927),
(18) R. W. James, I. Waller, and D. R. Hartree, Proc. Roy. Soc. A, cxviii. p. 334 (1928).
(19) R. W. James and G. W. Brindley, Proc. Roy. Soc. A, cxxi. p. 155 (1928).
(20) R. W. James, G. W. Brindley, and R. G. Wood, Proc. Roy. Soc. A, cxxv. p. 401 (1929).
(21) L. H. Thomas, Camb. Phil. Soc. Proc. xxiii. p. 542 (1927).
(22) E. Fermi, *Z. f. Phys.* xlviii. p. 73 (1928).
(23) H. Mark and L. Szillard, *Z. Phys.* xxxiii. p. 688 (1925).
(24) A. H. Armstrong, Phys. Rev. xxxiv. p. 931 (1929).
(25) R. W. G. Wyckoff, Phys. Rev. xxxv. p. 215 (1930); xxxvi. p. 1116 (1930).

(26) I. Waller, Upsala Dissertation (1925).
(27) R. W. James, Phil. Mag. xlix. p. 585 (1925).
(28) E. Schrödinger, *Phys. Zeitschr.* xx. p. 474 (1919).
(29) R. W. G. Wyckoff and A. H. Armstrong, *Z. f. Krist.* lxxii. p. 433 (1930).
(30) R. J. Havighurst, Phys. Rev. xxviii. p. 869 (1926).
(31) G. W. Brindley, Phil. Mag. ix. p. 193 (1930).
(32) N. F. Mott, Proc. Roy. Soc. A, cxxvii. p. 658 (1930).
(33) H. Bethe, *Ann. der. Phys* lxxxvii. p. 55 (1928).
(34) H. Mark and R. Wierl, *Z. f. Phys.* lx. p. 741 (1930).

The following papers deal with some determinations of f not specifically mentioned in the paper :—

(35) R. J. Havighurst, Phys. Rev. xxviii. p. 882 (1926).
(36) D. A. McInnes and T. Shedlovsky, Phys. Rev. xxvii. p. 130 (1926).
(37) R. W. James and J. T. Randall, Phil. Mag. i. p. 1202 (1926).
(38) J. Bearden, Phys. Rev. xxix. p. 20 (1927).
(39) A. H. Armstrong, Phys. Rev. xxxiv. p. 1115 (1929).
(40) R. W. G. Wyckoff and A. H. Armstrong, *Z. f. Krist.* lxxii. p. 319 (1929).
(41) R. W. G. Wyckoff, *Z. f. Krist.* lxxiii. p. 181 (1930).
(42) A. A. Rusterholz, *Z. f. Phys.* lxv. p. 226 (1930).
(43) D. K. Froman, Phys. Rev. xxxvi. p. 1330 (1930).
(44) G. W. Brindley, Phil. Mag. ix. p. 204 (1930); Proc. Leeds Phil. Soc. i. p. 402 (1929).

Reference should also be made to the paper by W. L. Bragg in the Report of the Solvay Conference, 1928, for a general account of scattering by atoms in crystals.

Manchester University,
November 30, 1930.

VII. *The Electrical Conductivity of Single Aluminium Crystals in Directions inclined at various Angles to the Crystal Axes.* *By* Malcolm Fraser, *M.A., D.Phil.**

METALS ordinarily crystallize as aggregates of a very large number of small crystals of the order of a million per cubic centimetre. Hence any theoretical explanation of their physical properties is complicated because the physical property of the aggregate will possess some mean value of the physical property of the individual crystals, and, further, complications may be introduced by the crystal boundaries. From the point

*Communicated by Prof. F. A. Lindemann, Ph.D., F.R.S.

of view of the theoretical explanation of physical properties, therefore, measurements on single crystals are most important.

The determination of the electrical conductivity of single crystals has been undertaken by a number of workers. For non-cubic crystals the measurements have been made in directions inclined at various angles to the crystal axes[1], but, apart from one rough experiment[2], it seems that this has not been done in the case of cubic crystals. The reason for this is not obvious, for although some of the experimenters who have measured the conductivity of cubic crystals in one direction only have declared that the conductivity is independent of direction[3], they seem to have no experimental ground for their assumption.

What is to be expected theoretically is not altogether clear, as up to the present no entirely satisfactory theory of electronic conduction has been put forward. It was in the hope of throwing some light on the theoretical side that the present research was undertaken.

Preparation of the Single Crystals of Aluminium.

The single crystals were prepared by the method due to Carpenter and Elam[4]. Briefly it consists of two heatings and one stretching. The first heating, which is for six hours at 550° C., is to remove the strain received during the rolling and to make the minute crystals equiaxed. The stretching by an amount so as to increase the length of the specimen by 1–2 per cent. strains all these crystals, while the second heating, during which the temperature is raised from 450° C. to 550° C. over the period of a week, is to produce recrystallization.

The aluminium used was of three different purities: (1) The ordinary 99·6 per cent. "pure aluminium" of the British Aluminium Company, containing approximately 0·2 per cent iron and 0·2 per cent. silicon; (2) some special aluminium of 99·7 per cent. purity presented by the British Aluminium Company (the impurities in this were not known accurately, but were chiefly iron and silicon); (3) aluminium of 99·95 per cent. purity obtained by Messrs. Hopkin and Williams from a German source (the impurities in this material were ·017 per cent. copper, ·012 per cent. silicon, ·012 per cent. iron, and ·003 per cent.

titanium). This metal was in the form of an ingot, and the British Aluminium Company kindly undertook the task of recasting it into suitable form and then rolling it into a sheet from which the test pieces were stamped. The pieces were $\frac{1}{8}$ in. thick, and some were of the shape shown in fig. 1, while others had been milled to the shape shown in fig. 2. In all seven different batches were prepared.

For the purpose of ascertaining whether single crystals had been formed the specimens were etched with 10 per cent. caustic soda solution, as recommended by Carpenter. After this treatment the individual crystals were visible as light and dark patches on the surface. Twenty-seven test pieces which had recrystallized suitably were selected. Each consisted of one single crystal over the whole length of the narrow portion MN. Fifteen were of 99·6 per cent. purity aluminium, eight of 99·7 per cent., and four of 99·95 per cent.

Fig. 1.

Fig. 2.

Determination of the Orientation of the Crystal Axes.

By placing etched crystals in parallel beams of light and noting the directions of the reflected rays both Bridgman [5] and Shimizu [6] have determined the orientations of the crystal axes. However, as tarnished surfaces and multiple reflexions complicated matters, this method, although tried, was abandoned in favour of the simple X-ray method of Majima and Togino [7]. These experimenters have taken a series of Laue photographs of an aluminium crystal at intervals of 5°. It is thus possible, by taking one Laue photograph of an aluminium crystal and comparing it with the given photographs, to obtain the orientation of its axes to within 2°.

The source of X-rays used was a Coolidge tube operating at 8 milliamps. and 35,000 volts. The rays passed through two pin-holes 1·5 mm. in diameter in two lead screens 4 cm. apart, and then fell on the crystal, where they were

diffracted, a Wellington X-ray plate placed at a distance of 3·2 cm. from the crystal receiving the diffracted rays. To prevent fogging of the plate by scattered radiation it was covered by a lead screen in which there was a small hole in order to allow the direct beams of X-rays to escape. An exposure time of three hours was used.

The orientation of the geometrical axis OQ (see fig. 3) of the specimen along which the conductivity was measured relative to the crystal axes OX, OY, and OZ was defined by the angles θ and ϕ, which its projections on the planes XY and XZ respectively made with the X axis. As aluminium crystals are cubic the axes are interchangeable, so it could always be arranged that $45° > \theta > \phi$.

Fig. 3.

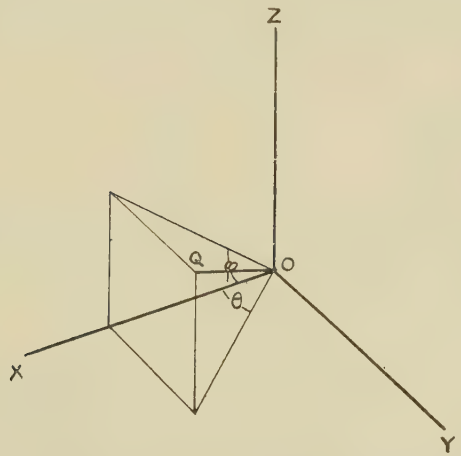

Actually, however, the orientation obtained from the Laue photograph was that of the beam of X-rays which was at right angles to the geometric axis of the specimen. It was the orientation of the latter which was required. This orientation was obtained from the former by stereographic projection.

Determination of the Resistance.

The determination of the resistance was more difficult than would appear at first sight, since it was extremely small, being of the order of 10^{-5} ohm. The following was the method adopted :—

A current of about 9 amperes was passed through the

single crystal by means of screw contacts at K and L (see figs. 1 and 2), and the potential difference between two points near the middle of its narrow portion was compared with the potential difference between two points on a copper rod, $\frac{1}{4}$ in. diameter, through which the same current was passed, the latter serving as a standard resistance. The tappings were taken off the single crystal by means of two brass pins fixed 4 cm. apart in an ebonite block. One of the points on the copper rod was movable and was adjusted until the potential difference between it and the fixed point was equal to that between the two brass pins on the single crystal. As it would have been difficult to measure the position of the movable point on the copper rod with sufficient accuracy, the following modification was adopted. A copper wire 5 metres long was placed in parallel with the rod, and the tapping off

Fig. 4.

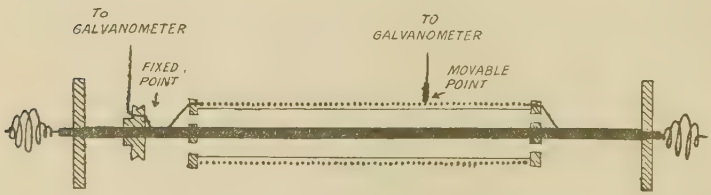

was made from the wire. For convenience this wire was wound on an insulating cylinder (a brass tube 4 cm. diameter which had been coated with asbestos paper and shellac). The copper rod was the axis of the cylinder. The apparatus, which might be named a potentiometer resistance, is shown in fig. 4.

The two points on the crystal and the two points on the potentiometer resistance were connected in turn to the galvanometer, the slide on the resistance being adjusted until the same deflexion was observed in each case. For increased accuracy an adjustable opposing e.m.f. was introduced into the galvanometer circuit and adjusted so that the galvanometer deflexion was zero. This had the further advantage that since the galvanometer took no current the lines of flow in the conductor were not disturbed by the tappings. The circuit is shown in fig. 5.

The whole circuit except the galvanometer was placed in a bath of paraffin oil whose temperature was kept

constant at 25° C. to within 0·1° C. by means of a toluene-mercury thermostatic regulator operating an electric heater. The bath was kept well stirred by rotating vanes. These precautions, besides ensuring that the resistances were measured at a constant temperature, reduced thermoelectric e.m.f.'s. to negligible values.

The potentiometer resistance was calibrated by observing the galvanometer deflexion when connected across adjacent turns of the potentiometer coil, and the resistances of the aluminium crystals were found in terms of this as a standard. As only relative resistances were required, it was not necessary to determine its absolute resistance.

Fig. 5.

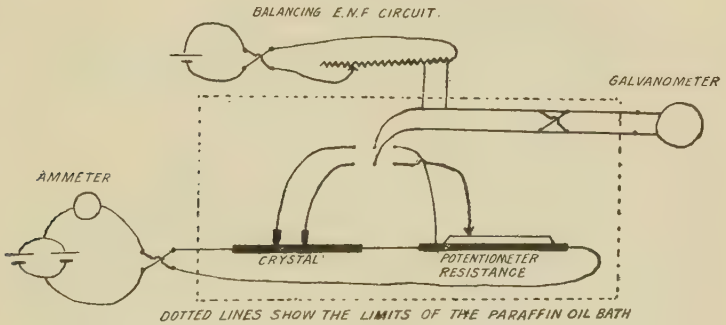

Determination of the Cross-sectional Area.

As the cross-section of a test piece was only approximately rectangular none of the straightforward methods for the measurement of its area could be used. The first method to be tried was to obtain the contour of the surfaces, using a high-power microscope. This, however, besides being very tedious, was only accurate to 1 per cent., which was not sufficient for these experiments.

The method finally adopted was to immerse the crystal to two known depths in paraffin oil, the difference in the weight of the crystal in the two cases being a measure of its volume and hence of its cross-sectional area.

The crystal was suspended vertically from one arm of the beam of a balance in a cylindrical glass vessel B (see fig. 6), which could be filled with paraffin from the pipette C or emptied by means of the two-way tap E, the pipette C being filled from the reservoir D by means of the tap G.

The paraffin having been adjusted to the level b in B and to the mark d in C, the crystal was weighed. Tap E was then opened, G being closed, and when the paraffin had flowed from C to B, its new level being c, the crystal was reweighed.

Fig. 6.

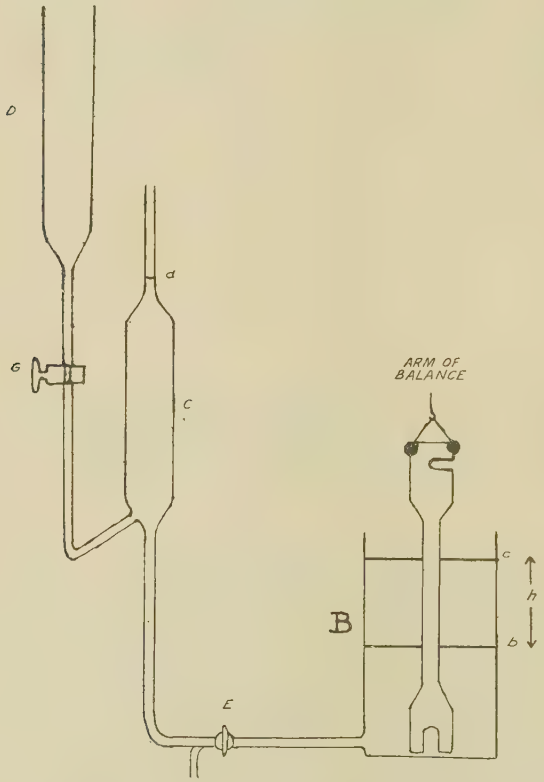

Let W = difference in weight of the crystal in the two cases,

h = distance bc.

ρ = density of the paraffin,

a = cross-sectional area of crystal.

Then $W = g\rho ha$.

Now, as only relative cross-sectional areas were required, W was taken as a measure of a, since g, ρ, and h are constants. Actually, small corrections had to be made to allow for the variation of ρ and h with temperature and for the second order effect of a on h.

The dimensions of the apparatus were chosen so that h should be approximately 4 cm.. the distance apart of the brass pins between which the potential difference was measured. Thus it was assured that levels b and c could be made to coincide with the positions on the crystal where the brass pins had rested.

Accuracy of the Results.

In order to obtain as accurate results as possible it was necessary to see what errors were likely to arise in the various measurements, and to minimize those which were of a large magnitude.

Errors in the Determination of the Orientation of the Crystal.

The crystal could be set relative to the beam of X-rays and to the photographic plate, so that its position was known to within 1°. When the Laue photograph did not coincide with one of the comparison photographs, interpolation between adjacent photographs had to be resorted to. The error involved was not greater than 2°. Owing to inaccuracies in drawing the stereographic projection a further error of not more than 2° in both θ and ϕ might be expected.

Hence the maximum error in the values of θ and ϕ was 5°.

Errors in the Determination of the Cross-sectional Area.

The crystals were weighed to half a milligram, and as the difference between the weight with the paraffin at level b and that with the paraffin at c was of the order of 0·8 gm. this gave an accuracy of 1 part in 1600.

Immediately the second weighing was completed the temperature of the paraffin was taken, and a correction was made to reduce the readings to a standard temperature (20° C.).

Let $3\alpha_{Al}$, $3\alpha_G$, and $3\alpha_P$ be the coefficients of cubical expansion of aluminium, glass, and paraffin respectively.

Let V = volume of the pipette,
A = cross-sectional area of the cylindrical glass vessels − cross-sectional area of the crystal,
a = cross-sectional area of the crystal,
ρ = density of paraffin,
W = difference in weight of the crystal,
W_1 = difference in weight of the crystal, at (20 + T) C,
} at 20°C.

At (20 + T°) C. difference in height of the two levels

$$= \frac{V(1+3\alpha_G T)}{A(1+2\alpha_G T)} = \frac{V(1+\alpha_G T)}{A};$$

$$\therefore\ W = g\frac{\rho}{1+3\alpha_P T}\cdot a(1+2\alpha_{Al}T)\cdot\frac{V(1+\alpha_G T)}{A};$$

$$\therefore\quad a = \frac{W_1 A}{g\rho V}\{1+(3\alpha_P-\alpha_G-2\alpha_{Al})T\}.$$

Substituting values for α_{Al}, α_G, and α_P,

$$a = \frac{W_1 A}{g\rho V}\left\{1+\frac{90-0{\cdot}9-5{\cdot}1}{10^5}T\right\}$$

$$= \frac{W_1 A}{g\rho V}\left\{1+\frac{84}{10^5}T\right\}.$$

Thus $$W = W_1\left\{1+\frac{84}{10^5}T\right\}.$$

As T was seldom more than 5° C., the correction for temperature was usually less than 4 parts in 1000. Consequently any errors involved were of the second order and could be ignored.

Another correction had to be applied, for the height which the paraffin rose in the cylindrical vessel B, although constant for any one crystal, varied slightly from crystal to crystal owing to differences in their cross-sectional areas.

Let h_1 = height paraffin rose when no crystal was in the vessel,

h_2 = height paraffin rose when a crystal of cross-sectional area a was present.

Then $$h_1(A+a)=h_2A,$$

or $$h_1=h_2\left(1-\frac{a}{A}\right).$$

Now $A+a$ was 41 sq. cm. and a cross-sectional area of 0·29 sq. cm. was equivalent to a difference in weight of 0·95 gm.;

$$\therefore \quad h_1=h_2\left(1-\frac{0\cdot29\ W_{observed}}{40\cdot7\times0\cdot95}\right)$$

$$=h_2\,(1-0\cdot0074\,W_{observed});$$

$$\therefore\ W_{corrected}=W_{observed}\left(1-0\cdot0074\,W_{observed}\right).$$

This correction, too, was small, being just over $\frac{1}{2}$ per cent.; so errors in it could be ignored.

Paraffin was used as the liquid because it wets aluminium and forms a horizontal surface of contact. It also possessed the property of dissolving any slight amount of grease which might have been on the surface of the crystal. Hence its surface tension was not likely to be altered seriously by the condition of the aluminium surface. Now the surface tension was 27 dynes per cm. and the perimeter of a crystal 2·4 cm., so that a factor of 65 dynes, or 0·065 gm., was introduced into the weighing. A variation therefore of 1 per cent. in either the perimeters at *b* and *c*, or the surface tension between the two weighings would affect the result by 0·00065 gm., or 1 part in 1400. To minimize changes in the surface tension the crystal was washed in paraffin, which was then allowed to drain. Having been suspended from the balance, it was immersed to well above the level *c* in paraffin, which was afterwards allowed to drain off before any weighings were attempted. It was unlikely, therefore, that the surface conditions would alter further when the crystal was again immersed in paraffin during the weighings. Changes of temperature, although affecting the surface tension and therefore individual weighings, cancelled out when the differences were taken.

That the crystal was suspended vertically was determined by means of two plumb lines, hung in the front and at the side of the balance case respectively. As the deviation from the vertical was certainly less than 2°, the error from the source was less than 1 part in 2000.

The same paraffin was used in all the determinations. As it had been fractionated several times there was little chance of its density changing owing to the evaporation of its more volatile constituents. However, as a check a standard test piece was kept whose cross-section was measured periodically, but no apparent change was observed.

The crystal was always allowed to drain before any series of weighings was commenced. A period of half an hour was found to be necessary, after which time its weight was found to remain constant.

That the cross sectional area of the glass vessel B was uniform was tested by suspending a test piece at various heights in it and measuring its cross-section between the same two marks on the aluminium. No measurable variation was noted. Even if the cross-section had varied, it would not have mattered provided the level b was initially the same in all the measurements.

The height h was not 4 cm. exactly, but only 3·85 cm. This was allowed for by varying the initial level b over a distance of 2 mm. and repeating the weighings several times; but as the crystals were found to be of such uniform cross-section no great trouble was taken to correct for this.

Owing to the etching producing small surface pits the cross-section measured was slightly larger than that which carried the electric current. The error due to this was negligible, as the value obtained for the specific resistance of an unetched crystal was found to be the same as that obtained after etching.

Thus it seemed that the maximum error in the determination of the cross-sectional area would be 2 parts in 1000. This was borne out by repeatingly determining the cross-sectional area of the standard test piece. Eleven determinations were made, and the maximum deviation from the mean was 0·16 per cent.

As the determination of the cross-sectional area was repeated twice (and in many cases four times) for each crystal, the mean being taken, the probable accuracy of the result was 1 part in 1000.

Errors in the Measurement of the Electrical Resistance.

The difference in the potential of the two brass pins was 3×10^{-5} volt when a current of 1 ampere was passed

through the crystal. Now, as the thermal e.m.f. might be of the same magnitude, it was necessary to make errors due to it as small as possible. By immersing the whole circuit except the galvanometer in a bath of paraffin oil whose temperature was kept constant to within 0·1° C., differences in temperature of bimetallic junctions were reduced. Brass pins were used to make contact with the aluminium, as brass-aluminium has the small thermal e.m.f. of $0{\cdot}3\times10^{-6}$ volt per degree. However, other bimetallic junctions existed in the circuit, as it was impracticable to have all the connexions including the galvanometer coils made of brass. They were all copper-brass junctions (thermal e.m.f. $3{\cdot}5\times10^{-6}$ volt per degree), but they were placed in pairs near together and were fairly massive, so that differences in temperature of more than 0·05° C. were not likely to occur. Thus the maximum thermal e.m.f. likely to exist in the circuit was $0{\cdot}35\times10^{-6}$ volt. By increasing the current through the crystal to 9 amperes the potential difference between the pins was raised to 27×10^{-5} volt, which reduced the maximum error to 1 part in 800. The error was still further reduced by reversing the galvanometer connexions and by reversing the current through the crystal, and taking the mean of the four readings. Also, when a balance had been obtained the current through the crystal and the balancing e.m.f. current were quickly shut off. The galvanometer was then connected in turn to the crystal and to the potentiometer resistance to see if any thermal e.m.f. existed to deflect the galvanometer. This and the previous precaution were, however, really unnecessary, as the thermal e.m.f.'s. never exceeded 1 part in 2000.

Errors due to changes of resistance with temperature were negligible. A variation of 0·1° C. in the temperature of the bath would have affected the relative resistances of the aluminium crystal and the potentiometer by 1 part in 20,000. A difference in their relative temperatures of 0·1° C., however, would have involved an error of 1 part in 2000.

Care was taken to see that all contacts were clean and free from moisture, as galvanic action could have produced appreciable errors.

Erratic or large variations in the main current or in the balancing e.m.f. circuit would have been a source of difficulty. It was found satisfactory to use two large

capacity accumulators arranged in parallel to produce the main current, while a small accumulator was sufficient for the balancing e.m.f. circuit.

The galvanometer, which was of the Broca type, had its sensitivity adjusted so that $1{\cdot}5\times10^{-7}$ volt deflected the spot of light 1 cm. at 1 metre distance. As readings to the nearest cm. were taken, this meant that the sensitivity was 1 part in 2000.

Fig. 7.

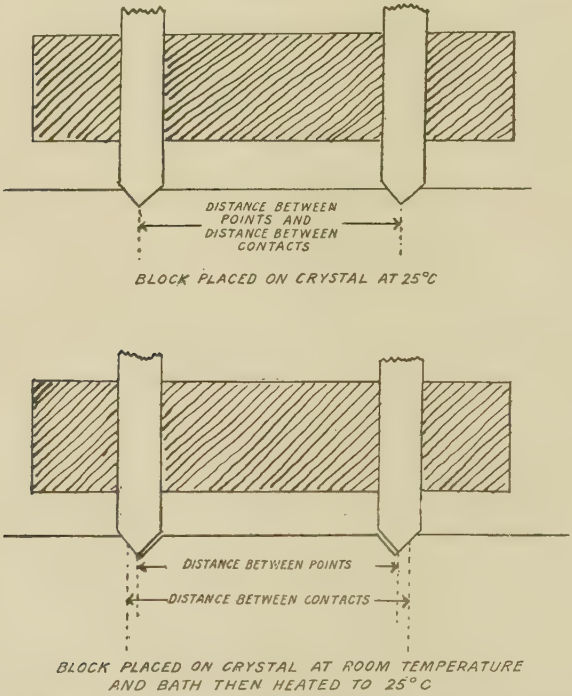

The position of the sliding contact on the potentiometer resistance could be read to 1 part in 2000. The potentiometer wire was calibrated, but was found to be uniform to this degree of accuracy.

The distance between the two brass pins was constant in all the experiments, as the temperature was constant. Nevertheless a potential source of error existed at the contacts which might easily have been overlooked. When the ebonite block with the brass pins was placed on the crystal before the bath was heated, and the temperature

raised to 25° it was found that the resistance of the crystal was 0·5 per cent. greater than when the ebonite block was placed on the crystal at 25° C. This was due to the fact that in the former instance, owing to the greater expansion of ebonite than aluminium, the brass pins pressed against the outsides of the depressions they had made instead of being central. This increased the distance between the points of contact, giving an apparent increase in resistance. Fig. 7 shows this in an exaggerated form. It was therefore essential for the bath to be at 25° C. before the block was placed on the crystal..

The length of the parallel portion of the crystals was 9 cm., and the potential difference was taken between points 4 cm. apart in the middle of this section. That parallel lines of flow existed in this central portion was shown by shifting the position of the ebonite block containing the points 1 cm. from the central position, no change in resistance being observed. Further, the lines of flow were not disturbed by the tappings, as in the balanced position the galvanometer took no current.

Thus it seemed that the maximum error in the measurement of the resistance would be 1 part in 1000. Repeated determinations showed that the error was actually somewhat less than this.

Errors due to Impurities in the Aluminium.

The conductivity of metals is affected greatly by traces of impurity, especially when the metals are in a very pure condition. Large variations in the amount of impurity in the aluminium were unlikely, as the test pieces of each different purity were obtained in one batch. Actually the eleven test pieces of the 99·95 per cent. aluminium were stamped out of the same sheet of the metal. The conductivities of these, measured before treatment, varied by 0·6 per cent. Hence it seemed likely that variations of greater magnitude would occur for the other purities. Unfortunately with nearly all the 99·6 per cent. aluminium, and with about half of the 99·7 per cent. aluminium, the single crystals had already been made before the apparatus for measuring the specific resistances had been completed. Thus it was not possible to measure their resistances before treatment, and so obtain more accurate comparisons of their conductivity as single crystals.

Errors due to Deformation of the Atomic Lattice.

The single crystals were not ground, polished, or worked in any way. This rendered any deformation of the atomic lattice unlikely.

RESULTS.

Per cent. purity aluminium.	Identification mark.	Treatment batch.	Relative specific resistance in the states :— Rolled.	Annealed.	Stretched.	Single crystal.	Orientation: θ.	φ.
99·6	G10	C	—	—	—	1937	42	38
	A18	C	—	—	—	1936	*	
	A9	A	—	—	—	1934	35	33
	G8	C	—	—	—	1934	11	1
	15	C	—	—	—	1933	43	17
	1	G	1937	1920	—	—	—	—
	A6	A	—	—	—	1930	37	29
	A10	A	—	—	—	1929	32	17
	A8	A	—	—	—	1928	30	4
	G6	C	—	—	—	1927	33	12
	4	E	—	1910	—	1927	26	4
	3	F	1932	1909	1911	1930	*	
	A3	A	—	—	—	1921	41	34
	A20	C	—	—	—	1921	40	31
	A1	A	—	—	—	1919	35	14
	A5	A	—	—	—	1917	23	8
99·7	Y7	C	—	—	—	1912	11	2
	Y5	A	—	—	—	1911	28	8
	V4	C	—	—	—	1910	45	3
	A16	C	—	—	—	1906	29	3
	V10	E	—	1879	—	1902	17	11
	V7	E	—	1878	—	1900	*	
	V8	E	—	1879	—	1899	*	
	V9	E	—	1879	—	—	—	—
	V6	E	—	1878	—	—	—	—
	V11	E	—	1875	—	—	—	—
	2	E	1875	1873	—	1898	*	
99·95	C	E	—	1855	—	—	—	—
	I	E	—	1850	—	—	—	—
	F	F	1849	1849	1850	—	—	—
	K	F	1848	1849	1845	1864	*	
	G	E	—	1849	—	1869	34	12
	H	F	1853	1848	1849	—	—	—
	D	F	1842	1846	1843	—	—	—
	J	E	—	1845	—	1866	22	21
	E	E	—	1844	—	—	—	—
	B	D	—	—	—	1863	*	

* Orientation not determined.

Results.

The results showing the relative specific resistances of the twenty-seven single crystals and of test pieces in the various stages of their treatment appear in the table. It must be remembered that as the accuracy was 1 part in 500 there may be an error of 4 in the last figure of each result.

In considering these results the following points were noted :—

(1) The fifteen single crystals of 99·6 per cent. purity aluminium show a variation in their specific resistances of 1·0 per cent., the eight single crystals of 99·7 per cent. purity aluminium show a variation of 0·7 per cent., while the four single crystals of 99·95 per cent. purity show a variation of 0·3 per cent. The results were plotted graphically against the orientations, but no connexion could be found between the variations in specific resistance and the orientation of the specimen relative to the crystal axis. The conclusion is, therefore, that the resistance is independent of direction.

(2) Annealing for six hours at 550° C. reduced the resistance of the 99·6 per cent. purity aluminium by 1 per cent., but had no effect on the resistances of the purer aluminium.

(3) Permanently stretching the annealed aluminium by 1–2 per cent. had no measurable effect on the specific resistance.

(4) The specific resistances of the single crystals of all three purities of aluminium were found to be about 1 per cent. greater than those of the annealed test pieces from which they were made.

(5) The specific resistance of the 99·95 per cent. purity aluminium was 2 per cent. less than that of the 99·7 per cent. purity aluminium, which, in turn, was 1 per cent. less than that of the 99·6 per cent. purity aluminium.

Discussion of Results.

Aluminium crystals belong to the face-centred cubic system, so the experimental results are in agreement with the theories of Drude, Bridgman [8], and Sommerfeld [9], all of which predicted that cubic crystals are isotropic.

Whether Lindemann's theory[10] is in agreement cannot be said definitely, as unfortunately it does not lend itself to detailed mathematical treatment.

The 1 per cent. increase in specific resistance of aluminium when converted into a single crystal may at first appear curious, but the explanation is probably that the prolonged annealing causes the impurities to go into solid solution. Microscopic examination shows that this does happen, so that an increase in specific resistance is to be expected. The fact that the increase is approximately the same for all three degrees of purity is, however, strange, since the 99·6 per cent. aluminium contains eight times as much impurity as the 99·95 per cent. material. On the other hand, it is known that the first small amounts of impurity cause a relatively greater effect than later additions, so that the results are not altogether improbable, and can hardly be discussed further until a more detailed knowledge of the effects of small amounts of impurity is available. Another possible explanation is that the boundaries of the microcrystals are much better conductors than the crystals themselves; but if this conception is to give results of the right magnitude, the boundaries will have to be almost supraconducting at ordinary temperatures, which appears improbable.

In conclusion, I should like to thank Professor Lindemann for suggesting the subject of the research, Dr. W. Hume-Rothery for his invaluable help and advice, and Mr. R. G. Milton, along with many others, for numerous suggestions and criticisms.

I must also thank the British Aluminium Company, and particularly Dr. A. G. C. Gwyer, for the great help which they gave in connexion with this work. Not merely did they present the 99·7 per cent. material, but they arranged specially to roll down the 99·95 per cent. material and to stamp it into suitable shape. Their generous assistance in this matter has materially assisted in bringing this research to a conclusion, and is acknowledged with gratitude.

Summary.

Single crystals of aluminium of 99·6, 99·7, and 99·95 per cent. purity were prepared by the method of Carpenter and Elam, and the orientations of the crystal axes were

determined by the Laue-spot method of Majima and Togino. The cross-sectional areas were determined by weighing with different levels immersed in paraffin, and the electrical resistances were measured by a potentiometer method. Within the accuracy of the experimental methods (1 per cent.) the specific resistance of a single crystal of given purity was found to be independent of the orientation relative to the crystal axes. The specific resistance of a single crystal was about 1 per cent. greater than that of the annealed material from which it was prepared, a result ascribed to the gradual solution of impurities during the long annealing process used for preparing the single crystal.

References.

(1) Bridgman, Proc. Amer. Acad. lx. p. 305 (1925); Gruneisen und Goens, *Zs. Phys.* xxvi. p. 250 (1924).
(2) Masima and Sachs, *Zeits. f. Phys.* l. p. 171 (1928).
(3) Bridgman, *loc. cit.*
(4) Carpenter and Elam, Proc. Roy. Soc. A, c. p. 329 (1921).
(5) Bridgman, Proc. Amer. Acad. lx. p. 313 (1925).
(6) Shimizu, Sci. Report Tohoku Univ. xvi. p. 621 (1927).
(7) Majima and Togino, Sci. Papers Inst. Chem. & Phys. Res. Tokio, no. 111 (1927).
(8) Bridgman, Phys. Rev. xvii. p. 161 (1921).
(9) Sommerfeld, *Naturwissenschaften*, xv. p. 825 (1927).
(10) Lindemann, Phil. Mag. xxix. p. 170 (1915).

Clarendon Laboratory,
Oxford.
December 1930.

VIII. *The Elastic Ring acted upon by Equal Radial Forces.* *By* C. E. Larard, *M.Inst.C.E.**

THIS investigation deals with a circular elastic ring of uniform cross-sectional area A, subjected to the action of any number N, of radial forces P, as indicated in fig. 1, and also in addition the same number of radial forces Q as indicated in fig. 4; such that

$$2\alpha N = 2\pi \quad \text{or} \quad \alpha = \frac{\pi}{N}.$$

The ring may be considered as free in space with its centre stationary. It is assumed that the radial thickness

* Communicated by the Author.

or dimension of the ring and the radial strain or displacement at any point in the ring are very small compared with the radius of the ring.

The following are the principal results obtained analytically :—

(*a*) The hoop-stresses of the ring ;

(*b*) the radial shear forces ;

(*c*) the flexural moments ;

(*d*) the work of deformation ;

(*e*) the radial deformations ; and

(*f*) a special proof of the Maxwell–Rayleigh reciprocal relationship when considered in connexion with the elastic ring, so as to include separately the reciprocity between forces and strains due to flexure, direct stresses, and shear forces respectively.

Fig. 1.

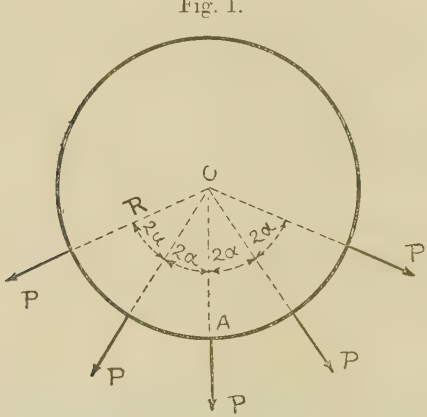

N equal radial forces such that $N \cdot 2\alpha = 2\pi$.

Consider first the case of N equal radial forces P, as in fig. 1, remembering that $\alpha = \frac{\pi}{N}$.

Flexural Couple and Forces at any Radial Section of Ring.

Consider the arc interval AB between two adjacent forces P and P (fig. 2). At each radial section A or B there are a direct tangential force T_1, a shear force $P_1 = \frac{P}{2}$, and a flexural moment M_1.

Resolving the forces parallel to OC, the median radial line, gives

$$2P_1 \cos\alpha = 2T_1 \sin\alpha,$$

from which
$$T_1 = P_1 \cot\alpha = \frac{P}{2}\cot\alpha. \quad . \quad . \quad . \quad . \quad (1)$$

The flexural moment M at angle θ is given by

$$M = M_1 + \frac{P}{2} R \sin\theta - T_1 R(1-\cos\theta). \quad . \quad . \quad (2)$$

Fig. 2.

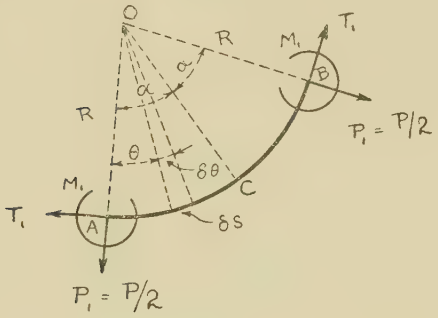

Since there is no change of slope at A or B, and since M_1 has a particular value determined by the flexural strain energy of AB, ${}_{M}U_{2\alpha}$ being a minimum *,

$$\therefore \qquad \frac{d\,{}_{M}U_{2\alpha}}{d\,M_1} = 0.$$

The work function for bending

$${}_{M}U_{2\alpha} = \frac{1}{2EI}\int_0^{2\alpha} M^2 ds = \frac{R}{2EI}\int_0^{2\alpha} M^2 d\theta, \quad . \quad . \quad (3)$$

where E denotes Young's modulus of elasticity, I the second moment of area of the cross-section, and M the variable moment in AB.

Differentiating (3) and equating to zero

$$\frac{d\,{}_{M}U_{2\alpha}}{dM_1} = \frac{R}{EI}\int_0^{2\alpha} M\frac{dM}{dM_1}\,d\theta = 0. \quad . \quad . \quad . \quad (4)$$

* Castigliano Theorem: 'L'Equilibre des Systèmes Elastiques,' 1879. (Translated by E. S. Andrews.)

Substitute in (4) the value of M given in (2) and write $\frac{dM}{dM_1} = 1$, giving

$$\frac{d_M U_{2\alpha}}{d M_1} = \frac{R}{EI}\int_0^{2\alpha}\left[M_1 + \frac{PR}{2}\sin\theta - T_1 R(1-\cos\theta)\right]d\theta = 0. \quad . \quad . \quad . \quad (5)$$

Integrating and solving give the value

$$M_1 = \frac{PR}{2}\left(\cot\alpha - \frac{1}{\alpha}\right), \quad . \quad . \quad . \quad . \quad . \quad (6)$$

which is the maximum negative bending-moment in the ring.

Substituting this value and (1) in (2),

$$M = \frac{PR}{2}\left[\left(\cot\alpha - \frac{1}{\alpha}\right) + \sin\theta - \cot\alpha(1-\cos\theta)\right] \quad (7\,a)$$

$$= \frac{PR}{2}(\sin\theta + m\cos\theta - n), \quad . \quad . \quad . \quad . \quad . \quad . \quad (7\,b)$$

Fig. 3.

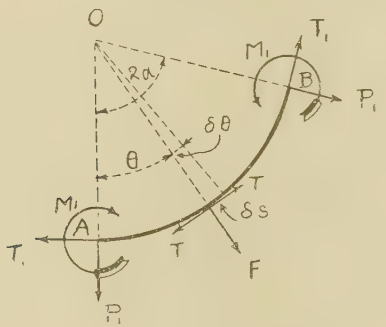

where $m = \cot\alpha$ and $n = \frac{1}{\alpha}$.

When $\theta = \alpha$ the moment at point C becomes

$$M_C = \frac{PR}{2}\left(\operatorname{cosec}\alpha - \frac{1}{\alpha}\right). \quad . \quad . \quad . \quad . \quad (8)$$

The hoop-stress T at angle θ (see fig. 3)

$$= \frac{P}{2}\sin\theta + T_1\cos\theta = \frac{P}{2}(\sin\theta + \cot\alpha\,.\cos\theta), \quad . \quad (9)$$

the shear force F (fig. 3)

$$= \frac{P}{2}\cos\theta - T_1\sin\theta = \frac{P}{2}(\cos\theta - \cot\alpha\sin\theta). \quad . \quad (10)$$

Flexural resilience or strain energy is given by the work function ${}_{M}U_{2\alpha}$ in equation (3).

Substituting in this equation the value of M given in (7 *b*),

$$ {}_{M}U_{2\alpha} = \frac{R}{2EI}\int_0^{2\alpha}\left[\frac{PR}{2}(\sin\theta + m\cos\theta - n)\right]^2 d\theta, \quad (11) $$

which, on integration and simplification, becomes

$$ {}_{M}U_{2\alpha} = \frac{P^2R^3}{8EI}\left[\alpha\,\mathrm{cosec}^2\alpha + \cot\alpha - \frac{2}{\alpha}\right]. \quad . \quad . \quad (12) $$

Hoop-stress resilience or strain energy ${}_{T}U_{2\alpha}$ is

$$ {}_{T}U_{2\alpha} = \frac{R}{2EA}\int_0^{2\alpha} T^2 . d\theta. \quad . \quad . \quad . \quad . \quad (13) $$

Substituting in this equation the value of T given in (9),

$$ {}_{T}U_{2\alpha} = \frac{R}{2EA}\int_0^{2\alpha}\left[\frac{P}{2}(\sin\theta + \cot\alpha\cos\theta)\right]^2 d\theta \; . \quad (14) $$

$$ = \frac{P^2R}{8EA}\left[\alpha\,\mathrm{cosec}^2\alpha + \cot\alpha\right]. \quad . \quad . \quad . \quad . \quad (15) $$

Shear resilience, ${}_{F}U_{2\alpha}$.

$$ {}_{F}U_{2\alpha} = \frac{CR}{2GA}\int_0^{2\alpha} F^2 d\theta. \quad . \quad . \quad . \quad . \quad (16) $$

Substituting in (16) the value of F given in equation (10),

$$ {}_{F}U_{2\alpha} = \frac{CR}{2GA}\int_0^{2\alpha}\left[\frac{P}{2}(\cos\theta - \cot\alpha\cos\theta)\right]^2 d\theta, \quad (17) $$

which on simplification gives

$$ {}_{F}U_{2\alpha} = \frac{CRP^2}{8GA}\left[\alpha\,\mathrm{cosec}^2\alpha - \cot\alpha\right]. \quad . \quad . \quad (18) $$

In this equation G denotes the transverse modulus of elasticity and C is a constant depending upon the form of the cross-section.

The total strain energy of the ring, U, is N times the sum of work quantities given by equations (12), (15), and (18) ; that is

$$ U = N({}_{M}U_{2\alpha} + {}_{T}U_{2\alpha} + {}_{F}U_{2\alpha}) \quad . \quad . \quad . \quad . \quad . \quad . \quad . \quad . \quad (19) $$

$$ = \frac{NP^2R}{8}\left[\frac{R^2}{EI}\left(\alpha\,\mathrm{cosec}^2\alpha + \cot\alpha - \frac{2}{\alpha}\right)\right. $$

$$ \left. + \frac{1}{EA}(\alpha\,\mathrm{cosec}^2\alpha + \cot\alpha) + \frac{C}{GA}(\alpha\,\mathrm{cosec}^2\alpha - \cot\alpha)\right]. $$

$$. \quad . \quad . \quad (20) $$

Writing

$$I = Ak^2, \qquad G = rE,$$

$$\frac{R^2}{k^2} = h, \quad \text{and} \quad \frac{c}{r} = l,$$

equation (20) takes the form

$$U = \frac{NRP^2}{8EA}\left[\alpha \operatorname{cosec}^2\alpha(h+1+l) + \cot\alpha(h+1-l) - \frac{2h}{\alpha}\right]. \quad . \quad . \quad . \quad (21)$$

The last two additive terms in the brackets ( ) show that the strain energy due to tension and shear are relatively small compared with the work of flexure.

Radial Strain or Displacement of the Point of Application of each P.

Let y_p denote the radial strain at each P, regarding the centre O of the ring as stationary.

The external work done on the ring by the forces P equals $N \times \frac{1}{2}Py_p$, and this must equal the stored strain energy given by (19);

i. e., $$U = \tfrac{1}{2}NPy_P = N({}_M U_{2\alpha} + {}_T U_{2\alpha} + {}_F U_{2\alpha}), \quad . \quad (22)$$

from which

$$y_P = \frac{2}{P}({}_M U_{2\alpha} + {}_T U_{2\alpha} + {}_F U_{2\alpha}). \quad . \quad (23)$$

Substituting the values given in (12), (15), and (18) in (23),

$$y_P = \frac{PR^3}{4EI}\left[\alpha \operatorname{cosec}^2\alpha + \cot\alpha - \frac{2}{\alpha}\right] + \frac{PR}{4EA}\left[\alpha \operatorname{cosec}^2\alpha + \cot\alpha\right] + \frac{CRP}{4GA}\left[\alpha \operatorname{cosec}^2\alpha - \cot\alpha\right] \quad . \quad . \quad . \quad (24)$$

$$= \left\{\begin{matrix}\text{displacement}\\ \text{due to flexure}\end{matrix}\right\} + \left\{\begin{matrix}\text{displacement due}\\ \text{to hoop-stress}\end{matrix}\right\} + \left\{\begin{matrix}\text{displacement}\\ \text{due to shear}\end{matrix}\right\};$$

or combining these three terms as for (21),

$$y_P = \frac{PR}{4EA}\left[\alpha \operatorname{cosec}^2\alpha(h+1+l) + \cot\alpha(h+1-l) - \frac{2h}{\alpha}\right]. \quad . \quad . \quad . \quad (25)$$

The same result as in (24) is obtained by using a Castigliano principle *, namely, that the displacement at the point of application of a force is found by taking the

* Proof in Castigliano's work, indicated in footnote on p. 131.

partial differential coefficient of the work function with respect to the force; thus differentiating both sides of (22) with respect to P_1, and remembering that $P = 2P_1$, we have

$$y_P = \frac{\partial}{\partial P_1}({}_M U_{2\alpha} + {}_T U_{2\alpha} + {}_F U_{2\alpha}) \quad . \quad . \quad . \quad . \quad . \quad (26\,a)$$

$$= \frac{\partial}{\partial P_1}({}_M U_{2\alpha}) + \frac{\partial}{\partial P_1}({}_T U_{2\alpha}) + \frac{\partial}{\partial P_1}({}_F U_{2\alpha}), \quad (26\,b)$$

or the total radial strain at A (see fig. 1), or at the point of application of any P, is the sum of the strains due to flexure, tension, and shear, and is given by taking the sum of the partial differential coefficients of the three work functions for the arc interval between two adjacent forces P.

In its expanded form equation (26 *b*) becomes

$$y_P = \frac{\partial}{\partial P_1}\left[\frac{R}{2EI}\int_0^{2\alpha} M^2 d\theta + \frac{R}{2EA}\int_0^{2\alpha} T^2 d\theta + \frac{CR}{2GA}\int_0^{2\alpha} F^2 d\theta\right] \quad . \quad . \quad . \quad (27\,a)$$

$$= \frac{R}{EI}\int_0^{2\alpha} M \frac{\partial M}{\partial P_1} d\theta + \frac{R}{EA}\int_0^{2\alpha} T \frac{\partial T}{\partial P_1} d\theta + \frac{CR}{GA}\int_0^{2\alpha} F \frac{\partial F}{\partial P_1} d\theta. \quad . \quad . \quad . \quad (27\,b)$$

Substituting the values of the variables M, T, and F given previously, together with their partial differentials with respect to P_1, equation (27 *b*) gives identically the same value for y_p as that given by (24), with the advantage that we avoid having to square the binomial or trinomial terms.

The equation given for y_p gives the radial displacement of the point of application of each P, whether N is an odd or an even number. If N is an even number, then two P's act oppositely in the same line through the centre O, and the total alteration in the diameter of the ring is obviously twice the radial strain at each P.

Consider next the case of the elastic ring with N equal radial forces P together with N equal radial forces Q, acting on the ring as indicated in fig. 4, so that

$$2N\alpha = 2\pi \quad \text{or} \quad \alpha = \frac{\pi}{N},$$

as before.

The following strains will be determined:—

(*a*) The radial displacement at the point of application of each P.

(*b*) The radial displacement at the point of application of each Q.

The Maxwell-Rayleigh reciprocal relationship will then be considered by making the P's and Q's each in turn take zero values.

Consider the equilibrium of the arc interval AC between P and Q (figs. 4 & 5).

Fig. 4.

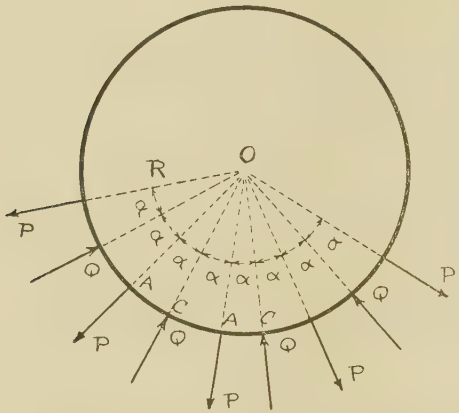

N equal forces P, and N equal forces Q.

Fig. 5.

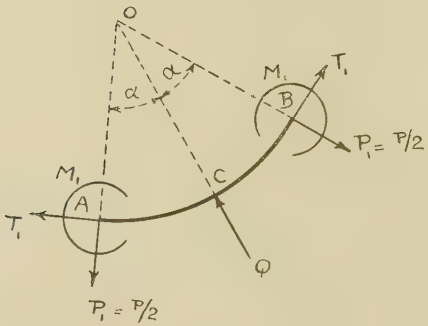

Resolving the forces

$$2P_1\cos\alpha - 2T_1\sin\alpha - Q = 0\ ;$$

$$\therefore \qquad T_1 = \frac{P\cos\alpha - Q}{2\sin\alpha}. \qquad \ldots\ldots \quad (28)$$

The flexural moment at angle θ (fig. 6) is given by

$$M = M_1 + \frac{P}{2} R \sin\theta - T_1 R(1-\cos\theta), \quad . \quad . \quad (29)$$

$$\frac{\partial M}{\partial M_1} = 1.$$

Let ${}_M U_\alpha$ = work of flexure for the arc AC.
Since there is no change of slope at A

$$\frac{\partial {}_M U_\alpha}{\partial M_1} = 0.$$

Fig. 6.

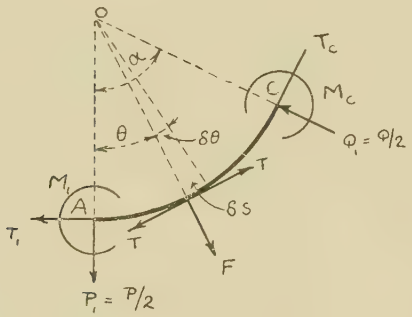

The flexural work

$${}_M U_\alpha = \frac{1}{2EI}\int_0^\alpha M^2 ds$$

$$= \frac{R}{2EI}\int_0^\alpha M^2 d\theta,$$

and the differential of this is

$$\frac{d_M U_\alpha}{dM_1} = \frac{R}{EI}\int_0^\alpha M \frac{dM}{dM_1} d\theta. \quad . \quad . \quad . \quad . \quad (30)$$

Substituting in (30) the values of M and its differential given in (29)

$$\frac{d_M U_\alpha}{dM_1} = \frac{R}{EI}\int_0^\alpha \left[M_1 + \frac{PR}{2}\sin\theta - T_1 R(1-\cos\theta)\right] d\theta = 0,$$

. . . (31)

which on integration and reduction, and taking the value of T_1 as given in (28), gives

$$M_1 = \frac{PR}{2}\left(\cot\alpha - \frac{1}{\alpha}\right) + \frac{QR}{2}\left(\frac{1}{\alpha} - \operatorname{cosec}\alpha\right). \quad . \quad (32)$$

Substituting this value for M_1 in (29),

$$M = P_1R\left[\sin\theta + \cot\alpha\cos\theta - \frac{1}{\alpha}\right] + Q_1R\left[\frac{1}{\alpha} - \operatorname{cosec}\alpha\cos\theta\right], \quad . \quad . \quad . \quad (33)$$

$$\frac{\partial M}{\partial P_1} = R\left(\sin\theta + \cot\alpha\cos\theta - \frac{1}{\alpha}\right), \quad . \quad . \quad . \quad . \quad . \quad . \quad . \quad (34)$$

$$\frac{\partial M}{\partial Q_1} = R\left(\frac{1}{\alpha} - \operatorname{cosec}\alpha\cos\theta\right). \quad . \quad . \quad . \quad . \quad . \quad . \quad . \quad (35)$$

Radial Displacement at Point of Application of each Q.

Referring to fig. 6 it will be seen that for a radial section of arc at angle θ the direct hoop-stress

$$T = T_1\cos\theta + P_1\sin\theta, \quad . \quad . \quad . \quad (36)$$

and substituting (28) for T_1

$$T = P_1(\sin\theta + \cot\alpha\,.\,\cos\theta) - \frac{Q_1\cos\theta}{\sin\alpha}, \quad . \quad . \quad (37)$$

$$\frac{\partial T}{\partial P_1} = (\sin\theta + \cot\alpha\cos\theta), \qquad \frac{\partial T}{\partial Q_1} = -\frac{\cos\theta}{\sin\alpha}. \quad (38)$$

The shear force

$$F = P_1(\cos\theta - \cot\alpha\sin\theta) + Q_1\frac{\sin\theta}{\sin\alpha}, \quad . \quad . \quad (39)$$

$$\frac{\partial F}{\partial P_1} = (\cos\theta - \cot\alpha\sin\theta), \qquad \frac{\partial F}{\partial Q_1} = \frac{\sin\theta}{\sin\alpha}. \quad (40)$$

The total strain energy for the arc AC is

$$U = U_M + U_T + U_F, \quad . \quad . \quad . \quad . \quad (41)$$

where the terms on the right represent, respectively, the work for flexure, for direct hoop-stress, and for shear.

By the Castigliano principle

$$y_Q = \frac{\partial U}{\partial Q_1} = \frac{\partial U_M}{\partial Q_1} + \frac{\partial U_T}{\partial Q_1} + \frac{\partial U_F}{\partial Q_1}, \quad . \quad . \quad (42)$$

giving the radial strain or displacement at the point of application of each Q.

Writing equation (42) in the expanded form for calculation

$$\frac{\partial U}{\partial Q_1} = \frac{\partial}{\partial Q_1}\left[\frac{R}{2EI}\int_0^\alpha M^2 d\theta + \frac{R}{2EA}\int_0^\alpha T^2 d\theta + \frac{CR}{2GA}\int_0^\alpha F^2 d\theta\right] = y_{Q_1}$$

$$= \frac{R}{EI}\int_0^\alpha M\frac{\partial M}{\partial Q_1}d\theta + \frac{R}{EA}\int_0^\alpha T\frac{\partial T}{\partial Q_1}d\theta + \frac{CR}{AG}\int_0^\alpha F\frac{\partial F}{\partial Q_1} = y_{Q_1}. \quad . \ . \ . \quad (43)$$

The values of M, T, and F and their partial differentials are given, respectively, in (33), (37), (39), and (35), (38), and (40).

Substituting these in (43) and keeping the three terms distinct throughout for the purpose of further analysis, we have

$$y_Q = \frac{R}{EI}\int_0^\alpha \left[P_1 R\left(\sin\theta + \cot\alpha\cos\theta - \frac{1}{\alpha}\right) + Q_1 R\left(\frac{1}{\alpha} - \operatorname{cosec}\alpha\cos\theta\right)\right] R\left(\frac{1}{\alpha} - \operatorname{cosec}\alpha\cos\theta\right)d\theta$$

$$+ \frac{R}{EA}\int_0^\alpha \left[P_1(\sin\theta + \cot\alpha\,.\,\cos\theta) - \frac{Q_1\cos\theta}{\sin\alpha}\right]\left(-\frac{\cos\theta}{\sin\alpha}\right)d\theta$$

$$+ \frac{CR}{GA}\int_0^\alpha \left[P_1(\cos\theta - \cot\alpha\sin\theta) + \frac{Q_1\sin\theta}{\sin\alpha}\right]\left(\frac{\sin\theta}{\sin\alpha}\right)d\theta. \quad . \ . \ . \quad (44)$$

Integrating and reducing, equation (44) becomes

$$y_Q = \frac{PR^3}{4EI}\left[\frac{2}{\alpha} - \operatorname{cosec}\alpha(\alpha\cot\alpha + 1)\right] + \frac{QR^3}{4EI}\left[\alpha\operatorname{cosec}^2\alpha + \cot\alpha - \frac{2}{\alpha}\right] \quad (45a)$$

$$+ \frac{PR}{4EA}\left[-\operatorname{cosec}\alpha(1 + \alpha\cot\alpha)\right] + \frac{QR}{4EA}\left[\alpha\operatorname{cosec}^2\alpha + \cot\alpha\right] . \ . \quad (45b)$$

$$+\frac{CRP}{4GA}[\operatorname{cosec}\alpha(1-\alpha\cot\alpha)]$$

$$+\frac{CRQ}{4GA}[\alpha\operatorname{cosec}^2\alpha-\cot\alpha]. \quad . \quad (45\,c)$$

Line (45 *a*) gives the radial displacement at Q due to the flexural moments, line (45 *b*) the radial displacement due to hoop-stress, (45 *c*) the radial strain at Q due to the shear forces, and the sum of the three gives the total radial strain at Q when all three straining actions are taken into account.

Radial Displacement y_P *at the Point of Application of each* P.

This displacement is arrived at in a similar way to that of y_Q, that is

$$y_P=\frac{\partial U}{\partial P_1}=\frac{\partial U_M}{\partial P_1}+\frac{\partial U_T}{\partial P_1}+\frac{\partial U_F}{\partial P_1} \quad . \quad . \quad . \quad . \quad . \quad . \quad (46)$$

$$=\frac{R}{EI}\int_0^\alpha M\frac{\partial M}{\partial P_1}d\theta+\frac{R}{EA}\int_0^\alpha T\frac{\partial T}{\partial P_1}d\theta+\frac{CR}{GA}\int_0^\alpha F.\frac{\partial F}{\partial P_1}d\theta. \quad . \quad . \quad . \quad (47)$$

Substitute in (47) the values of the three variables and their differentials with respect to P_1 given in (33), (34), (37), (38), (39), and (40), giving

$$y_P=\frac{R}{EI}\int_0^\alpha\left[P_1R\left(\sin\theta+\cot\alpha\cos\theta-\frac{1}{\alpha}\right)+Q_1R\left(\frac{1}{\alpha}-\operatorname{cosec}\alpha\cos\theta\right)\right]\left\{R\left(\sin\theta+\cot\alpha\cos\theta-\frac{1}{\alpha}\right)\right\}d\theta$$

$$+\frac{R}{EA}\int_0^\alpha\left[P_1(\sin\theta+\cot\alpha\cos\theta)-\frac{Q_1\cos\theta}{\sin\alpha}\right](\sin\theta+\cot\alpha\cos\theta)\,d\theta$$

$$+\frac{CR}{GA}\int_0^\alpha\left[P_1(\cos\theta-\cot\alpha\sin\theta)+\frac{Q_1\sin\theta}{\sin\alpha}\right](\cos\theta-\cot\alpha\sin\theta)\,d\theta, \quad . \quad . \quad . \quad (48)$$

which on simplification becomes

$$y_P=\frac{PR^3}{4EI}\left[\alpha\operatorname{cosec}^2\alpha+\cot\alpha-\frac{2}{\alpha}\right]+\frac{QR^3}{4EI}\left[\frac{2}{\alpha}-\operatorname{cosec}\alpha(\alpha\cot\alpha+1)\right] \quad (49a)$$

$$+\frac{PR}{4EA}[\alpha\,\mathrm{cosec}^2\alpha+\cot\alpha]$$

$$+\frac{QR}{4EA}[-\mathrm{cosec}\,\alpha(1+\alpha\cot\alpha)] \quad . \quad (49b)$$

$$+\frac{CRP}{4GA}[\alpha\,\mathrm{cosec}^2\alpha-\cot\alpha]$$

$$+\frac{CRQ}{4GA}[\mathrm{cosec}\,\alpha(1-\alpha\cot\alpha)]. \quad . \quad (49c)$$

(49*a*), (49*b*), (49*c*) and the sum of these give respectively the radial displacement at the point of application of each P due to flexure, hoop-stress, shear-stress, and for the three together.

Equations (49) and (45) are set out in Tables I. and II. respectively, showing clearly the constituent radial strains when the forces P and the forces Q have definite values. The tables are also introduced for simplicity of reference in considering the following special cases :—

1. If each of the forces Q is made equal to zero, the total radial strain at the point of application of each P is given by the sum of the expressions in columns (1), (3), and (5) in Table I., the resulting equation being identical with (24). Also, the sum of the expressions in columns (7), (9), and (11) in Table II. gives the radial strain at each of the points in the ring midway between the points of application of adjacent forces P.

2. For the sake of easy reference let the forces P act at points A on the ring and the forces Q at the mid-points C (see fig. 4).

(*a*) If the forces Q at the points C are each zero, the sum of the expressions in columns (7), (9), and (11) gives the radial strain at each point C due to the forces P at the points A.

(*b*) If the forces P at the points A are each zero, and if the forces Q at the points C become the forces P, then the sum of columns (2), (4), and (6) gives the radial strain at each of the points A due to the forces P acting at the points C instead of at A, and this sum is identically the same as for (*a*) above.

That is to say, the N equal forces P applied at the points A produce the same strain at the mid-points C that would

Table I.

Total Deflexion at P due to Flexure, Hoop-Stress, and Shear =

Radial Deflexion due to Flexure		+	Radial Deflexion due to Hoop-Stress		+	Radial Deflexion due to Shear.	
1	2		3	4		5	6
$\frac{PR^3}{4EI}\left[\alpha\,\mathrm{cosec}^2\alpha+\cot\alpha-\frac{2}{\alpha}\right]$	$+\frac{QR^3}{4EI}\left[\frac{2}{\alpha}-\mathrm{cosec}\,\alpha(\alpha\cot\alpha+1)\right]$	$+$	$\frac{PR}{4EA}[\alpha\,\mathrm{cosec}^2\alpha+\cot\alpha]$	$+\frac{QR}{4EA}[-\mathrm{cosec}\,\alpha(1+\alpha\cot\alpha)]$	$+$	$\frac{CRP}{4GA}[\alpha\,\mathrm{cosec}^2\alpha-\cot\alpha]$	$+\frac{CRQ}{4GA}[\mathrm{cosec}\,\alpha(1-\alpha\cot\alpha)]$

Table II.

Total Deflexion at Q due to Flexure, Hoop-Stress, and Shear =

Radial Deflexion due to Flexure		+	Radial Deflexion due to Hoop-Stress		+	Radial Deflexion due to Shear.	
7	8		9	10		11	12
$\frac{PR^3}{4EI}\left[\frac{2}{\alpha}-\mathrm{cosec}\,\alpha(\alpha\cot\alpha+1)\right]$	$+\frac{QR^3}{4EI}\left[\alpha\,\mathrm{cosec}^2\alpha+\cot\alpha-\frac{2}{\alpha}\right]$	$+$	$\frac{PR}{4EA}[-\mathrm{cosec}\,\alpha(1+\alpha\cot\alpha)]$	$+\frac{QR}{4EA}[\alpha\,\mathrm{cosec}^2\alpha+\cot\alpha]$	$+$	$\frac{CRP}{4GA}[\mathrm{cosec}\,\alpha(1-\alpha\cot\alpha)]$	$+\frac{CRQ}{4GA}[\alpha\,\mathrm{cosec}^2\alpha-\cot\alpha]$

be produced at the points A if the forces P were applied at the mid-points C instead of at the points A.

This should be expected; the only difference in the two cases is that in the first case the radius is increased by the amount of the strain, while in the second case the radius is decreased.

The Maxwell–Rayleigh* reciprocal force-displacement relationship states that "a force P applied at a point A produces the same displacement at another point D that would be produced at A if P is applied at D instead of at A."

It is interesting to note from Tables I. and II. (by first writing $P=0$ and then $Q=0$, as explained above) how beautifully the reciprocal relationship holds for the three kinds of straining actions considered separately or taken together when derived by the stored strain energy method.

The determination of the moments, hoop-stresses, shear forces, internal energy, and radial deformations for special cases where the number of radial forces has definite value such as 2, 3, 4, . . . N are easily found by writing in the equations given, $\alpha = \frac{\pi}{2}, \frac{\pi}{3}, \frac{\pi}{4}, \ldots \frac{\pi}{N}$ respectively, and the expressions for them become simple in form.

March 18th, 1931.

IX. *A Comparison of the Crystal Structures of Cu_5Zn_8 and Cu_5Cd_8.* *By* A. J. Bradley, *M.Sc.*, *Ph.D.*, *and* C. H. Gregory, *M.Sc.* †

A. Structure of Cu_5Zn_8.

THE γ-phase of the Cu–Zn series of alloys was shown by Westgren and Phragmèn [1] to have a cubic structure with 52 atoms per unit cell. This structure was afterwards worked out in detail by Bradley and Thewlis [2], who utilized the data published by Westgren and Phragmèn, which included Laue photographs, rotation crystal photographs, and powder diagrams. A structure was obtained which has the symmetry of the space-group T_d^3, and an attempt was made to fix the positions of all the atoms in the structure. The general form of the proposed structure and the values of some of the parameters defining the atomic positions were

* Clerk-Maxwell, Phil. Mag. xxvii. (1864). Rayleigh, Lond. Math. Soc. iv. (1873). *Loc. cit.* Phil. Mag. xlvii. (1873); xlix. (1874).

† Communicated by Prof. W. L. Bragg, F.R.S.

both arrived at by assuming values for the interatomic distances suggested by those existing in the pure metals, and no attempt was made to show that the solution so obtained was a unique solution of the experimental data. The structure so obtained did, however, account quite well for the observed reflexions on both the single crystal and the powder photographs.

In view of the frequency with which this type of structure occurs it seemed to us advisable to attempt to deduce the structure by more rigid reasoning, and to test it by comparison with a set of quantitative measurements. We have therefore tried to determine the exact positions of the atoms from the intensity measurements, and by this means to get definite experimental evidence regarding the interatomic distances.

Experimental.

The alloys were annealed in powder form at 250–300° for one hour, and X-ray powder photographs taken.

The intensities were calculated from measurements of the blackening of the powder photographs, obtained by means of a Cambridge microphotometer [3].

The values are integrated by subtracting the background readings from the peak readings, and then making an allowance for the slightly varying widths of the lines. Actually this correction makes very little difference to the results, as the lines measured for intensity purposes have for the most part about the same width. This is largely due to the fact that no use was made of the lines towards the outside of the film where the α-doublet opens out, and that there are no lines towards the centre of the film. These values were further corrected by calibrating from the blackening curve of the films. This correction has very little effect because within the range of the films examined the change of blackening between the lines and the background was on an almost linear portion of the curve, with the exception of one very strong line ($\Sigma h^2=18$) on either film. A much more important possible source of error is the uncertainty with which the background readings can be measured. This gives rise to some difficulty in measuring the weak lines. No claim is made that the values here obtained are precise measures of the intensities, but at least they are satisfactory enough for the purpose of structure determinations.

In order to compare the observed with the calculated values they must first be corrected for the effects of absorption, which has the effect of weakening the inner lines more

than the outer ones. A comparatively simple way of allowing for this effect has recently been suggested by Claassen [4]. The corrections to be applied are shown in Table I. The magnitude of the absorption effect is not great in the Cu–Zn photographs, but is very noticeable in the Cu–Cd photographs. The effect has in both cases been minimized by using a very thin specimen diluted with Canada balsam, with which the powdered alloy is mounted.

The intensity values so corrected are given in Table I. for all planes up to $\Sigma h^2=78$. Lines occurring at greater angles were not photometered owing to the opening of the α-doublet and the increasing tendency at high angles for reflexions from different planes to be superimposed. The measurements of the positions of the high angle reflexions given in Table II. were, however, utilized to determine the lattice constant. The lattice constant so obtained was then used to calculate values of $\sin^2\theta$ at lower angles. These latter values are inserted in Table I. as a check on the indices there allotted to the observed reflexions.

The intensity values given in Table I. are in each case on a purely arbitrary scale. In order to compare them with the calculated values given in Table IV. they were arbitrarily reduced to approximately the same scale as the calculated values.

Deduction of Structure.

The unique deduction of the structure proceeds as follows:— The single crystal data of Westgren and Phragmèn show that the structure is body-centred cubic and has T_d, O, or O_h symmetry, and that the number of atoms per unit cell is not a multiple of 8. The only possible space-groups are T_d^3, O^5, and O_h^9. Now each of these space-groups is characterized by the possession of intersecting 3-fold axes. The number of possible structure types is therefore comparatively small, and a unique determination of the structure is much simpler than might appear at first sight. The possible combinations of atoms giving a total of 52 per unit cell are:—

Space-group T_d^3.

(1) $12+8+8+8+8+8$,
(2) $12+8+8+8+8+6+2$,
(3) $12+12+12+8+8$,
(4) $12+12+12+8+6+2$,
(5) $24+12+8+8$,
(6) $24+12+8+6+2$.

TABLE I.

		Cu–Zn.				Cu–Cd.			
		$\sin^2\theta$.		Intensity.		$\sin^2\theta$.		Intensity.	
Σh^2.	hkl.	Calc.	Obs.	Obs.	Corr. for absorption.	Calc.	Obs.	Obs.	Corr. for absorption.
2	110	·015	—	—	—	·013	—	—	—
4	200	·030	—	—	—	·025	—	—	—
6	211	·045	—	—	—	·038	—	—	—
8	220	·060	—	—	—	·051	—	—	—
10	310	·076	—	—	—	·064	·065	7	23
12	222	·091	·092	11	17½	·076	·077	9	27
14	321	·106	·107	9½	14½	·089	·091	17	47
16	400	·121	—	—	—	·102	—	—	—
18	411, 330	·136	·137	139	205	·115	·116	145	363
20	420	·151	·153	2	3	·127	—	—	—
22	332	·167	·168	13	18	·140	·141	23	49
24	422	·182	·183	7	9½	·153	·154	16	32
26	510, 431	·197	·198	7½	10	·165	·167	8	15
30	521	·227	·228	3	4	·191	?	2	3
32	440	·242	?	1	1	·203	—	—	—
34	530, 433	·257	?	1½	1½	·217	·217	7	10
36	600, 442	·273	·274	24	26	·229	·230	9	13
38	611, 532	·288	·289	4½	5	·242	·243	6	8
40	620	·303	—	—	—	·254	·256	4	5
42	541	·318	—	—	—	·267	·269	9	12
44	622	·333	·334	1	1	·280	·281	7	8
46	631	·348	·350	8	9	·293	·294	16	19
48	444	·363	·365	13	13	·306	·306	16	18
50	{ 710 / 550, 543 }	·379	·380	8½	8½	·319	·319	18	19
52	642	·394	·395	2½	2½	·331	—	?	?
54	{ 721 / 633, 552 }	·409	·410	47	46	·344	·345	45	46
56	642	·424	·425	3	3	·357	·357	4	4
58	730	·439	?	1½	1½	·369	·369	2	2
62	732, 651	·469	·470	6	5	·395	·396	12	10½
64	800	·495	?	1	1	·407	—	—	—
66	{ 811 / 741, 554 }	·500	·501	25½	22	·420	·421	13	11½
68	820, 644	·515	·515	5½	5	·433	·434	9	7
70	653	·530	·530	3	2	·446	·446	6	4½
72	822, 660	·545	·546	11	9	·458	·459	8	6
74	{ 831 / 750, 743 }	·560	·561	2½	2	·471	·471	3	2
76	662	·575	·576	6	5	·484	·486	8	5½
78	752	·591	·591	4	3	·497	·497	11	7½

Table II.

Σh^2.	hkl.	Cu–Zn. Doublet.	Cu–Zn. $\sin^2\theta$. Obs.	Cu–Zn. $\sin^2\theta$. Calc.	Cu–Zn. Estimated intensity.	Cu–Cd. Doublet.	Cu–Cd. $\sin^2\theta$. Obs.	Cu–Cd. $\sin^2\theta$. Calc.	Cu–Cd. Estimated intensity.
80	840		—	·606	—		·511	·510	v.v.w.
82	910, 833		·622	·621	w.		·523	·522	w.
84	842		—	·636	—		·537	·535	v.v.w.
86	921 761, 655		·651	·651	w.		·547	·548	w.
88	664		—	·666	—		—	·561	—
90	930 851, 754	α_1 α_2	·680 ·684	·680 ·684	w.–m.		·573	·573	w.
94	933 763	α_1 α_2	— —	·710 ·714	—		·599	·599	v.w.
96	844	α_1 α_2	— —	·725 ·730	—		·611	·612	v.w.
98	941 853, 770	α_1 α_2	·741 ·745	·741 ·745	m.		·624	·624	st.
100	10 0 0 860	α_1 α_2	— —	·756 ·760	—		·637	·637	v.w.
102	10 1 1 772	α_1 α_2	·771 ·776	·771 ·775	m.–w.		·649	·650	w.
104	10 2 0 862	α_1 α_2	·786 ·790	·786 ·790	w.		·663	·663	v.w.
106	950 943	α_1 α_2	— —	·801 ·806	—		·675	·675	w.
108	10 2 2 666	α_1 α_2	·816 ·821	·816 ·821	m.–w.		·687	·688	m.
110	10 3 1 952, 765	α_1 α_2	·830 ·835	·831 ·836	v.–w.		·701	·701	w.
114	871 855, 774	α_1 α_2	·861 ·866	·861 ·866	st.	α_1 α_2	·724 ·728	·725 ·729	m.
116	10 4 0 864	α_1 α_2	— —	·876 ·881	— —	α_1 α_2	— —	·738 ·742	—
118	10 3 3 961	α_1 α_2	·892 ·896	·892 ·896	w.	α_1 α_2	— —	·751 ·754	—
120	10 4 2	α_1 α_2	·907 ·912	·907 ·912	m.–w.	α_1 α_2	— —	·763 ·767	— —
122	11 1 0 954, 873	α_1 α_2	? —	·922 ·927	v.w.	α_1 α_2	·775 ·780	·776 ·780	w. w.
126	11 2 1 10 5 1, 963	α_1 α_2	·952 ·957	·952 ·958	st.	α_1 α_2	·801 ·805	·802 ·806	st.
128	880					α_1 α_2	·814 ·818	·814 ·818	w.
130	11 3 0 970					α_1 α_2	? —	·827 ·831	v.w.
132	10 4 2 882					α_1 α_2	·840 ·845	·840 ·844	w.
134	11 3 2, 776 10 5 3, 972					α_1 α_2	·852 ·857	·852 ·857	m.
136	10 6 0 866					α_1 α_2	·865 ·870	·865 ·870	w.
138	11 4 1 875					α_1 α_2	·877 ·882	·878 ·882	w.
140	10 6 2					α_1 α_2	— —	·891 ·895	— —
142	965					α_1 α_2	·903 ·908	·903 ·908	w.
144	12 0 0 884					α_1 α_2	·916 ·921	·916 ·921	w.
146	12 1 1, 11 5 0 11 4 3, 981, 974					α_1 α_2	·929 ·933	·929 ·934	m.
148	12 2 0					α_1 α_2	— —	·942 ·946	—
150	11 5 2, 10 7 1 10 5 5					α_1	·955	·954	m.
Lattice constant			8·84 A.					9·635 A.	
Density			7·9					9·0	
Composition by weight			61 per cent. Zn.					73·0 per cent. Cd.	

Each of the above numbers represents a group of structurally equivalent atoms derived from a single atom by the symmetry operations of the space-group. Each atom in a group of 6 or 2 must lie at the intersection of 4-fold alternating axes. Each atom of an 8 group must lie on a 3-fold axis. (These are referred to below as A atoms). 12 groups may be either of two types—on 4-fold alternating axes which are lines of intersection of planes of symmetry (C atoms), or on 4-fold alternating axes which are not on planes of symmetry (C′ atoms) *. 24 groups may also be of two types—atoms on reflexion planes of symmetry (D atoms), or atoms on 4-fold alternating axes which are not on planes of symmetry (D′ atoms). (See fig.)

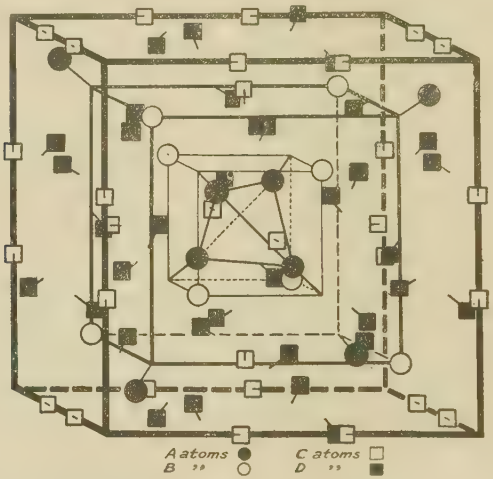

Unit cell of Gamma structure, of which Cu_5Zn_8 and Cu_5Cd_8 are examples. The short lines indicate the way in which the atomic positions are changed by varying the parameter values, which are not the same for Cu_5Zn_8 and Cu_5Cd_8.

Space-group O_h^9.

This differs from T_d^3 only in detail. Two groups of eight atoms, which are not related by symmetry in T_d^3, now become members of a group of 16 atoms. The atoms of a D group above now lie on 2-fold axes. No position exists corresponding to D′ above, for this would give atoms in a 48-fold position, and it would be impossible to assign

* C′ is a special case of D′, with coordinates $\frac{1}{2}$, 0, $\frac{1}{4}$, etc.

positions to the remaining 4 atoms. In short, this space-group may be regarded as a special case of T_d^3, and the two may be considered simultaneously.

Space-group O^5.

Except in the most general case with groups of 48 atoms this space-group is indistinguishable from O_h^9. In the present instance, therefore, it need not be considered as an additional possibility, since the 48-fold positions are impossible.

There are thus six possible combinations of groups of atoms, and an attempt has been made to deduce directly from the experimental evidence which of these is correct. For this purpose we have collected the set of quantitative figures of intensity measurements given in Table II., obtained photometrically from powder photographs of the alloys, and we have tried to show that the data so obtained can be explained by only one of the above six structure types.

At first only a few salient features of the intensity measurements need be taken into account, thus:—(330) and (411) are extremely strong; (200), (220), (310), and (400) are absent, and (440) and (800) are the weakest recorded intensities. Structures (1) and (2) can be eliminated at once, because with so many atoms on the 3-fold axes it follows at once from the nature of the structure factor formula that such arrangements would give strong reflexions from almost all $hh0$ planes, whereas (220) is absent and (440) extremely weak. Structures (3) and (4), with so many atoms on 4-fold axes of symmetry, should give strong reflexions from planes $(h00)$. Most of such planes are, as a matter of fact, absent or extremely weak, so that only (5) and (6) are left for detailed treatment.

Structures (5) and (6) differ only in detail, so that they may be considered simultaneously. They may belong to either of the space-groups T_d^3 or O_h^9. In these space-groups a 24 group may be of two possible kinds. One of these, however, would place all the atoms on 4-fold alternating axes of symmetry, giving rise to a large structure factor for planes of the type $(h00)$, and can therefore be ruled out. 24 groups must therefore be of the type D with atoms lying on planes of symmetry.

Typical coordinates of an atom which is a member of a D group would be *dde* (see set of coordinates in next section), and the next stage in the analysis is to fix the values of d and e. For this purpose the same procedure may be employed as was used to determine the structure of

α-manganese[5]. The unit cell is divided into 4096 (16^3) cubes, and each of the 4096 corners of these cubes is considered in turn as a possible position for a typical D atom. A preliminary test was applied by rejecting ranges of the parameters (*dde*) which could not explain the intensely strong line for which $\Sigma h^2=18$, *i. e.*(411) and (330), which is the most striking feature of all the γ structures. In doing this account was taken of all possible variations in the contributions of the remaining atoms. The values of (*dde*) not so eliminated are tabulated below, and a further choice is made by considering the effect on other spectra, again taking into account the contributions of the remaining atoms.

Table III. summarizes the process of elimination, which finally leads to the conclusion that the fifth of the above

Table III.

Typical coordinates (*dde*) of a D atom.	Possible objections to such values of (*dde*).
i. 7/16, 7/16, 0.	200 and 220 would be too big.
ii. 3/8, 3/8, 0.	200 too big.
iii. 5/16, 5/16, 0.	411 too small.
iv. 3/8, 3/8, 1/16.	411 too small; 200 too big.
v. 5/16, 5/16, 1/16.	All satisfactory.
vi. 5/16, 5/16, 1/8.	220 too big.
vii. 5/16, 1/16, 1/16.	200, 211, 310 too big.
viii. 1/4, 1/16, 1/16.	330 too small; 110, 200 too big.
ix. 3/8, 1/16, 1/16.	200, 220 too big.

sets of parameter values is approximately correct. The fact that (411) must be strong as well as (330) follows from an examination of rotation photographs.

The approximate value of the (*dde*) parameters is thus 5/16, 5/16, 1/16, and it is now possible to get a rough idea of the values of the other parameters. Two possible types of 12 group are mentioned above, but of these the C′ atoms may be eliminated at once, because they are bound to give excessively large contributions to (400) and (800). We are left with 12 atoms of the C type with typical coordinates (c00). Using the same tests as above, it is easily seen that the typical atom of a 12 group C must have coordinates about 1/3, 0, 0. The typical atom of an A group of eight atoms must have coordinates preferably about 1/3, 1/3, 1/3, but with possible alternative values about 1/8, 1/8, 1/8.

It is now possible to eliminate structure 6. This has $2+6$ atoms lying at the point of intersection of 4-fold axes, and in whatever manner the parameters are adjusted reflexions from $h00$ and $hh0$ planes are found to be too large. The only possible type of structure is therefore 5, consisting of the following groups:—$24+12+8+8$. Of the two sets of 8 atoms one has typical coordinates approximately 1/8, 1/8, 1/8, and the other has typical coordinates approximately 1/3, 1/3, 1/3. The translation $\frac{1}{2}$, $\frac{1}{2}$, $\frac{1}{2}$ (body-centred cubic lattice) makes the latter equivalent to $-1/6$, $-1/6$, $-1/6$, and this last set of coordinates are used below.

Exact Evaluation of the Parameter Values.

The structure of γ Cu–Zn consists of four sets of equivalent positions (see fig.), with the coordinates:—

(8 A) (aaa) $(a\bar{a}\bar{a})$ $(\bar{a}a\bar{a})$ $(\bar{a}\bar{a}a)$ $(\frac{1}{2}+a, \frac{1}{2}+a, \frac{1}{2}+a)$
$(\frac{1}{2}+a, \frac{1}{2}-a, \frac{1}{2}-a)$ $(\frac{1}{2}-a, \frac{1}{2}+a, \frac{1}{2}-a)$
$(\frac{1}{2}-a, \frac{1}{2}-a, \frac{1}{2}+a)$.

(8 B) $(\bar{b}\bar{b}\bar{b})$ $(\bar{b}bb)$ $(b\bar{b}b)$ $(bb\bar{b})$ $(\frac{1}{2}-b, \frac{1}{2}-b, \frac{1}{2}-b)$
$(\frac{1}{2}-b, \frac{1}{2}+b, \frac{1}{2}+b)$ $(\frac{1}{2}+b, \frac{1}{2}-b, \frac{1}{2}+b)$
$(\frac{1}{2}+b, \frac{1}{2}+b, \frac{1}{2}-b)$.

(12 C) $(c00)$ $(\bar{c}00)$ $(0c0)$ $(0\bar{c}0)$ $(00c)$ $(00\bar{c})$ $(\frac{1}{2}+c, \frac{1}{2}, \frac{1}{2})$
$(\frac{1}{2}-c, \frac{1}{2}, \frac{1}{2})$ $(\frac{1}{2}, \frac{1}{2}+c, \frac{1}{2})$ $(\frac{1}{2}, \frac{1}{2}-c, \frac{1}{2})$
$(\frac{1}{2}, \frac{1}{2}, \frac{1}{2}+c)$ $(\frac{1}{2}, \frac{1}{2}, \frac{1}{2}-c)$.

(24 D) (dde) $(d\bar{d}\bar{e})$ $(\bar{d}d\bar{e})$ $(\bar{d}\bar{d}e)$ $(\frac{1}{2}+d, \frac{1}{2}+d, \frac{1}{2}+e)$
$(\frac{1}{2}+d, \frac{1}{2}-d, \frac{1}{2}-e)$ $(\frac{1}{2}-d, \frac{1}{2}+d, \frac{1}{2}-e)$
$(\frac{1}{2}-d, \frac{1}{2}-d, \frac{1}{2}+e)$.

(ded) $(d\bar{e}\bar{d})$ $(\bar{d}e\bar{d})$ $(\bar{d}\bar{e}d)$ $(\frac{1}{2}+d, \frac{1}{2}+e, \frac{1}{2}+d)$
$(\frac{1}{2}+d, \frac{1}{2}-e, \frac{1}{2}-d)$ $(\frac{1}{2}-d, \frac{1}{2}+e, \frac{1}{2}-d)$
$(\frac{1}{2}-d, \frac{1}{2}-e, \frac{1}{2}+d)$.

(edd) $(e\bar{d}d)$ $(\bar{e}d\bar{d})$ $(\bar{e}\bar{d}d)$ $(\frac{1}{2}+e, \frac{1}{2}+d, \frac{1}{2}+d)$
$(\frac{1}{2}+e, \frac{1}{2}-d, \frac{1}{2}-d)$ $(\frac{1}{2}-e, \frac{1}{2}+d, \frac{1}{2}-d)$
$(\frac{1}{2}-e, \frac{1}{2}-d, \frac{1}{2}+d)$.

It has been shown above that the approximate values of a, b, c, d, and e are 1/8, 1/6, 1/3, 5/16, and 1/16 respectively. A more precise determination must proceed by methods of

trial and error. It is necessary to calculate the intensity values for a given set of parameter values, and then modify the latter in the direction indicated by the observed intensities. This process brings us to the set of parameter values which were given in the original paper on the structure of γ-brass. In the investigation then made there were certain assumptions concerning the interatomic distances. We have now obtained the same structure without these assumptions, and the quantitative data enable the parameters to be more accurately determined.

In general structure 5, which has been demonstrated to be the only possible structure, might correspond to either of the space groups T_d^3 or O_h^9, but with the set of parameter values found the holohedral space-group is impossible. The only possible space-group is therefore T_d^3.

In comparing observed and calculated intensity values a formula was used based upon the intensity formulæ given by Bragg and West [6], following on the lines of a paper by Darwin [7].

The most convenient quantity to calculate is the total radiation received from a reflexion at a glancing angle θ on a strip of film of constant breadth, the breadth being small in proportion to the radius of the powder photograph camera used. Let this quantity be P_l, I_0 the intensity per unit area in the neighbourhood of the crystal. Then

$$\frac{P_l}{I_0} = \left(\frac{Ne^2}{mc^2} \cdot F\right)^2 . \lambda^3 . \frac{I + \cos^2 2\theta}{2 \sin 2\theta} . \frac{p}{2} . \cos\theta . \frac{M}{\rho} . \frac{l}{2\pi r \sin 2\theta};$$

$N = 1/V$, where V is the volume of the unit cell (in c.c.);

$\frac{e^2}{mc^2} = 2{\cdot}816 \times 10^{-13}$; λ (for CuK_α radiation) $= 1{\cdot}54 \times 10^{-8}$ cm.;

p is the number of planes of the form $[hkl]$; M and ρ are the mass and density respectively for the whole specimen; l is the breadth of the strip of film under consideration, and r the radius of the camera; F, the structure factor, involves the scattering power of the atoms in question. This was derived from a set of values calculated from data recently supplied by Prof. Hartree.

In addition, a factor correcting for absorption should be introduced into the above equation. In practice it has been found more convenient to correct the observed values. The factor $l/2\pi r$ differs from camera to camera, and as a device for comparing results obtained with different cameras we have adopted the practice of expressing the observed results as if for a film of breadth $2\pi r$.

Table IV.

Comparison of Observed and Calculated Intensities.

		Cu–Zn.			Cu–Cd.					
			Calc.			Calc.				
h^2.	*hkl*.	Obs.	*a*.	*b*.	Obs.	*a*.	*b*.	*c*.	*d*.	Obs. *
2	110	—	17	8	—	19	17	74	2	—
4	200	—	0	2	—	0	4	2	2	—
6	211	—	7	4	—	8	27	6	8	—
8	220	—	1	2	—	1	11	0	3	—
10	310	—	2	0	60	3	2	13	59	50
12	222	45	46	48	70	62	125	58	75	60
14	321	37	32	38	120	41	85	38	97	100
16	400	—	0	0	—	0	0	1	14	—
18	411, 330	520	690	750	910	910	780	830	810	800
20	420	8	5	9	—	6	12	2	3	—
22	332	46	59	41	120	82	119	123	106	110
24	422	24	33	21	80	46	70	92	79	75
26	510, 431	26	22	24	40	32	45	49	29	35
30	521	10	6	11	10	9	27	7	6	10
32	440	2	3	2	—	5	9	8	4	—
34	530, 433	3	4	3	25	7	16	11	19	25
36	600, 442	67	42	62	35	61	33	25	32	35
38	611, 532	13	17	12	20	24	23	21	18	20
40	620	—	0	0	15	0	0	2	10	15
42	541	—	0	1	40	1	4	12	35	45
44	622	2	2	2	20	4	9	8	13	20
46	631	23	30	28	50	43	57	44	56	55
48	444	34	39	37	45	55	55	45	47	50
50	710 / 550, 543	22	33	24	50	49	53	53	54	55
52	642	6	3	6	?	5	8	1	3	?
54	721 / 633, 552	116	110	129	115	170	136	175	182	140
56	642	7	10	8	10	14	18	17	13	12
58	730	3	2	3	5	4	5	2	5	6
62	732, 651	14	21	14	26	34	43	44	34	34
64	800	2	1	1	?	2	6	2	3	?
66	811 / 741, 554	57	47	66	29	73	65	34	36	39
68	820, 644	12	14	9	18	20	17	21	27	25
70	653	6	4	7	11	5	7	6	13	15
72	822, 660	23	23	24	15	35	27	48	32	21
74	831 / 750, 743	5	8	5	5	12	14	11	7	7
76	662	12	14	13	14	20	27	16	20	21
78	752	8	11	10	19	15	15	29	40	28

(*a*) Former parameters.

(*b*) Modified parameters.

(*a*) "Normal" Gamma structure.

(*b*) "Normal" parameters, Cu in B and C, Cd in A and D.

(*c*) Modified parameters, atoms at random.

(*d*) Modified parameters, Cu in A and B, Cd in C and D.

* Allowing for heat motion.

A comparison of the observed and calculated intensities, using the parameters given in the former paper, shows that considerable discrepancies exist (see Table IV.). Some of these were pointed out then, but, as no quantitative data then existed, no attempt was made to get a better adjustment. Table V. indicates how the necessary adjustments were found.

Table V.

Σh^2.	hkl.	Relation of obs. to calc. int. (former parameters).	Required direction of change in parameter values.				
			a.	*b*.	*c*.	*d*.	*e*.
20	420	stronger	−	+		+	−
22	332	weaker	+			+	−
24	422	weaker	+		(+)	+	−
30	521	stronger	+		+	+	−
36	600 / 442	stronger	+			+	−
52	642	stronger		+	−	+	−
62	732 / 651	weaker	+	+	−		−
70	653	stronger	+	+		+	−

The above table indicated definite adjustments to be made in the *a*, *b*, *d*, and *e* parameters. Finally, a set of values was obtained which gives a much better agreement with the observations. The values now obtained were $a=0{\cdot}110$, $b=0{\cdot}172$, $c=0{\cdot}355$, $d=0{\cdot}313$, $e=0{\cdot}036$. The intensities calculated from these values are shown in column *b* of Table IV. Almost all the observed values lie between the two sets of calculated values, but much closer to the new set. Probably the correct values of the parameters are not much more than about 0·003 from the above set. This is equivalent to a maximum difference of about 0·025 Å. The maximum possible error in the parameter values calculated from the above values should then be $2\sqrt{3}$ of this amount, *i. e.*, less than 0·1 Å. The values given in the former paper were at most 0·007 from the present values, *i. e.*, about 0·06 Å. The corresponding difference in the interatomic distance is therefore not greater than about 0·2 Å.

The calculated values, using the new set of parameter values, *derived solely from the experimental intensity data,* are tabulated below in Table VIII. From these figures the only definite information to be deduced at this stage is the approximate constancy of interatomic distance, a fact of considerable importance which can be interpreted more

definitely when we compare the evidence obtained from the Cu–Cd alloy, an account of the analysis of which is given below.

B. Structure of Cu_5Cd_8.

Professor Westgren of Stockholm was kind enough to send us copies of some powder photographs of copper-cadmium alloys containing 73 and 75 per cent. by weight of cadmium, together with photograms of a copper-zinc alloy for comparison. The alloy of Cu and Cd containing 73 per cent. of cadmium corresponds roughly to the formula Cu_5Cd_8, whilst that of the copper-zinc alloy corresponded to the formula Cu_5Zn_8. It might therefore be expected that there would be a considerable resemblance in the powder photographs of the two alloys. There is, however, a striking difference between the photographs, which makes it clear that, although the structure of the copper-cadmium alloy must be very like that of Cu_5Zn_8, there is some important difference between the two structures. It was not unreasonable to suppose that this consists simply in the replacement of zinc atoms by cadmium atoms, but an attempt to interpret the difference in this simple fashion did not meet with success. It was apparent that some other factor was operative. We therefore decided to obtain quantitative data from the two alloys. Powder photographs were taken and photometer measurements made on them, in the manner described in the earlier part of this paper.

There are striking differences between the intensities of certain corresponding lines as recorded by the photometer. Tables I. and II. give the measurements for Cu–Cd obtained in the same way as for Cu–Zn. In attempting to explain the observed values for the Cu–Cd structure we proceeded as follows:—

In the first place it was supposed, as mentioned above, that cadmium atoms simply replaced the zinc atoms, and an attempt was made to get agreement between calculated and observed values by adjusting the parameters *. This was found to be obviously impossible, and it was evident that, although the difference was partly due to changes in the parameters, it would also be necessary to interchange certain groups of copper and cadmium atoms. Two problems had therefore to be solved—the new values of the parameters and the distribution of copper and cadmium atoms, amongst the positions of the metal atoms.

* The scattering factors for Cu and Cd were calculated from the Thomas formula (Bragg and West, *loc. cit.*).

A first step towards the solution of the first problem was made by replacing in the calculations Cu and Cd atoms by an atom of average scattering power at each atomic position. Assuming this mean atom, the general trend of the necessary corrections in the parameters can be seen from Table VI.

Table VI.

Σh^2.	*hkl*.	Observed relation of intensity of Cu–Cd line to that of corresponding Cu–Zn line.	Required direction of change in parameter values.				
			a.	*b*.	*c*.	*d*.	*e*.
10	310	stronger	−	+	−		
14	321	stronger				+	−
20	420	weaker	+	−		−	+
22	332	stronger	−			−	+
24	422	stronger	−		(−)	−	+
32	440	weaker	−	+	+	+	
34	530 433	stronger	−	+	−	−	
36	600 442	weaker	−	−		−	+
40	620	stronger ?					
42	541	stronger ?					
44	622	stronger	−	−			+
52	640	weaker		−	+	−	+
66	811 741 554	weaker		−		−	
70	653	stronger	+	+		+	−

Clearly *a* and *d* must be made smaller and *e* increased By doing this an improved agreement can be obtained for 22, 24, 30, 34, 36, 52, and 66. It is impossible, however, to obtain the precise values of the parameters until the second problem has been solved and the Cu and Cd atoms partitioned out between the available positions.

Table VII.

Σh^2.	*hkl*.	Observed relation of intensity of Cu–Cd line to that of corresponding Cu–Zn line.	Position of copper and cadmium atoms so indicated.			
			A.	B.	C.	D.
10	310	stronger	Cu	Cu	Cd	Cd
14	321	stronger	Cu	Cu		Cd
32	440	weaker	Cu		Cd	
40	620	stronger	Cu	Cu	Cd	Cd
42	541	stronger	Cu	Cu	Cd	Cd
44	622	stronger	Cu	Cu		Cd

Table VII. shows where the copper and cadmium atoms must be placed in order to improve the agreement for 10, 14, 32, 42, and 44. It will be seen that the results are concordant, assigning Cu to the A and B positions and Cd to the C and D positions. This being determined, it is now possible to find the precise values of the parameters in order to get agreement between observed and calculated intensities. The best set of values was found to be :

$$a=0{\cdot}097,\ b=0{\cdot}161,\ c=0{\cdot}352,\ d=0{\cdot}300,\ e=0{\cdot}055.$$

The process by which the structure was arrived at can be followed by considering columns (*a*), (*b*), (*c*), (*d*) in Table IV. and comparing them with the observed intensities. Column (*a*) shows the effect of a random arrangement of Cu and Cd atoms in the positions of a structure which we may call the "normal" Gamma type, since it is one which as nearly as possible gives an equal interatomic distance throughout. Such a structure forms a convenient starting-point for calculations. In the stage in column (*b*) we have placed Cd in the A and D positions and Cu in the B and C positions by analogy with the Cu–Zn structure. This arrangement, as mentioned above, cannot be made to agree by any parameter changes. Lines 10 and 12, for instance, show a divergence from observation which it is impossible to correct by altering the parameters, because they are of such a low order. In column (*c*) we have gone back to the random arrangement (mean atom), so as to test what can be done by parameter changes. There is still considerable divergence. In column (*d*) Cd atoms have been placed in C and D positions, Cu in A and B, and final adjustments to the parameters have been made. The agreement is now excellent throughout. The observed results tend to be smaller than the calculated results at higher angles, but this is very naturally explained by assuming an allowance for heat motion such as that given in the last column, which is of course quite empirical.

Discussion of Results.

Our examination has led us to a very definite conclusion which was rather unexpected. Although the positions occupied by the 52 atoms are similar in Cu–Zn and Cu–Cd, the distributions of the atoms in these positions are quite different in Cu–Cd from those which were found previously for Cu–Zn. A curious point now arises. It is clear that

there is a concentration of Cd in C and D positions, but *according to the composition of this phase there are insufficient* Cd *atoms to occupy all these places.* The composition Cu_5Cd_8 corresponds to 20 Cu atoms and 32 Cd atoms, whereas there are 36 positions of the C and D type. If 16 Cu atoms are assigned to A and B, and 36 Cd atoms to C and D, the composition should be Cu_4Cd_9, and *such a composition is not included in the range of this structure.*

Two possible explanations suggest themselves. Either four Cu atoms are distributed quite at random amongst the 36 C and D positions, or there is some tendency towards a more regular arrangement by confining the Cu atoms to one or other of these groups. The question has been tested by calculating the intensities obtained in each case. It was obvious that excluding Cu atoms from the C positions tended to make agreement worse ; it was doubtful whether agreement was better or worse by excluding them from D positions. The best agreement was got by supposing 4 Cu atoms and 32 Cd atoms to be arranged in the C and D positions in a random way, and we put this forward tentatively as our nearest approach to a solution.

According to this the structure of the Cu–Cd alloy may be described as one of the Gamma type, with 20 Cu atoms in A and B positions, and a group of 4 Cu atoms and 32 Cd atoms in the C and D positions, the members of the latter group being interchanged in a random way.

A remarkable amount of information is given by a study of the interatomic distances tabulated in Table VIII. The most important point is that the atoms in positions A and B, which are all Cu atoms, have the normal interatomic distances for copper as found in the element. The interatomic distances both inside the C and D groups and between members of these and the other two groups are considerably larger. This suggests that the C and D groups are behaving essentially like cadmium, in the structure of which the interatomic distances are much greater than in copper.

On comparing the structure now obtained with the structure of Cu_5Zn_8 one is immediately led to question the way in which the positions of the Cu and Zn atoms were placed when the structure was originally obtained. The evidence for placing the Cu atoms in B and C positions and the Zn atoms in A and D positions was derived solely from the analogy with the similar alloys of zinc with Ag and Au, because of course the scattering of Cu and Zn is so similar that they cannot be distinguished by X-ray analysis. It seemed that the intensities of the lines on the powder

photographs of the Ag–Zn and the Au–Zn alloys could be explained if the Ag or Au atoms were placed in B and C positions and the Zn atoms in A and D positions; the positions of the Cu and Zn atoms in the Cu–Zn alloy then followed by analogy. This argument is now seen to have

TABLE VIII.

Interatomic Distances in Cu_5Zn_8 compared with those in Cu_5Cd_8 and in the Constituent Elements.

	Cu_5Zn_8.		Cu_5Cd_8.		Elements.
	Neighbouring atoms.	Dist. in Å.	Neighbouring atoms.	Dist in Å.	Dist. in Å.
Zn–Zn...	A–D	2·6			2·65
	D–D	2·65			2·9
	A–A	2·75			
Cu–Zn...	B–D	2·55			
	C–D	2·55			
	B–A	2 6			
	B–D	2·6			
	C–A	2·6			
	C–D	2·8			
	C–D	2·8			
Cu–Cu...	C–C	2·55	A–A	2·55	2·55
	B–C	2·7	A–B	2·6	
Cu–Cd...			A–D	2·75	
			B–D	2·75	
			A–C	2·8	
			B–D	2·8	
			B–C	2·85	
Cd–Cd...			C–C	2·85	2·95
			C–D	2·9	3·2
			C–D	2·95	
			D–D	3·0	
			D–D	3·2	
			C–D	3·4	

been unsound, since a similar argument leads one to assign analogous positions to Zn and Cd, and this has proved not to be the case.

The problem of fixing the positions of the Cu and Zn atoms in the Cu–Zn structure would thus appear insoluble, but fortunately light is thrown on the problem from two independent sources. In the first place the corrected values of the interatomic distances in the Cu–Zn alloy given in

Table VIII. show that *the* A *atoms in the* Cu–Zn *structure are definitely further apart than either the atoms in the pure* Cu *lattice or the* A *atoms in the* Cu–Cd *alloy*. There is therefore definite evidence in favour of placing the larger atoms, *i. e.*, the Zn atoms, in the A position. Moreover, there is evidence obtained by us during investigations of ternary alloys of Cu, Zn, and Al [8] that a series of alloys exist with structures intermediate between those of γ Cu–Zn and δ Cu–Al, and it appears certain that the change-over from the one structure to the other is perfectly continuous. In δ Cu–Al [9] it is certain that all B and C positions are occupied by Cu, and the continuity of the ternary alloys suggests that they must be all occupied by Cu in Cu–Zn also.

To confirm the argument one must show that a discontinuous series of alloys is obtained when the atomic arrangement of the corresponding binary structures is widely different. For example, the ternary alloys of Cu–Zn and Cu–Cd should show a discontinuity in the range of the Gamma structures. This series has not yet been investigated, but other series which we have examined show a discontinuity in the Gamma range. These are series intermediate between Cu–Zn and Cu–Sn, and between Cu–Al and Cu–Sn. The Cu–Sn structure is different both from that of Cu–Zn and from that of Cu–Al [10, 11], and in each case there is a decided break in continuity. A detailed discussion of the results obtained in the investigation of the ternary alloys is reserved for a later paper.

Summary.

1. The structures of Cu_5Zn_8 and Cu_5Cd_8 are both of the Gamma type, with 52 atoms in the unit cell, occupying very nearly the same general positions in each case. These atoms fall into four groups of structurally equivalent positions, containing respectively 8, 8, 12, 24 atoms.

2. A reinvestigation of the structure of Cu_5Zn_8 from first principles leads to a more accurate and reliable set of parameter values. Since the scattering powers of Cu and Zn for X-rays are so similar, the X-ray investigation can only determine atomic positions, and cannot distinguish which atoms are Zn and which Cu. In a previous paper this distinction had been made by assuming Cu_5Zn_8 to be analogous to Ag_5Zn_8 and Au_5Zn_8, when of course the atoms can be identified owing to the large difference in scattering power.

3. An attempt was then made to explain the powder photograph of Cu_5Cd_8 by assuming a structure similar to

that of the above group. It was found that it was both necessary to alter the parameters slightly and to redistribute the atoms between the 52 positions in a different manner. In Ag_5Zn_8 and Au_5Zn_8, also in Cu_5Zn_8 if it is analogous to those alloys, there are 20 (Cu, Ag, Au) atoms in groups of 8 and 12, and 32 Zn atoms in groups of 8 and 24; in Cu_5Cd_8 there are 16 Cu atoms in groups of 8 and 8, and 4 Cu atoms and 32 Cd atoms apparently distributed at random amongst groups of 12 and 24.

4. In Cu_5Cd_8, where the scattering power of the atoms is different, the very good agreement between calculated and observed intensities appears to us to give satisfactory evidence that positions and parameters have been correctly assigned. This is checked by the interatomic distances, for the distances Cu–Cu are smaller than the distances Cd–Cd, both agreeing well with the distances in the pure metals. The distances Cu–Cd are intermediate.

5. In Cu_5Zn_8 the atoms cannot be distinguished by X-rays, and, in addition, the interatomic distances are closely the same. Formerly we were confident that the analogies with Ag_5Zn_8 and Au_5Zn_8 placed the Cu and Zn atoms, but the fact that Cu_5Cd_8 has so different a distribution proves that this argument cannot be relied upon. We believe, however, that the positions we have assigned are correct, because Cu_5Zn_8 forms a continuous series of alloys with Cu_9Al_4, a definitely known structure which we have recently checked by further investigation.

6. Even though the evidence for the atomic distribution in Cu_5Zn_8 is not so conclusive, there is no doubt that the distribution in Ag_5Zn_8 and Au_5Zn_8 at least is radically different from that in Cu_5Cd_8. There is thus no direct connexion between chemical composition and atomic distribution in these alloy structures, in spite of the fact that the general type of structure is the same.

The authors thank Professor W. L. Bragg, F.R.S., for his kind interest and help in the investigation, and Mr. A. P. M. Fleming, O.B.E., M.Sc. (Tech.), Director of Research of Metropolitan Vickers Electrical Co., Ltd., for enabling the research to be carried out.

References.

(1) A. Westgren and G. Phragmèn, Phil. Mag. l. p. 311 (1925).
(2) A. J. Bradley and J. Thewlis, Proc. Roy. Soc. A, cxii. p. 678 (1926).
(3) G. M. B. Dobson, Proc. Roy. Soc. A, civ. p. 248 (1923).
(4) A. Claassen, Phil. Mag. ix. p. 57 (1930).

(5) A. J. Bradley and J. Thewlis, Proc. Roy. Soc. A, cxv. p. 456 (1927).
(6) W. L. Bragg and J. West, *Zeit. für Krist.* lxix. p. 118 (1928).
(7) C. G. Darwin, Phil. Mag. xliii. p. 800 (1922).
(8) A. J. Bradley and C. H. Gregory, Mem. & Proc. Man. Lit. & Phil. Soc. p. 91 (1927–8).
(9) A. J. Bradley, Phil. Mag. vi. p. 878 (1928).
(10) A. Westgren and G. Phragmèn, *Zeit. Metallkunde*, xviii. p. 279 (1926).
(11) J. D. Bernal, 'Nature,' cxxii. p. 54 (1928).

X. *Experiments on Time-lag in Gas-filled Photoelectric Cells.* *By* Prof. E. L. E. Wheatcroft, *M.A.**

General.

The question of time-lag or "fatigue" in gas-filled photoelectric cells has not so far been the subject of much attention, although such cells are now in very general use. For the engineer the point of interest is the current-light ratio at higher audio frequencies, and in this connexion some manufacturers have stated that no change in "response" can be detected up to 10,000 cycles, while others have found quite an appreciable reduction at much lower frequencies. Campbell and Stoodley † have discussed this reduction in response, and published curves for various types of cell.

For the physicist the time-lag may form a clue to the processes operating in the cell. It is not at all surprising that the time of ionization should become large with potentials near the glow-potential or that it should increase with increasing magnification. The experiments described in the two parts of this paper confirm the oscillogram published in a note by the above-mentioned authors †, and establish, within these limits, certain simple differential equations as representing the behaviour of the cell.

Part I.

Introduction.

THE author was engaged for some time in an attempt to measure in oscillographs of the Duddell type the lag between current and displacement at various frequencies between 50 and 2500 cycles. For this purpose a gas-filled

* Communicated by the Author.

† "Photoelectric Cells and their Applications": Joint Discussion of the Physical and Optical Societies, June 4-5, 1930, p. 64 *et seq.*

photoelectric cell was used, since at the time of commencing the investigation vacuum cells were not made sufficiently sensitive for the purpose. It became clear after a while that the lag in the photoelectric cell was by no means negligible at these frequencies, but was in fact a considerable fraction of the apparent lag of the oscillograph. Moreover the lag varied between different series of tests. The author therefore endeavoured to measure the cell-lag, and to do so by an absolute method rather than by that of comparing one cell with another.

Apparatus used.

Fig. 1 shows in diagrammatic form the apparatus which was used. On a rigid frame A are mounted two brass bridges G, H, and two electromagnets B, C. A tungsten wire D E F is stretched between the bridges after the manner of a violin string, and, passing between the poles of the two electromagnets, is kept taut by weights at one end.

Fig. 1.

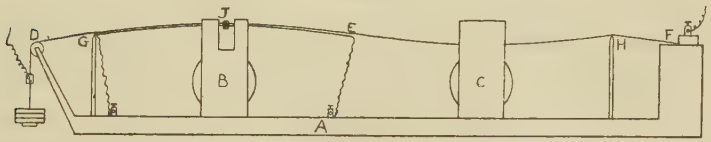

This tungsten wire, which is 0·122 mm. in diameter, is conveniently described as the carrier wire. The wire, of course, has a natural frequency of transverse vibration, and if a current be passed through it at this frequency (or any multiple) it will vibrate with a comparatively large amplitude due to the force exerted by the two magnetic fields. The polarities of the magnets may be in opposite directions, and in that case the wire will vibrate with a node at the point E, and the oscillator frequency must be an even harmonic of the fundamental frequency of the wire.

An enamelled copper wire, ·051 mm. diameter, is attached to the carrier wire by a binding of silk thread and shellac in such a manner that it conforms to the vibrations of the carrier wire aver the portion G E. This copper wire, which is conveniently described as the generator wire, has an electromotive force induced into it as it vibrates between the poles of the magnet B along with the carrier wire to which it is attached.

The magnet B is slotted in the centre to expose a small paper target J also fixed to both wires, and light from an

incandescent lamp is brought to a focus on this target, the rays travelling perpendicular to the plane of fig. 1 and parallel to the lines of force of magnet B. Such rays as are not cut off by the target fall on the cathode of the photo-electric cell. The total illumination of the cell then consists of a constant component superimposed on an alternating component which is essentially *in phase with the displacement* of the target.

If the field of the magnet B be made uniform, the e.m.f. induced in the generator wire is proportional to the velocity of the wire, and is essentially *in phase with the velocity* of the target. Since the target is executing simple harmonic motion about its mean position, there must therefore be

Fig. 2.

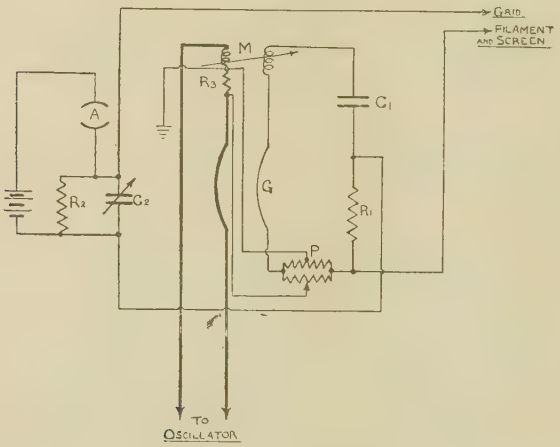

between the generator e.m.f. and the light falling on the cell a phase difference of exactly 90°, or $\frac{1}{4}$ cycle, at whatever be the frequency of oscillation.

Fig. 2 shows in diagrammatic form the electrical circuit used to compare the generated e.m.f. with the current in the photoelectric cell. In order first to balance out the effect of the current in the carrier wire the variable mutual inductance M and the potentiometer device P are adjusted to give silence in the detector, with the wire stationary. Then, when the wire is allowed to vibrate the current in the resistance R_1 bears to the net generated e.m.f. a relation which is calculable from the constants of the generator circuit. Similarly the photo-cell current bears a known

relation to the current in R_2 calculable from the values of C_2 and R_2. By adjusting the exciting current of the generator field magnet and the variable condenser C_2 the potential across R_1 can be made equal to that across R_2, and a balance obtained.

Adopting the complex number notation, let $j = \sqrt{-1}$, $\omega = 2\pi \times$ frequency, E = generated e.m.f., I = photo-cell current. Then the potential drop across R_1 is

$$\frac{E.R_1}{R_4 - \frac{j}{\omega C_1}},$$

where R_4 is the total resistance of the generator circuit. But at balance this is also the drop across R_2, so that the cell current is given by

$$I = \frac{E.R_1}{R_4 - \frac{j}{\omega C_1}}\left[\frac{1}{R_2} + j\omega C_5\right],$$

where C_5 is the total capacity of the photo-cell circuit, Then, since j represents a *lead* of 90°, the cell current I leads the e.m.f. E by an angle

$$\tan^{-1}\omega C_5 R_2 + \tan^{-1}\frac{1}{\omega C_1 R_4}$$
$$= \tan^{-1}\omega C_5 R_2 + 90° - \tan^{-1}\omega C_1 R_4.$$

But the displacement leads the e.m.f. by 90°, so that the displacement leads the current I by an angle α, given by

$$\alpha = \tan^{-1}\omega C_1 R_4 - \tan^{-1}\omega C_5 R_2.$$

The apparatus used has the following general characteristics:—

Resistance R_1.—347 ohms bifilar wound Eureka on a wooden bobbin.

Resistance R_2.—137,000 ohms, consisting of two "Dumetohm" resistors of 0·25 megohm nominal value, mounted in a screened box. This resistance "aged" slowly from a value of 133,000 to 137,000 during six months, and therefore was calibrated before each series of tests.

Condenser C_1.—Substandard mica condenser with plug top, giving values 0·2–1·0 microfarad.

Condenser C_2.—Variable air condenser mounted in screened box, with a range 17–1050 micro-micro-farad.

Mutual inductance M.—About 1 microhenry maximum value; the self-inductance of the coils is entirely negligible.

Potentiometer device P.—Together with the shunt R_3 the effective value is about ·005 ohm. The shunt R_3 is of no. 18 S.W.G. Eureka, 1 in. long, while the potential slide is made of no. 36 S.W.G. Eureka, 18 in. long.

The detector is a special three-valve screened amplifier which can be tuned to the working frequency. This has the effect of keeping any harmonics out of the telephones and making the ear much more sensitive to the balance of the fundamental frequency.

The screening embraces the photoelectric cell, the resistance R_2, the condenser C_2, the amplifier, and the connexion from the photo-cell circuit to the grid of the first valve. This screening, which for simplicity is omitted from fig. 2, is electrically connected to the filament of the amplifier and is practically at earth potential.

The total resistance of the generator circuit measured at 1000 cycles is 358 ohms. The self-inductance of the circuit is calculated to be entirely negligible.

The capacity between the carrier and generator wires was measured as 230 micro-microfarads.

The additional capacity of the photo-cell circuit was measured as 5 micro-microfarads. The A.C. admittance, $\frac{\partial i}{\partial e}$, was calculated as negligible.

Experimental Results.

(1) The first tests were directed to ascertaining whether there was any effect due to variation in the intensity or quality of illumination, and it appeared that within the accuracy of experiment there was no observable effect. This being so it was possible to increase the illumination at lower cell potentials, thus keeping the greatest possible sensitivity.

(2) Next, as a check on the accuracy of calibration of the apparatus a series of tests were made at various values of the condenser C_1, keeping the photo-cell conditions unvaried.

The angle α was found constant even when it was obtained by subtraction of two large measured angles.

(3) Although this experiment is designed to give an absolute measure of the lag, yet it may be considered a confirmation of the method that the lag found with a vacuum cell is zero within the accuracy of reading.

Fig. 3.

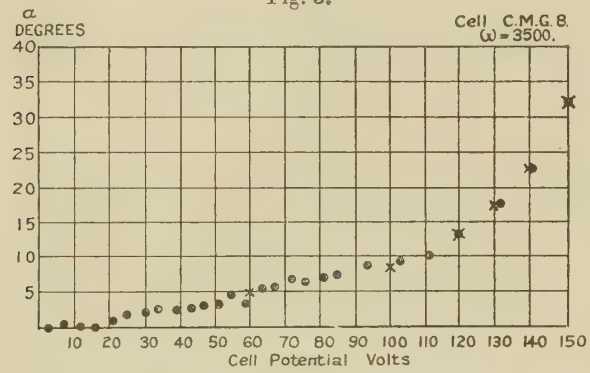

Fig. 4.

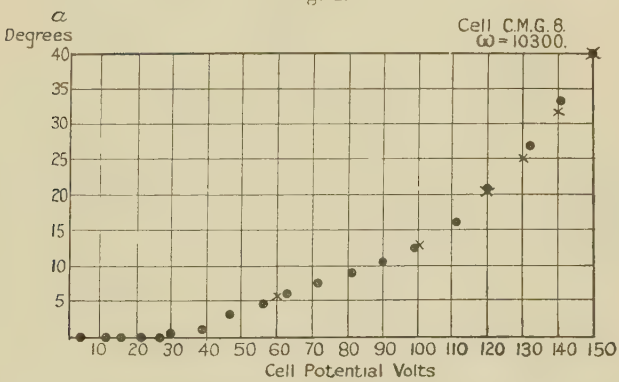

(4) Figs. 3, 4, and 5 show the values of α for a gas-filled cell at three different frequencies, having values very nearly in the ratio 1 : 3 : 5.

Consideration of Results.

The results of these experiments are illuminating in the light of the experiments of Campbell and Stoodley *.

* "Photoelectric Cells and their Applications": Joint Discussion of the Physical and Optical Societies, June 4–5, 1930, p. 64 *et seq.*

These investigators applied to their cells a light which varied with a rectangular wave form, so that at each half-period the illumination was instantaneously put on and off. They found that, if a sudden change ΔL be made in the illumination, the change in cell current ΔI after a time interval T is given by

$$\Delta I = \Delta L(a - bf(T)),$$

and the shape of the function was such as to suggest the equation

$$\Delta I = \Delta L(a - be^{-\lambda T}).$$

Fig. 5.

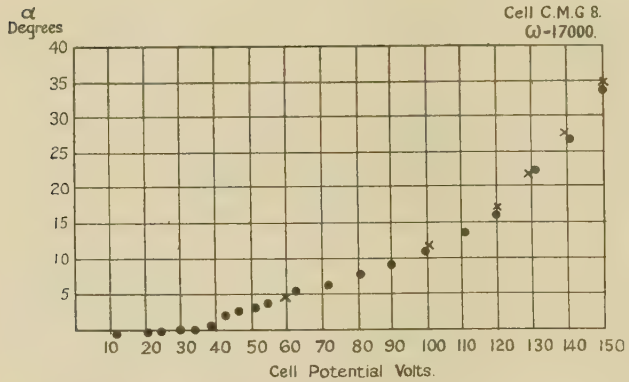

If this is the true equation, and it can be held to apply additively to infinitesimal changes, it is possible to deduce general equations, as follows :—

$$I = I_1 + I_2, \quad . \quad . \quad . \quad . \quad . \quad . \quad . \quad (1)$$

$$I_1 = (a - b)L, \quad . \quad . \quad . \quad . \quad . \quad . \quad . \quad (2)$$

$$\frac{dI_2}{dt} + \lambda I_2 = \lambda b L. \quad . \quad . \quad . \quad . \quad . \quad . \quad (3)$$

The application of these equations to a sinusoidally varying light is best treated by the complex number method, as follows :—

$$I = I_1 + I_2, \quad . \quad . \quad . \quad . \quad . \quad . \quad . \quad (1a)$$

$$I_1 = (a - b)L, \quad . \quad . \quad . \quad . \quad . \quad . \quad . \quad (2a)$$

$$I_2 = \frac{\lambda b L}{\lambda + j\omega}. \quad . \quad . \quad . \quad . \quad . \quad . \quad . \quad (3a)$$

These three complex equations are represented graphically in fig. 6, where OQ represents I_1, QP I_2, and OP consequently I.

Let QPS be drawn a right angle, as shown. Then

$$QS = \frac{QT^2 + TP^2}{QT},$$

$$QT = \frac{\lambda^2 b L}{\lambda^2 + \omega^2},$$

$$TP = \frac{\omega \lambda b L}{\lambda^2 + \omega^2}.$$

$\therefore$ QS $= bL$ and is independent of ω.

Thus as ω varies P describes a circle on QS as diameter. Also

$$\tan \phi = \frac{TP}{QT} = \frac{\omega}{\lambda}.$$

Fig. 6.

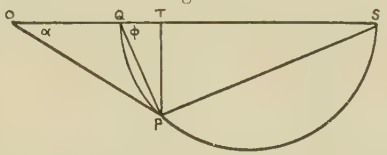

The diagram of fig. 6 shows clearly that the angle of lag, α, should be zero both at very low and at very high frequencies ($\tan \phi = 0$ and $\tan \phi = \infty$), and should show a maximum at some intermediate value.

The accompanying table shows certain values of α found experimentally and extracted from these plotted graphically in figs. 3, 4, and 5. The existence of the expected maximum angle is quite clear.

Cell CMG 8.

e.	ω.	α.	tan α.
150	3,500	32° 0′	·625
	10,300	40° 30′	·854
	17,000	33° 30	·662
100	3,500	8° 50′	·155
	10,300	13° 0′	·231
	17,000	10° 50′	·191
60	3,500	4° 45′	·083
	10,300	5° 30′	·096
	17,000	4° 50′	·084

Part II.

Introduction.

The circle diagram of fig. 6 is directly deduced from the equations (1), (2), (3) given in Part I., and the existence of such a relation would therefore be strong confirmation of the exponential curve suggested for Campbell and Stoodley's oscillograms. The author therefore undertook a second set of tests with that object.

Apparatus used.

In this case a simple alternating current bridge was used to compare the current of a vacuum cell with the current of the gas-filled cell which was being tested.

Illumination from a 30-watt gas-filled lamp was interrupted by a toothed wheel attached to the shaft of a direct-current motor, and suitable lenses brought the rays to a focus on a small right-angled prism which reflected part of the light. The reflected rays illuminated the cathode of the vacuum cell, and the refracted rays passed to the gas-filled cell. A suitable shutter was arranged so that the variation in light was approximately sinusoidal at a frequency determined by the speed of the motor. Tests were conducted with this sinusoidally varying illumination of different frequencies from $\omega = 1615$ to $\omega = 12950$ radians per second, the cell potential being kept constant for any one test. The frequency was measured by stroboscopic comparison of the speed of the motor with a vibrating fork.

Since the illuminations of the two cells have a fixed ratio (dependent on the setting of the prism), and the vacuum cell current I_v is at every instant proportional to the light falling on it, the lag of the gas-filled cell current I behind I_v will be a measure of α, and the ratio $\frac{I}{I_v}$ will be a measure of the ratio $\frac{I}{L}$. It is therefore to be expected, if the equations (1), (2), (3) hold true, that a vector making an angle α with the horizontal and having a length equal to $\frac{I}{I_v}$ will trace out a circle corresponding exactly to the circle QPS of fig. 6, and in particular that the angle ϕ (see fig. 6) will vary so that

$$\tan \phi = \text{constant} \times \omega.$$

Fig. 7 shows diagrammatically the circuit used to compare the vacuum-cell current I_v with the gas-filled cell current I. When a balance is attained there is no alternating potential drop across the detector. Therefore

$$\frac{I_v}{1/R_2 + j\omega C_2} = (I - I_v)R_1.$$

Hence

$$\frac{I}{I_v} = 1 + \frac{R_2}{R_1} \cdot \frac{1 - j\omega C_2 R_2}{1 + (\omega C_2 R_2)^2}.$$

Experimental Results.

Fig. 8 (*a*) shows a plot of points for a gas-filled cell at a potential of 115 volts. The figures marked against each point are values of ω ($= 2\pi \times$ frequency). It will be seen that a

Fig. 7.

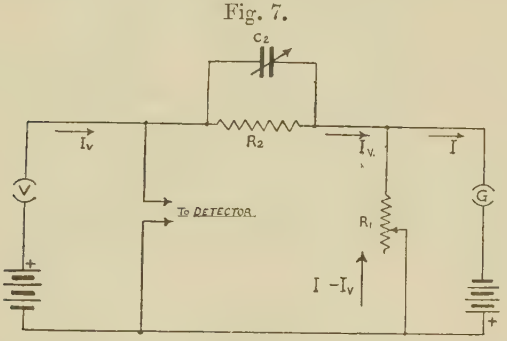

very good circle may be drawn through the points, and, as will be seen from fig. 8 (*b*), the values of $\frac{\tan\phi}{\omega}$ show no definite deviation from constancy.

Some difficulty was experienced in obtaining the circle diagrams, as the cell showed uncontrollable fluctuations of output which, though small in themselves, were sufficient to spoil the test for the purpose of determining the circles. The points plotted were found by conducting a series so quickly that the unknown cause of variation did not operate. Since, however, many circles were actually obtained which, like the circle plotted in fig. 8, conform very well to that demanded by the equations, it is concluded that these equations fit very well the behaviour of the cell at any given moment, although the "constants" vary somewhat from time to time.

Similar circles were obtained for other applied potentials, and fig. 9 shows, taking the average circle values for each

Fig. 8.

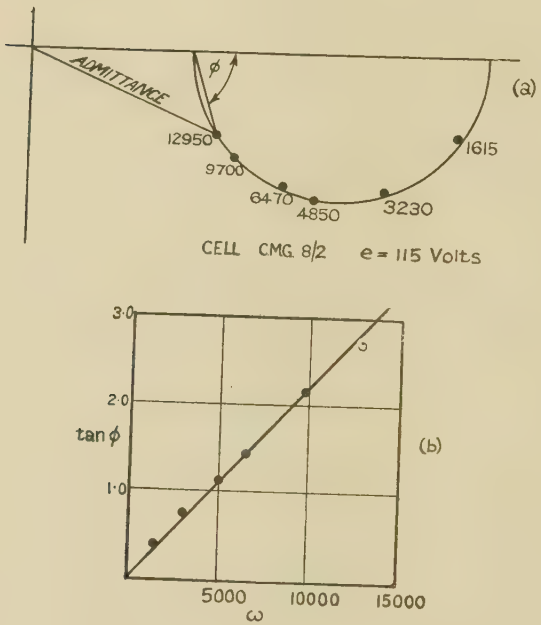
ADMITTANCE
φ
(a)
12950
9700
6470
4850
3230
1615
CELL CMG. 8/2 e = 115 Volts
3·0
2·0
1·0
tan φ
(b)
5000
10000
15000
ω

Fig. 9.

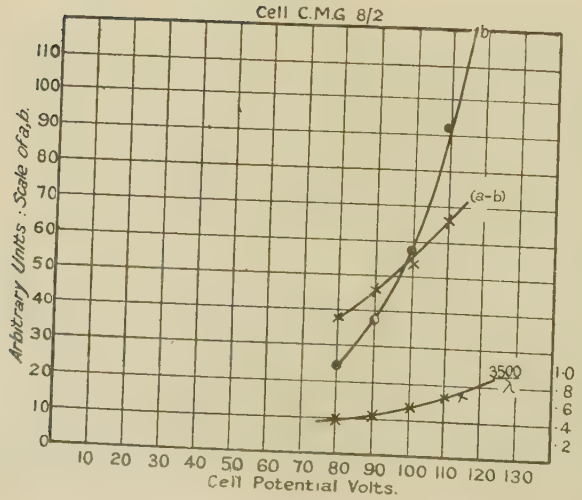
Cell C.M.G. 8/2
Arbitrary Units : Scale of a, b.
110
100
90
80
70
60
50
40
30
20
10
0
b
(a-b)
a
3500
λ
1·0
·8
·6
·4
·2
10 20 30 40 50 60 70 80 90 100 110 120 130
Cell Potential Volts.

potential, how the two components of current vary with applied potential over the range for which these tests were conducted. It is noticeable that both components of current increase with increasing potential.

Conclusion.

It is natural to inquire whether these experiments and those of Campbell and Stoodley throw any light on the processes of ionization in the cell. We may conclude as a result that the internal behaviour of the cells can be represented by equations of the type (1), (2), (3). Now the variation with applied potential found in the current I_1 appears to be of the right magnitude to be accounted for by the effect of electron collisions only, and it therefore seems probable that the delay is to be found in the action of the positive ions, at any rate if it is to such action that the high final current in a glow discharge is attributable. Equation (3) would result if it were supposed that the ions collect in a layer near the cathode, discharging at a rate proportional to the number collected, and by their presence or discharge releasing a proportionate number of additional electrons. Rothe * has found that gas attached to the cathode may have a large effect on the rate of decay of current in a glow-tube, and it is possible that a similar cause may hold up the discharge of positive ions in a gas-filled cell.

Acknowledgment.

I have to thank Prof. Whiddington for much valuable advice, and to acknowledge the advice and assistance of the Research Staff of the General Electric Co., in particular Dr. Campbell and Mr. Stoodley.

XI. *The Photoelectric Emission of Thin Films.* By N. R. Campbell. (Communication from the Research Laboratories of the General Electric Co., Ltd., Wembley.) †.

Summary.

§ 1. The thin films studied are those formed by heating oxidized silver (and some other metals) in cæsium vapour.

* *Physik. Zeitschr.* xxxi. pp. 520–539 (1930).

† Communicated by C. C. Paterson, Director.

§ 2. Apparatus is described for the gradual introduction of known quantities of cæsium into the cell.

§ 3. The changes in the emission during such introduction are described. They indicate that the cæsium undergoes a chemical reaction with the oxidized silver and that the final cathode is a thin film of cæsium on the products of the reaction.

§ 4. From the ratio of oxygen absorbed to cæsium reacting with it it is concluded that the reaction is, as might be expected, $2Cs + Ag_2O = Cs_2O + 2Ag$.

§ 5. It is impossible, however, that the support for the thin film should be simply a mixture of Cs_2O and Ag, for the cathode does not resemble thin films deposited on either of these substances in the absence of the other.

§ 6. Evidence is presented that excess of Cs may alloy with the Ag and thus bring about the production of a substance in which Cs_2O and Ag are intermingled on the molecular scale. This substance is sometimes, if not always, the support of the thin cæsium film.

§ 7. Measurements of the thermionic emission indicate that cathodes of this nature have all nearly the same b but widely different A. Those with the highest A (and therefore the largest thermionic emission) have in general the lowest mean photoelectric emission Σ. This result is consistent with Fowler's theory of selective emission. The value of b determined thermionically does not accord with the photoelectric threshold.

---

1. THE experiments described here were designed to throw light on the constitution of the cæsium-silver-oxygen photoelectric cathode, first described by Koller *, which has a greater sensitivity to white light and to the red end of the spectrum than any other known cathode. The work is by no means complete ; but since some of our conclusions are at variance with those recently presented by Koller *, the results that seem already established are published without further delay.

Cathodes of the type with which we are here concerned are produced by heating an oxidized silver surface in cæsium vapour and finally removing " excess " cæsium. The changes in the photoelectric emission during this

* L. R. Koller, Gen. Elec. Rev. xxxi. p. 476 (1928).

process have already been described qualitatively * ; in the first set of experiments they were investigated quantitatively by a method very similar to that described by Koller †.

2. For this purpose a cell (A, fig. 1) of normal construction with a silver cathode was connected through a capillary B with a small bulb C. The cathode in A was sometimes a coating of silver deposited chemically on the walls, sometimes a plate of silver suspended in the middle

Fig. 1.

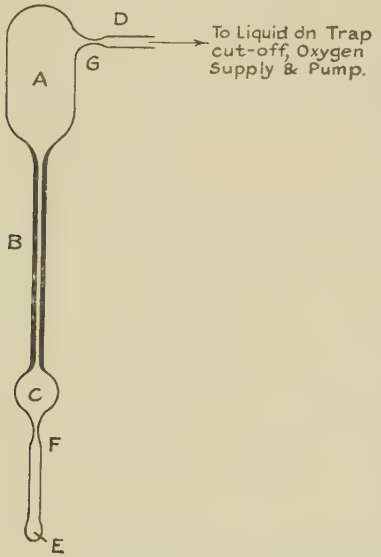

of the cells. The anode was of nickel ; a central wire, coated, like the walls, with silver in the first type of cell, in the second a cylindrical gauze not coated with silver. No difference in behaviour was found between the two arrangements except such as might be attributed to the better thermal insulation of the suspended plate. The cell was baked and exhausted as usual through D ; it was then filled with oxygen at a pressure of about 1 mm. and a discharge passed with the silver as cathode until

* N. R. Campbell, 'Photoelectric Cells and their Applications' (Phys. Soc. London, 1930), pp. 10–18.

† L. R. Koller, Phys. Rev. xxxvi. p. 1639 (1930).

a suitable quantity of oxygen had been absorbed. The remaining oxygen was then removed; cæsium azide in E was decomposed by heat, the nitrogen pumped away, and the cæsium metal distilled into C. The apparatus was then sealed off at F and G.

The cell and its attachment were now introduced completely into a bath of aniline vapour (184° C.). The cæsium diffused through the capillary into the cell; if it reacts there with the silver oxide and disappears immediately—this assumption is to be noted—the quantity that has entered and combined with the silver is proportional to the period that the cell has been in the bath—except for a slight correction for the time (of the order of 1 minute) required for the glass to assume the temperature of the bath. The relation between the emission from the cathode and the quantity of cæsium can therefore be traced.

At first both the photoelectric and the thermionic emissions were measured; but it appeared that the changes in one followed closely the changes in the other. The ratio of the emissions was not constant, the thermionic emission increasing more rapidly than the photoelectric emission under white light; but an increase or decrease in one was always accompanied by an increase or decrease in the other. Accordingly in the later observations the photoelectric emission was not measured; the nearly saturated thermionic emission alone was measured by simply connecting cathode and anode in series with a galvanometer and a battery of about 20 volts.

3. The result of one experiment of this kind is shown in fig. 2, in which the thermionic emission (log. scale) is plotted against the time since the cell was placed in the bath. After an initial period—seldom as long as shown in the figure, and clearly due to a delay in establishing a steady flow of cæsium vapour—the emission rises rapidly to a sharp maximum at A, and then falls even more rapidly; during this fall the insulation resistance between the electrodes decreases greatly. The slight minimum at B was usually, but not always, detected. If the supply of cæsium was stopped before A was reached, by sealing off the capillary, and the heating of the cell was continued, the emission, both thermionic and photoelectric, decreased and finally vanished almost entirely. If it

was stopped after A in the same way, further baking had practically no effect on the emission ; but if it was stopped by cooling C (in fig. 1) while A was heated, so that any free cæsium would return to C, the emission rose to about the value characteristic of A and remained constant.

These facts, taken in conjunction with those described by Koller (*loc. cit.*) and by de Boer and Teves *, admit of only one explanation. During the increase up to A

Fig. 2.

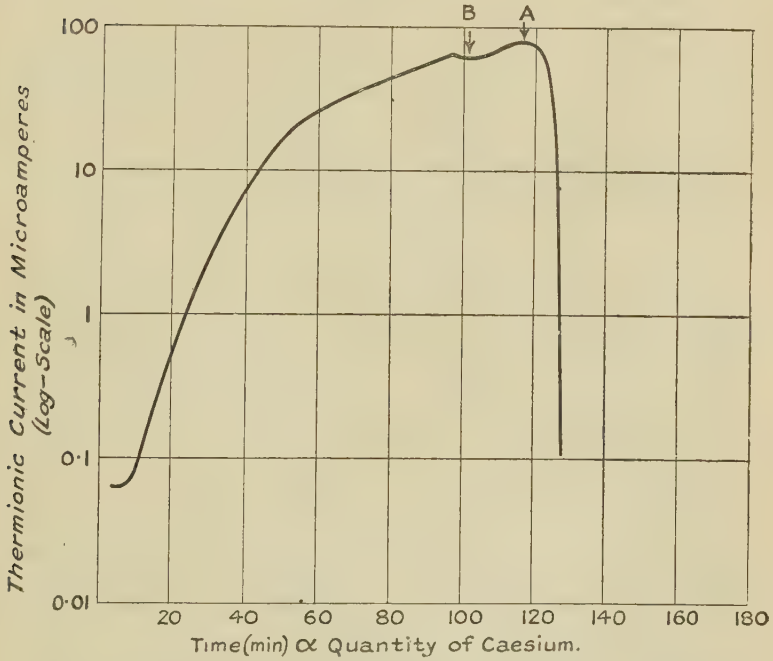

the cæsium that enters is disappearing by chemical reaction with the silver oxide to form an inactive compound ; thermionic and photoelectric emission occur only because there is present on the surface a film of the metal, probably monatomic, that has not yet had time to combine ; if the supply is stopped, this film combines like the rest, and the emission vanishes. At A the reaction is complete ; any further cæsium forms a thicker layer

* J. H. Boer and M. C. Teves, *Zeit. f. Phys.* lxv. p 489 (1930).

on the cathode and on the glass insulation ; the emission decreases and an insulation leak develops. If this excess cæsium is removed the emission at A is restored. The minimum at B perhaps represents the stage when the reaction is complete at one part of the surface, and the emission of that part becomes rather less than its maximum value owing to the presence of a layer of cæsium more than one atom thick.

However, this theory, though nobody will doubt its main features, is rather too simple. It suggests that the emission, up to B or possibly A, ought to be proportional to the area of the cathode surface on which the reaction is complete, and therefore to the quantity of cæsium that has entered. Actually it increases much more rapidly than this quantity, estimated by the time of heating. The discrepancy lies doubtless in the existence of stages intermediate between that of a surface untouched by the reaction and a surface on which the reaction is complete, covered with a monatomic layer of excess cæsium. I tried to base some more complete and accurate theory on the form of the curve in fig. 2, but abandoned the attempt when I found that, though the curves in different experiments are generally similar, it was impossible to find any simple formula by means of which they could all be exhibited as the same curve with different parameters depending on measurable quantities, such as the amount of oxygen originally absorbed.

Accordingly the only quantitative deduction that I propose to make from these curves is that A represents truly the amount of cæsium necessary to complete the reaction, and that the time occupied in reaching A in different experiments (with the same capillary and the same temperature of the bath) is proportional to the quantity of cæsium required to complete the chemical reaction. Two objections may be raised :—First, that the reaction may not be instantaneous, but occupy a time comparable with t. The sharpness of the maximum at A and of the subsequent fall, somewhat concealed by the logarithmic scale, seems to dispose of this objection, unless the whole theory is abandoned. Second, that A represents the quantity of cæsium required to form a monatomic layer in addition to that required to complete the reaction. But the former quantity must be negligibly small compared with the latter. The area of the cathode

was never greater than 50 cm.^{2}; if the radius of the Cs atom is $2{\cdot}5 \times 10^{-8}$ cm., the mass required to form a monatomic layer is $3{\cdot}3 \times 10^{-6}$ gm. The total quantity of cæsium introduced, estimated from the data given below, was never less than $2{\cdot}5 \times 10^{-3}$ gm.; the monatomic layer is never more than 0·13 per cent. of the total cæsium, which is much less than the error in determining t.

Fig. 3.

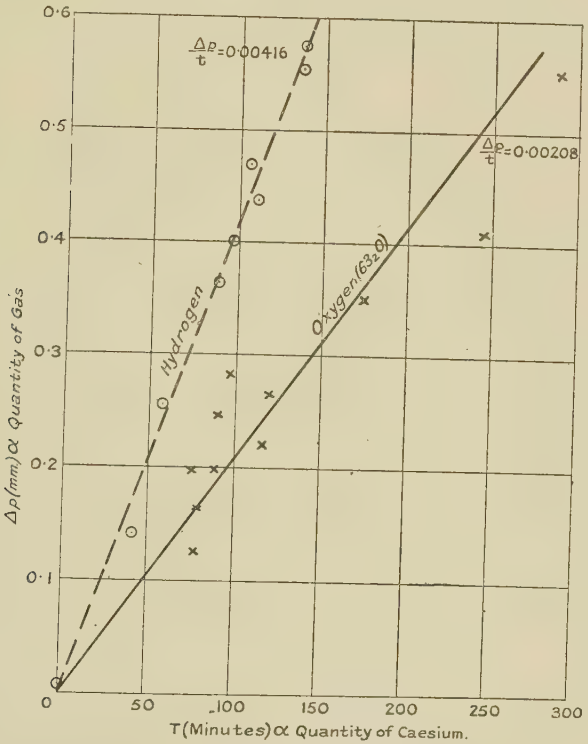

4. If the oxygen absorbed in the discharge is involved in the reaction—and this can hardly be doubted—the quantity of oxygen absorbed should be proportional to the quantity of cæsium required to react with it. The volume V in communication with the cell during the oxidation is always the same. Hence, if Δp is the reduction in pressure during the discharge, t ought to be proportional to Δp, and the ratio of proportionality should be consistent with some compound likely to be formed. In

fig. 4 the crosses show the values of Δp and t obtained in all the experiments, of the kind described in paragraph 3, which led to any result at all. They indicate clearly that Δp and t generally increase together; further, if a straight line from the origin has to be drawn among them and the divergences attributed to casual error, it must lie not very far from the full line drawn. (This line is actually drawn to represent the median $\Delta p/t$, so that equal numbers of points lie on each side of it.) But the divergences cannot be attributed wholly to experimental error. Errors may

Fig. 4.

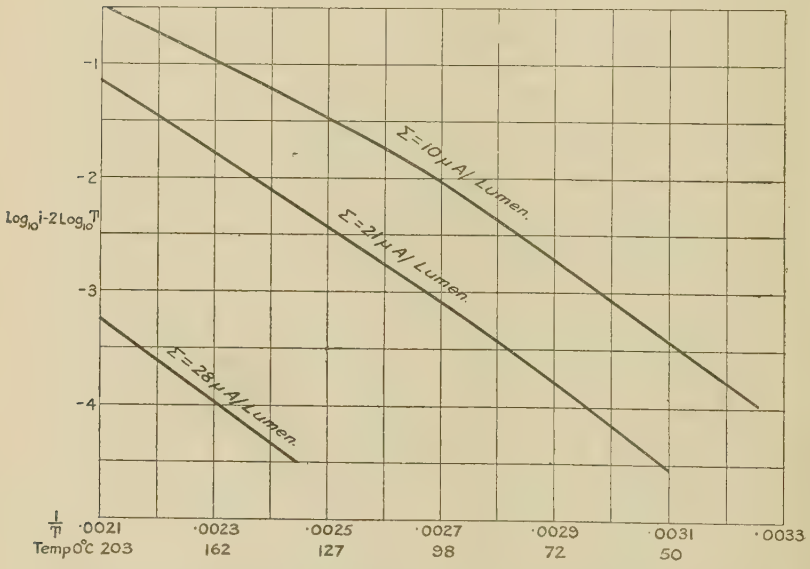

arise in the determination of Δp and t, in the temperature of the aniline bath, and in differences of the capillary tube, which had to be replaced occasionally owing to breakage; the maximum error is estimated at 15 per cent; six points are at a greater distance from the line than this. All these 6 points are suspect for one reason or another, but there is not sufficient reason to reject any of them as completely irrelevant. My conclusion is that, while there are circumstances determining the relation of oxygen to cæsium that are not accounted for wholly by our theory, the points lying near the line

drawn represent the normal behaviour which would always appear in ideal conditions that cannot be defined precisely at present; in such conditions $\Delta p/t$ would be constant and about 0·002.

In order to determine to what stoichiometric ratio this value corresponds a calibration is necessary. It might be derived from V, the dimensions of the capillary, and the recorded properties of cæsium vapour. But it seemed easier and more satisfactory to derive it experimentally by subjecting the cæsium to a known reaction. For this purpose A was replaced by a vessel of the same size as the cell, but containing no silver or other metal; the oxidation process was omitted, and after the cæsium had been introduced into B the apparatus was left on the pump and the aniline bath placed around it with the tube D protruding. The walls of the bath were of glass; the distillation of the cæsium from B into A could be watched, and the time after which the last traces disappeared from B determined with an error of not more than 2 per cent. This time corresponds to t. The cut-off leading to the pump was now closed, so that the volume V was shut off as during the oxidation process, and water vapour was admitted to it by removing the liquid air round a trap in which it was condensed. The water immediately reacted with the cæsium; the water was then frozen out again and the pressure of the resulting hydrogen measured *. This pressure corresponds to Δp and may be called $\Delta p'$. The values of $\Delta p'$ and t are shown by circles in fig. 4; they define closely the dotted straight line for which $\Delta p'/t = 0{\cdot}0042$.

If the reaction with water is

$$2Cs + H_2O = 2CsOH + H_2,$$

and if we suppose that the reaction with silver oxide is essentially

$$2nCs + O_2 = 2Cs_nO,$$

* At first I tried to make the cæsium absorb oxygen rather than evolve hydrogen; but the reaction of Cs and O_2 at low pressures appears to be very capricious, and no consistent results could be obtained. It should be added that after Koller's results appeared I calculated the calibration constant by his method from Kundsen's law and the dimensions of the capillary, and obtained a value differing by a factor of about 3 from that reached by the direct experimental method, and giving a correspondingly greater value of n (below). I have not tried to explain the discrepancy, for greater weight must clearly be attributed to a method which involves fewer quantities, and none not measured in strictly comparable conditions.

then, for the same amount of cæsium,

$$n = \Delta p' / \Delta p.$$

The only integer that can represent the value of $\Delta p' / \Delta p$ according to the experiments is 2. (The exact coincidence with 2 is, of course, merely fortuitous.) There is no reason therefore to suppose that the chemical reaction in the cell is other than that which would be anticipated, namely

$$2Cs + Ag_2O = Cs_2O + 2Ag.$$

The cathode finally produced consists of a thin film of cæsium on cæsium oxide and silver. Since thin layers of cæsium on silver are known to have photoelectric emission quite different from the cathodes studied here (they possess no maximum of emission in the visible or infra-red, and have a much smaller emission for white light), the natural conclusion is that the characteristic emission is that of cæsium on cæsium oxide.

5. But if this were so, cathodes of identical properties ought to be obtained by depositing thin layers of cæsium on Cs_2O produced by other means. Thus it may be produced by oxidizing cæsium * or by substituting for silver some other metal, the oxide of which is similarly reducible by cæsium, and carrying through the process studied here. Both these alternatives have been investigated. In the second copper and nickel were used and curves similar to fig. 1 obtained. With copper it was found that the Cs/O ratio, determined as in fig. 2, was the same as that with silver. With nickel, which cannot be oxidized by the discharge, the difficulty of estimating the amount of oxygen absorbed was not overcome; but neither of them produced quite the same results as the process employing silver. The mean emission † for light

* J. H. Boer and M. C. Teves, *loc. cit.*

† Purists sometimes object to the use in scientific work of the mean emission rather than the emission curve; but they forget that the emission curve is useless as a means of identification unless it can be interpreted as a function of a small number of parameters. Possible parameters are the threshold, the position, and the height of the maximum. The threshold cannot be determined with any accuracy; the position and height of the maximum certainly do not determine the whole form of the curve. Determinations of the emission curve agreed with those of other observers as well as these agree among themselves (*cf.* Koller and Boer and Teves (*loc. cit.*), and J. W. Ballard, J. Opt. Soc. Amer. xx. p. 608 (1930); but there were no indications that the facts would appear

from tungsten at 2800°K. could never be made to exceed 10 μ A/lumen, and was usually considerably less. The emission of the silver cells is often, and perhaps normally, not much above this limit, but it is seldom below it and sometimes it is very much greater; 49·3 μ A/lumen is the highest that I have observed.

6. It appears therefore that the support of the thin film cannot be simply Cs_2O or simply Ag; it must be some complex involving both. Evidence for this conclusion can be adduced from facts previously published*, but not mentioned here so far.

If, when the cathode has reached stage A, a large excess of cæsium is introduced quickly into the cell the appearance of the cathode changes completely. At stage A it is of a dark colour, tinged either with green or red. Under the action of the excess of cæsium it changes rapidly and becomes indistinguishable in appearance from the original metallic silver before oxidation. The mean emission decreases greatly, and the characteristic maximum at 700-800 mμ almost vanishes. The photoelectric properties are more like those of cæsium on unoxidized silver. Previously I interpreted this change as indicating that the original state had really been restored, and that the combination of the cæsium and oxygen had been mysteriously reversed, the oxygen being pumped away and the cæsium appearing free on the walls of the cell. This interpretation is false; estimation of the free cæsium by means of water in the manner described has shown that, despite the appearance of the film of metal on the walls, it is usually a small fraction of the total cæsium that has been introduced into the cell, and represents only a part of the excess introduced after reaching A. The cæsium introduced up to stage A must still be present in a combined form that does not react with water to liberate hydrogen; there is no reason to believe that it is not still present in the form Cs_2O on or in the silver cathode.

It seems now that the explanation is to be found in the existence of an alloy of silver and cæsium, liquid (or

simpler if stated in terms of them rather than in terms of the mean emission. Among silver cells an increase of mean emission is usually the result of an increase of emission at almost all wave-lengths; the position of the maximum varies little, and no correlation could be found between its exact position and any other characteristic.

* N. R. Campbell, *loc. cit.*

at least capable of two dimensional flow) at temperatures below 200°. If sufficient excess of cæsium is present in sufficient concentration it alloys with the silver and the alloy flows over the cæsium oxide and conceals it. Of the existence of an alloy there is direct evidence in a lowering of the vapour pressure of the cæsium; the complete removal of excess cæsium by distillation from a cell that has reached this stage is a very long business; the concealment of the cæsium oxide by it is more hypothetical, but is supported in some degree by other facts.

For the cathodes possessing an emission greater than the normal of 10–12 μA/lumen appear to represent a a stage intermediate between A and that arising from large excess of cæsium. They are never produced unless cæsium has been present in considerable excess at some stage, and they are relatively light in colour. The exact circumstances of their production is the subject of present inquiry; but all that is known of them is consistent with the view that in them the surface on which the monatomic film of cæsium rests is a complex produced by the merging of the Cs_2O and Ag (and possibly Cs) into one another. Such merging might be the beginning of the supposed two-dimensional flow of the Cs—Ag alloy over the Cs_2O.

7. Finally, brief mention may be made of measurements on the thermionic emission of these cathodes, similar to those already reported by Koller *. Fig. 4 shows the Richardson lines characteristic of three typical cathodes, $\log i$—2 log T being plotted 1/T. The mean photoelectric emission Σ of the cathodes are marked against each curve.

It will be seen that the lines are not straight. This may be because the surfaces are not homogeneous; the photoelectric emission varies by at least 30 per cent. over their surface, and the lines may be compounded of several straight lines of different slope; or, again, it may be because, as wave-mechanics indicate, the Richardson line should not be strictly straight for cathodes of very small work function. But it is remarkable that the lines are nearly parallel, so that the cathodes differ in their A rather than in their b, and that A is larger for the cathode with the smaller mean photoelectric emission.

* L. R. Koller, Phys. Rev. xxxiii. p. 1082 (1929).

Mr. Fowler has pointed out to me that such a result is consistent with the theory of selective emission that he has proposed*. A high selective emission requires the presence of a well-developed "valley" between two "peaks" in the potential curve of the surface layer; such a valley is most likely to occur if the layer is relatively thick. On the other hand, A should decrease as the thickness of the layer increases, if the height of the peaks is constant.

The value of b calculated from the part of the lines corresponding to higher temperatures is about 0·6 volt, which is, I believe, the lowest value of b yet recorded. It corresponds to a threshold at 2 μ, but all attempts to detect any photoelectric emission beyond 1·3 μ have failed. This discrepancy shows that a theory which indicates that the work function determined from the Richardson equation should also determine the threshold is faulty at some point; but no suggestion can be made at present where the fault lies.

It may be mentioned incidentally that the thermionic emission of these cathodes is perfectly stable over long periods of time, and that, since it varies very rapidly with the temperature, photoelectric cells of this nature might be useful for some purposes as thermometers in the range from 100° to 200° C.

XII. *The Bending of a Thin Circular Plate.* *By* J. J. Vincent, *M.Sc., Shirley Institute, Didsbury, Manchester* †.

WHEN a thin flat plate, supported at its edge, is bent by a normal pressure, the stretching of the middle surface is negligible only when the deflexion of any point of the plate from its unstrained position or from a developable surface is small compared with the thickness of the plate. If the stretching of the middle surface be neglected, the deflexion of a point of a flat circular plate from its unstrained position is proportional to the pressure; but as the pressure increases, so that the deflexion is no longer small compared with the thickness of the plate, the deflexion for a given pressure will be less than that given by the relation of

* R. H. Fowler, Proc. Roy. Soc. A, cxxviii. p. 123 (1930).

† Communicated by Dr. John Prescott, M.A., College of Technology, Manchester.

proportionality, because, roughly speaking, part of the load is supported by the stretched middle surface, in the same way as a load is supported by a stretched non-rigid membrane. The equations giving the displacement at any point of a thin flat plate, which apply so long as the angle in radians between any two tangent planes to the bent plate is small compared with unity, are given in Prescott's 'Applied Elasticity,' chapter xv., and an approximate method for their solution, using a pseudo-energy equation, is given.

An attempt is made in this paper to obtain by another method approximate solutions to these equations applied to a thin, flat, circular plate. As long as the deflexion has not reached the point at which the rigidity is less effective than the tensions, the required deflexion can be expressed as a series of odd powers of the pressure, p. When p is small, the first power of p is alone important, and this term in p is the usual solution obtained when the deflexion is small compared with the thickness of the plate. Using this solution as a first approximation to the more general equation, and assuming that the terms in higher powers of p are small in comparison, a second approximation containing p^3 is obtained. Repeating this process, we get a third approximation containing p^5. To continue the process beyond this stage becomes laborious. A solution of this kind is obtained for the two cases :

(I.) when the plate is supported with its rim everywhere at the same level;

(II.) when the circumference of the plate is held fixed so that the radial strain is zero at the circumference.

The results for Case I. are compared with the results of an experiment by Mr. P. T. Steinthal *, and a fair agreement is obtained, especially as there is some doubt as to the experimental conditions. When Mr. Steinthal (who was the same person as the late Dr. Telford Petrie) was asked, a few years ago, under what precise boundary conditions his experiments were made, he admitted that he was not quite clear after all these years ; and, moreover, he had no suspicion of any effect that tension might have on his results, and so, he remarked, he would have taken no care to avoid holding the rim in tension. It should be noted that the experimental results lie between those for Case I. and Case II. For a given deflexion the pressure is much higher in Case II. than

* "Some Experimental Data on the Flexure of Flat Circular Plates within the Elastic Limits," by P. T. Steinthal, M.Sc., 'Engineering,' xci. p. 677.

Case I., as is to be expected from the different boundary conditions ; but the divergence soon becomes so great as to indicate that the solution for Case II. is only valid for much smaller deflexions than that for Case I. The way in which the deflexion begins to diverge from a linear function of p when p has such values that the maximum deflexion is of the order of the thickness, shows how accurate is the remark, in Thomson and Tait's 'Natural Philosophy,' that the usual formulæ for deflexion of plates (*i. e.*, with no allowance for stretching) are quite true only when the maximum deflexion is an infinitely small fraction of the thickness of the plate.

Let

p = uniform pressure applied normally to plate.

E = Young's Modulus.

σ = Poisson's ratio.

$$E' = \frac{E}{1-\sigma^2}.$$

$2h = d$ = thickness of plate.

a = radius of plate.

I = moment of inertia of unit length of a normal section of the plate about a line where the middle surface meets this section.

w = displacement, measured from the level of the centre of the middle surface, of a particle of middle surface distant r from centre ; w and p are measured in the same direction.

Then it has been shown by Prescott ('Applied Elasticity,' p. 443) that w is given by

$$p = E'I\nabla_1^4 w - \frac{2hE}{r} \cdot \frac{d}{dr}\left(\frac{d\phi}{dr} \cdot \frac{dw}{dr}\right), \quad . \quad . \quad . \quad (1)$$

where

$$\nabla_1^2 \equiv \frac{1}{r}\frac{d}{dr}\left(r\frac{d}{dr}\right), \quad \nabla_1^4 \equiv \nabla_1^2(\nabla_1^2),$$

and ϕ is a function connected to w by the equation

$$\nabla_1^4 \phi = -\frac{1}{2r}\frac{d}{dr}\left(\frac{dw}{dr}\right)^2. \quad . \quad . \quad . \quad . \quad (2)$$

Case I.

The boundary conditions are :—

(i.) The bending moment about the circumference is zero.

(ii.) The mean radial tension is zero for $r = a$.

Condition (i.) gives

$$\frac{d^2w}{dr^2}+\frac{\sigma}{r}\frac{dw}{dr}=0 \quad \text{at} \quad r=a, \quad . \quad . \quad . \quad (3)$$

and „ (ii.) gives

$$\frac{d\phi}{dr}=0 \quad \text{at} \quad r=a. \quad . \quad . \quad . \quad . \quad . \quad (4)$$

If the stretching of the middle surface be neglected, ϕ is zero, and if w_0 is the corresponding value of w,

$$p=\mathrm{E'I}\nabla_1{}^4w_0. \quad . \quad . \quad . \quad . \quad . \quad . \quad (5)$$

The solution of this, satisfying (3), is (*loc. cit.* p. 402)

$$w_0=\frac{pr^4}{64\mathrm{E'I}}-\frac{(3+\sigma)pa^2}{32(1+\sigma)\mathrm{E'I}}r^2 \quad . \quad . \quad . \quad (6)$$

$$=\alpha r^4+\beta r^2, \quad . \quad . \quad . \quad . \quad . \quad . \quad . \quad . \quad (7)$$

where

$$\alpha=\frac{p}{64\mathrm{E'I}}, \quad . \quad . \quad . \quad . \quad . \quad . \quad . \quad . \quad (8)$$

$$\beta=-\frac{(3+\sigma)pa^2}{32(1+\sigma)\mathrm{E'I}}. \quad . \quad . \quad . \quad . \quad . \quad . \quad (9)$$

When ϕ is small, w_0 is an approximate solution of (1). Therefore, put $w=w_0+w_1$, where w_1 is small compared with w_0, and let ϕ_1 be the corresponding value of ϕ.

Substituting $w=w_0+w_1$ in (1), and using (5), we get approximately, neglecting squares and products of small quantities,

$$\nabla_1{}^4w_1=\frac{\gamma}{r}\frac{d}{dr}\left(\frac{d\phi_1}{dr}\cdot\frac{dw_0}{dr}\right), \quad . \quad . \quad . \quad . \quad (10)$$

where

$$\gamma=\frac{2h\mathrm{E}}{\mathrm{E'I}}, \quad . \quad . \quad . \quad . \quad . \quad . \quad . \quad . \quad (11)$$

and substituting in (2), we have approximately,

$$\nabla_1{}^4\phi_1=-\frac{1}{2r}\frac{d}{dr}\left(\frac{dw_0}{dr}\right)^2. \quad . \quad . \quad . \quad . \quad (12)$$

Integrating thrice successively, we get

$$\frac{d\phi_1}{dr}=-\frac{\alpha^2r^7}{6}-\frac{\alpha\beta r^7}{3}-\frac{\beta^2r^3}{4}+\frac{\mathrm{K}r}{2}, \quad . \quad . \quad (13)$$

where K is an arbitrary constant, the other two constants which arise being zero, since $\frac{dw}{dr}$ and $\frac{d\phi}{dr}$ are both finite when $r=0$.

From (13), (4),

$$\mathrm{K} = \frac{\alpha^2 a^6}{3} + \frac{2\alpha\beta a^4}{3} + \frac{\beta^2 a^2}{2} \quad . \quad . \quad . \quad . \quad (14)$$

Integrating (10) once, and putting the arbitrary constant equal to zero, since $\frac{dw}{dr} = 0$ at $r = 0$, we get

$$r\frac{d}{dr}(\nabla_1^2 w_1) = \gamma \frac{d\phi_1}{dr} \cdot \frac{dw_0}{dr}$$

$$= -\gamma(4\alpha^3 + 2\beta r)\left(\frac{\alpha^2 r^7}{6} + \frac{\alpha\beta r^5}{3} + \frac{\beta^2 r^3}{4} - \frac{\mathrm{K}r}{2}\right)$$

from (7) and (13).

Dividing by r and integrating,

$$\frac{1}{r}\frac{d}{dr}\left(r\frac{dw_1}{dr}\right)$$

$$= -\gamma\left[\frac{\alpha^3 r^{10}}{15} + \frac{5\alpha^2\beta r^8}{24} + \frac{5\alpha\beta^2 r^6}{18} + \frac{(\beta^3 - 4\alpha\mathrm{K})r^4}{8} - \frac{\beta\mathrm{K}r^2}{2}\right] + \mathrm{L},$$

where L is an arbitrary constant.

Multiplying by r and integrating,

$$r\frac{dw_1}{dr} = -\gamma\left[\frac{\alpha^3 r^{12}}{180} + \frac{\alpha^2\beta r^{10}}{48} + \frac{5\alpha\beta^2 r^8}{144}\right.$$

$$\left. + \frac{(\beta^3 - 4\alpha\mathrm{K})r^6}{48} - \frac{\beta\mathrm{K}r^4}{8}\right] + \frac{\mathrm{L}r^2}{2},$$

the constant of integration being zero since $\frac{dw_1}{dr} = 0$ at $r = 0$.

Dividing by r and integrating, using $w = 0$ when $r = 0$,

$$w_1 = -\gamma\left[\frac{\alpha^3 r^{12}}{2160} + \frac{\alpha^2\beta r^{10}}{480} + \frac{5\alpha\beta^2 r^8}{1152}\right.$$

$$\left. + \frac{(\beta^3 - 4\alpha\mathrm{K})r^6}{288} - \frac{\beta\mathrm{K}r^4}{32}\right] + \frac{\mathrm{L}r^2}{4} \quad . \quad . \quad . \quad (15)$$

$$\equiv a_{12}r^{12} + a_{10}r^{10} + a_8 r^8 + a_6 r^6 + a_4 r^4 + a_2 r^2 \quad . \quad . \quad . \quad . \quad (16)$$

From (3), (15),

$$\mathrm{L} = \frac{2\gamma}{1+\sigma}\left[\frac{(11+\sigma)}{180}\alpha^3 a^{10} + \frac{(9+\sigma)}{48}\alpha^2\beta a^8 + \frac{5(7+\sigma)}{144}\alpha\beta^2 a^6\right.$$

$$\left. + \frac{(5+\sigma)}{48}(\beta^3 - 4\alpha\mathrm{K})a^4 - \frac{(3+\sigma)}{8}\beta\mathrm{K}a^2\right] \quad . \quad . \quad . \quad (17)$$

Let $(w_0+w_1+w_2)$ and $(\phi_1+\phi_2)$ be third approximations to w and ϕ respectively ; then, proceeding as before, we get

$$\frac{d\phi_2}{dr}=-\frac{3}{14}a_{12}\alpha r^{15}-\frac{(5a_{10}\alpha+3a_{12}\beta)}{21}r^{13}-\frac{(8a_8\alpha+5a_{10}\beta)}{30}r^{11}$$
$$-\frac{(3a_6\alpha+2a_8\beta)}{10}r^9-\frac{(4a_4\alpha+3a_6\beta)}{12}r^7$$
$$-\frac{(a_2\alpha+a_4\beta)}{3}r^5-\frac{a_2\beta}{2}r^3+\frac{\mathrm{M}r}{2}, \quad . \quad . \quad (18)$$

where

$$\mathrm{M}=\frac{3}{7}a_{12}\alpha a^{14}+\frac{2(5a_{10}\alpha+3a_{12}\beta)}{21}a^{12}$$
$$+\frac{(8a_8\alpha+5a_{10}\beta)}{15}a^{10}+\frac{(3a_6\alpha+2a_8\beta)}{5}a^8$$
$$+\frac{(4a_4\alpha+3a_6\beta)}{6}a^6+\frac{2(a_2\alpha+a_4\beta)}{3}a^4+a_2\beta a^2, \quad . \quad (19)$$

and

$$w_2=\frac{\mathrm{A}_{17}r^{20}}{18\,.\,20^2}+\frac{\mathrm{A}_{15}r^{18}}{16\,.\,18^2}+\frac{\mathrm{A}_{13}r^{16}}{14\,.\,16^2}+\frac{\mathrm{A}_{11}r^{14}}{12\,.\,14^2}+\frac{\mathrm{A}_9r^{12}}{10\,.\,12^2}$$
$$+\frac{\mathrm{A}_7r^{10}}{8\,.\,10^2}+\frac{\mathrm{A}_5r^8}{6\,.\,8^2}+\frac{\mathrm{A}_3r^6}{4\,.\,6^2}+\frac{\mathrm{A}_1r^4}{2\,.\,4^2}+\frac{\mathrm{N}r^2}{4}, \quad . \quad . \quad (20)$$

where

$$\left.\begin{aligned}
\mathrm{A}_{17}&=-\frac{20}{17}a_{12}\alpha^2\gamma,\\
\mathrm{A}_{15}&=-\gamma\left(\frac{55}{21}a_{10}\alpha^2+5a_{12}\alpha\beta\right),\\
\mathrm{A}_{13}&=-\gamma\left(\frac{12}{5}a_8\alpha^2+\frac{94}{21}a_{10}\alpha\beta+\frac{23}{7}a_{12}\beta^2\right),\\
\mathrm{A}_{11}&=-\gamma\left(\frac{11}{5}a_6\alpha^2+4a_8\alpha\beta+\frac{17}{6}a_{10}\beta^2-6a_{12}\mathrm{K}\right),\\
\mathrm{A}_9&=-\gamma\left(2a_4\alpha^2+\frac{18}{5}a_6\alpha\beta+\frac{12}{5}a_8\beta^2-5a_{10}\mathrm{K}\right),\\
\mathrm{A}_7&=-\gamma\left(\frac{5}{3}a_2\alpha^2+\frac{64}{21}a_4\alpha\beta+\frac{25}{14}a_6\beta^2-4a_8\mathrm{K}\right),\\
\mathrm{A}_5&=-\gamma\left(\frac{10}{3}a_2\alpha\beta+\frac{5}{3}a_4\beta^2-3a_6\mathrm{K}\right),\\
\mathrm{A}_3&=-\gamma\left(\frac{3}{2}a_2\beta^2-2a_4\mathrm{K}-2\mathrm{M}\alpha\right),\\
\mathrm{A}_1&=\gamma(a_2\mathrm{K}+\mathrm{M}\beta)\,;
\end{aligned}\right\} \quad . \quad . \quad (21)$$

$$N = -\frac{2}{1+\sigma}\left[\frac{(19+\sigma)}{18.20}\cdot A_{17}a^{18} + \frac{(17+\sigma)}{16.18}\cdot A_{15}a^{16}\right.$$
$$+ \frac{(15+\sigma)}{14.16}\cdot A_{13}a^{14} + \frac{(13+\sigma)}{12.14}\cdot A_{11}a^{12}$$
$$+ \frac{(11+\sigma)}{10.12}\cdot A_9 a^{10} + \frac{(9+\sigma)}{8.10}\cdot A_7 a^8$$
$$+ \frac{(7+\sigma)}{6.8}\cdot A_5 a^6 + \frac{(5+\sigma)}{4.6}\cdot A_3 a^4$$
$$\left. + \frac{(3+\sigma)}{2.4}\cdot A_1 a^2\right]. \quad . \quad . \quad . \quad . \quad . \quad . \quad . \quad (22)$$

Therefore, to this degree of approximation,

$$w = w_0 + w_1 + w_2$$
$$= \frac{A_{17}}{18.20^2}r^{20} + \frac{A_{15}}{16.18^2}\cdot r^{18} + \frac{A_{13}}{14.16^2}r^{16} + \frac{A_{11}}{12.14^2}r^{14}$$
$$+ \left(\frac{A_9}{10.12^2} + a_{12}\right)r^{12} + \left(\frac{A_7}{8.10^2} + a_{10}\right)r^{10} + \left(\frac{A_5}{6.8^2} + a_8\right)r^8$$
$$+ \left(\frac{A_3}{4.6^2} + a_6\right)r^6 + \left(\frac{A_1}{2.4^2} + a_4 + \alpha\right)r^4 + \left(\frac{N}{4} + a_2 + \beta\right)r^2.$$
$$. \quad . \quad . \quad (23)$$

Case II.

If the boundary of the plate is kept fixed, the boundary conditions are :—

(i.) The bending moment about the circumference is zero.

(ii.) The radial displacement is zero for $r = a$.

Therefore, equation (4) is replaced by

$$\frac{d^2\phi}{dr^2} - \frac{\sigma}{r}\frac{d\phi}{dr} = 0 \text{ when } r = a. \quad . \quad . \quad . \quad (24)$$

Proceeding as before, we get

$$\frac{d\phi_1}{dr} = -\frac{\alpha^2 r^7}{6} - \frac{\alpha\beta r^5}{3} - \frac{\beta^2 r^3}{4} + \frac{K'r}{2}, \quad . \quad . \quad (25)$$

where

$$K' = \frac{2}{1-\sigma}\left[\frac{(7-\sigma)}{6}\alpha^2 a^6 + \frac{(5-\sigma)}{3}\alpha\beta a^4 + \frac{(3-\sigma)}{4}\beta^2 a^2\right] \quad (26)$$

and

$$w_1 = -\gamma\left[\frac{\alpha^3 r^{12}}{2160} + \frac{\alpha^2\beta r^{10}}{480} + \frac{5\alpha\beta^2 r^8}{1152} + \frac{(\beta^3 - 4\alpha \mathrm{K}')r^6}{288} - \frac{\beta \mathrm{K}' r^4}{32}\right] + \frac{\mathrm{L}' r^2}{4} \quad . \quad . \quad (27)$$

$$\equiv a_{12}r^{12} + a_{10}r^{10} + a_8 r^8 + a_6' r^6 + a_4' r^4 + a_2' r^2 \quad . \quad . \quad . \quad . \quad (28)$$

where

$$\mathrm{L}' = \frac{2\gamma}{1+\sigma}\left[\frac{(11+\sigma)}{180}\alpha^3 a^{10} + \frac{(9+\sigma)}{48}\alpha^2\beta a^8 + \frac{5(7+\sigma)}{144}\alpha\beta^2 a^6 + \frac{(5+\sigma)}{48}(\beta^3 - 4\alpha \mathrm{K}')a^4 - \frac{(3+\sigma)}{8}\beta \mathrm{K}' a^2\right]; \quad (29)$$

$$\frac{d\phi_2}{dr} = -\frac{3}{14}a_{12}\alpha r^{13} - \frac{(5a_{10}\alpha + 3a_{12}\beta)}{21}r^{13} - \frac{(8a_8\alpha + 5a_{10}\beta)}{30}r^{11} - \frac{(3a_6'\alpha + 2a_8\beta)}{10}r^9 - \frac{(4a_4'\alpha + 3a_6'\beta)}{12}r^7 - \frac{(a_2'\alpha + a_4'\beta)}{3}r^5 - \frac{a_2'\beta}{2}r^3 + \frac{\mathrm{M}' r}{2}, \quad . \quad (30)$$

where

$$\mathrm{M}' = \frac{2}{1-\sigma}\left[\frac{(45-3\sigma)}{14}a_{12}\alpha a^{14} + \frac{(13-\sigma)}{21}(5a_{10}\alpha + 3a_{12}\beta)a^{12} + \frac{(11-\sigma)}{30}(8a_8\alpha + 5a_{10}\beta)a^{10} + \frac{(9-\sigma)}{10}(3a_6'\alpha + 2a_8\beta)a^8 + \frac{(7-\sigma)}{12}(4a_4'\alpha + 3a_6'\beta)a^6 + \frac{(5-\sigma)}{3}(a_2'\alpha + a_4'\beta)a^4 + \frac{(3-\sigma)}{2}a_2'\beta a^2\right]; \quad . \quad . \quad . \quad (31)$$

$$w = \frac{\mathrm{A}_{17}r^{20}}{18 \cdot 20^2} + \frac{\mathrm{A}_{15}r^{18}}{16 \cdot 18^2} + \frac{\mathrm{A}_{13}r^{16}}{14 \cdot 16^2} + \frac{\mathrm{A}_{11}'r^{14}}{12 \cdot 14^2} + \left(\frac{\mathrm{A}_9'}{10 \cdot 12^2} + a_{12}\right)r^{12} + \left(\frac{\mathrm{A}_7'}{8 \cdot 10^2} + a_{10}\right)r^{10} + \left(\frac{\mathrm{A}_5'}{6 \cdot 8^2} + a_8\right)r^8 + \left(\frac{\mathrm{A}_3'}{4 \cdot 6^2} + a_6'\right)r^6 + \left(\frac{\mathrm{A}_1'}{2 \cdot 4^2} + a_4' + \alpha\right)r^4 + \left(\frac{\mathrm{N}'}{4} + a_2' + \beta\right)r^2, \quad . \quad . \quad . \quad (32)$$

where A_{11}', A_9', A_7', A_5', A_3', A_1' are given by the expressions for A_{11}, A_9, A_7, A_5, A_3, A_1, respectively, by replacing a_2, a_4, a_6, K, M, by a_2', a_4', a_6', K', M'; and N' is given by replacing A_{11}, A_9, A_7, A_5, A_3, A_1 in the expression for N by A_{11}', A_9' . . . A_1', respectively.

Evaluation of the Constants.

Case I.

$$\text{Let } \sigma = \frac{1}{4}.$$

Then from (8), $$\alpha = 0{\cdot}176\frac{p}{Ed^3}; \quad . \quad . \quad . \quad . \quad . \quad . \quad (33)$$

,, (9), $$\beta = -0{\cdot}914\frac{a^2p}{Ed^3}; \quad . \quad . \quad . \quad . \quad . \quad (34)$$

,, (11), $$\gamma = \frac{11{\cdot}2}{d^2}; \quad . \quad . \quad . \quad . \quad . \quad . \quad . \quad . \quad (35)$$

,, (14), $$K = 0{\cdot}321\frac{a^6p^2}{E^2d^6}; \quad . \quad . \quad . \quad . \quad . \quad (36)$$

,, (17), $$L = 0{\cdot}771\frac{a^{10}p^3}{E^3d^{11}}; \quad . \quad . \quad . \quad . \quad . \quad (37)$$

,, (15),
$$\left.\begin{aligned} a_{12} &= -0{\cdot}00003\frac{p^3}{E^3d^{11}},\\ a_{10} &= 0{\cdot}00066\frac{a^2p^3}{E^3d^{11}},\\ a_8 &= -0{\cdot}00717\frac{a^4p^3}{E^3d^{11}},\\ a_6 &= 0{\cdot}0387\frac{a^6p^3}{E^3d^{11}},\\ a_4 &= -0{\cdot}103\frac{a^8p^3}{E^3d^{11}},\\ a_2 &= 0{\cdot}193\frac{a^{10}p^3}{E^3d^{11}}; \end{aligned}\right\} \quad . \quad . \quad . \quad . \quad . \quad (38)$$

from (19), $$M = -0{\cdot}115\frac{a^{14}p^4}{E^4d^{14}}; \quad . \quad . \quad . \quad . \quad . \quad (39)$$

from (21),

$$\left.\begin{aligned}
A_1 &= 1{\cdot}87\frac{a^{16}p^5}{E^5d^{19}},\\
A_3 &= -3{\cdot}91\frac{a^{14}p^5}{E^5d^{19}},\\
A_5 &= 3{\cdot}20\frac{a^{12}p^5}{E^5d^{19}},\\
A_7 &= -1{\cdot}43\frac{a^{10}p^5}{E^5d^{19}},\\
A_9 &= 0{\cdot}497\frac{a^8p^5}{E^5d^{19}},\\
A_{11} &= -0{\cdot}0997\frac{a^6p^5}{E^5d^{19}},\\
A_{13} &= 0{\cdot}0117\frac{a^4d^5}{E^5d^{19}},\\
A_{15} &= -0{\cdot}00079\frac{a^2p^5}{E^5d^{19}},\\
A_{17} &= 0{\cdot}00003\frac{p^5}{E^5d^{19}};
\end{aligned}\right\} \quad . \quad . \quad . \quad . \quad . \quad (40)$$

$$N = -0{\cdot}418\frac{a^{18}p^5}{E^5d^{19}}. \quad . \quad . \quad . \quad . \quad . \quad (41)$$

Therefore, from (23), when $r = a$,

$$w_a = -0{\cdot}738\frac{a^4p}{Ed^3} + 0{\cdot}122\frac{a^{12}p^3}{E^3d^{11}} - 0{\cdot}0662\frac{a^{20}p^5}{E^5d^{19}},$$

and if b is the deflexion of the centre measured from the level of the rim,

$$b = -w_a,$$

and $$\frac{b}{d} = 0{\cdot}738\frac{a^4p}{Ed^4} - 0{\cdot}122\left(\frac{a^4p}{Ed^4}\right)^3 + 0{\cdot}066\left(\frac{a^4p}{Ed^4}\right)^5.$$

Inverting this, we get

$$\frac{a^4p}{Ed^4} = 1{\cdot}35\left(\frac{b}{d}\right) + 0{\cdot}410\left(\frac{b}{d}\right)^3 - 0{\cdot}0369\left(\frac{b}{d}\right)^5. \quad . \quad (42)$$

$\frac{a^4p}{Ed^4}$ is plotted against $\frac{b}{d}$ as shown. The straight line is the tangent to this curve at the origin, viz., the line $\frac{a^4p}{Ed^4} = 1{\cdot}35\frac{b}{d}$. If p_0 is the value of p satisfying this last equation, that is,

the value of p when stretching is neglected, and p_0 the value given by (42), then values of $\frac{p}{p_0}$ may be compared with the corresponding values obtained from Steinthal's curves, and are shown in the following table.

		$d = 0{\cdot}142''$.				$d = 0{\cdot}268''$.			
b/d.		0·705	1·06	1·41	1·70	0·56	0·75	0·93	1·12
$\frac{p}{p_0}$	Steinthal...	1·24	1·47	1·80	2·10	1·16	1·27	1·36	1·50
	Calculated	1·15	1·29	1·49	1·65	1·09	1·16	1·24	1·34

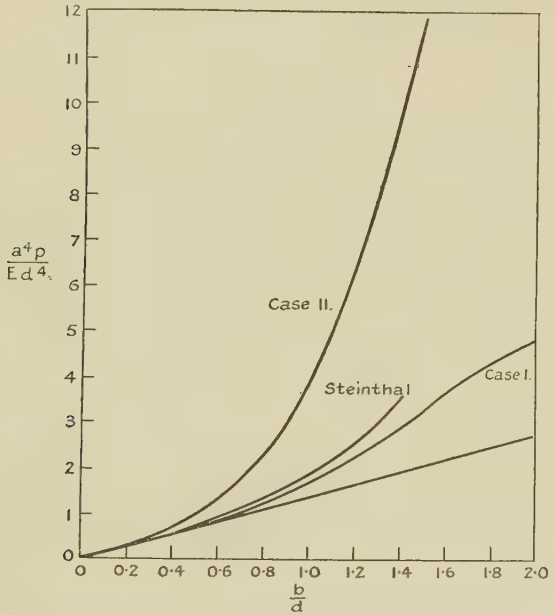

Steinthal's curve for $d = 0{\cdot}142''$ is shown on the graph by making its tangent at the origin coincide with the tangent to (42) at the origin. In effect this means that we are taking the value of E for Steinthal's disks from his own experiments.

Case II.

From (26),

$$K' = 0{\cdot}946\frac{a^6 p^2}{E^2 d^6}; \quad . \quad . \quad . \quad . \quad . \quad (43)$$

„ (29),

$$L' = 4{\cdot}08\frac{a^{10} p^3}{E^3 d^{11}}; \quad . \quad . \quad . \quad . \quad . \quad (44)$$

from (28),

$$\left.\begin{aligned} a_6' &= 0{\cdot}0558\frac{a^6p^3}{\mathrm{E}^3d^{11}},\\ a_4' &= -0{\cdot}304\frac{a^8p^3}{\mathrm{E}^3d^{11}},\\ a_2' &= 1{\cdot}02\frac{a^{10}p^3}{\mathrm{E}^3d^{11}}; \end{aligned}\right\} \quad . \quad . \quad . \quad . \quad . \quad (45)$$

from (31),

$$\mathrm{M}' = -1{\cdot}95\frac{a^{14}p^4}{\mathrm{E}^4d^{14}}; \quad . \quad . \quad . \quad . \quad . \quad (46)$$

„ (32),

$$\left.\begin{aligned} \mathrm{A}_1' &= 31{\cdot}0\frac{a^{16}p^5}{\mathrm{E}^5d^{19}},\\ \mathrm{A}_3' &= -28{\cdot}6\frac{a^{14}p^5}{\mathrm{E}^5d^{19}},\\ \mathrm{A}_5' &= 12{\cdot}7\frac{a^{12}p^5}{\mathrm{E}^5d^{19}},\\ \mathrm{A}_7' &= -3{\cdot}51\frac{a^{10}p^5}{\mathrm{E}^5d^{19}},\\ \mathrm{A}_9' &= 0{\cdot}771\frac{a^8p^5}{\mathrm{E}^5d^{19}},\\ \mathrm{A}_{11}' &= -0{\cdot}114\frac{a^6p^5}{\mathrm{E}^5d^{19}},\\ \text{and}\quad \mathrm{N}' &= -12{\cdot}6\frac{a^{18}p^5}{\mathrm{E}^5d^{19}}. \end{aligned}\right\} \quad . \quad . \quad . \quad . \quad . \quad (47)$$

Therefore, from (32), when $r = a$,

$$w_a = -0{\cdot}738\frac{a^4p}{\mathrm{E}d^4} + 0{\cdot}766\frac{a^{12}p^3}{\mathrm{E}^3d^{11}} - 2{\cdot}36\frac{a^{20}p^5}{\mathrm{E}^5d^{19}};$$

and if $b = -w_a$,

$$\frac{b}{d} = 0{\cdot}738\frac{a^4p}{\mathrm{E}d^4} - 0{\cdot}766\left(\frac{a^4p}{\mathrm{E}d^4}\right)^3 + 2{\cdot}36\left(\frac{a^4p}{\mathrm{E}d^4}\right)^5.$$

Inverting this, we get

$$\frac{a^4p}{\mathrm{E}d^4} = 1{\cdot}35\left(\frac{b}{d}\right) + 2{\cdot}58\left(\frac{b}{d}\right)^3 + 0{\cdot}0168\left(\frac{b}{d}\right)^5. \quad . \quad (48)$$

$\frac{a^4p}{\mathrm{E}d^4}$ is plotted against $\frac{b}{d}$ as shown.

XIII. *Theory of Dielectrics.*

To the Editors of the Philosophical Magazine.

GENTLEMEN,—

IN a letter addressed to the Editors of the Philosophical Magazine, Dr. J. H. J. Poole remarks that the experimental results obtained by Dr. H. H. Poole and confirmed by H. Schiller and others do not agree with the formula that I have deduced in my paper published in the Philosophical Magazine for February 1931.

I should like to point out that, in my opinion, the contradiction in question is but apparent and that, on the contrary, the results mentioned complete or supplement mine. Indeed, the empiric formula proposed by Dr. H. H. Poole is verified for *intense electric fields*, while my study is built on the observation of what takes place in weaker fields.

After all, the phenomenon we observe here is similar to the phenomenon produced by the passage of electricity through gases. When we progressively increase the field, the observed current first increases almost proportionately to the field, then increases more slowly till it has reached the constant value of the saturation-current. If we further increase the field, the current increases again rapidly and ultimately reaches the high value corresponding to the disruptive potential.

In the present case, too, I have experimentally observed a current nearly proportional to the field (*Mem. Ac. Roy. Belg.* t. xi.). The formula deduced from the theory I proposed enables us to foresee the existence of a saturation-current. By analogy with what takes place in gases, we may deduce that for more intense fields we shall observe a further growth of the current and consequently a growth of conductivity which will reach the value corresponding to the field piercing the dielectric. It is this phase of the current in the solid dielectrics which seems to have been studied by Dr. H. H. Poole; the results he obtained are given by the formula he mentions.

Yours faithfully,

Université de Liége,
May 5th, 1931.

G. GUÉBEN.

XIV. *Notices respecting New Books.*

Intermediate Mechanics: Statics and Mechanics. By D. Humphrey. (Longmans, Green and Co., 1931. 10*s.* 6*d.*)

THE present volume completes the work by Mr. Humphrey on Intermediate Mechanics, of which the volume on Dynamics has already been published. The two volumes together are planned to cover all the requirements for the Higher Certificate and University Scholarship examinations. It is a feature of the treatment that the methods of the Calculus are used whenever possible, and this certainly makes it a useful work for those who have some knowledge of differential and integral calculus. The text is supplemented by a large number of examples of all kinds. Specially useful will be the illustrative examples, which are fully worked out. This book can be recommended.

Practical Physical Chemistry. By Alexander Findlay. With 114 figures in the text. Fifth edition, revised and enlarged. Pp. xii + 312. (Longmans, Green and Co. 1931. 7*s.* 6*d.*)

The bibliographical note at the beginning of Professor Findlay's book is evidence of its usefulness and popularity. Originally appearing at a time when Physical Chemistry was not subject to such a systematic attack as is now made upon it both in school and in University laboratories, it has grown with its subject so that it can still fulfil for the student the same primary function. It is an excellent guide to the simple application of physical principles in chemistry and therein lies its great value. Its recommendation need not end there, for it contains a happy blend of theoretical instruction with practical advice, and insists on just that amount of refinement which is necessary for the most useful result. More full-grown chemists might read with advantage the first chapter, on limits of accuracy and the validity of results, and even advanced research workers will find in the book many hints on the construction of efficient apparatus. The relegation to footnotes of further refinements for specific purposes adds greatly to the utility of the book for reference, and at the same time to the clarity and simplicity of the text.

Among the more noticeable of the modern features of the book are the references to parachor determination and its significance, an excellent if somewhat modest introduction to the concept of activity, and an instance of the application of the thermionic valve to potentiometric method. The chapter on electromotive force is a long one and a good one, but even so, it seems almost too succinct for the exposition of such important material. For a practical book it compares very favourably, from the reading standpoint, with many texts of a more narrative character. Its figures, its instructions, and its purpose are all equally clear.

XV. *Proceedings of Learned Societies*

GEOLOGICAL SOCIETY.

[Continued from vol. xi. p. 1256.]

April 22nd, 1931.—Prof. E. J. Garwood, M.A., Sc.D., F.R.S., President, in the Chair.

THE following communications were read:—

1. 'Xenoliths of Igneous Origin in the Trégastel-Ploumanac'h Granite, Côtes-du-Nord, France.' By Herbert Henry Thomas, M.A., Sc.D., F.R.S., V.P.G.S., and Walter Campbell Smith, M.C., T.D., M.A., Sec.G.S.

In the neighbourhood of Trégastel, about 7 miles north of Lannion, a red porphyritic biotite-granite crops out along the coast and forms the rising ground for several miles inland, In parts, this granite is remarkable for the abundance of xenoliths which it contains. Some of these are of sedimentary origin, but the majority are of the kind usually referred to as 'basic segregations.' A patch of basic rock covering an area of about a mile and a half from north to south and about half a mile wide is entirely surrounded by granite. Its most basic portions are of biotite-bearing olivine-norite. Impregnation by, and reaction with, the invading granite has given rise to a whole series of hybrid rocks varying through hypersthene-gabbro, augitic quartz-biotite-diorite, to quartz-biotite-diorite, and even to a biotite-rich granitic stage. Near the junction of the granite with the hybrid rocks, 'basic segregations' are very numerous. When examined, they prove to have a structure and mineral composition corresponding to the various stages presented by the basic hybrids, and on the extreme margin of the hybrid rock the xenoliths may be seen in the process of separation from the parent mass. The occasional presence of large felspars in the xenoliths is discussed, and the Authors are of opinion that these are xenocrysts and have not grown in place. Evidence is produced to show that the basic mass from which the xenoliths were derived was most probably part of the roof of the granite.

Comparisons are made with rocks from other areas.

2. 'The Loch Doon "Granite" Area, Galloway.' By Charles Irving Gardiner, M.A., F.G.S., and Prof. Sidney Hugh Reynolds, M.A., Sc.D., F.G.S.

The Loch Doon 'granite' mass has a length of $11\frac{1}{2}$ and a maximum width of $6\frac{1}{2}$ miles and covers an area of about 47 square miles. The plutonic rocks are almost everywhere surrounded by high hills composed of metamorphosed Ordovician sediments.

The plutonic rocks are of three main types:—

1. The prevalent rock, intermediate in character, is a quartz-mica-diorite or tonalite with an average specific gravity of 2·71.
2. The central ridge is formed of biotite-granite with an average specific gravity of 2·63.
3. At the southern and north-western ends of the plutonic mass the rock is a norite with an average specific gravity of 2·81. A third mass of norite, probably analogous to the other two, is found in the isolated exposure of Burnhead, about $1\frac{1}{2}$ miles east of the plutonic boundary.

Analyses were prepared by Mr. E. G. Radley of each of these rock-types. The most interesting problem concerning the plutonic mass is to determine the mutual relations of the rocks and to ascertain whether their different varieties may be considered to have arisen by differentiation subsequent to intrusion, or whether the facts point to each of the three rock-types being a separate intrusion.

The Authors believe the latter to be the true explanation for the following reasons:—

1. Throughout a narrow band along much of the norite-tonalite boundary, and a wider one along the tonalite-granite boundary, the rock is of transitional or hybrid character.
2. The marginal part of the norite sometimes shows signs of alteration—apparently by the tonalite.
3. Small areas of tonalite, presumably intrusions, occur within the limit of each mass of norite.

No evidence was found of contamination of the igneous magma by the incorporation of sedimentary material.

Great numbers of small intrusions, dykes, and perhaps sills, trending north-east to south-west, cut both the plutonic rocks and the surrounding altered sediments. The great majority belong to the same suite and are somewhat later than the plutonic rocks, as they are not metamorphosed. Others show metamorphism, and must be pre-plutonic or at any rate pre-tonalite. The considerable majority of the minor intrusions are fine-grained porphyrites, but more acid types—microgranites, granophyres, and quartz-porphyries—occur. There are also numerous dioritic and lamprophyric dykes, most of the lamprophyres bearing hornblende.

Except for the Arenig cherty series, the sediments surrounding the Loch Doon plutonic mass form a somewhat monotonous series of grits and flags with no calcareous rocks. Biotite-cordierite-hornfels is the prevalent rock-type formed by their metamorphism. The highest grade of metamorphism is found in the xenoliths enclosed in the tonalite; these occasionally contain corundum.

The Arenig cherts become recrystallized as quartzites with biotite, pyroxene, garnet, and occasionally schorl in the interstices between the quartz grains.

FIG. 1.

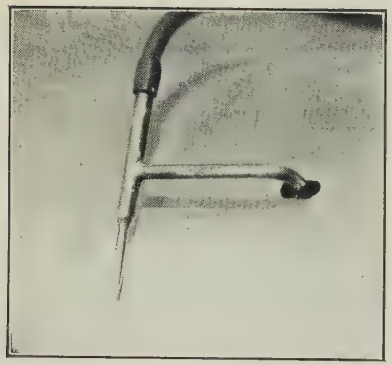

FIG. 2.

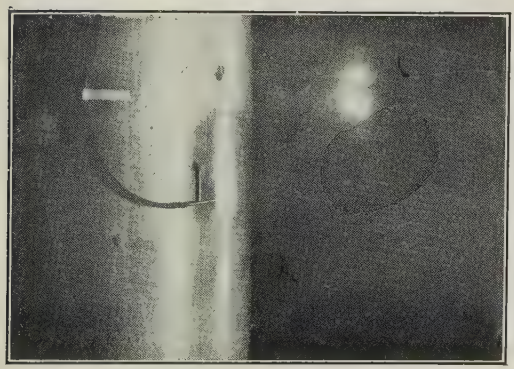

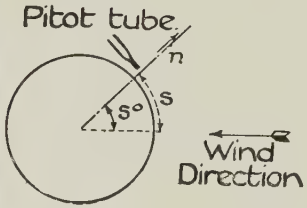

FIG. 3.

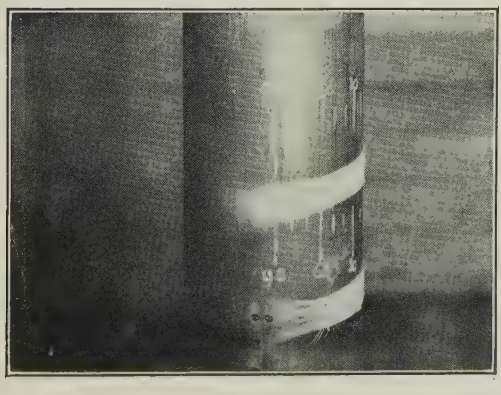

FIG. 4.

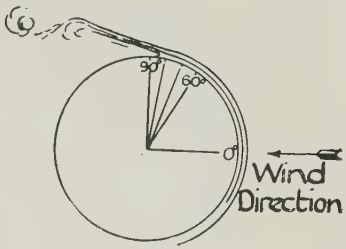

FIG. 5.

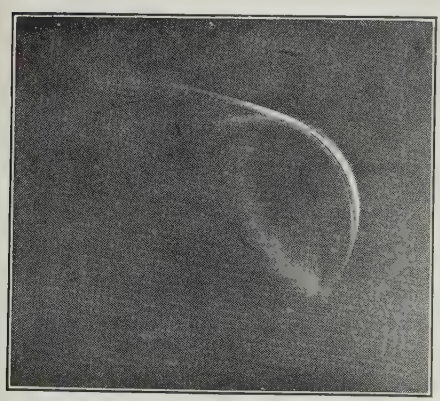

FIG. 6.

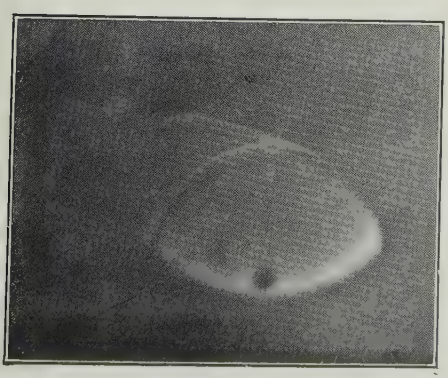

Fig. 7.

Fig. 8.

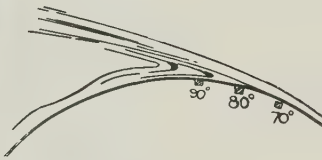

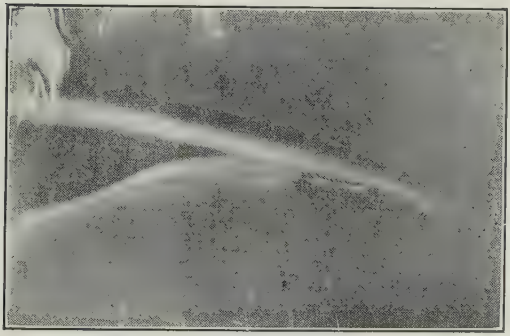

Fig. 9.

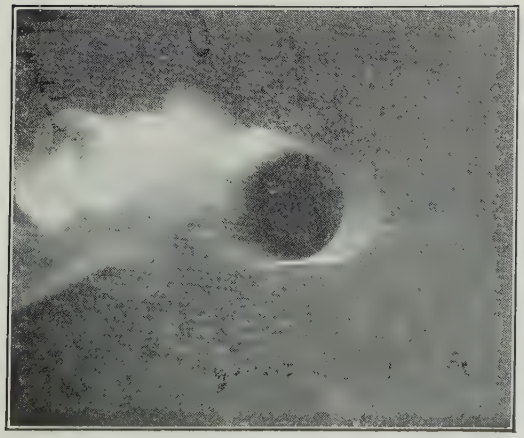

Phil. Mag. Ser. 7, Vol. 12, Pl. IV.

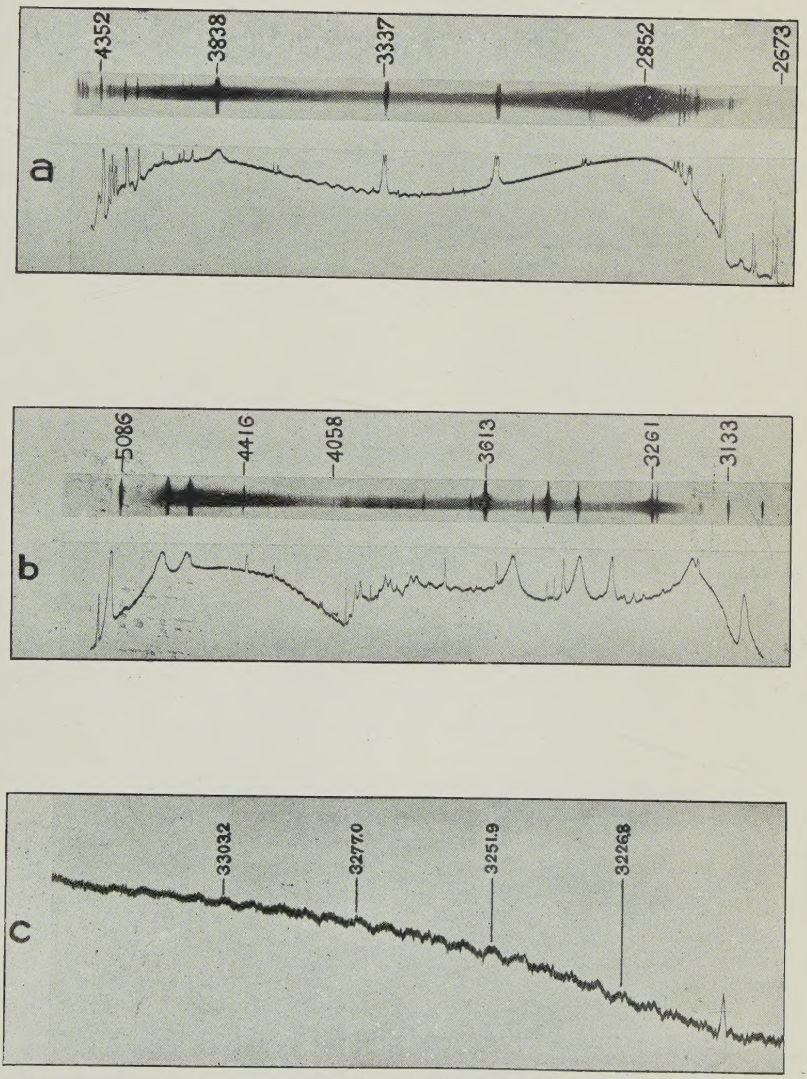

a. Mg_2 (2^1P_1).
b. Cd_2 (2^3P_0 and 2^3P_1).
c. Hg_2 (2^3P_1).

Phil. Mag. Ser. 7, Vol. 12, Pl. V.

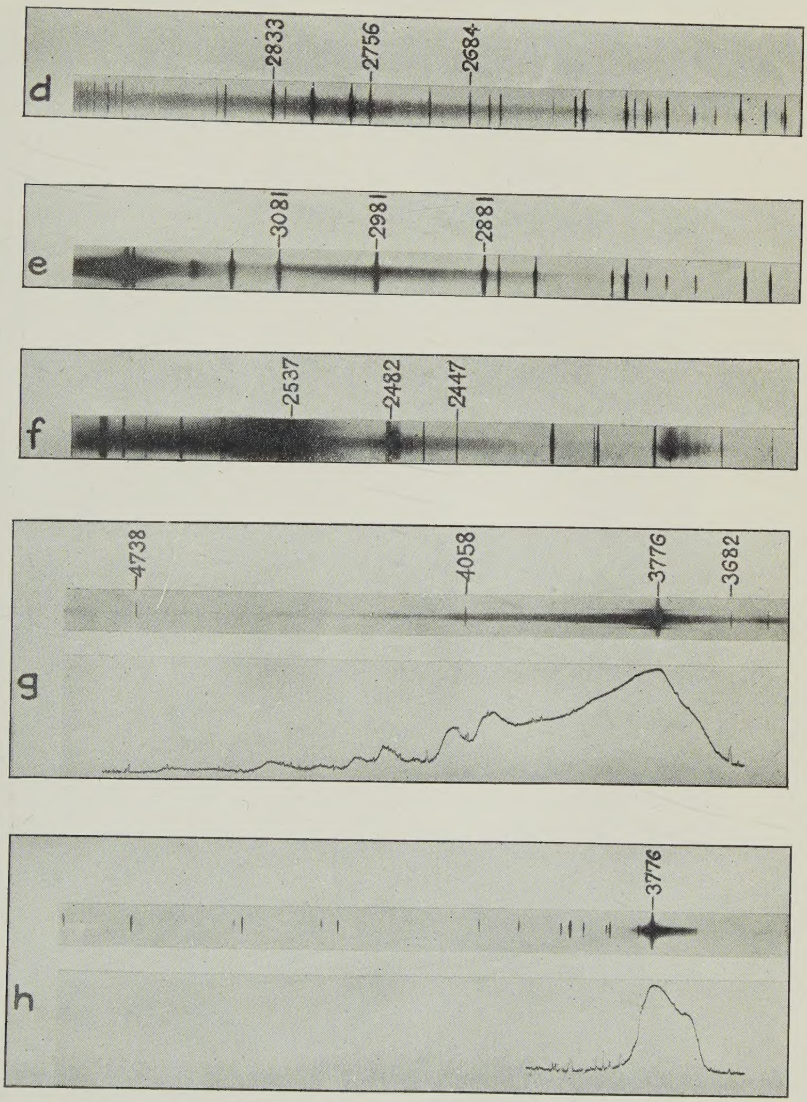

d. Zn_n.
e. Cd_n.
f. Hg_n.
g & *h*. Tl_n.